Annales Societatis Geologorum Poloniae (2008), vol. 78: 151–280.

THE RED-BED-TYPE PRECIOUS METAL DEPOSIT IN THE SIEROSZOWICE-POLKOWICE COPPER MINING DISTRICT, SW POLAND

Jadwiga PIECZONKA[1], Adam PIESTRZYŃSKI[1], Jacek MUCHA[1], Adam GŁUSZEK[2], Maciej KOTARBA[1] & Dariusz WIĘCŁAW[1]

[1] *Faculty of Geology, Geophysics and Environmental Protection, AGH University of Science and Technology, Al. Mickiewicza 30, 30-059 Kraków, Poland; e:mail: piestrz@geol.agh.edu.pl*
[2] *KGHM PM S.A., ul. M. Skłodowskiej-Curie 48, 59-301 Lubin, Poland*

Pieczonka, J., Piestrzyński, A., Mucha, J., Głuszek, A., Kotarba, M. & Więcław, D., 2008. The red-bed-type precious metal deposit in the Sieroszowice-Polkowice copper mining district, SW Poland. *Annales Societatis Geologorum Poloniae*, 78: 151–280.

Abstract: Since 50 years copper-silver ores have been extracted from the Lubin-Sieroszowice deposit located on the border between the Lower and Upper Permian sediments. It is a world class stratoidal type deposit. In the whole world the Kupferschiefer unit is recognized as a black, clayey organic-rich shale. The Cu-Ag deposit is a part of the Fore-Sudetic Monocline, and is located on the border of the Lower and Upper Permian strata The monocline includes three rock complexes. The first is the basement, which comprises Proterozoic crystalline rocks and Carboniferous sediments. It is overlain by monoclinally dipping Permian and Triassic sedimentary rocks.

In this work, study on ore mineralisation of the red variety of the Kupferschiefer are presented. Oxidation of the Kupferschiefer as an epigenetic phenomena.The oxidized zones reveal low concentrations of simple copper sulphides with the dominating chalcopyrite accompanied by bornite, pyrite, covellite, galena, clausthalite, chalcocite, digenite, spioncopite, geerite, native Au, electrum, tetraauricupride, naumannite, native Pb, Pd-arsenides and minerals of mixed composition: Au-Ag-Pb-Bi-Se-Te, Au-Ag-Pb-Te, Bi-Cu, Bi-Pd and Pd-As-O. Most important are natural alloys of precious metals, Pd-arsenides and oxidized phases (mostly Pd ones), which strongly influence the effectiveness of froth flotation. Precious metals form several parageneses: i – clausthalite - native Pb - electrum - $AuPb_2$, ii – Pt-native Au - native Pd - sobolevskite - native Pb, iii – native Au - haematite - bornite - minerals of covellite-chalcocite group, iiii – electrum - tetraauricupride - chalcocite, iiiii – electrum - Pd-arsenides - tellurides - selenides - BiPd and CuBi natural alloys - Pd-oxides.

The red Kupferschiefer variety is distinctly lower in carbonates and resembles rather a marl. Average Fe_2O_3 content is about 5 times higher than that in the grey Kupferschiefer. The average TOC content in the red Kupferschiefer is about 10 times lower than that in the black Kupferschiefer and about 5 times lower than that in the grey Kupferschiefer. Average Cu content is 1,070 ppm at variability coefficient 81% . The grey Kupferschiefer contains 3 times higher contents of Cu and its variability coefficient is 2 times higher, which points out to quantitative changes during the leaching of copper when secondary oxidation of deposit proceeded. Thus, low Cu and TOC values can be indicative for oxidizing environment and, consequently, can be good exploration guides to zones enriched in precious metals.

Average Au content in the red Kupferschiefer is high 15.419 ppm, is much higher than that for the grey Kupferschiefer. Comparison of metal contents in samples from the oxidized zones reveal high variability of Au values in the red, which may change from a few ppm to over 100 ppm. Negative Cu-Au correlation supports the hypothesis on the introduction of gold into the red Kupferschiefer during the leaching of copper. Au horizon is continuous and located close to the bottom contour of Cu deposit. It includes the top part of the sandstone and extends down, even beneath 1 m from the top of the sandstone. The average thickness of the high-Au zones is 0.2 m, and various from 0 up to 1.4 meters. The Au and PGE deposit described in this paper fit well in the world criteria for economic-grade accumulations.

Key words: Kupferschiefer – Poland, precious metals, geology, petrology.

Manuscrip received 22 March 2004, accepted 17 December 2008

INTRODUCTION

The research project carried out in the Lubin–Sieroszowice copper deposit in the years 1995–1997 enabled the authors to conclude the regularities of the occurrence of precious metals in the study area. It was found that precious metals are related to secondary oxidation zones of rocks and are hosted mostly in the sandstones, and in the bottom part of the Kupferschiefer, but are less common in the carbonate rocks (Report AGH, 1996, 1997).

Maps and cross-sections produced for that project allowed the authors to estimate the size of oxidized zones, directions of their extension and accumulated reserves of gold. Basing on these data, the southwestern and western parts of the mining lease were selected as most promising for the future exploration for precious metals.

In the late 1990ties the selected parts of the deposit area were not enough well recognized as intensive development works were at the stage of planning. The development of the mining works in this part of copper deposit, that took place in the following years, enabled the authors to access the new fields and evaluated the concentrations of precious metals.

Taking into account that several years have passed since the completion of the early research, the new project has been proposed, focused on both the basic and applied studies. Accumulation of such a large amount of gold at the bottom of the copper ore zone and, commonly, also in the sandstone beneath the copper zone can be regarded as a gold deposit proper and, simultaneously, may rise serious legal problems influencing its economic value.

Studies planned and completed for the following project were the continuation of the already completed, early research. Hence, in the first chapter provides the summary of previous results, in order to clarify the problem. The monograph is a set of papers written by various authors under the common title.

Sincere thanks are due to the Staff of the Geological Department at the Polkowice-Sieroszowice Mine, particularly to Mr. A. Michalik, Mr. R. Leszczyński, Mr. J. Byra and Mr. R. Rożek for their kind assistance and discussions during the sampling of the deposit. The authors are indebted also to Ms. E. Szwed, Mr. H. Czerw, Mr. D. Bembenista and Mr. P. Lenik for assistance in processing of graphic materials.

METHODS

SAMPLING

The sampling was accomplished in underground workings of the Polkowice-Sieroszowice Mine. From the area occuppied by the secondary oxidized copper deposit 35 channel samples were collected from the full heights mine workings. Sampling procedure was consistent with that applied by the KGHM Polska Miedź S.A. Company, i.e. each channel sample was divided into 20-cm-long interval samples related to copper ore lithology. Such procedure gave totally 314 interval samples from which 204 samples were selected for chemical analyses for Au, Pt and Pd. From the all collected interval samples the polished sections were cut for microscopic studies. Additional 200 polished sections were prepared from samples collected in the zones potentially enriched in noble metals. Next 1,120 interval samples collected for earlier research projects (Report AGH, 1996, 1997; Pieczonka, 1998) were included into the microscopic studies as well as into the microprobe WDS and EDS analyses. Total number of samples derived from the noble metal zone exceeded 1,500. Localization of sampling sites is shown in Fig. 1.

MICROSCOPIC STUDIES

All microscopic observations were carried on at the Department of Ore and Evaporite Deposits, Faculty of Geology, Geophysics and Environment Protection at the AGH-University of Science and Technology (UST) in Kraków. Both the NIKON and OPTON microscopes were used, equipped with the integrated systems of optical photography and computer imaging using the MULTISCAN 1106 software.

Microscopic observations enabled the selection of samples for the mircoprobe chemical analyses, which were applied for identification of grains too small (<5 μm across) to be credibly identified under the microscope. This procedure led to the discovery of over 20 new minerals and first appearances of minerals in Poland.

MICROPROBE ANALYSES

Chemical composition of native gold, electrum and accompanying minerals was analyzed with the microprobe. Before the year 2000 analyses were run at the Research Institute of Non-ferrous Metals, Gliwice (eng. L. Kubica) with the Jeol Superprobe 753 apparatus using the WDS method. The later analyses were carried on at the Department of Ore and Evaporite Deposits, AGH-UST in Kraków with the ARL SEMQ probe and at the Institute of Earth Sciences, Jagiellonian University, also with the ARL SEMQ instrument (EDS method). Despite two different analytical devices, all analyses were carried out under the identical analytical parameters: acceleration voltage 20 kV, current 20 mA and sample current 10 nA. The following analytical lines and standards were used: S Kα, Fe Kα (FeS_2), Ag Lα (100%), Au Lα (100%), Hg Lα (HgS), Pd Lα (100%), Bi Mα (100%), Se Lα (100%), Cu Kα (100%), Pt Lα (100%), As Kα.

The EDS analyses were carried on at the Laboratory of Scanning Microscopy for Biological and Geological Sciences, Faculty of Biology and Earth Sciences at the Jagiellonian University with the HITACHI S-4700 supplied with the FESEM and EDS devices. The EDS method was applied for obtaining the BSE images, element mapping and quantitative analyses.

METHODS OF GEOCHEMICAL ANALYSES

All geochemical analyses were performed at the Department of Environmental Analyses, Cartography and Economic Geology, Faculty of Geology, Geophysics and Envi-

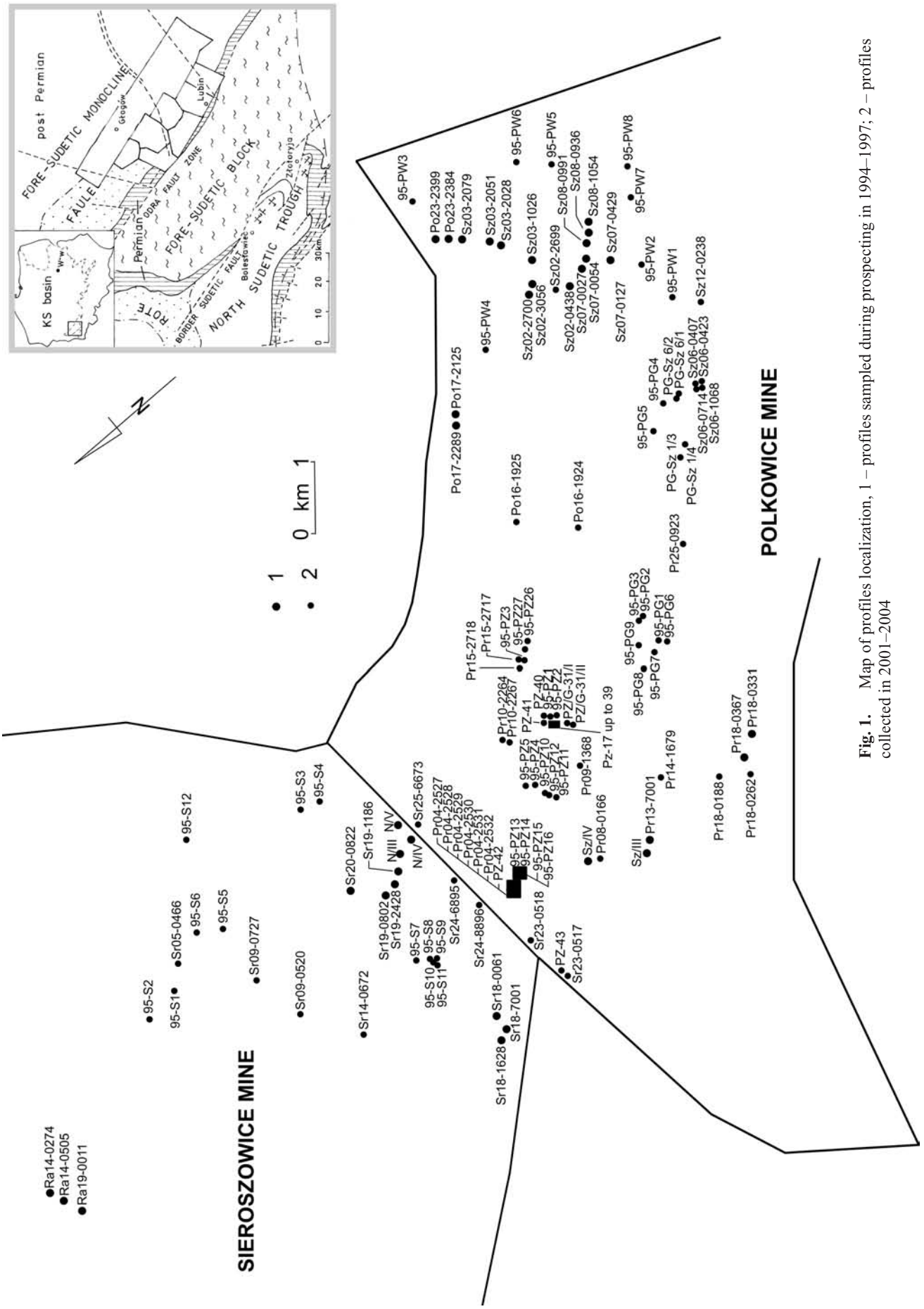

Fig. 1. Map of profiles localization, 1 – profiles sampled during prospecting in 1994–1997; 2 – profiles collected in 2001–2004

ronmental Protection at the AGH-University of Science and Technology in Kraków.

The **Rock-Eval pyrolysis** was developed by the French Petroleum Institute (Espitalié *et al.*, 1977; 1985). Results of the Rock-Eval analysis enable to determine the quantity and tentatively genetic type and maturity of organic matter dispersed in the analyzed samples (e.g., Espitalié *et al.*, 1985; Peters, 1986). In Poland this method has been applied for over 20 years in petroleum geochemistry (see e.g., Kotarba & Szafran, 1985; Wilczek & Merta, 1992).

The sulphate and the pyritic sulphur contents were determined according to the Polish Standards PN-77/G-04514.09 and PN-77/G-04514.11, respectively.

In order to determine the contents of bitumens and elemental sulphur, first the bitumens were extracted from rock samples (20 to 300 g each) in the Soxhlet apparatus with the azeotropic 93:7 v/v mixture of dichloromethane (DCM) and methanol (MeOH). The encountered native sulphur crystals were removed and determined quantitatively by adding metallic copper to the bitumens solution.

The separation of bitumen fractions was carried out in two stages. First, asphaltenes were removed by precipitation in *n*-heksane. The resulting maltenes were dissolved in a few ml of *n*-hexane and supplied to chromatographic column filled with silica gel and aluminum oxide (1:2 v/v). After elution of saturated hydrocarbons with *n*-heksane the aromatic hydrocarbons fraction was eluated with benzene. The remaining resins were eluated with the 1:1 v/v benzene-methanol mixture. Fraction composition of bitumens was calculated in relation to the total received mass (including asphaltenes).

Distribution of *n*-alkanes and isoprenoids. The saturated hydrocarbons fraction was analyzed with the Hewlett Packard 5890 Series II gas chromatograph supplied with the flame ionization detector (FID) and capillary column (25 m × 0.32 mm internal diameter) coated with the HP-1 phase (Methyl Silicone Gum, 0.52 μm film thickness), and temperature-programmed from 110 to 310°C.The flow rate of carrier gas (nitrogen) was 2.7 ml/min.

The distribution of **methylphenanthrenes and methyldibenzothiophenes** and theirs homologues were determined on the same instrument equipped with a 50 m × 0.32 mm capillary column coated with HP-5 phase, and temperature-programmed from 80 to 250°C.

After extraction of bitumens and removal of carbonates with hydrochloric acid, rock samples selected for **stable carbon isotope analysis** of kerogen were combusted in an on-line system. Preparation of previously extracted bitumens and their fractions was performed by the same procedure. Stable carbon isotope analyses were performed using a Finnigan Delta Plus mass spectrometer. The stable carbon isotope data are presented in the δ-notation relative to PDB standard, with an analytical precision estimated to be ±0.2‰.

In order to separate the pure **kerogen**, the residue left after bitumens extraction was treated with the concentrated acids: HCl (18 wt.%, for 2 hours) and HF (50 wt.% for at least 16 hours). Undissolved residue was separated from the solution by centrifugation (1,600 1/min., 10 min.) and decantation. Neoformed fluoride phases were removed with hot concentrated HCl. Resulted kerogen concentrate was purified by heavy liquid separation (aqueous $ZnBr_2$ solution, density 2.1 g/ml) and repeat-extracted with the above mentioned DCM-MeOH mixture. Before elemental analysis samples were homogenized and analyzed for moisture and ash according to Polish Standards PN-80/G-04511 and PN-80/G-04512, respectively. The amount of pyrite contaminating kerogen concentrate was determined as total iron with the Philips PU 1100X spectrophotometer using the standard AAS procedure provided by the producer. Samples were combusted at 815°C and ash was dissolved in analytically pure HCl. Measurements were carried on the obtained Fe ion solutions diluted in measuring flasks.

The (C, H, N, S) elemental analysis was carried on with the Carlo Erba EA 1108 analyzer. Combustion products were separated chromatographically and measured with the TDC detector. The results were processes with the EAGER 200 software. Oxygen content was calculated to 100% considering the moisture and mineral matter contents. The organic sulphur contents in kerogen were determined with the formula:

$$S = S_{TOT} - S_{pyrite}$$

where: S_{TOT} – total sulphur determined with elemental analyser (wt.%), S_{pyrite} – content of pyritic sulphur (wt.%), $S_{pyrite} = 64.12 \cdot Fe_{TOT}/55.85$, Fe_{TOT} – total iron in kerogen sample (wt.%).

STATISTICAL AND GEOSTATISTICAL METHODS

Due to specific character of geostatistical analysis, details of applied methods were described in chapter "*Distribution...*". For the initial description of the variability of deposit parameters the classic statistical method was applied, i.e., preparation of histograms characterizing the probabilistic variability structure of parameters and calculation of principal variability measures: arithmetic mean and extreme values, variance, variability coefficients (as measures of dispersion) and assymmetry coefficient (as a measure of distribution skewness). Additionally, the percentage of samples in particular sampling sites which met the economic criterion (Au content > 0.5 ppm) was calculated.

Methods of map preparation

In order to draw the contour maps of parameters, the Surfer 8.0 (Golden Software) program was applied. Values of parameters calculated in a dense grid (25 × 25 m) were smoothed with the 5 × 5 matrix in which the central value obtained the weight 2. Such data processing enabled the elimination of a substantial part of local variability from the contour pattern.

Values of specific parameters in nodes of the square grid were calculated with the point kriging method using the standardized variograms whereas the empirical variograms were obtained from the analysis of the whole sample population.

The experimental data processing revealed that the best fitting of empirical variograms was obtained by the combi-

nation of spherical or linear (range below 500 m) models with the random model. Analysis of Pt+Pd contents disclosed the presence of the "*Hole effect*", i.e. at the range over 500 m the empirical variograms became regular sinusoids of a period about 1,500 m.

Final map and cross-section processing was carried on with the Microstation J software. Cross-sections were not localized in the maps due to confidential character of data.

Methods of chemical analyses

Basic chemical analyses for Au, Pt and Pd were carried out by the ACTLABS (Canada) with the ICP-MS method. In order to eliminate the nugget effect, 30-gram portions were prepared from each sample. Analytical precision was 2 ppb for Au, 5 ppb for Pt and 4 ppb for Pd. Bulk analyses for 48 elements were carried on by the ACTLABS, as well, with the XRF method for main elements and ICP-MS one for trace elements. From each sample 11-gram portions were prepared. Analytical precision was 0.01% for 10 main elements and 0.1 to 10 ppm for the remaining 38 trace elements.

Analyses of selected metals: PGE, As, Hg, Bi, Re, Sb, Se, Mo and Te in special samples were carried on with the ICP-MS method (the Perkin Elmer ELAN 6100 apparatus) at the Department of Hydrogeology and Engineering Geology, Faculty of Geology, Geophysics and Environmental Protection, AGH-University of Science and Technology in Kraków. From each sample 1-gram portions were prepared for analysis. Analytical precision varied from 0.1 to 1.0 ppb, except for Te.

GEOCHEMISTRY OF Au AND PGE

Jadwiga Pieczonka

INTRODUCTION

Concentrations of Au and PGE in the Earth crust usually do not exceed 5 ppb (Crocket, 1993), but for chemical and fine-clastic sediments similar to those encountered in the Fore-Sudetic Monocline much lower values were quoted (about 1 ppb, Tab. 1). Table 2 shows Au contents in various volcanic and igneous complexes, which are generally less than 2 ppb. Higher values (up to 22.5 ppb) were reported only from rhyolites and ignimbrites from the Okhotsk region (Russia), but in most cases contents below 5 ppb were quoted. Au contents in samples from Lower Permian igneous and volcanic rocks in the Fore-Sudetic Monocline are much higher than presented in Tables 1 and 2. For exploration purposes such contents are regarded as anomalous and are positive directories for further works.

Table 1

Average Au content in some selected sedimentary rocks [ppb]

Rock type/localization	Au (Min-max)	References
Claystones, sandstones: Tuva, Taymyr, Yenisey, Russia	2.7(0.5-7.0)	Korobejnikov A.F., 1986: Gold distribution in black shale association. Geochem. Int. 23, 114-124
Conglomerates, sandstones and claystones: Undino-Dainski Basin, Eastern Transbaikalia, Russia	8.75(0.5-19)	Polikarpochkin V.V., Korotajeva I.Ya., 1976: Distribution of gold in the sedimentary rocks of the Udino-Dainsk basin (eastern Transbajkalia). Geochem. Int. 13/2, 57-62
Mudstones and greywackes: Bohemian Massif, Czechoslovakia (R.C.)	4.6(1-19)	Moravek P., Pouba Z., 1984: Gold mineralization and granitoides in the Bohemia Massif, Czechoslovakia. In: Gold'82, Forster ed. Balkema, 713-729
Tuffogenic mudstones (Archean): Superior, Canada	1.1(0.1-8.8)	Kwong Y.T.J., Crocket J.H., 1978: Background and anomalous gold in rock of an Archean greenstone assemblage, Kakagi Lake area, northwestern Ontario. Econ. Geol. 73, 50-63
Claystones:Kuznetsk, Sayan, Tuva, Taymyr, Yenisey, Russia	2.2(0.1-8.3)	Korobejnikov A.F., 1986: Gold distribution in black shale association. Geochem. Int. 23, 114-124
Claystones and limestones: Sayan, Tuva, Taymyr, Yenisey, Russia	6.7(0.1-29)	Korobejnikov A.F., 1986: Gold distribution in black shale association. Geochem. Int. 23, 114-124
Barren schists: Witwatersrand Basin, South Africa	4.1(0.3-23)	Kwong Y.T.J., Crocket J.H., 1978: Background and anomalous gold in rock of an Archean greenstone assemblage, Kakagi Lake area, northwestern Ontario. Econ. Geol. 73, 50-63
Shales (Paleocene): Gubbio, Italy	1.85(0.4-5.8)	Crocket J.H., 1993: Distribution of gold in the Earth's crust. In: Gold metallogeny and exploration Forster R.P. ed., Chapman & Hall., 1-36
Limestones, dolostones, marl slates: Kuznetsk, Altay, Sayan, Tuva, Russia	2.5(0.2-5.5)	Korobejnikov A.F., 1986: Gold distribution in black shale association. Geochem. Int. 23, 114-124
Pelagic limestones (Turonian-Paleocene): Gubbio, Italy	1.1(0.3-4.6)	Crocket J.H., 1993: Distribution of gold in the Earth's crust. In: Gold metallogeny and exploration Forster R.P. ed., Chapman & Hall., 1-36
Limestones (Upper Jurassic): Central Asia, Russia	0.71(0.6-1.0)	Popov V.S., 1975: Geochemistry of gold in the Upper Jurassic evaporite formation on the southern part of Soviet Central Asia. Dokl. Acad. Sci. USSR, Earth Sci. Section 224, 204-207
Evaporites, (Jurassic): Central Asia, Russia	1.4(0.4-7.0)	Popov V.S., 1975: Geochemistry of gold in the Upper Jurassic evaporite formation on the southern part of Soviet Central Asia. Dokl. Acad. Sci. USSR, Earth Sci. Section 224, 204-207

Table 2

Average Au content in some selected volcanogenic rocks [ppb]

Rock type/localization	Au (Min-max)	References
Rhyolite, dacite (Cainozoic): Kuril-Kamchatka Province, Russia	1.79	Anoshin G.N., Kepezhinskas V.V., 1972: Petrochemical features related to gold distribution for the Cenozoic volcanic rocks of the Kuril-Kamchatka province. Geochim. Int. 9, 618-629
Andesite (Cainozoic): Kuril-Kamchatka Province, Russia	1.88	Anoshin G.N., Kepezhinskas V.V., 1972: Petrochemical features related to gold distribution for the Cenozoic volcanic rocks of the Kuril-Kamchatka province. Geochim. Int. 9, 618-629
Basalt (Cainozoic): Kuril-Kamchatka Province, Russia	1.73	Anoshin G.N., Kepezhinskas V.V., 1972: Petrochemical features related to gold distribution for the Cenozoic volcanic rocks of the Kuril-Kamchatka province. Geochim. Int. 9, 618-629
Rhyolite + ash cover (Cretaceous): Okhotsk-Chukotka complex, Russia	1.23	Mints, M.V., 1975: Gold in igneous rocks of southwester part of Ulinsk superposed downwrap (Okhotsk - Chukotka volcanic belt). Int. Geol. Rev. 17/5, 604
Granite (Cretaceous): Okhotsk-Chukotka complex, Russia	0.98	Anoshin G.N., Kepezhinskas V.V., 1972: Petrochemical features related to gold distribution for the Cenozoic volcanic rocks of the Kuril-Kamchatka province. Geochim. Int. 9, 618-629
Andesite, basalt (Cretaceous): Okhotsk-Chukotka complex, Russia	1.98	Mints, M.V., 1975: Gold in igneous rocks of southwester part of Ulińsk superposed downwrap (Okhotsk - Chukotka volcanic belt). Int. Geol. Rev. 17/5, 604
Rhyolite (Cretaceous): Okhotsk-Chukotka complex, Russia	1.47	Mints, M.V., 1975: Gold in igneous rocks of southwester part of Ulińsk superposed downwrap (Okhotsk - Chukotka volcanic belt). Int. Geol. Rev. 17/5, 604
Basalt, andesite (Cretaceous-Paleocene): Okhotsk, Russia	3.2	Yudin S.S., Yudina V.N., Shilin N.L., 1972: Gold concentration in volcanic series in the central part of the Okhotsk volcanic belt. Dokl. Acad. Sci. USSR, Earth Science Sec. 207, 39-441
Rhyolite, ignimbrite (Cretaceous-Paleocene): Okhotsk, Russia	9.6 (1.5-22.5)	Yudin S.S., Yudina V.N., Shilin N.L.,1972: Gold concentration in volcanic series in the central part of the Okhotsk volcanic belt. Dokl. Acad. Sci. USSR, Earth Science Sec. 207, 39-441
Basalt, andesite (Miocene, Pleistocene): Cascade Mountains, USA	5.6 (0.1-19)	Gottfried D., Greenland L.P., 1972: Distribution of gold in igneous rock US. Geol. Surv. Prof. Pap. 727, 42 pp
Basalts and bimodal igneous rocks: Western USA	1.8 (0.2-6.1)	Gottfried D., Greenland L.P., 1972: Distribution of gold in igneous rock US. Geol. Surv. Prof. Pap. 727, 42 pp

Average contents of most the PGE in the Earth crust are lower than those of Au and usually do not exceed 1 ppb for particular element and 10 ppb for total PGE (Tab. 3, Pasava *et al.*, 2003). However, in the rocks of exploration potential for PGE their combined contents are usually 10 times higher (Tab. 3). In the highest-grade known Ni-Cu deposit – Norilsk-Talnakh (Russia) – PGE contents in sulphide ores are over 100 ppm (Distler *et al.*, 1993). Average PGE contents in the layered mafic intrusions are from several to a dozen of ppm (Zientek, 1993, *vide* Barrie, 1995) (Tab. 3) but highest amounts were observed in macroscopically visible, disseminated sulphides. Most of the PGE-enriched sulphide associations hosted in pegmatoidal pyroxenite from the Bushveld Complex (South Africa) and in chromite deposit of the Sopchezeero LMI (Kola Peninsula, Russia) are of hydrothermal origin. However, some LMIs – e.g. the Duluth and the Muskox intrusions – do not host economic-grade deposits despite the common presence of disseminated Ni-Cu sulphides (Barns & Francis, 1995).

An untypical, Au-Pt-Pd deposit is the Serra Pelada (Northern Brasil, Cabral *et al.*, 2002). Average content of combined precious metals in this locality is high (about 20 ppm) whereas Cu content is below 0.1% (Tab. 3). Maximum Au concentrations in the "*bonanzas*" were up to 13.5%. Ore is hosted in brecciated, haematitized and silicified, carbonate metamudstones containing 10% of amorphous carbon. Its origin is related to the low-temperature hydrothermal processes (Cabral *et al.*, 2002).

GOLD AND PGE IN LOWER PERMIAN ROCKS OF THE FORE-SUDETIC MONOCLINE

Table 4 presents gold contents in Lower Permian rocks from the Fore-Sudetic Monocline. All analyzed core fragments reveal increased amounts of Au whereas PGE contents are below detection limit (5 ppb). The exception is Ir, which was detected in three samples, although in amounts below 1 ppb (Tab. 4).

All analyzed Lower Permian rocks originating from various parts of the Fore-Sudetic Monocline reveal distinct traces of hydrothermal processes – hematitization of Fe-silicates, zeolitization and carbonatization. It is supported by the results of petrographic studies, e.g. Siemaszko (1978), Ryka (1978) and Speczik (1979, 1985). In one of drill cores abundant sulphide mineralization was found, which also proves the presence of hydrothermal activity. Typical are high contents of Au, particularly in the rocks from the Fore-Sudetic Monocline and from the North-Sudetic Trough (Tab. 4). The lowest Au contents were found in volcanics from the Wolsztyn High (Tab. 4).

The earlier monographs (Speczik, 1979, 1985) clearly demonstrated the presence of hydrothermal processes in the basement of the Fore-Sudetic Monocline. In Carboniferous rocks hydrothermal mineralization includes: hematite, pyrite, cobaltite, safflorite, pyrrhotite, arsenopyrite, chalcocite, sphalerite, chalcopyrite, cubanite, bornite, marcasite, native Bi, enargite, galena, tetrahedrite and hypergenic as-

Table 3

Concentrations of Au and PGM in some selected igneous rocks and selected deposits [ppb]

Rock type/localization	Au	Cu [ppm]	Os	Ir	Ru	Rh	Pt	Pd	Remarks/references
Tuffs, Bohemian Massif	42.9	162		0.36	1.92	0.26	9.81	20.52	average content Pasava *et al.*, 2003
Basalt, Namibia	4.6	179		2.29	9.5	-	80	23	average content Borg *et al.*, 1987
Felsite rocks, Namibia	7.4	40		3.61	10	-	57	116	average content Borg *et al.*, 1987
Peridotite, Stare Ransko, Czech Republic	24.1	874		3.14	2.8	4.6	57.2	75.6	subeconomic Ni-Cu Pasava *et al.*, 2003
Troctolite, Stare Ransko, Czech Republic	5.3	99		0.16	0.5	0.1	2.3	1.6	barren Pasava *et al.*, 2003
Anorthosite, Impla, South Africa	4.0	2	4	7.7	47	24.0	157	28	BB-A barren, Bushveld Maier, Barnes 2003
Pyroxenite, Impla, South Africa	1.1	22	3	4.3	22	16.0	93	39	BB-B barren, Bushveld Maier, Barnes, 2003
Basalt, Karoo, South Africa		101		0.04		0.3	5	7	Caroo Formation Maier *et al.*, 2002
Massive sulphides, Ndzongiseni, South Africa	1062.6	Ni-	71.0	6.60	<17	28.7	17390	21169	Caroo Formation Maier *et al.* 2002
Hartley Pt mine, Zimbabwe	1100	613	46	160	240	359	6540	2350	Geat Dyke, PGE-3 zone, Oberthür *et al.*, 2003
Hartley Pt mine, Zimbabwe	260	544	36	120	170	270	2780	3390	Great Dyke, PGE-2 zone, Oberthür *et al.*, 2003
Pyroxenite, Rustenburg, South Africa	1476	2479	825	1774	10151	3538	43003	13353	RPM, Bushveld Maier, Barnes, 2003
Stillwater Complex, Montana, USA				178	372	384	128852-4600	217665-8000	Talkington, Lipin, 1986
Fedorov Pansky, Kola Peninsula, Russia	130-140	0.16-0.22 %	-	-	-	130-140	560-550	2650-2420	PGE ore (lenses A-B) Schissel *et al.*, 2002
Sulphide ores, Sudbury, Canada	78-862	1.97-5.73 %	3-40	0.11-144	2-225	0.16-287	413-4719	701-5213	Eckstrand, 1995
Sulphide ores, Norilsk, Russia	240-5500	5.5-21 %	40-120	10-160	90-290	20-1240	980-24200	3340-101800	Distler *et al.*, (1993)
Sulphide ores, Kambalda, Australia	339	0.22 %	110	60	220	50	326	425	Australian Ni (2.96%) Hudson, 1986
Serra Pelada, Brasil	15200	8-560		5-1100			1890	4090	Cabral *et al.*, 2002
Earth crust	0.002	25	0.00005	0.00002	0.0001	0.00006	0.0015	0.0005	Reference level http://www.earthref.org

semblage: malachite, azurite, covellite, chalcocite and tenorite (Speczik, 1979). Moreover, silicification, chloritization, carbonatization, kaolinization and pyritization of these rocks were noticed (Speczik, 1979). Hydrothermal minerals formed in a wide range temperatures, from high to low (Speczik, 1979). Results of studies carried out in the 1980-ties suggested that the Variscan orogenic epoch played crucial role in the metallogenesis of the Fore-Sudetic Monocline basement (Speczik, 1985). The mineral assemblages newly described from the copper deposit allow the authors to revise this concept. Chemical analyses of volcanics from the basement of the Fore-Sudetic Monocline point out to their secondary, pulsatory saturation with alkalies, which resulted in secondary depletion in Fe (Siemaszko, 1978). Hydrothermal activity in the basement rocks presumably affected the sedimentary cover composed of clastics and chemical sediments. However, it is difficult to recognize the chronology of the events. The crucial feature is the vertical permeability, which was responsible for fluid transfer from deep basement. Additional, new data on the structure of consolidated basement of the Fore-Sudetic Monocline provided by geophysical studies point to the presence of deep fracture and basic intrusives in this area (Koblański, 1996).

Table 4

Concentration of Au, PGE and Re in selected volcanogenic rocks from drill cores, Lower Permian, Fore-Sudetic Monocline [ppb]

Sample, borehole	Au	Os	Ir	Ru	Rh	Pt	Pd	Re	Type of rock	Geological unit
Drogomin 1	13	n.a.	n.a.	n.a.	n.a.	-5	-4	n.a.	rhyolite	Wolsztyn High
Międzyrzecz 2	23	n.a.	n.a.	n.a.	n.a.	-5	-4	n.a.	rhyolite	Wolsztyn High
Zbąszynek IG3	27	n.a.	n.a.	n.a.	n.a.	-5	-4	n.a.	rhyolite	Wolsztyn High
Czeklin 1	17	n.a.	n.a.	n.a.	n.a.	-5	-4	n.a.	andesite	Fore-Sudetic Monocline
Niwiska 1	96	-2	0.4	-5	-0.2	-5	-2	-5	andesite	Fore-Sudetic Monocline
Jagodzin 1	130	-2	0.2	-5	-0.2	-5	-2	-5	andesite	North-Sudetic Trough
Chrząstowo 1	6.1	-2	0.2	-5	-0.2	-5	-2	-5	melaphyre	Wolsztyn High

n.a. – not analyzed

Table 5

Concentrations of precious metals in black shale formations

Hosting formation	Au [ppm]	Pt [ppm]	Pd [ppm]	Other elements	Age	References
Selwyn Basin,Yukon, Canada	0.086	0.410	0.214	Ni, Zn, Mo, As	Devonian	Hulbert *et al.*, 1992, SHMS-type deposit
Oklahoma shale, USA	0.019	0.15		Mo	Devonian-Mississippian	Coveney, Nansheng, 1991
Chattanooga Shale, Indiana, USA	0.004	0.063	0.16	V	Devonian-Mississippian	Coveney, Nansheng, 1991
Bohemian Massif, Czech Republic	0.062, max.-0.133	0.015, max.-0.025 Ru-0.006	0.067 max.-0.102 Rh-0.0017	Cu, Ni, V, As, Zn	Proterozoic	Pasava *et al*., 1990
Timsk, Kursk, Russia	0.106	0.260 Os=3.5	0.020	Zn, Cu, piryt	Proterozoic	Chernyshov, Korobkina, 1995
Puolanka, Finland	0.035, max.- 0.170			Pyrite, C_{org}-7%	Proterozoic 2.0-2.1 Ga	Loukola-Ruskeeniemi, 1991, black shales
Black shale, Jormula, Finland	0.016, max.-0.180		Max.-0.069	Pyrite C_{org}-7%	Proterozoic 1.96 Ga	Loukola-Ruskeeniemi, 1991, ophiolitic complex
Black shale, Talvivaara, Finland	0.015	0.027, Ir-0.042	0.073	Ni, Cu, Zn	Proterozoic 1.96-1.97 Ga	Loukola-Ruskeeniemi, Heino, 1996
Kalahari Copperbelt, Namibia	0.007-0.046	0.034-0.12 Ir- 0.00015-0.00103	0.0-0.008	Cu=2.5-3,3%, Ni	Middle Proterozoic	Borg *et al.*, 1987 black shales

GEOCHEMISTRY OF PRECIOUS METALS IN BLACK SHALES

Contents of precious metals in black shales are usually higher than in other rocks. For Au values from 4 to 180 ppb, for Pt – 25–410 and for Pd – 0–240 ppb were quoted (Tab. 5). Contents of the remaining PGE typically do not exceed a few ppb (Tab. 5). Highest contents of both Au and PGE were noticed in black shales accompanying the massive sulphide deposits. Hence, it can be assumed that precious metals are present in the dispersion aureoles of these deposits. Among all studied black shales (Tab. 5 and 6) the most interesting appear the Cambrian black shales from Southern China where economic-grade accumulations were found of Ni (2.6–3.6%) and Mo (3.9–5.7%) (Mao *et al.*, 2002). Some metals: Mo, Ni, Se, Re, Os, As, Hg and Sb are enriched over 1,000 time above the reference value (Tab. 7) (Mao *et al.*, 2002) whereas Ag, Au, Pt and Pd occur in amounts 100 times higher that the reference value. Contents of organic carbon and vanadium are similar to those known from the Kupferschiefer of the Fore-Sudetic Monocline.

Considering black shales of various ages (Tab. 5), contents of Au and PGE in the Zechstein Kupferschiefer from the Fore-Sudetic Monocline are similar to other world occurrences (Tab. 6). Mean Au content is 5.78 ppb for n = 77. Variability coefficient and standard deviation point out to

Table 6

Concentrations of precious metals in the black variety of the Kupferschiefer
(Au = mean content) (after AGH Report, 1996)

Sample	Au [ppb] (min.-max.)	Pt [ppb]	Pd [ppb]	Ag [ppm]	n
LW-1	2.0	≤5	≤4	45	1
LW-2	4.0	5	6.0	82	1
LW-3	6.1(3-15)	≤5	≤4	82-452	3
LW-4	2.4 (2-4)	≤5	≤4	15-2180	4
LW-5	2.7 (2-3)	≤5	≤4	158-825	2
LW-6	3.3 (2-9)	≤5	≤4	83-350	4
LG-1	5.9 (2-9)	≤5	≤3	402-451	5
LG-2	2.4 (2-3)	≤5	≤3	232-687	3
LG-3	2.0 (2-2)	≤5	≤3	33-939	4
LZ-4	6.0 (5-7)	≤5	≤4	42-237	2
LZ-5	≤2	≤5	≤4	370	1
LZ-8	15 (5-20)	≤5	≤4	1530-1730	2
LZ-9	13.0	≤5	≤4	1970	1
RG-1	13.0	≤5	≤3	193	1
RG-2	8.0	≤5	≤3	263	1
RG-3	7.0	≤5	≤3	160	1
RG-4	5.0	≤5	≤3	160	1
RG-5	3.0	≤5	≤3	1040	1
RG-6	4.0	≤5	≤3	708	1
RG-7	5.7 (5-6)	≤5	≤3	221-261	3
RG-8	7.0	≤5	≤3	144-319	3
RG-9	11.0	≤5	≤3	555	1
RG-10	8.0	≤5	≤3	1100	1
RN-1	6.8 (4-8)	≤5	≤3	263-702	3
RN-2	5.4 (4-6)	≤5	≤3	26-274	2
RN-3	12.9 (4-26)	≤5	≤3	580-735	3
RN-4	4.7 (3-6)	≤5	≤3	580-735	3
RZ-1	3.4 (2-5)	≤5	≤3	126-150	3
RZ-2	2.0	≤5	≤3	39	1
RZ-3	4.0 (3-5)	≤5	≤3	87-89	2
RZ-4	6.3 (6-8)	≤5	≤3	127-225	3
RZ-5	4.0	≤5	≤3	373	1
RZ-6	6.0	≤5	≤3	485	1
RZ-7	6.0 (6-6)	≤5	≤3	96-170	2
RZ-8	3.6 (2-6)	≤5	≤3	16-50	3
RZ-9	4.6 (4-5)	≤5	≤3	41-602	3
$\bar{x}$	5.78	≤5	≤3		
s	3.43				
S^2	11.75				
V	59.31 %				

V – variability coefficient; $\bar{x}$ - an average; s – standard deviation; S^2 – variance

moderate variability of Au contents in the Kupferschiefer. It must be emphasized that in the whole population of analyses only 5 samples showed values over 10 ppb (Tab. 6), hence, the true content of Au is about 3 ppb. It means that Au contents in the Kupferschiefer from the Fore-Sudetic Monocline are only 1.5 times higher that the reference level whereas the black, metal-bearing shales from China reveal over 100-times enrichment (see Tab. 7). The higher values of Au (Tab. 6) can be connected with the high contents of Ag, as revealed by Salamon (1979). Contents of Pt and Pd are low, and usually fall below the detection limit in the population of samples analyzed for exploration project. Concentrations of these metals are presented in chapter "*Geochemistry of host rocks...*". For comparison, Ag contents in black shales from China exceed 10,000 times the reference level (Tab. 7) (mean content Ag = 50 ppm) and those in the Kupferschiefer from the Fore-Sudetic Monocline are 672,000 times higher than the reference level (maximum Ag content 3,360 ppm, Salamon, 1979). It must be emphasized that contents of V, Ni, Co and organic carbon in these formations are similar and concentrations of U is 10 times higher in Chinese black shales than in the Kupferschiefer from the Fore-Sudetic Monocline (see Piestrzyński, 1990; Mao *et al.*, 2002). Simultaneously, the Chinese black shales contain only 0.06–0.26% Cu. Obviously, differences in metal concentrations in the black shales hosting the economic-grade accumulations are significant. It may result from various sources of metals precipitated with the same process. Sulphur in black-shale-type deposits from Southern China shows highly diversified ^{34}S, from +22 to –22‰. According to Mao *et al.*, (2002), such values indicate biogenic origin of sulphur. Since Collier (1985) has demonstrated that Mo concentrations in sea water are higher than the remaining metals, the presence of this element in bottom sediments is regarded as diagnostic for reducing environment in the bottom layer of sea water (Jacobs *et al.*, 1987).

CONTENTS OF Au AND PGE IN UNCONVENTIONAL DEPOSITS

Several genetic types of Au deposits and over 2,000 deposits themselves are known worldwide. However, there are only a few PGE deposits (in the LMI- Layered Mafic Intrusions). In the following paper the authors focused attention exclusively on unconventional accumulations of precious metals. Undoubtedly, one of such deposits is located in the Fore-Sudetic Monocline (Piestrzyński *et al.*, 2002), the others are porphyry Cu-Au deposits with PGE (Piestrzyński *et. al.*, 1991) and Pt-Pd-Au accumulations in unconformity-type uranium deposits (Tab. 7). The latter host not only the economic-grade U concentrations but also increased contents of Ni, Mo, Pb, Zn, As, Cu and V. An interesting group includes deposits from the Tennant Creek area in Australia (Skirrow & Walshe, 2002) where 600 occurrences of hematite bodies were found from which about 25% contains also Au, Cu or Bi (Skirrow & Walshe, 2002). The highest-grade body – "Eldorado" – is low in sulphides but hosts hematite and high amounts of Se, Au and Bi along

Table 7

Concentrations of precious metals in unconventional deposits [ppm]

Deposit/ localization	Au [ppm]	Pt [ppm]	Pd [ppm]	Accompanying elements	Type of deposit	Age	Remarks/ references
Coronation Hill, N. Territory, Australia	4.85	0.19	0.65	U	UN	Proterozoic	Carville *et al.*, 1990
Jabiluka 2, N. Territory, Australia	up to 500		0.1-1.0	U	UN	Proterozoic	Carville *et al.*, 1990
Eldorado, Tennant Creek, Australia	20	-	-	Se, Bi, Cu	REDOX	Proterozoic	Skirrow, Walshe, 2002
Nick, Canada	0.086	0.149-0.618, Ir-0.003	0.091-0.319 Os-0.015	Ni, Pb, Zn, As, Mo	SHMS	Devonian	black shale Hulbert *et al.*, 1992
Sukhoi Log, Lena, Russia	2.45-31.97	1.45-5.0	1.6	Cu pyrite	SH ?	Proterozoic-Cambrian	metasediments, Pt-minerals Wild *et al.*, 2003
Zunyi Guizhou, China	0.7	0.3 Ir-0.03	0.4	Mo, V, Ni, U	BS	Cambrian	black shale Coveney, Nansheng, 1991
Sulphide layer, Southern China	0.334	0.295	0.300 Os-0.034	Ru-0.023 Rh-0.025	BS	Cambrian	Ni-2.6%, Mo-3.9% Mao *et al.*, 2002
Hunan, China	2.49	0.3	0.33	Mo, Ni, V	SH	Cambrian	black shale Fan, 1983
Udokan, Siberia, Russia	0.016-3.7	0.03-2.1	0.015-3.25	Cu, Ag, V, Mo, Ni, Zn	SHMS	Proterozoic	black shale Makariev *et al.*, 1999
Monterrosas, Peru	6.0 Ag= 20	?	?	Cu-1.0-1.2%	IOCG	Jurassic-Cretaceous	Sillito, 2003
Punta del Cobre, Chile	0.2-0.6 Ag=2-8	?	?	Cu=1.5%	IOCG	Jurassic-Cretaceous	Sillito, 2003
Lupin, Canada	10.75			As, pyrite	BIF,	Archean	Algoma type, Kerswill, 1995
Homstake, USA	8-9			As, pyrite	BIF	Proterozoic	Algoma type, Kerswill, 1995
Morro Velho, Minas Gerais, Brasil	10.0			As, pyrite, pyrrhotite	BIF	Archaean	iron-carbonate formation Kerswill, 1995
St. Tomas II, Phillippines	1.4	0.045	0.29	Cu, Bi, Te, Sb	PC	Tertiary	porphyry Cu-Au Piestrzyński *et al.*, 1994
Earth crust	0.002	0.0015	0.0005	Ir-0.00002	Ru-0.0001	Rh-0.00006 Os-0.00005	reference level http://www.earthref.org

Types of deposits: SH – sediment hosted, UN – unconformity related, IOCG – iron oxide-copper-gold, BIF – banded iron formation, PC – porphyry copper, BS – black shale, REDOX – redox boundary, SHMS – sediment-hosted massive sulphides

with the lower contents of Cu and Pb. Au accumulations are related to the latest deformation stage (Skirrow & Walshe, 2002).

GEOLOGICAL SETTING

Jadwiga Pieczonka

LITHOLOGY, STRATIGRAPHY AND TECTONICS

Lithology, stratigraphy

Geological setting of the Polish copper deposits in which Au deposit is hosted (Fig. 2) has been described in a great number of papers. The deposit is part of the Fore-Sudetic Monocline. The Monocline includes three rock complexes. The first is the basement, which comprises Proterozoic crystalline rocks and Carboniferous sediments. It is overlain by monoclinally dipping Permian and Triassic sedimentary rocks. In the southeastern part of the Monocline (Opole region) Upper Cretaceous sediments were discordantly deposited onto Triassic and Permian strata or onto the older rocks of the Fore-Sudetic Block. The Permian–Triassic complex is unconformably covered by younger Paleogene–Neogene and Quaternary sediments (Konstantynowicz, 1971; Kłapciński *et al.*, 1984; Kłapciński & Peryt, 1996).

Crystalline basement

This unit includes schists, greywackes, hornfelses, granodiorites and gneisses (Kłapciński *et al.*, 1975; Tomaszewski, 1978; Koblański, 1996).

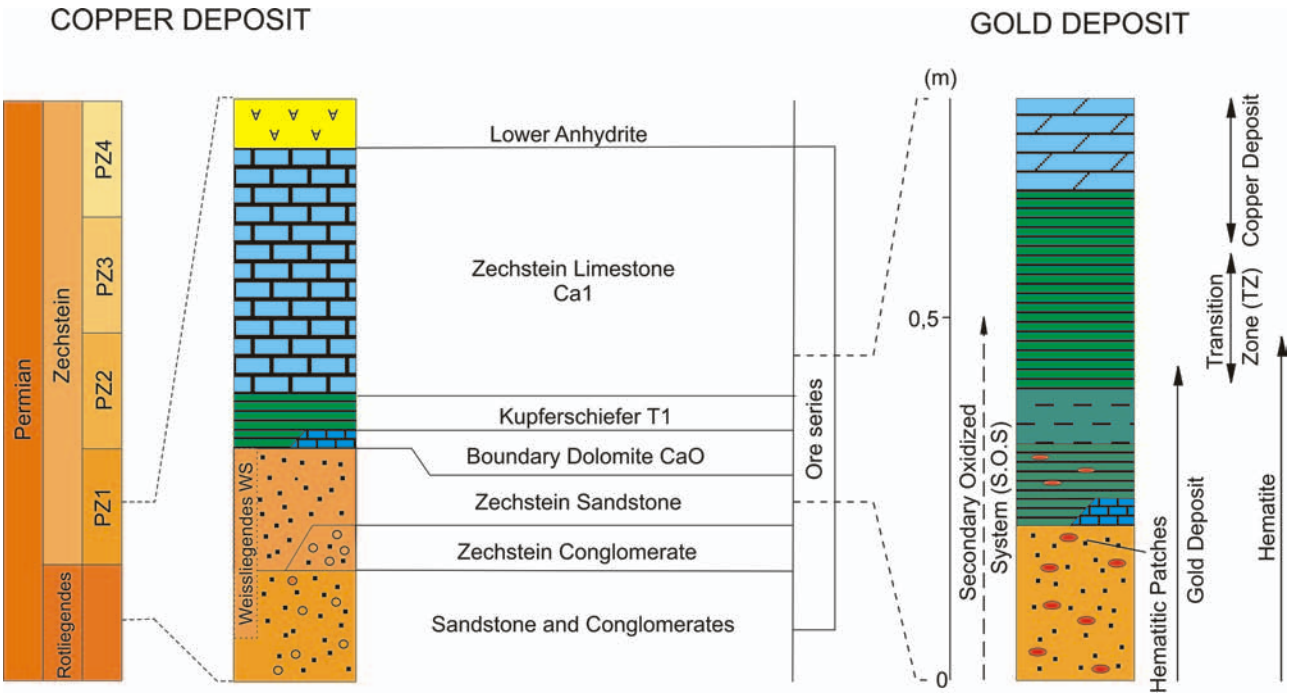

Fig. 2. Lithostratigraphic column through copper deposit (modified after Oszczepalski, 1999), gold deposit after Piestrzyński *et al.* (2002)

Permian

This unit comprises Rotliegend and Zechstein strata. Deposition of Rotliegend sediments is related to the final stage of the Variscan orogeny. Its stratigraphy and sedimentation were described by Kłapciński (1971), Pokorski (1978, 1981) and Pokorski and Ryka (1978). Two members were distinguished: lower – Autunian and upper – Saxonian. The Autunian comprises conglomerates, brownish-red sandstones and shales, quartzitic conglomerates and volcanics (Ryka, 1981), the latter represented by rhyolites and rhyolitic tuffs and breccias (Juroszek *et al.*, 1981; Kłapciński *et al.*, 1988). The Saxonian is a succession of brownish-red sandstones with shales intercalations only locally underlain by conglomerates. Higher in the sequence, grey and white greywacke sandstones appear (Kłapciński, 1971; Pokorski, 1978, 1981).

In the Polkowice deposit the average thickness of red sandstones is 296.2 m, and that of white sandstones is 6.89 m (after archival data, Geological Dept. of the Polkowice-Sieroszowice Mine).

Transition from the Rotliegend to the Weissliegend is usually gradual (Oberc & Tomaszewski, 1963; Jerzykiewicz *et al.*, 1976; Nemec & Porębski, 1977). The age of a part of the Weissliegend is controversial (Krasoń & Grodzicki, 1964; Wyżykowski, 1964, 1971; Rydzewski, 1969; Podemski, 1973; Jerzykiewicz *et al.*, 1976).

Description of the Zechstein was excerpted from Kłapciński (1964, 1971). For practical purposes, the Kupferschiefer is widely accepted as the lowest unit of the Zechstein succession (and, simultaneously, of the *PZ_1 cyclothem*). However, beneath the Kupferschiefer the carbonate horizon, up to 30 cm thick, is locally developed. This is the Basal Limestone or its local equivalent – the Boundary Dolomite (Krasoń, 1964). Thickness of the Kupferschiefer varies usually from 30 to 60 cm (Salski, 1968; Konstantynowicz, 1971). The Kupferschiefer is overlain by the Zechstein Limestone (Tomaszewski, 1978), which shows distinct cyclicity in some localities (Peryt, 1984). Higher in the sequence, the Lower Anhydrite appears (Kłapciński, 1966; Kłapciński & Peryt, 1996) followed by the Oldest Halite and/or the Upper Anhydrite strata. Significant thickness of anhydrite is correlated with low thickness of the Oldest Halite and *vice versa* (Kłapciński, 1966; Kłapciński & Peryt, 1996).

In the Polkowice area, the Zechstein oldest member is the Boundary Dolomite of average thickness about 0.03 m. The Kupferschiefer, of average thickness 0.31 cm, forms continuous layer in the eastern and northern parts of the mine. Thickness of overlying carbonates and of the Lower Anhydrite is 50.73 m each. The Oldest Halite member occurs only in the Sieroszowice area (after archival data, Geological Dept. of the Polkowice-Sieroszowice Mine and Tomaszewski, 1962b). The *PZ_2 cyclothem* begins with the Main Dolomite member followed by the Basal Anhydrite and the Older Halite grading up the sequence into the potassium salts (Kłapciński, 1967, 1991; Kłapciński & Peryt, 1996). In the southern part of the Monocline the Older Halite is followed by anhydrites (Kłapciński, 1991).

In the Polkowice area the Main Dolomite is 6.4 m thick, whereas the anhydrite series thickness reaches up to 16.8 m (after archival data, Geological Dept. of the Polkowice-Sieroszowice Mine).

Development of the *PZ_3 cyclothem* varies in various parts of the Monocline. In the southern part the succession includes the Platy Dolomite which contains up to 40% of anhydrite. The basal part of this member includes clayey

carbonates (Peryt, 1988). In the northern part of the Monocline the equivalent of the Platy Dolomite is the shale horizon with dolomite layer overlain by the Main Anhydrite (Kłapciński, 1967, 1986) and the Younger Halite. In the vicinity of Nowa Sól intercalations of potassium salts appear (Kłapciński & Peryt, 1996).

Average thicknesses of the Platy Dolomite and the Main Anhydrite are 4.3 and 19.7 m, respectively (after archival data, Geological Dept. of the Polkowice-Sieroszowice Mine).

The *PZ_4 cyclothem* begins with brownish-red clayey shales with gypsum and anhydrite intercalations and lenses, followed by the Pegmatite Anhydrite. In the northern part of the Monocline anhydrite member is overlain by the Youngest Halite covered by brownish-red shales (Kłapciński, 1991; Kłapciński & Peryt, 1996).

In the Polkowice area thickness of the Pegmatite Anhydrite is 0.5 m and that of overlying clayey shales is 17.8 m (after archival data, Geological Dept. of the Polkowice-Sieroszowice Mine).

The Zechstein stratigraphy in the southern part of the Fore-Sudetic Monocline brings several problems as in this area the cyclothems are reduced or absent (Fig. 2), (Tomaszewski, 1978; Wagner *et al.*, 1978). Further to the north, all four cyclothems appear (Peryt, 1977). Zechstein stratigraphy of the Sieroszowice-Lubin area was described by Tomaszewski (1966, 1978, 1981), Kłapciński (1967), Kłapciński *et al.* (1984) and Tomaszewski and Kienig (1972).

Triassic

Sequence of this unit includes the Bunter Sandstone, the Muschelkalk and the Keuper stages (Tomaszewski, 1962a; Deczkowski, 1977; Kłapciński *et al.*, 1984). The Lower Bunter comprises mainly arcosic sandstones, rarely quartz sandstones with intercalations of shales, gypsum and sandy limestones (Kłapciński, 1958). The Middle Bunter shows similar lithology (Kłapciński *et al.*, 1984; Kłapciński & Peryt, 1996) whereas the Roethian is developed only in the northeastern part of the Monocline. Its lower horizon includes dolomites with anhydrites, marls and limestone intercalations whereas the upper horizon embraces marls interbedded with limestones and gypsum (Kłapciński & Peryt, 1996).

In the Polkowice area the Triassic succession is reduced to the Lower Bunter of thickness 82.2 m (after archival data, Geological Dept. of the Polkowice-Sieroszowice Mine).

The Muschelkalk occurs in the vast areas of the Fore-Sudetic Monocline. The lowest part of the succession includes platy limestones interbedded with marls, the middle part consists of dolomites with marls, anhydrites and gypsum interbeds and the upper part comprises platy limestones and sandy dolomites (Kłapciński *et al.*, 1984; Kłapciński & Peryt, 1996).

The Lower Keuper strata include clays interbedded with sandstones and dolomites and intercalated with clayey shales and gypsum. These are overlain by clayey shales with anhydrite, gypsum, arcosic sandstones and mudstones of the Upper Keuper. The Roethian strata are clayey shales interbedded with mudstones, sandstones and dolomites (Kłapciński *et al.*, 1984; Kłapciński & Peryt, 1996).

Cretaceous

The Cretaceous sediments were found in the Opole Trough, in the eastern part of the Fore-Sudetic Monocline. These are mainly sandstones, conglomerates and marls unconformably covering the older strata (Kłapciński & Peryt, 1996).

Paleogene

The Paleogene sequence comprises various sands (calcareous, quartz-glauconitic, quartz and micaceous) overlain by a lignite seam (Dyjor, 1978; Kłapciński *et al.*, 1984; Kłapciński & Peryt, 1996).

In the Polkowice area the stratigraphic gap includes sediments from the Lower Bunter to the Eocene. Thickness of Oligocene strata (clays, muds, sands and conglomerates) is significant (48.4 m) (after archival data, Geological Dept. of the Polkowice-Sieroszowice Mine).

Neogene

The Neogene succession comprises quartz conglomerates, sands, clays and lignite seams (Kłapciński *et al.*, 1984; Kłapciński & Peryt, 1996) of thickness exceeding 300 m (after archival data, Geological Dept. of the Polkowice-Sieroszowice Mine).

Quaternary

The Quaternary deposits reveal high lithological variability. The sediments are sands and quartz gravels containing granite and lydite pebbles. These are overlain by clays, muds, sands, gravels and clays, and rare peats (Kłapciński *et al.*, 1984; Kłapciński & Peryt, 1996).

In the Polkowice area, average thickness of Quaternary strata (muds, sands, sandy clays) is 37.2 m (after archival data, Geological Dept. of the Polkowice-Sieroszowice Mine).

Tectonics

The most intensive tectonic movements in the Fore-Sudetic Monocline took place during the Laramide orogeny, at the Cretaceous/Paleogene break. Structural history of this area includes several phases. The oldest, NW–SE-trending fault system with accompanying fissures and fractures originated from the Old Cimmerian phase, i.e. at the Keuper/Rhaetian boundary. Further faulting took place in the Young Cimmerian phase (Late Jurassic). At the end of the Late Cretaceous the existing structures were rearranged and new, mostly continuous deformations developed (Salski, 1975a, b, 1977, 1996).

The Fore-Sudetic Monocline is bordered from the southwest by the Fore-Sudetic Block along the Middle Odra River Fault, which is, in fact, a fault system of lower order in comparison to the Main Sudetic Thrust and to the Silesia-Lubusz Deep Fracture (Oberc, 1967, 1995). In the Fore-Sudetic Monocline the strata dip generally to the northeast at low angle (2–5°, Preidl, 1967), although higher dip angles (up to 25°) were locally noticed (Błaszczyk, 1981).

The copper deposit is located in the marginal, southwestern part of the Monocline, close to the boundary with the Fore-Sudetic Block (Wyżykowski, 1961; Salski, 1996).

Three fault sets were identified: NW–SE; W–E and N–S (Tomaszewski, 1963; Preidl, 1967; Sokołowski, 1967) with dominating, NW–SE set of roughly parallel faults spaced from 0.5 to 2 km.

Apart from dip-slip faults, also the strike-slip dislocations were observed. The most common is the NE–SW set. The lateral displacements of single faults do not exceed 1 m, however, the cumulative displacements in larger areas may reach even tens of meters (Salski, 1977, 1996).

Due to diversified lithology of the ore deposit the rocks reveal intensive fracturing. At the Polkowice Mine three fracture systems were identified with the dominating NNW–SSE-trending one (Salski, 1975a, 1975b.).

The presence of large-scale, flat, brachyanticlinal and brachysynclinal structures of general NW–SE trend is related to the elevations of the Zechstein basement.

OXIDIZED ZONES

Detailed studies on the occurrence of precious metals in the copper deposit were carried out in the Lubin-Sieroszowice area in the years 1995–1997 and managed by Professor Adam Piestrzyński. The results allowed the authors to develop the concept that the increased contents of precious metals are related to the oxidized zones. Consequently, the Polkowice-Sieroszowice area was selected as a potential site of economic-grade accumulations of precious metals and the following research projects was focused on these zones. The oxidized zones, particularly their origin and influence on the genesis of the whole deposit were always a matter of highest interest. Selected genetic concepts are presented below.

Definition of the "Rote Fäule"

The "Rote Fäule" facies was defined for the first time by Gillitzer (1936) as an oxidized facies of the Kupferschiefer. According to this author, this is a synsedimentary facies deposited in a shallow basin. Richter (1941), Kautzch (1942) and Jung (1960) presented similar opinions. Jung and Knitzschke (1976) proposed the slopes of paleohighs as deposition sites of the "Rote Fäule". Among Polish authors the syngenetic origin of the "Rote Fäule" was advocated by Konstantynowicz (1965) and Krasoń and Grodzicki (1965).

Oszczepalski (1980, 1989, 1999) and Oszczepalski and Rydzewski (1983) assumed more complex, syngenetic-early diagenetic formation model of this facies. According to their idea, hematitization is presumably a secondary feature except for these red rocks, which origin is related to the elevations of the Rotliegend basement.

As early as in 1930-ties the epigenetic theory of the Kupferschiefer oxidation has emerged thanks to, among others, Schneiderhöhn (1926) and Fulda (1928), and was later continued by Jowett (1986) and more recently by: Kucha and Pawlikowski (1986) and Piestrzyński *et al.* (2002).

The recent papers suggested the existence of more than one "Rote Fäule" facies and related the economic-grade mineralisation to only a few types of these rocks. Moreover, strong links between basement structure, mineralisation and "Rote Fäule" facies were underlined (Rentzsch, 1991, 1995; Kucha, 1995; Piestrzyński, 1995). According to Piestrzyński (1995), the "Rote Fäule" defined as synsedimentary oxidized facies did not affect at all the mineralizing processes. On the contrary, there is an important relationship between the mineralizing processes and the oxidizing conditions prevailing beneath the ore zone, in both the Weissliegend and the Rotliegend sandstones. The Rotliegend molasse might have been the source of metals, which were mobilized during the diagenesis and/or as a result of dynamic stress caused by halokinetic movements (Kucha & Pawlikowski, 1986).

According to Kucha (1995), the oldest red spots (i.e., the "Rote Fäule") were formed during synsedimenary or early diagenetic events and did not reveal any links to sulphide mineralisation. On the contrary, the younger, epigenetic red spots are closely connected with copper sulphides. Similarly to Piestrzyński (1995), Kucha (1995) also suggested the presence of the "Rote Fäule" facies beneath the copper deposit. The existence of two types of red spots: older ("Rote Fäule") originating from synsedimentary or early diagenetic processes and younger, epigenetic, related to the enrichment in precious metals was recently confirmed by Pieczonka (1998, 2000), Pieczonka and Piestrzyński (2000), and Piestrzyński *et al.* (2002).

The occurrence of rocks with red spots ("oxidized facies")

The distribution of rocks with red spots was described by Oszczepalski and Rydzewski (1996, 1997) from six areas of the Fore-Sudetic Monocline. The largest is the Gubin-Zielona Góra area, which extends westward and continuing up to the Lower Lusatia. To the south this area approaches the North-Sudetic Trough and its eastern boundary is the Polkowice-Sieroszowice deposit in which the oxidized facies includes the Weissliegend sandstone, the Kupferschiefer and the bottom part of the Zechstein Limestone. Thickness of the red-spot zone varies from tens of meters (in the southern part of the Żary Pericline) to some tens (locally to several) centimeters at the margin of the zone (Oszczepalski & Rydzewski, 1997). Much smaller areas were found in the vicinities of Ostrzeszów, Poznań (where six zones were distinguished) and in the Western Pomerania (Kamień Pomorski area) where the oxidized facies continues westward, towards Germany (Oszczepalski & Rydzewski, 1996, 1997).

The areas of red spots occurrence in Lower Zechstein strata in Poland are in various stages of recognition. Konstantynowicz (1965) described rocks (mostly marls) with red spots underlying the copper deposit in the North-Sudetic Trough. Red spots in marls and limestones occurring at the bottom and in the top of the copper zones were characterized by Skowronek (1968) from the Leszczyniec Trough.

Several authors, e.g.: Rydzewski (1976, 1978), Michalik (1979), Oszczepalski (1989), Jowett *et al.* (1991), Wodzicki and Piestrzyński (1994) and Kucha (1995) have already discussed problems of red spots occurrence in the rocks from the Fore-Sudetic Monocline. Here, red spots were observed mostly at the bottom of the copper zone, in

red- and brownish-grey-colored rocks containing hematite and Fe-hydroxides. The spots were encountered in all lithologic types of rocks. According to Michalik (1979), sandstones with red spots occur in almost whole area between Lubin and Sieroszowice. The range of clayey and carbonate rocks with red spots is much limited. These rocks form several isolated "islands" of diameters from several hundreds of meters to 2 kilometers, generally overlying the red-spotted sandstones. Detailed distribution of red-spot zones in relation to the copper deposit in the Polkowice-Sieroszowice area was described by Piestrzyński and Pieczonka (1997a, b), Pieczonka (2000) and Piestrzyński *et al.* (2002).

Distribution of red-spot zones in study area, in relation to the copper deposit

Vertical relationships

In order to determine the mutual relationships between the red-spot zones and the copper deposit, several geological cross-sections were drawn through various parts of the Polkowice-Sieroszowice area. Contents of Cu and Fe^{3+} together with macroscopically visible red spots were taken as indicators of the boundaries between the reducing, the transitional and the oxidized zones (Pieczonka, 1998, 2000).

One of the cross-sections was drawn through the Polkowice Main Field. In all the vertical profiles included into this cross-section (No. Sz06-1086, Sz06-0714, Sz06-0423 and Sz06-0407) red spots were macroscopically visible in the sandstones and the carbonates. The upper boundary of the first oxidized zone located in the sandstones follows the top surface of this rock whereas the lower boundary is unknown as it was localized in only a single sequence. The second oxidized zone includes a fragment of dolomite series. Between both oxidized zones the two transitional zones were found: the first in the Kupferschiefer or in the Kupferschiefer and in a part of the dolomite series and second in the dolomite series itself.

In both the oxidized and the transitional zones only traces of copper mineralisation were found, which is compensated by the presence of precious metals hosted mostly in the red sandstone as well as in the Kupferschiefer from transitional zones.

Another cross-section was drawn in the southwestern part of the Polkowice West Field (profiles No. Pr14-1604, Pr14-1605, Pr14-1600, Pr14-1606, Pr14-1610, Pr14-1614 and Pr14-1609). Most of these profiles record the copper deposit which then grades into the transitional zone. The boundary between the deposit and the transitional zone is almost vertical. A fragment of oxidized zone was found only at the bottom of carbonate series where it extends 1.5 m above the Kupferschiefer top surface. Rocks with typical red spots form a narrow offshoot, which penetrates the transitional zone.

The most complicated relationships between the zones are seen in the cross-section drawn through the western part of the Polkowice West Field (profiles No. Pr04-2527, Pr04-2528, Pr04-2530, Pr04-2529, Pr04-2532, Pr04-2531). This cross-section includes both the horizontal and the vertical boundaries between zones. The first, extended oxidized zone is located in the sandstone. The position of the upper boundary of the overlying transitional zone changes from horizontal, defined along an extended distance by the sandstone-Kupferschiefer lithological interface, to irregular, vertical one, separating the copper deposit and the oxidized zone. This zone includes all types of rocks. The second oxidized zone penetrates into the carbonate series form the southeast, immediately from above the Kupferschiefer. From the northwest it forms a vertical boundary of the transitional zone.

The copper deposit includes the Kupferschiefer and the carbonates. Towards the oxidized zone the copper grade abruptly decreases and in the oxidized zone itself it does not exceed 0.5 wt.% Cu. In both the oxidized and the transitional zones high amounts of precious metals appear. In the area represented by the cross-section the oxidized zone is dominated by native Au, whereas in the transitional zone electrum prevails. In the copper deposit native Au is rare and was encountered usually at the boundary with the transitional zone (Pieczonka, 1998, 2000).

The cross-sections demonstrate significant variability of thickness and geometry of particular oxidized zones. Apart from alternating zones located beneath the copper deposit, in which thickness changes are gradual, there are areas in which the zones extend upward and form additional, irregular, vertical boundaries as well as other areas in which the oxidized zone penetrates the copper deposit with narrow, irregular offshoots, usually above the top surface of the sandstone. Differences in geometry of these zones result from different formation conditions. In the sandstone the oxidized zone occupies vast area and the prepared cross-sections did not contour its boundaries. In the Kupferschiefer and in the carbonate series the oxidized zones form less extended, irregular restricted areas (red-shoot). Due to limited vertical range of studied sequences, an eventual presence of oxidized zone above the copper deposit can only be hypothesized.

Horizontal relationships

The occurrence of red-colored rocks is highly variable. Distribution of sandstones with red spots was recognized basing upon data after Nieć and Piestrzyński (1996) and that of the spotted Kupferschiefer and carbonate rocks was concluded from archival materials provided by the Geological Dept. of the Polkowice-Sieroszowice Mine (Archival materials, 1998). These materials include results of drillings and observations made by mining geologists during the development of the mine.

The sandstones with red spots occur in almost whole area of the deposit. These were observed in the southern and the western parts of the Sieroszowice area, and extend as irregular offshoots to its northern and eastern parts (Fig. 3). In the Polkowice mine, sandstones free of red spots form irregular fields in the northern and northeastern parts, and a single, isolated restricted red-shoot located closer to the center of the study area. These sandstones continue towards the Rudna and the Lubin mines where the spotted sandstones form only rare, isolated areas.

In both the Kupferschiefer and the carbonates red spots are less common. In the Polkowice and Sieroszowice mines

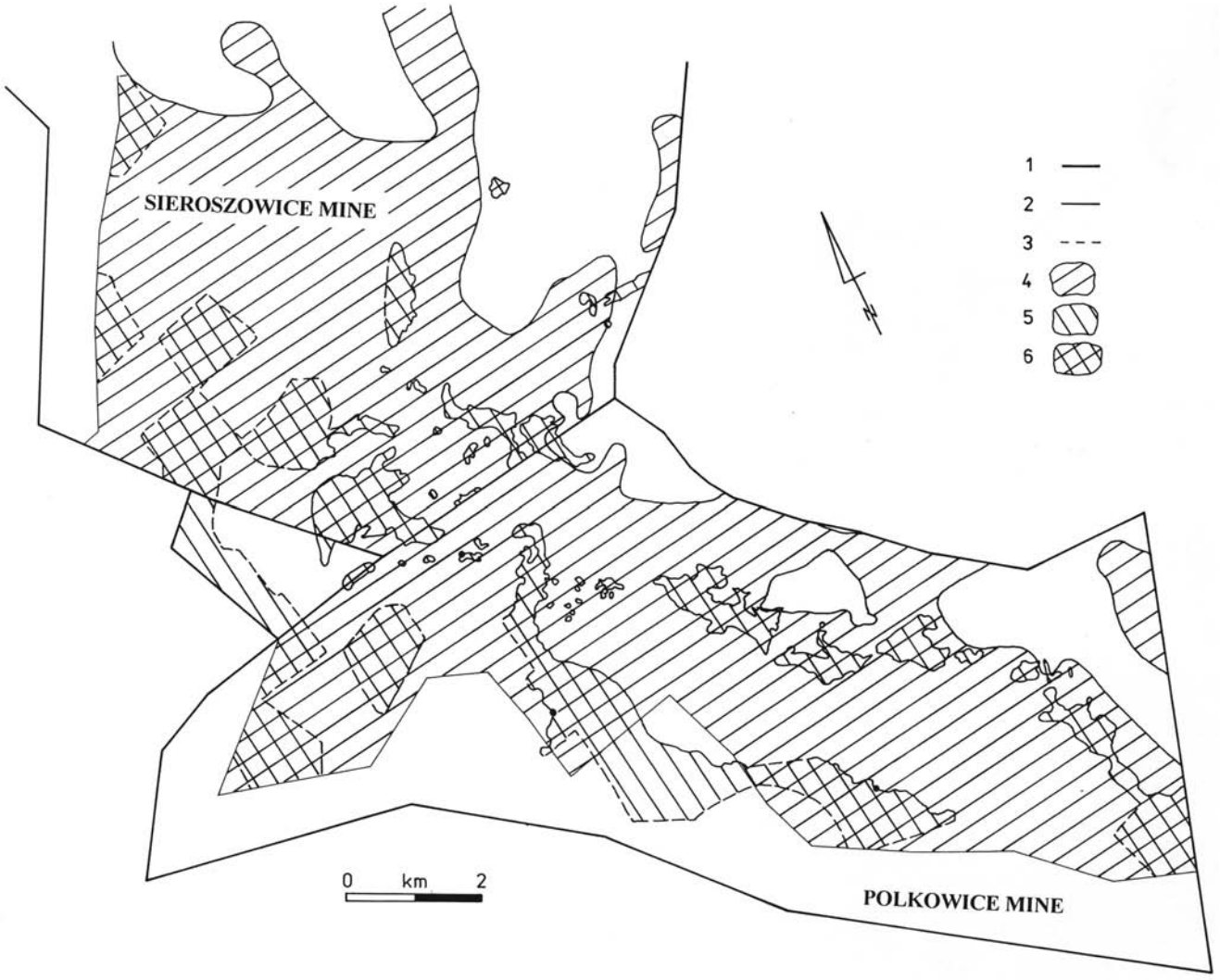

Fig. 3. Spatial relationship of oxidized areas and copper deposit (after Pieczonka, 2000). *1* – limit of mining concession; *2* – limit of the copper deposit; *3* – limit of the copper deposit based on bore holes; *4* – areas with oxidized Weissliegende sandstone; *5* – range of oxidized areas within the Kupferschiefer and dolomite; *6* – range of complete oxidized section in the copper zone

the spotted Kupferschiefer and dolomites form highly irregular, isolated red-shoots of various size. Only for some red-shoots, the boundaries could be defined accurately, for others the boundaries are still only approximate, because lack of mining works. In the Sieroszowice area the red-spotted Kupferschiefer and dolomites occur mostly in its southern and southwestern parts, over the red-spotted sandstones. In the Polkowice mine, red-shoots of the spotted Kupferschiefer and dolomites form two, locally parallel, NW–SE-trending belts. Interpretation of drilling data revealed that the red-spotted rocks occur also in the southwestern part of the Polkowice area and extend further northward, towards Radwanice and Sieroszowice. Generally, these rocks occur above the red-spotted sandstones (Pieczonka, 2000).

Considering the inadequate recognition of the southern and southwestern parts of the Polkowice-Sieroszowice deposit, the contour of red-spotted rocks zone in this part of the mine still remains unknown.

Similar pattern – i.e., isolated red-shoots of red-spotted Kupferschiefer and carbonates overlying the widespread zones of red-spotted sandstones – was described by Michalik (1979), basing upon data from 130 boreholes.

Both the irregular shapes and variable size of red-spotted zones as well as an enrichment in Cu in the areas adjacent to transitional zones, reported by mining geologists, confirmed the epigenetic origin of red spots in relation to the copper deposit (Pieczonka, 2000; Piestrzyński *et al.*, 2002).

Distribution of red spots in the rocks from the Polkowice-Sieroszowice deposit

The studies on the occurrence of the ”Rote Fäule” facies in the Fore-Sudetic Monocline were based mostly on data from drillings. Thanks to significant depth of boreholes, the distribution of red spots in particular rocks and their position in relation to the copper deposit were recognized.

Further studies carried out after the year 1995 (see Piestrzyński & Pieczonka, 1997a, b; Pieczonka, 2000; Piestrzyński *et al.*, 2002) were based upon macro- and microscopic analyses of specimens selected from channel samples taken in vertical sequences, whose localization followed the progressing development of the deposit. The thickness and the lithologies of sampled rocks depended on local, geological and mining conditions. In the Polkowice-Sieroszowice mine the copper deposit is located within the Kupferschiefer and the hanging wall carbonates. Hence, the mine workings are driven on the top surface of the sandstone. In the sequences sampled during the first stage of the research project only a single, point sample (sometimes two point samples, taken from 0 to 20 cm interval beneath the top of the sandstone) was collected from this rock. Results of their examinations allowed the authors to recognize the importance of the sandstone and gave rise to an expensive program of supplementary drillings down to 1.5 m depth from the top of the sandstone. Unfortunately, even these drillings did not provide sufficient data for credible, qualitative and quantitative evaluation of red spots distribution in the sandstone.

Red spots were observed in the sandstones, in the Kupferschiefer, and in the dolomites. Carbonates with red spots were usually encountered above the red-colored sandstones. In the Kupferschiefer separating these rocks red spots were often macroscopically invisible. In most samples collected from such shale the red internal reflections were observed under the ore microscope at crossed nicols. Intensive red coloration of the Kupferschiefer or the Boundary Dolomite was found only in small areas.

The Polkowice East Field

In the Polkowice East Field red spots were found first of all in the sandstone, in profiles No. Sz07-0012, Sz12-0238, 95-PW-1 and 95-PW-2 (Pieczonka, 1998) localized in the southern part of the field. Supplementary drillings down to 1.5 m depth from the top of the sandstone did not penetrate the lower boundary of the red-spots zone. Only in a single profile (No. 95-PW-8) red spots were encountered also in the bottom part of the carbonates, immediately over the spotted sandstone (Pieczonka, 1998, 2000). In 1999–2000 years several new profiles were sampled during the development of the new parts of copper deposit: No. Po23-2384, Po23-2399, Sz02-0438, Sz02-2700, Sz02-3056 (Fig. 4), Sz03-1026 (Fig. 5), Sz03-2028, Sz03-2059, Sz03-2079, Sz07-0027 (Fig. 6), Sz07-0054, Sz07-0429, Sz08-0936, Sz08-0991 and Sz08-1054 (Fig. 7). In sampled rocks the red spots were absent.

The Polkowice Main Field

In the Polkowice Main Field most of red spots were found also in the sandstone, even down to 1 m depth from its top surface (profiles: Sz06-0407, Sz06-0423, Sz06-0714, Sz06-1086, Po16-1925, 95-PG-3, 95-PG-4, 95-PG-5, 95-PG-7 and 95-PG-9, Pieczonka, 1998, 2000). Deeper supplementary wells were not drilled. In some sequences the whole top part of the sandstone was red-colored, whereas in other ones samples free of spots were collected (e.g., profile No. Po16-1925). In the southern part of the field red spots appeared above the top of the sandstone, in the Kupferschiefer (profiles: 95-PG-1, 95-PG-2, Pieczonka, 1998, 2000) and in the carbonates (profiles No. Sz06-0407, Sz06-0423, Sz06-1086, Pieczonka, 1998, 2000). In dolomites the spots were found immediately above the Kupferschiefer (profile No. Sz 06-0407) and 20–30 cm above its top surface (sequences No. Sz06-0423, Sz06-0714). Only in a single, 95-PG-3 profile red spots were encountered in the bottom part of the Kupferschiefer and in the lowermost interval sample taken from the dolomite. In the profiles Po17-2125 and Po17-2289 located close to the border with the Polkowice East Field red spots were not observed.

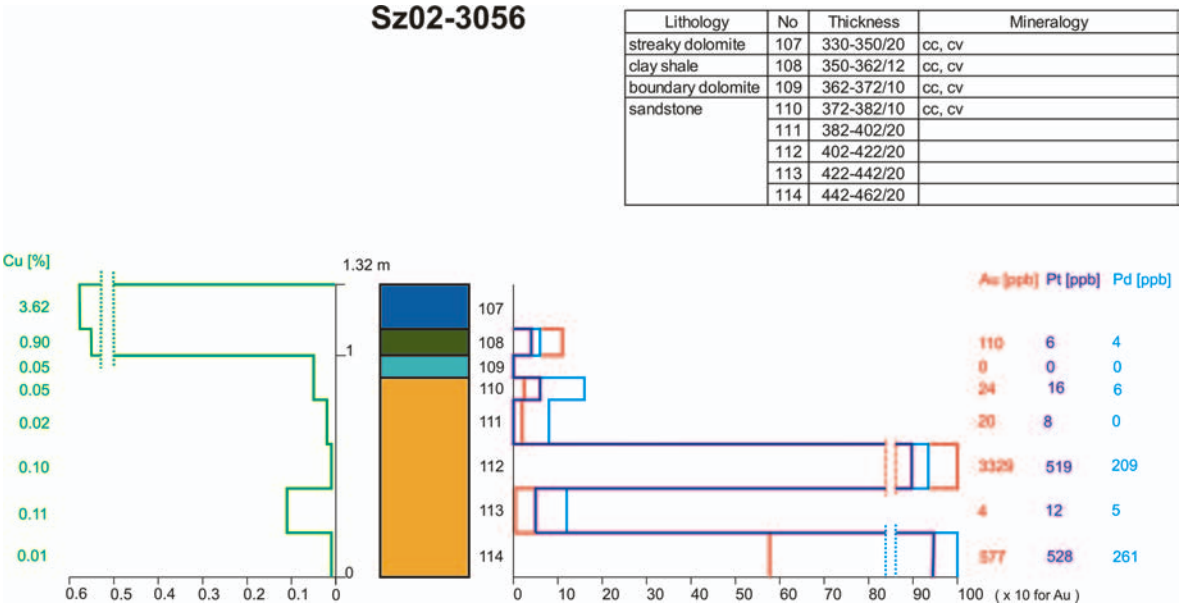

Fig. 4. Vertical distribution and correlation of copper and precious metals in the profile Sz02-3056 from Polkowice Mine, East Field. 114 – no of chip sample, cc – chalcocite, cv – covellite

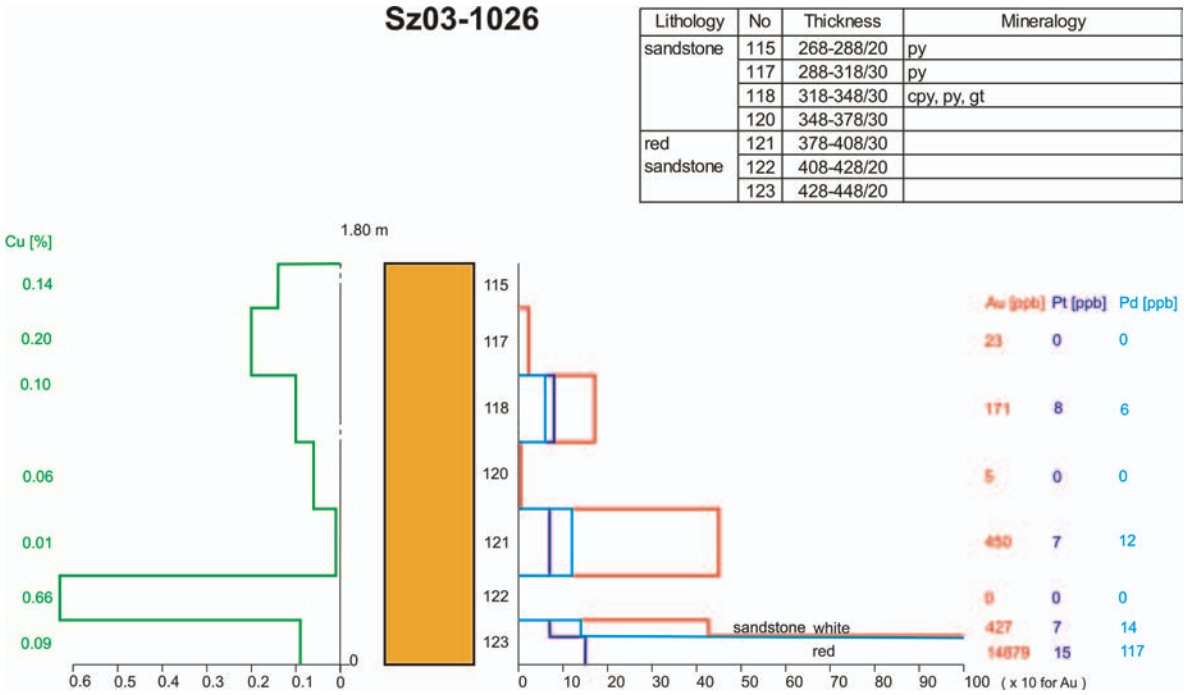

Fig. 5. Vertical distribution and correlation of copper and precious metals in the profile Sz03-1026 from Polkowice Mine, East Field. 123 – no of chip sample, cpy – chalcopyrite, py – pyrite, gt – goethite

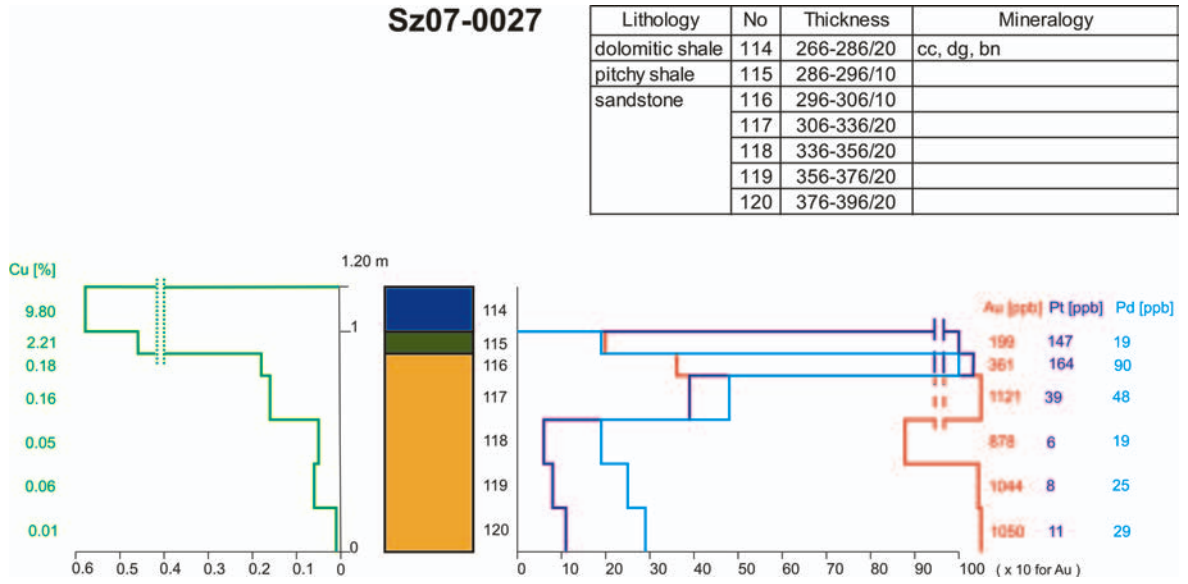

Fig. 6. Vertical distribution and correlation of copper and precious metals in the profile Sz07-0027 from Polkowice Mine, East Field. 120 – no of chip sample, bn – bornite, cc – chalcocite, dg – digenite

The Polkowice West Field

Red spots from this field revealed highest density and diversity. However, it must be emphasized that in this field the largest number of observations could be made due to intensive mining operations.

The sandstone

Apart from profiles: Pr18-0331 and Pr18-0367, in which red spots were not found, the red-colored sandstone was present in all the studied sequences, from which more than one sample was taken. However, the boundaries of the red spots zone could not be contoured, despite large number of samples. The spots occur in both the southern and central parts of the field, and at the boundary with the Sieroszowice area. In some sequences the full studied sandstone thickness contained red spots (profiles: Sr23-0517, Sr 23-0518, Pr10-2267 and Pr04-2529, Pieczonka, 1998, 2000) whereas in others the spots appeared at depth from 0 to 40 cm from the

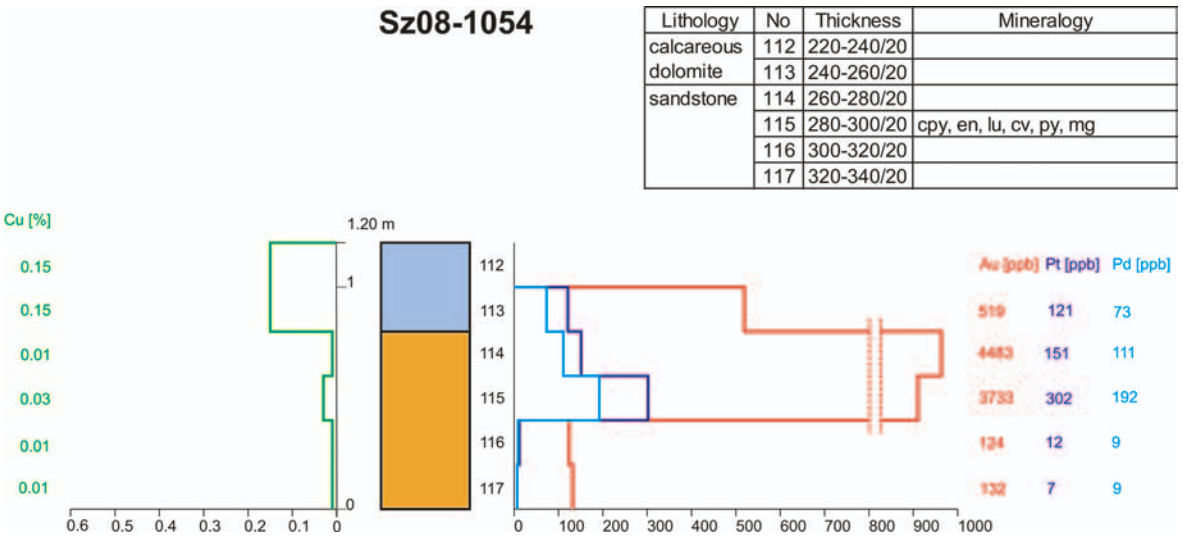

Fig. 7. Vertical distribution and correlation of copper and precious metals in the profile Sz08-1054 from Polkowice Mine, East Field. 117 – no of chip sample, cpy – chalcopyrite, cv – covellite, en – enargite, lu – luzonite, mg – magnetite, py – pyrite

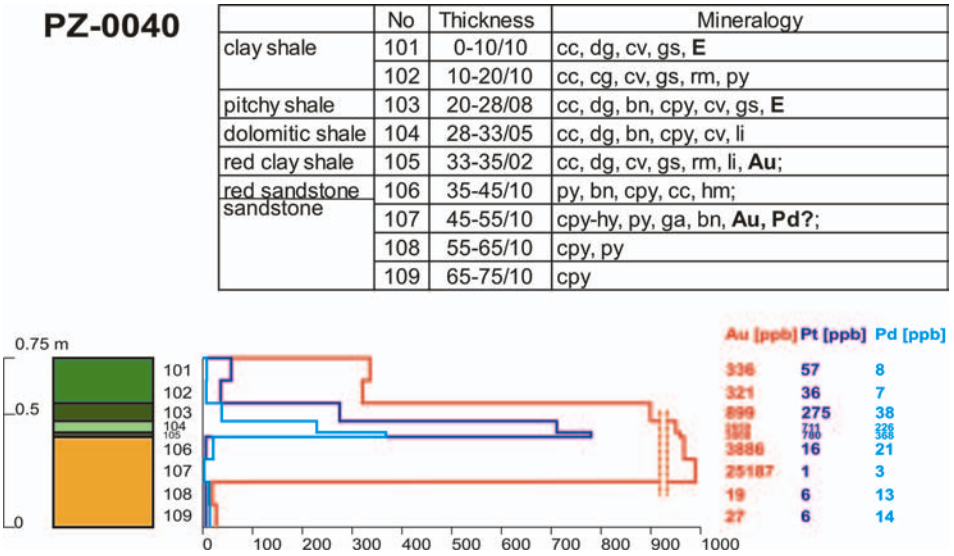

Fig. 8. Vertical distribution of precious metals in the profile PZ-0040 from Polkowice Mine, West Field. 109 – no of chip sample, bn – bornite, cpy – chalcopyrite, cc – chalcocite, cv – covellite, cg – castaingite, dg – digenite, ga – galena, gs – gersdorffite, rm – rammelsbergite, li – laitakarite, py – pyrite, hy – haycockite, E – electrum, hm – hematite, Au – native gold, Pd? – palladium arsenides

top surface (profiles: Pr04-2531, Pr04-2532, Pr08-0166, PZ-40 in Fig. 8, PZ-41 and PZ-43 in Fig. 9, Pieczonka, 1998, 2000, and Pr13-7001). Obviously, it does not mean that the spots do not occur at greater depths from sandstone top surface. Moreover, in some sequences, the alternating zones of grey and red sandstone were found (profile PR 18-0262) or red spots appeared some tens of centimeters down the top of the sandstone (sequence No. Pr 04-2527). Observations revealed not only the high variability of red spots distribution but also their highly irregular shape and size (Pieczonka, 1998, 2000).

The spots located in the top part of the sandstone, close to the boundary with the Kupferschiefer as well as those located down to 20 cm depth from this lithological interface reveal cherry-red colour, usually elongated shape and stable thickness over long distances. A randomly selected sampling site positioned in the central part of such a long spot may suggest the general, occurrence of syngenetic type of lamina in the sandstone (Fig. 10A) and consecutive samples taken from alternating, red and grey sandstone zones may "confirm" this observation (profile PR18-0262). Commonly, such a lamina pinches out or branches after a long distance (several meters) from the center. The case illustrated by PR18-0262 profile may result also from roughly parallel arrangement of several large spots or from clustering of smaller spots at various depths from the top surface of the sandstone. Insufficient recognition of sandstone in the study area gives rise to various possible interpretations (Pieczonka, 1998).

PZ-0043

Lithology	No	Thickness	Mineralogy
streaky dolomite with red patches	101	0-20/20	
	102	20-40/20	py, bn, cpy
	103	40-60/20	cpy
	104	60-80/20	cpy, cc, bn, hm, **Au**
	105	80-100/20	cpy, cc
	106	100-120/20	cpy, bn, cc, dg, hm, rm
	107	120-140/20	cpy
	108	140-160/20	hm
	109	160-180/20	cpy, hm, cc
	110	180-200/20	cpy, bn, dg, py, hm
	111	200-220/20	bn, dg
	112	220-233/13	cpy, bn, cc; hm
clay shale	113	233-239/06	cpy;
red sandstone	114	239-249/10	bn, cpy, hm;
	115	249-259/10	cpy, bn, cv, hm, cc, **Au**;
	116	259-279/20	cpy;

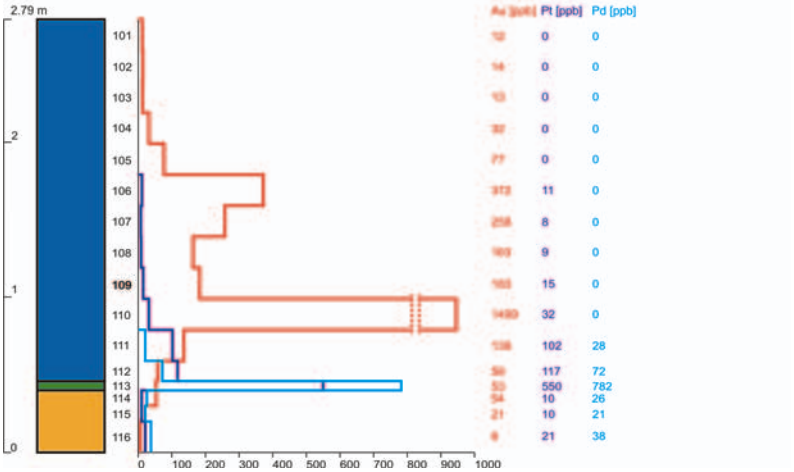

Fig. 9. Vertical distribution of precious metals in the profile PZ-0043 from Polkowice Mine, West Field. 109 – no of chip sample, bn – bornite, cpy – chalcopyrite, cc – chalcocite, cv – covellite, dg – digenite, rm – rammelsbergite, py – pyrite, Au – native gold, hm – hematite

In more compact, carbonate-cemented sandstone immediately underlying the Kupferschiefer the other type of spots was found – brownish-red, more regular in shape and smaller (Fig. 10B).

In several profiles only the top part of the sandstone (some 10 cm thick) was observed, immediately underlying the Kupferschiefer. This layer commonly hosted the red spots (profiles: 95-PZ-1, 95-PZ-2, 95-PZ-3, 95-PZ-15, 95-PZ-19, Fig. 11), (Pieczonka, 1998, 2000). In many sequences the sandstone was not sampled (profile Sz/III, Sz/IV) or the interval sample taken just beneath the Kupferschiefer represented the white sandstone variety. However, if red-colored Kupferschiefer or cabonates occurred in such sequences, it is very probable that red spots were present also in the sandstone, but at greater depths.

The Kupferschiefer

The red-spotted or brownish-red Kupferschiefer varieties encountered in the Polkowice West Field usually occupy lowermost position in the full thickness of this member. i.e., immediately above the top surface of the cherry-red sandstone (Fig. 10C, D). Such shale forms either a homogenous layer overlain successively by brownish-grey and dark-grey varieties (profiles: 95-PZ-1, 95-PZ-2, 95-PZ-13, 95-PZ-17, 95-PZ-18, Fig. 12, up to No. 95-PZ-25, Pieczonka, 1998, 2000) or intercalations of brownish-red and brownish-grey shale overlain by dark-grey variety (profiles: 95-PZ-27 to 95-PZ-38, Pieczonka, 1998). Therefore, in the Kupferschiefer layer some tens of centimeters thick one can observe transition from oxidized zone (red and brownish-red shale) to transitional zone (brownish-grey shale), to reducing zone (dark-grey shale with Cu mineralisation). Distribution of profiles revealed that the red-colored variety of the Kupferschiefer occurs mostly in the central and southern parts of the West field.

The carbonate rocks

In the cabonate rocks the red spots are rare and were observed in sequences localized along the southwestern boundary of the Polkowice West Field (profiles: PZ-43, Pr04-2531, Pr04-2532, Sr23-0517, Pieczonka, 1998, No. Pr13-7001, Fig. 13, No. Sz/III, Fig. 14 and No. Sz/IV, Fig. 15). In this part of the mining field carbonates are separated from the sandstone by the Kupferschiefer layer only a dozen of centimeters thick. Moreover, in some sites the shale does not contain macroscopically visible red spots. Low thickness of the Kupferschiefer was probably responsible for the expansion of oxidized zone into the carbonate series. Thick-

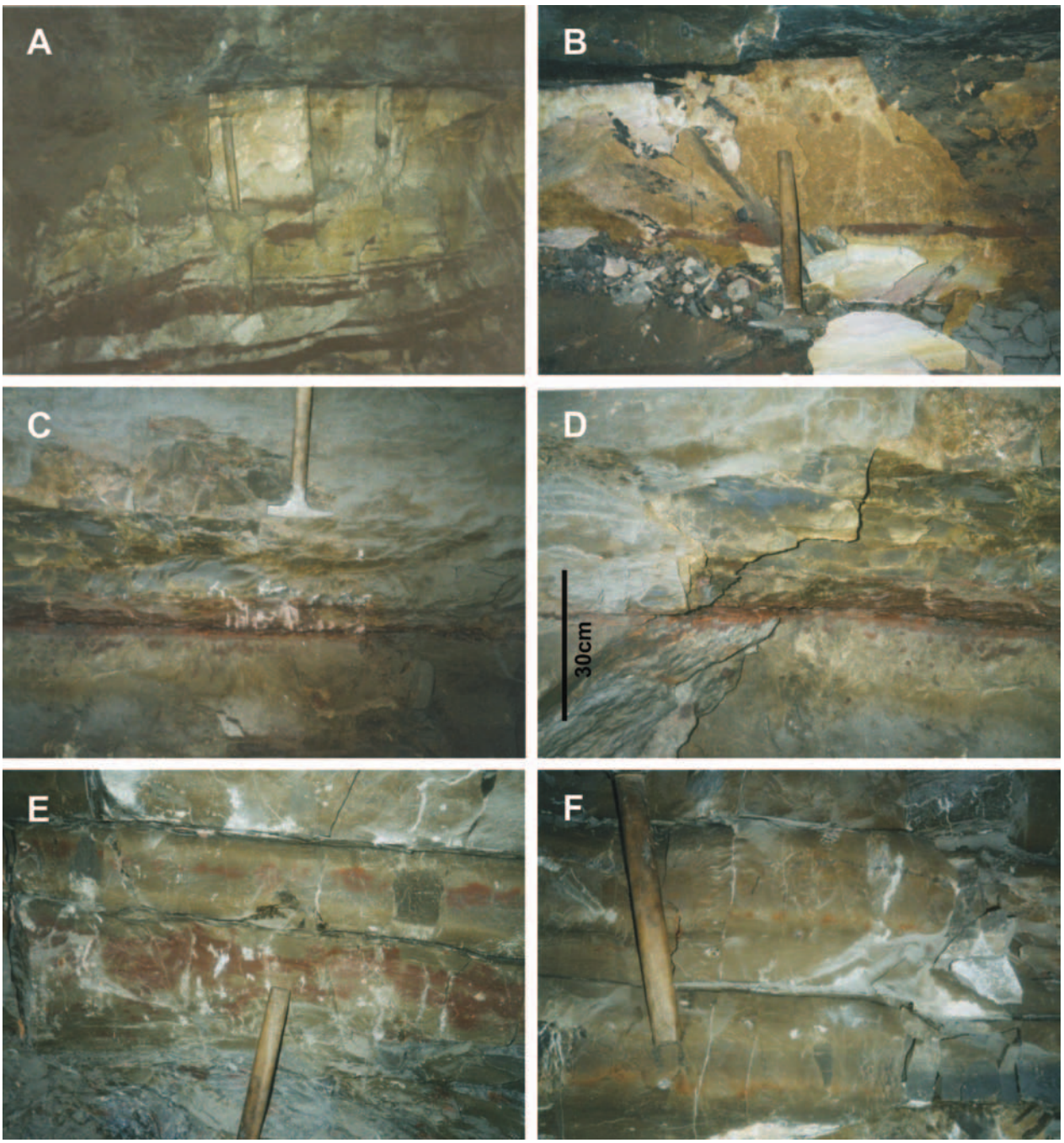

Fig. 10. Macrophotographs showing position of red patches in vertical sections of Zechstein strata, Polkowice Mine. **A** – red patches in the uppermost part of Weissliegende sandstone, profile PZ-G-31; **B** – red patches and spots random distributed in the uppermost part of Weissliegende sandstone, profile PZ-G-31; **C** – red patches at the contact of Weissliegende sandstone and Kupferschiefer, profile PZ-G-31; **D** – red patches and spots at the contact of Weissliegende sandstone and Kupferschiefer, profile PZ-G-31; **E** – secondary oxidized section of the lowermost part of PZ1 limestone, profile PZ-G-31; **F** – secondary maroon patches showing primary lamination of the lowermost part of PZ1 limestone, profile PZ-G-31

ness of red-spotted dolomites far exceeds 2 m and red spots were encountered in all collected interval samples except for sequences No. Pr04-2531 and Sz/IV where the red spots disappeared about 1 m above the top surface of the Kupferschiefer.

Size, shape and color of red spots are highly variable. A common variety includes spots arranged concordantly with dolomites bedding. These are large, irregular spots or clusters of closely packed, smaller, cherry-red spots arranged in streaks (Fig. 10E). Such streaks can be formed also by smaller, more regular, brownish-red spots (Fig. 10F). Intensity of color in specific layers is highly variable.

Apart from the areas where the main direction of spots arrangement is clear over long distances, there are sites where spots of various size are randomly scattered within the dolomite. However, even the large, elongated spots tend

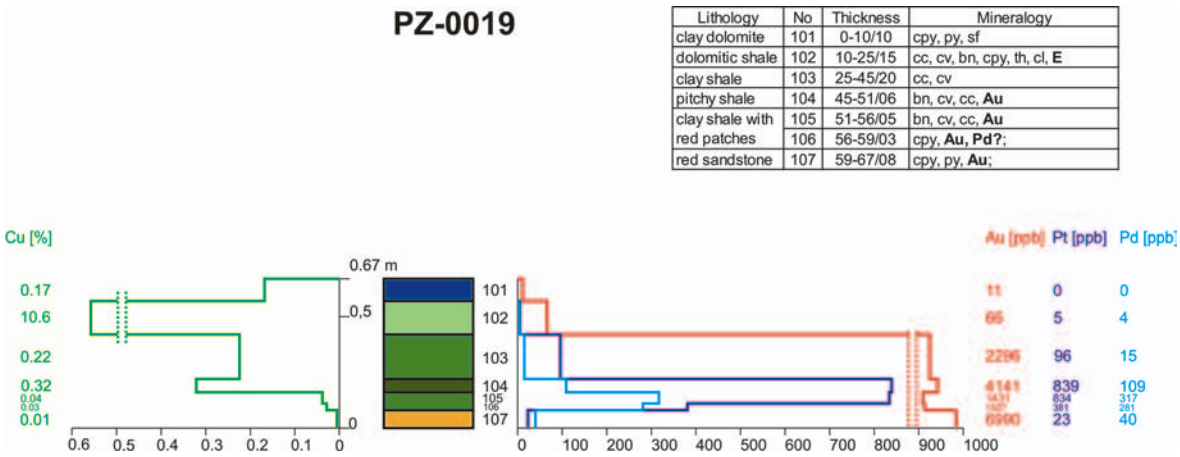

Fig. 11. Vertical distribution and correlation of copper and precious metals in the profile PZ-0019 from Polkowice Mine, West Field. 107 – no of chip sample, bn – bornite, cpy – chalcopyrite, cc – chalcocite, cv – covellite, sf – sphalerite, cl - calusthalite, py – pyrite, th – thucholite, E – electrum, Au – native gold, Pd – palladium arsenides

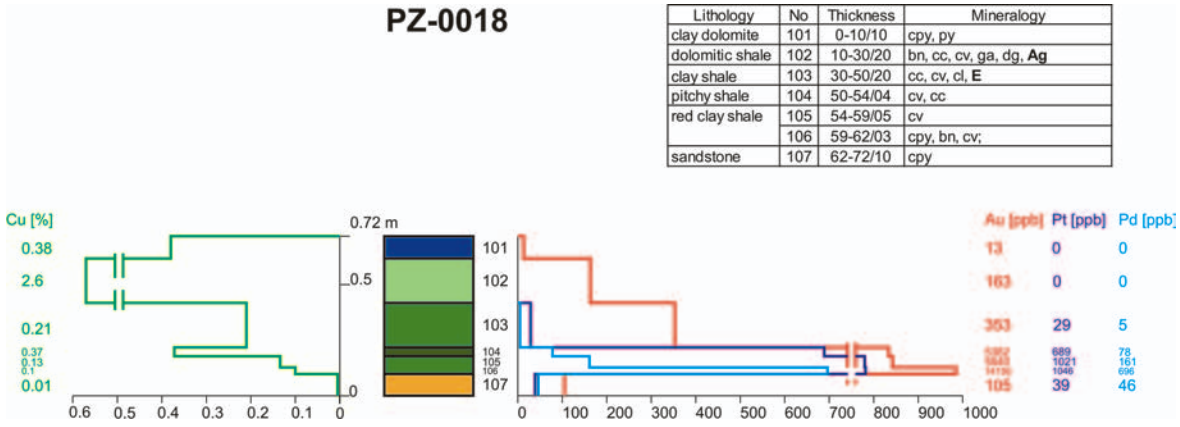

Fig. 12. Vertical distribution and correlation of copper and precious metals in the profile PZ-0018 from Polkowice Mine, West Field. 107 – no of chip sample, bn – bornite, cpy – chalcopyrite, cc – chalcocite, cv – covellite, ga – galena, cl – calusthalite, dg – digenite, py – pyrite, E – electrum, Ag – native silver

to position their longer axes parallelly to the bedding planes. Red-colored are also diagenetic sulphates encountered in nest-like structures (Pieczonka, 1998, 2000).

The Sieroszowice area

Before the year 2000, the occurrence of red spots in the Sieroszowice area was known only from a few profiles localized in the southeastern part of the mine (e.g., No. 95-S-7, Sr09-0520 and Sr09-0727, Pieczonka, 2000). The spots were rare and occurred at depths intervals 0–10 cm, 20–40 cm and 60–80 cm beneath the top of the sandstone. In the following years sampling was made in profiles localized in various parts of the mine: northwestern (No. Ra14-0274 and Ra14-0505), central (No. Ra19-0011), southwestern (No. Sr18-61"s", Sr18-1628 and Sr18-7002, Fig. 16), southern (No. Sr19-0802, Sr19-1186, Sr19-2428, Fig. 17, No. N/III, Fig. 18, No. N/IV, Fig. 19 and No. N/V, Fig. 20) and southeastern (No. Sr20-0822). In the profiles No. Sr18-1628, N/III, N/IV and N/V, large number of red spots was observed in all samples collected from the sandstone (even down to 1.5 m depth, as in No. N/III). Moreover, spots were observed also in the dolomites, in No. N/III profile (even in the highest interval sample taken 2.3 m above the top of the clayey dolomite) and in No. Sr18-7002 profile. In the remaining profiles red spots were not encountered. However, it must be noticed that the Sieroszowice area is poorly recognized in comparison with other mines, and observations could be carried out over a small area.

Summary

The spots were observed over long distances at the sandstone/Kupferschiefer boundary and within the sandstone, at depths about 20 cm beneath the top surface as well as in the bottom part of the carbonate series. Sometimes, these are clusters of spots locally following the bedding planes of the sandstone or dolomites, or the lamination of the Kupferschiefer. The spots may pinch our or branch in various directions. Usually, the spots reveal cherry-red color. Such arrangement of spots was a result of activity of oxidizing solutions flowing in a partly unconsolidated sediment, along the directions of most favorable physical properties. Local changes of these properties, if hampered the

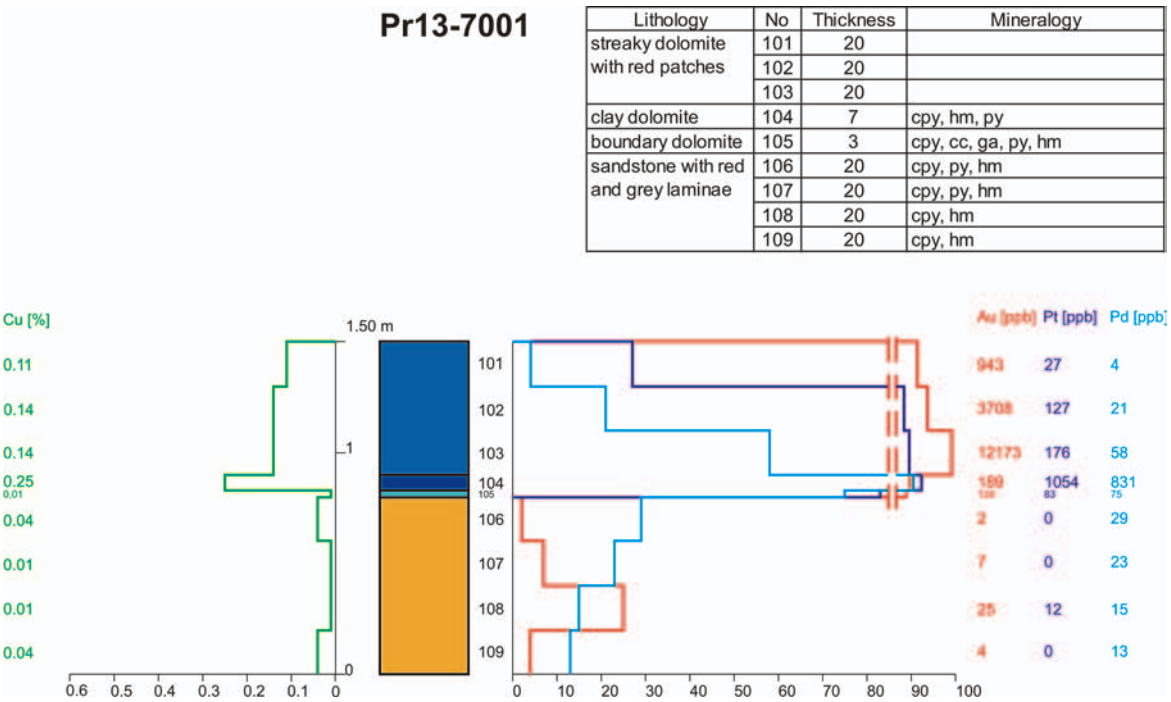

Lithology	No	Thickness	Mineralogy
streaky dolomite with red patches	101	20	
	102	20	
	103	20	
clay dolomite	104	7	cpy, hm, py
boundary dolomite	105	3	cpy, cc, ga, py, hm
sandstone with red and grey laminae	106	20	cpy, py, hm
	107	20	cpy, py, hm
	108	20	cpy, hm
	109	20	cpy, hm

Fig. 13. Vertical distribution and correlation of copper and precious metals in the profile Pr13-7001 from Polkowice Mine, West Field. 109 – no of chip sample, cpy – chalcopyrite, cc – chalcocite, ga – galena, hm – hematite, py – pyrite

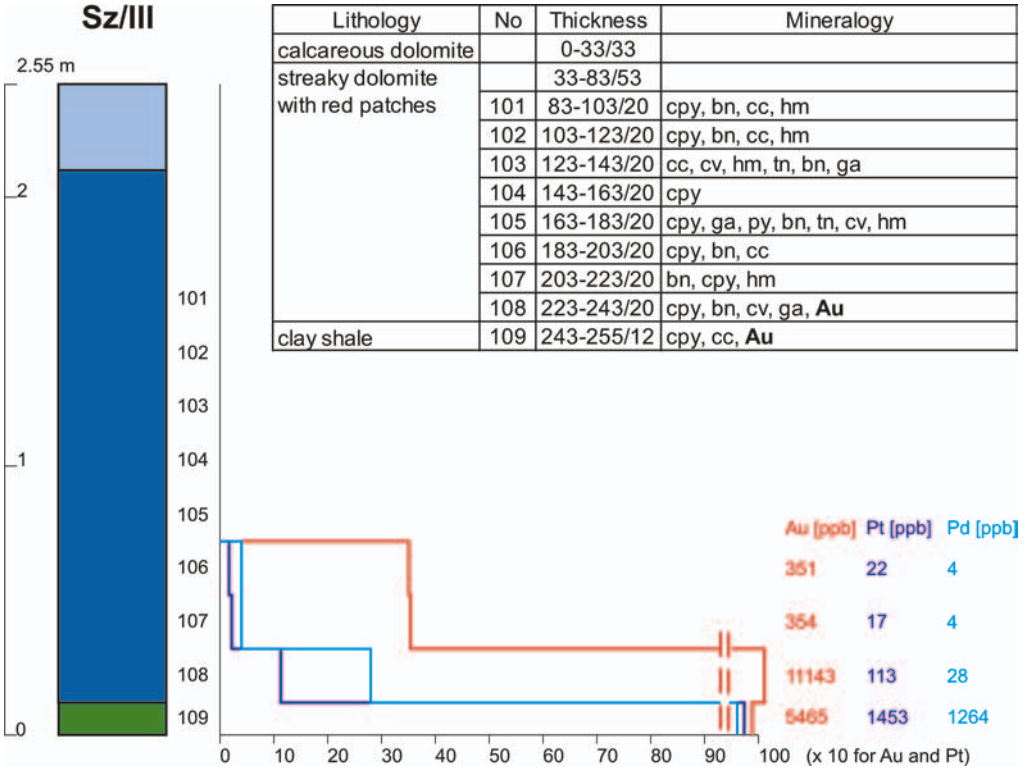

Lithology	No	Thickness	Mineralogy
calcareous dolomite		0-33/33	
streaky dolomite with red patches		33-83/53	
	101	83-103/20	cpy, bn, cc, hm
	102	103-123/20	cpy, bn, cc, hm
	103	123-143/20	cc, cv, hm, tn, bn, ga
	104	143-163/20	cpy
	105	163-183/20	cpy, ga, py, bn, tn, cv, hm
	106	183-203/20	cpy, bn, cc
	107	203-223/20	bn, cpy, hm
	108	223-243/20	cpy, bn, cv, ga, **Au**
clay shale	109	243-255/12	cpy, cc, **Au**

Fig. 14. Vertical distribution of precious metals in the profile Sz/III from Polkowice Mine, West Field. 109 – no of chip sample, bn – bornite, cpy – chalcopyrite, cc – chalcocite, cv – covellite, tn – tennantite, hm – hematite, ga – galena, py – pyrite, Au – native gold

solution transfer, caused the migration of fluids in various directions and the formation of variously shaped spots. At sites where solution transfer was highly obstacled by changes in porosity and permeability of rocks, small, isolated spots were formed. The barriers for free, vertical migration of solutions were, among others, the topmost, 20-cm-thick, compact, carbonate-cemented sandstone layer as well as the bottom surface of the Kupferschiefer and the higher portions of the dolomite series. The single, brick-red spots seen in the topmost sandstone layer are analogous to

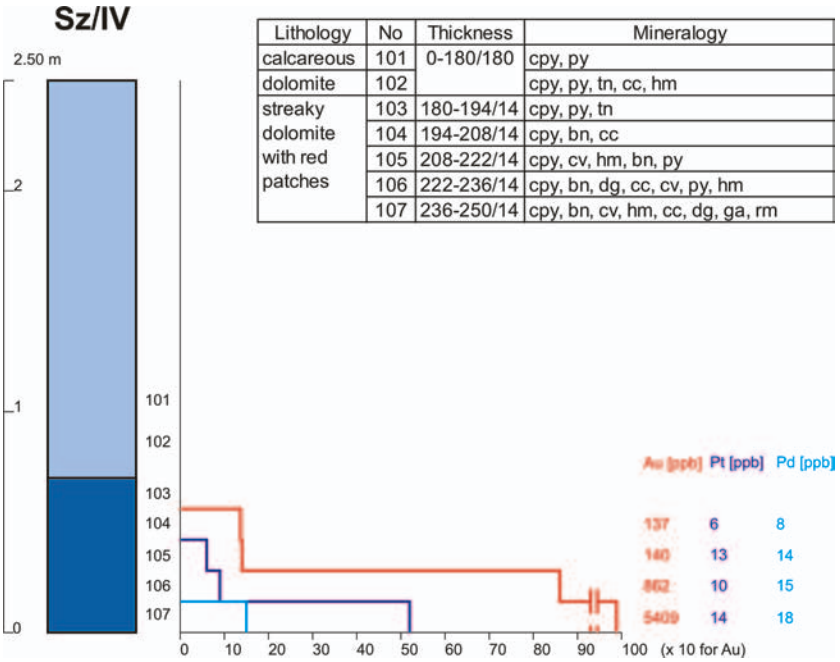

Lithology	No	Thickness	Mineralogy
calcareous	101	0-180/180	cpy, py
dolomite	102		cpy, py, tn, cc, hm
streaky dolomite with red patches	103	180-194/14	cpy, py, tn
	104	194-208/14	cpy, bn, cc
	105	208-222/14	cpy, cv, hm, bn, py
	106	222-236/14	cpy, bn, dg, cc, cv, py, hm
	107	236-250/14	cpy, bn, cv, hm, cc, dg, ga, rm

Fig. 15. Vertical distribution and correlation of copper and precious metals in the profile Sz–IV from Polkowice Mine, West Field. 107 – no of chip sample, bn – bornite, cpy – chalcopyrite, cc – chalcocite, cv – covellite, tn – tennantite, dg – digenite, ga – galena, rm – rammelsbergite, py – pyrite, hm – hematite

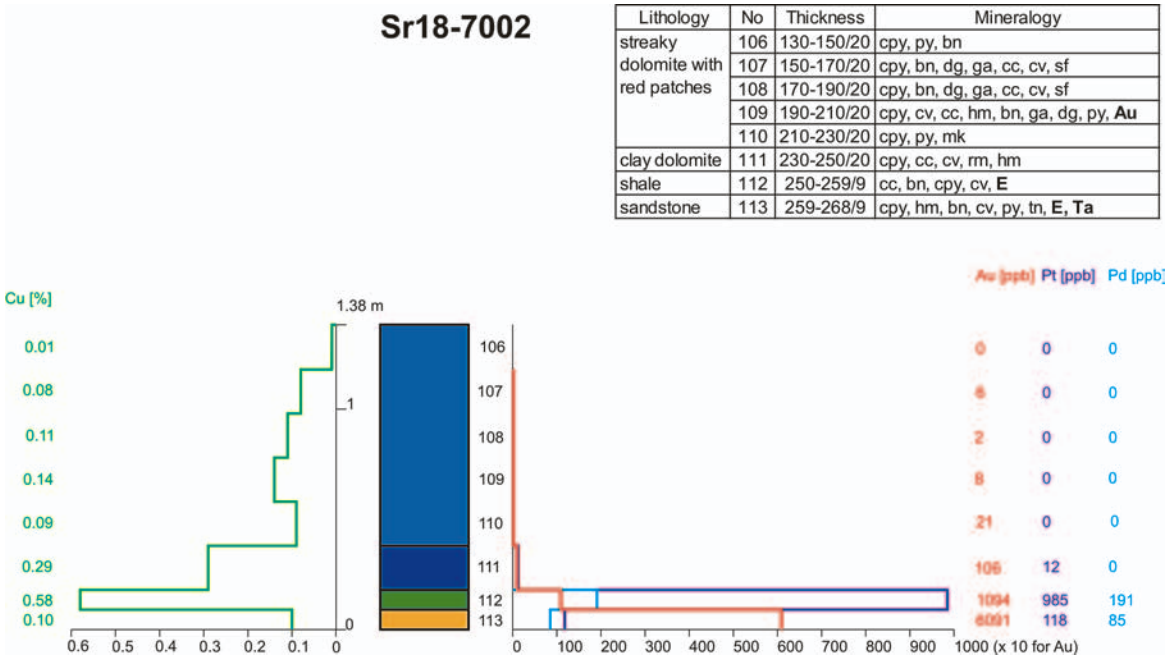

Lithology	No	Thickness	Mineralogy
streaky dolomite with red patches	106	130-150/20	cpy, py, bn
	107	150-170/20	cpy, bn, dg, ga, cc, cv, sf
	108	170-190/20	cpy, bn, dg, ga, cc, cv, sf
	109	190-210/20	cpy, cv, cc, hm, bn, ga, dg, py, **Au**
	110	210-230/20	cpy, py, mk
clay dolomite	111	230-250/20	cpy, cc, cv, rm, hm
shale	112	250-259/9	cc, bn, cpy, cv, **E**
sandstone	113	259-268/9	cpy, hm, bn, cv, py, tn, **E, Ta**

Fig. 16. Vertical distribution and correlation of copper and precious metals in the profile Sr18-7002 from Polkowice Mine, West Field. 113 – no of chip sample, bn – bornite, cpy – chalcopyrite, cc – chalcocite, cv – covellite, tn – tennantite, sf – sphalerite, ga – galena, dg – digenite, rm – rammelsbergite, py – pyrite, mk – marcasite, E – electrum, Au – native gold, Ta – tetraauricupride, hm – hematite

those observed in the carbonates together with the cherry-red spots. Their different shape, distribution in the rocks and color indicate that these spots were formed under conditions different from those of spots described above.

Basing upon macroscopic observations, two types of red spots can be distinguished, formed during two different oxidation stages (Pieczonka, 1998, 2000; Piestrzyński *et al.*, 2002).

Structures and types of red spots

The sandstone

Spots encountered in the sandstone show highly variable size and shapes, and different shades of red color. Dominant are brownish-red, occasionally cherry-red spots. Despite their size, all these spots reveal highly irregular shapes with numerous offshoots penetrating the host rock in

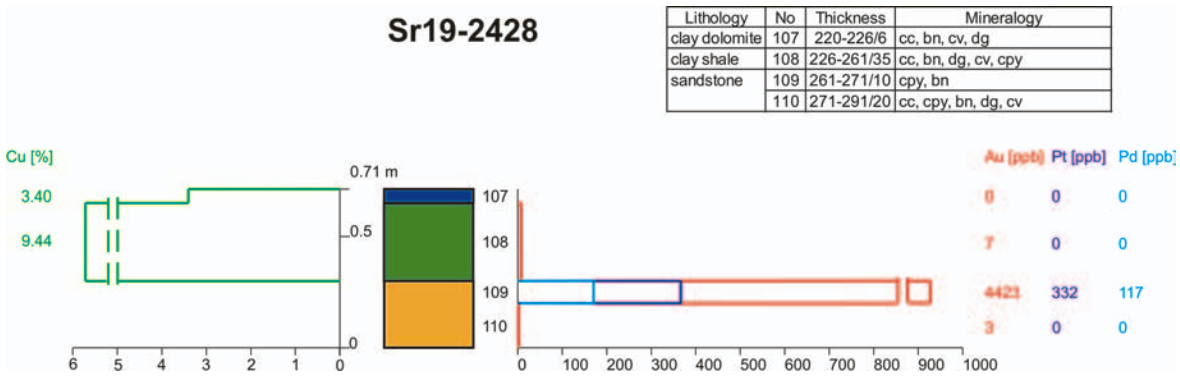

Fig. 17. Vertical distribution and correlation of copper and precious metals in the profile Sr19-2428 from Polkowice Mine, West Field. 110 – no of chip sample, bn – bornite, cpy – chalcopyrite, cc – chalcocite, cv – covellite, dg – digenite

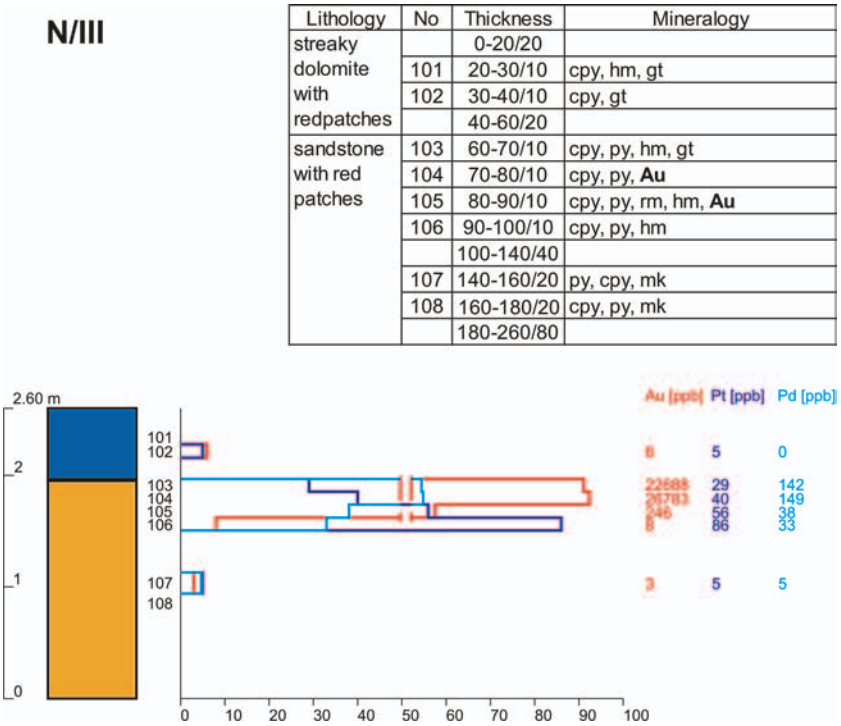

Fig. 18. Vertical distribution of precious metals in the profile N/III from Polkowice Mine, West Field. 108 – no of chip sample, cpy – chalcopyrite, gt – goethite, dg – digenite, rm – rammelsbergite, py – pyrite, mk – marcasite, Au – native gold, hm – hematite

various directions. In these spots and in surrounding, unaffected white sandstone, abundant sulphide accumulations were noticed (Fig. 21A, B, C, D). Changes in color of larger spots can be caused by various intensity of oxidizing solutions action or variable Fe contents in rocks penetrated by these solutions. Locally, over short distances, the red-colored, topmost zone of the sandstone resembles a layer. In a single profile the red sandstones were apparently laminated (laminae resulted from changes in sandstone color caused by horizontal solution transfer) and hosted distinct, dark-red (occasionally cherry-red) spots (Fig. 21E). These laminae disappeared about 0.5 m beneath the top surface of the sandstone.

The second type includes spots of more regular shapes, several centimeters in diameter, showing brownish-red, sometimes brick-red color and common dark rims (Fig. 21F, 22A, B). The rims composed of abundant hematite are distinct barriers between the spots and the enclosing sandstone. However, under the ore microscope, at crossed nicols, the rims boundaries are not so sharp. Within the spots hematite accompanies the coarse-crystalline carbonate cement, locally entirely replacing carbonate minerals. It also fills the cracks in various detrital grains up to complete replacement of the clastics. Hematite accumulations occur also outside the spots, within the carbonate cement of surrounding white sandstone (Pieczonka, 1998). Within the

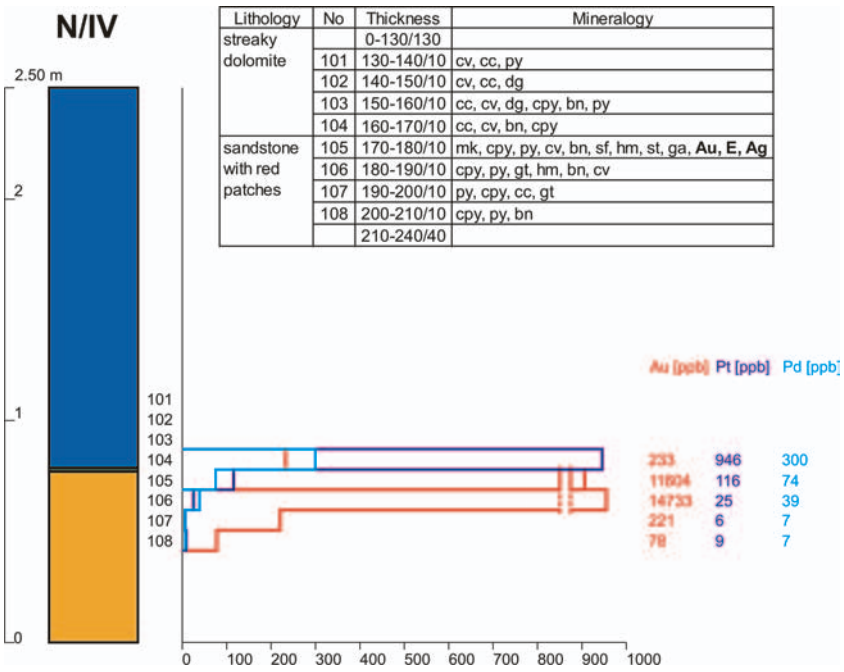

Fig. 19. Vertical distribution of precious metals in the profile N/IV from Polkowice Mine, West Field. 108 – no of chip sample, bn – bornite, cpy – chalcopyrite, gt – goethite, cc – chalcocite, cv – covellite, dg – digenite, ga – galena, sf – sphalerite, py – pyrite, mk – marcasite, Au – native gold, E – electrum, Ag – native silver, st – stromeyerite, hm – hematite

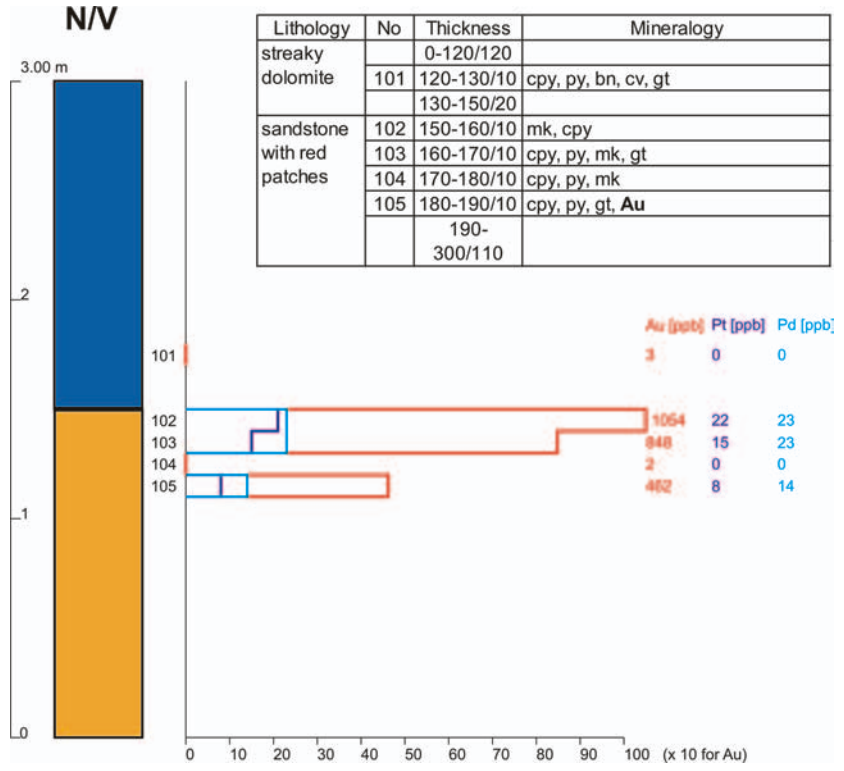

Fig. 20. Vertical distribution of precious metals in the profile N/V from Polkowice Mine, West Field. 105 – no of chip sample, bn – bornite, cpy – chalcopyrite, gt – goethite, cv – covellite, py – pyrite, mk – marcasite, Au – native gold

spots chalcopyrite and pyrite were observed as aggregates in sandstone cement and in cracks cutting the detrital grains. Outside the red spots sulphides are rare.

The two types of spots are secondary and were formed shortly after deposition of the sandstone (Pieczonka, 1998, 2000). For the first type of spots it is documented by their irregular shapes, arrangement in relation to sandstone bedding and the presence of sulphides. In many earlier papers (Piestrzyński, 1995; Kucha, 1995) the lack of relationships between the sulphide mineralisation and the syngenetic sed-

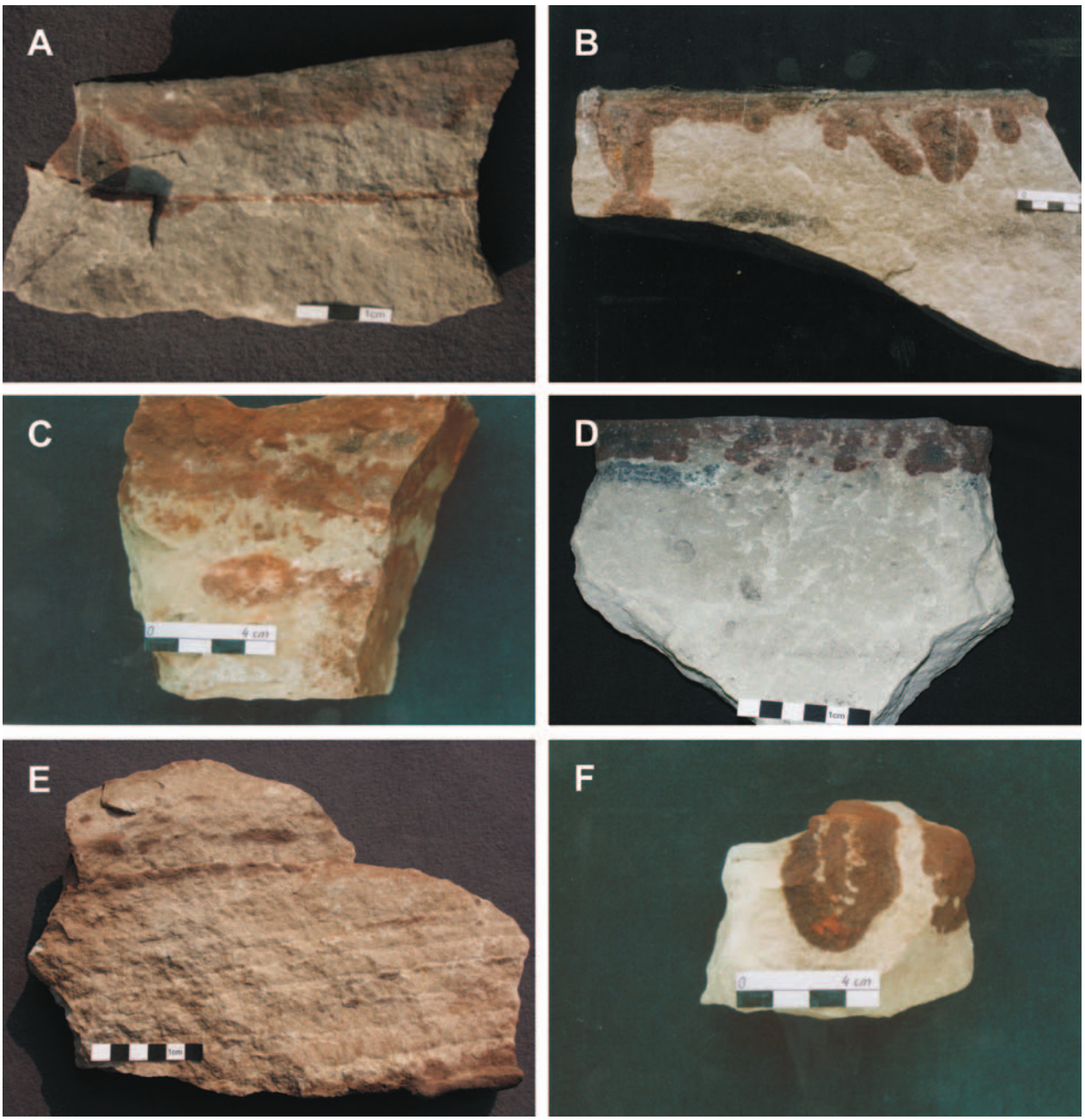

Fig. 21. Macrophotographs showing different shape of red patches in the Weissliegende sandstone, Polkowice Mine. **A** – red patches in the uppermost part of Weissliegende sandstone, solid red line is a shear plane, profile SW-G-=53; **B** – lens of sulphides (black) within the red patches and spots random distributed in the uppermost part of Weissliegende sandstone, profile SW-G-53; **C** – irregular red patches and nests of sulphides at the contact of Weissliegende sandstone and Kupferschiefer, profile SW-G-53; **D** – secondary oxidized section of the uppermost part of Weissligende sandstone and random distributed sulphide nests (dark blue), profile SW-G-53; **E** – red bed related maroon patches in Weissliegende sandstone, profile Pr13-7001/108; **F** – maroon patches regular in shape in Weissliegende sandstone, profile N/III/4

iments was advocated. The epigenetic origin of the second spot type is confirmed by the presence of sulphides and relics of white sandstones within the spots, and by the existence of coarse-crystalline carbonate cement unreplaced by hematite, well visible under the microscope. Hematite accompanies carbonates in sandstone cement and forms rims around the clastic grains, which are not closely packed. Hence, it has appeared in the rock after deposition of the sandstone (Pieczonka, 1998). A similar concept was presented earlier by Michalik (1979).

The Boundary Dolomite

The red-colored Boundary Dolomite was found only in the Polkowice West Field (profile PZ-G-31/2). It was described several times by Piestrzyński and Pieczonka (1997a, b), Pieczonka (1998, 2000) and Piestrzyński *et al.* (2002). Spots visible at the surface of specimens show a variety of shapes and shades of red color. Dolomite itself is light- to dark-grey. Distribution and shapes of red spots suggest their epigenetic character (Fig. 22C, D, E, F). The presence of two types of spots can be assumed, formed during the two

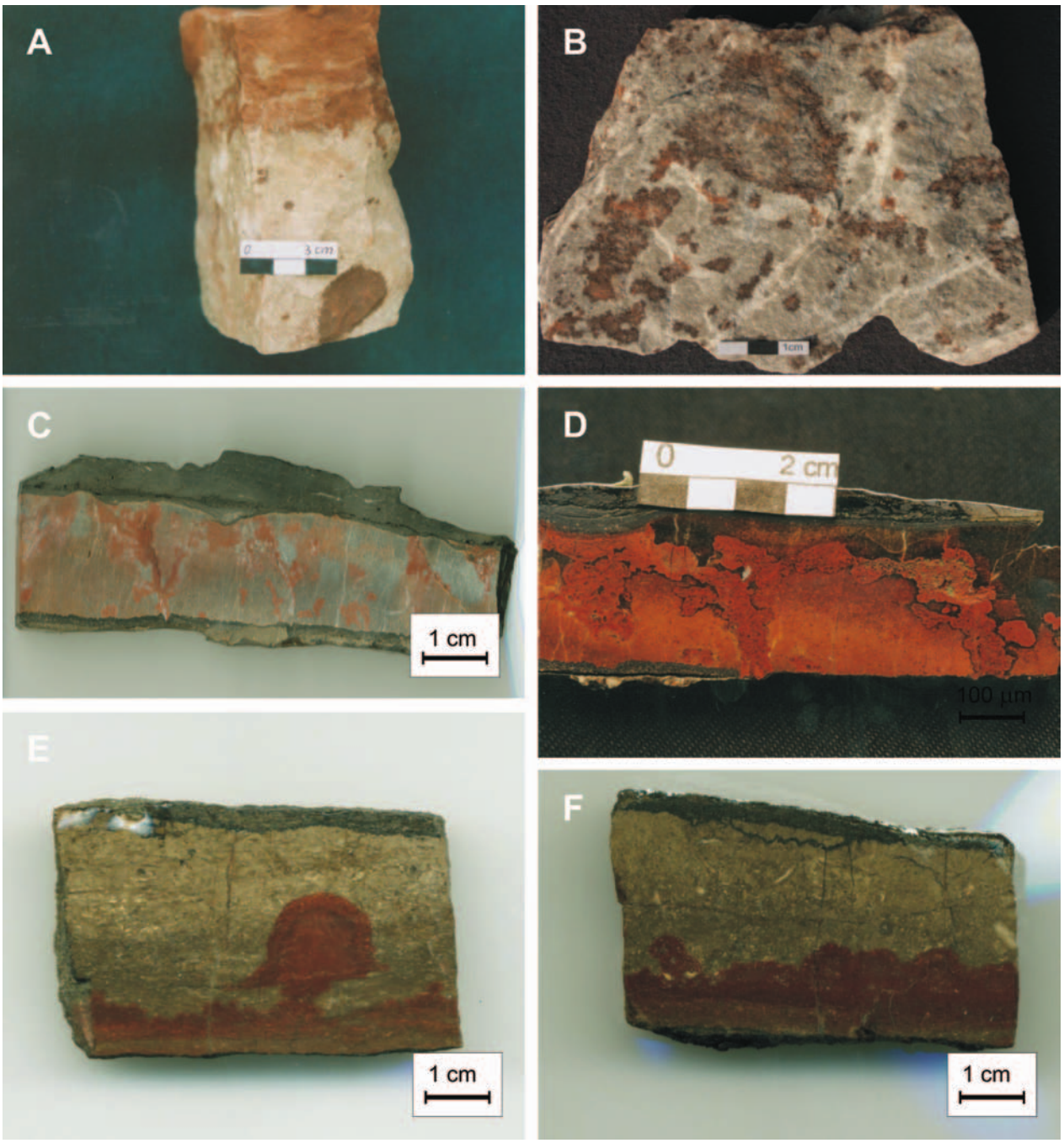

Fig. 22. Macrophotographs showing different shape and relationship of red patches in the secondary oxidized Permian strata, Polkowice Mine. **A** – regular red and maroon spots in the uppermost part of Weissliegende sandstone, profile N/III/6; **B** – random distributed red and maroon spots in Weissliegende sandstone, profile Sr18-1628; **C** – structurally controlled red spots in the boundary dolomite, profile PZ-G-31; **D** – two stages of oxidation: the older stage is characterized by red color, the youngest is structurally control and is represented by dark red (maroon), profile PZ-G-31; **E** – two stages of development of secondary oxidation systems in the boundary dolomite, profile Sr18-7002; **F** – peneconcordant red patches in the boundary dolomite, profile Sr18-7002

stages of oxidation. The first type includes spots of clearly lighter color and diffused boundaries. The second type comprises spots intensively colored, from brick-red to red with brownish shade. Microscopic observations revealed that some spots evolve from a narrow chimney located beneath the bottom surface of the Boundary Dolomite (Fig. 22C). Up the sequence the spots become wider and branch into bush-like structures. It can be assumed that these spots were sourced from beneath the Boundary Dolomite. The overlying Kupferschiefer provided a distinct barrier for solutions circulating within the Boundary Dolomite and, thus, forced the distribution of resulting red spots along the Dolomite/Kupferschiefer interface (Fig. 22C, D). In many sites spots of intensive red color cut the bright-red ones.

Results of microscopic studies supported the conclusions obtained from macroscopic observations. Under the reflected light a variety of structures and textures of Boundary Dolomite was recognized. Most part of rock is a micro-

spar of bright-red or dark-grey colors at crossed nicols. The dark-grey microspar hosts single spots of red internal reflections. Apart from pure microspar, the zones of microspar were observed full of nests and veinlets of sparite. Under the crossed nicols this zone was intensively red. Colors observed under the microscope and those seen macroscopically in specimens are identical. The bright-red spots formed presumably during the first oxidation stage of the Boundary Dolomite. At this stage most part of the rock remained unaffected, probably due to physical properties, e.g. permeability or porosity, which were among the factors decisive for the transfer of oxidizing solutions and, consequently, for the shapes of the spots. In the second oxidation stage intensively red spots were produced. Such intensive color may be an effect of either repeated oxidation of the same zones or the invasion of solutions showing much stronger oxidation potential. In these spots nests of uncolored carbonate sparite can be observed at crossed nicols (Pieczonka, 1998, 2000).

In all the zones the Boundary Dolomite hosts sulphides. The highest-grade, secondary mineralisation is related to veinlets and nests of carbonate sparite cutting these zones.

The Kupferschiefer

Morphology and color of red spots encountered in the Kupferschiefer also suggest their two-stage formation (Piestrzyński & Pieczonka, 1997a, b; Pieczonka, 1998, 2000). The red Kupferschiefer was found in profiles from the Polkowice West Field. Red-colored is mostly the dolomitic variety, rarely the clayey one.

Studies of small specimens may sometimes suggest the presence of red laminae, as described by Michalik (1979), (Fig. 23A, B). However, more detailed observations revealed that, when observed over longer distances, such ”laminae” pinch out into lenses or branch out into two or more streaks pointing in various directions and enclosed in unchanged, grey Kupferschiefer. Boundaries of the streaks are irregular and discordant in relation to the Kupferschiefer lamination. Numerous spots show various morphologies of lower and upper boundaries. The lower boundary is roughly concordant with the shale lamination whereas the upper boundary is irregular and repeatedly cuts discordantly the shale lamination (Fig. 23C). Locally, relics of grey, spot-free Kupferschiefer can be observed between the red spot and the overlying, dark-grey shale (Fig. 23C). Probably, the oxidizing solutions migrating along the lamination interfaces of the Kupferschiefer left unaffected the zones which physical properties hampered the solution transfer.

Various shades of red color are visible not only in adjacent spots but also within a single spot (Fig. 23C). Colors of neighboring spots may change from light, reddish-grey to brownish-red. Changes in shade within the individual spot are usually less pronounced and can be caused by local variations of chemical composition of the rock, e.g. changes in the initial Fe contents. The presence of adjacent spots of different colors and variable shapes together with the presence of sulphides allow the authors to conclude that these spots are epigenetic and were presumably produced from two solutions of different properties (Piestrzyński & Pieczonka, 1997a, b; Pieczonka, 1998, 2000).

In both the grey and dark-grey Kupferschiefer varieties accompanying the red shales and in the grey Kupferschiefer from sequences with red spots in the sandstones and carbonates, red internal reflexes are visible under the microscope – an effect of dispersed hematite.

The dolomite

Spots encountered in the dolomite can be intensively red, sometimes with a brick-red (Fig. 23D) and cherry-red (Fig. 23E, F) shades. Locally, both types of spots occur together or overlap each other. Cherry-red spots reveal diversified shapes and size, and rarely occur individually. Clusters of larger spots commonly form streaks parallel to the bedding planes (Fig. 10E).

Intensively red spots are often more regular and are randomly distributed in relation to the bedding, sometimes forming larger clusters. Some spots show darker rims which provide distinct boundaries between the spot and the enclosing, grey dolomite. Intensity of red color in various parts of a spot depends on the content of hematite, which concentrates particularly at the margins, forming macroscopically visible rims (Pieczonka, 1998).

In many sequences the dolomite hosts irregular, cherry-red spots of common diffused boundaries, which are accompanied by a network of fine, multidirectional, cherry-red veinlets. These are overlapped by red and brownish-red spots, and red veinlets. More intense red color appears also in the vicinity of nests filled with coarse-crystalline carbonates, which probably contain ankerite. In all the samples collected from the spotted dolomites traces of sulphides were found.

The color, shape and distribution of red spots in dolomites confirm genetic concept resulting from the analysis of the remaining types of spotted rocks. The spots are epigenetic and were formed in more than one stage of oxidation (Piestrzyński & Pieczonka, 1997a, b; Pieczonka, 1998, 2000).

Summary

Analysis of shapes, colors and distribution of red spots in various rocks was based upon macro- and microscopic observations. In the sandstone, in the Kupferschiefer and in the dolomites spots of similar structures were identified. These are: (i) spots resembling laminae, which cover vast areas, (ii) spots of variable size, very irregular in shape and showing diffused boundaries and (iii) spots of more regular, elliptical or lensoidal shapes, 1–2 cm in diameter. First two types usually show cherry-red shade whereas the latter type includes dark-red, sometimes brick-red spots. Assuming that the red “laminae” are only fragments of larger, irregular spots, the first two types can be united into one class. Finally, two types of spots were proposed, basing upon their structure and color (Pieczonka, 1998, 2000).

Skowronek (1968), Michalik (1979) and Kucha (1995) distinguished many more types of spots. The first two authors based their classification mostly on color and shape of spots, the latter – upon microscopic observations.

The results of studies summarized in the following paper do not allow to distinguish more than two types of red

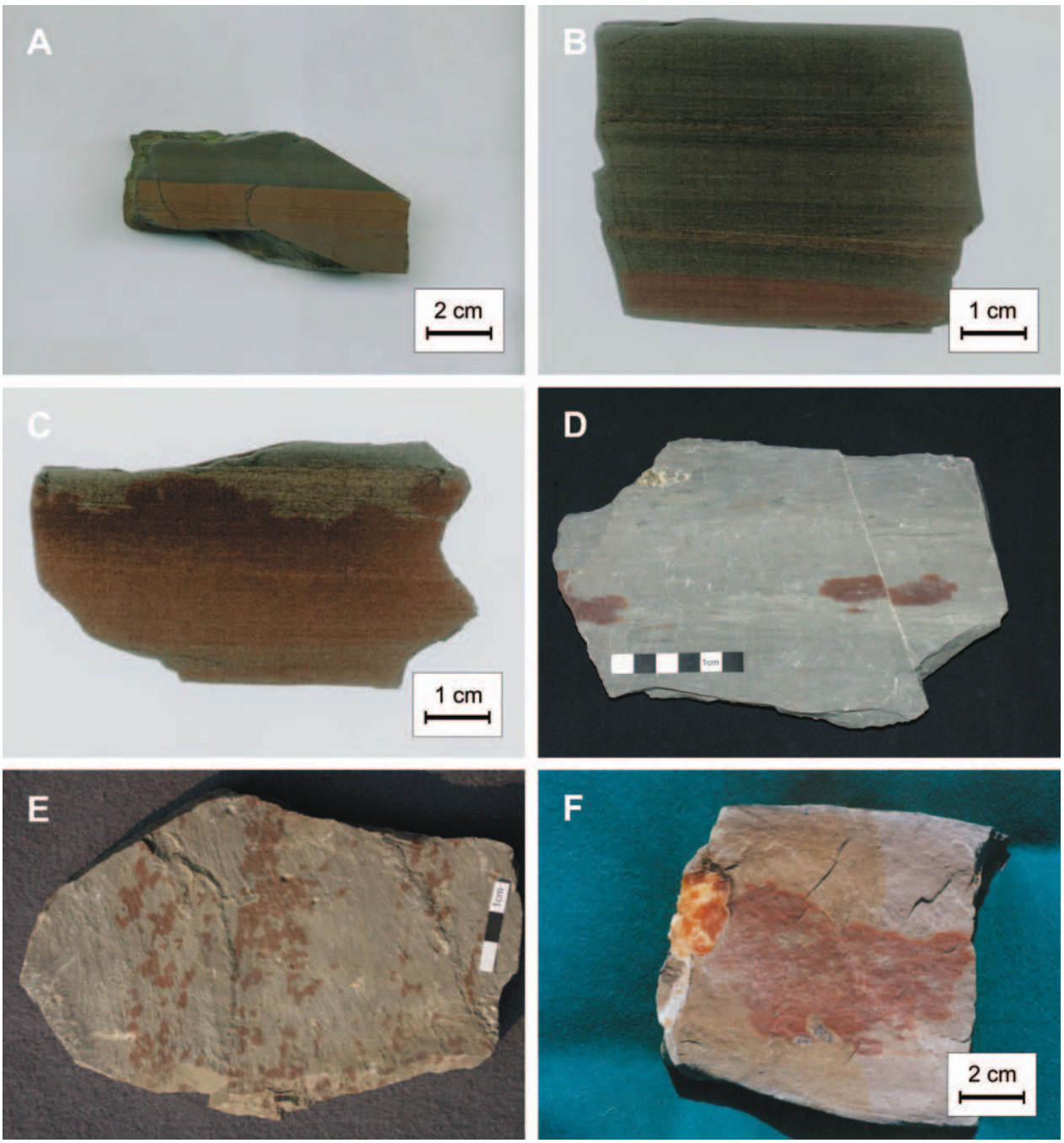

Fig. 23. Macrophotographs showing different shape and relationship of red patches in the secondary oxidized Permian strata, Polkowice Mine. **A** – regular contact of maroon shale with gray shale, profile PZ-G-31; **B** – regular maroon patches within the dark gray shale, profile PZ-22; **C** – irregular, secondary maroon patches in Kupferschiefer, profile PZ-41, **D** – maroon patches in dolomite (PZ1), profile Sr18-7002/108; **E** – random distributed maroon spots in dolomite (PZ1), profile PZ-G-2; **F** – big maroon spot on the edge of diagenetic gypsum nest, profile PZ-G-31

spots. Detailed studies support the field observations, from which the presence of two types of spots is evident, formed during two oxidation stages.

Assuming that in the undeveloped parts of the sandstone the red spots may occur, which were formed during synsedimenatry processes (marked "I"), the spots described in this paper and classified as epigenetic were marked "II". Two types of these spots were distinguished, formed probably in two stages:

II a – cherry-red spots of irregular shapes, variable size and commonly diffused boundaries,

II b – red or brick-red spots, more regular, several cm across, of sharp boundaries.

Analysis of red spots distribution in the host rocks revealed their clustering in the vicinity of various fractures and cracks or, at least, the distinct increase in number of spots at such sites. This feature is evident in the sandstones, but is rather rare in the carbonates (Fig. 23D). Moreover,

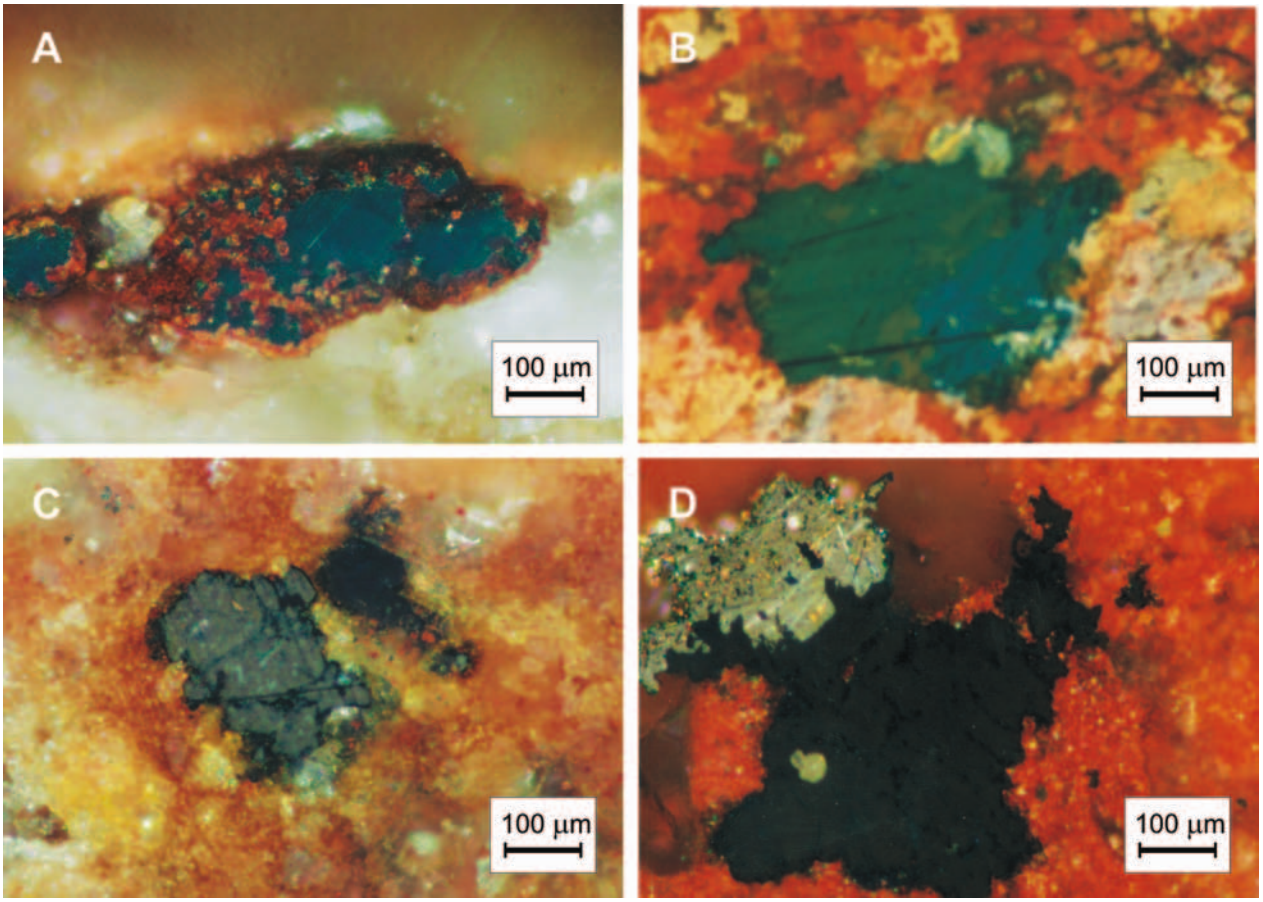

Fig. 24. Microphotographs in reflected light and crossed polars showing position of precious metals mineral assemblage from Polkowice Mine, West Field. **A** – structurally controlled oxidation of chalcopyrite (black), red is goethite, sample PZ-J-18; **B** – nest of chalcocite (black) and electrum in oxidized (red) boundary dolomite, sample PZ-G-31; **C** – nest of secondary sulphides in oxidized dolomite, sample Sz/III/2; **D** – intergrowth of bornite (black) and electrum (grey) in oxidized boundary dolomite (red), sample PZ-G-31/II

red spots expanding along the shear surfaces were observed (Fig. 21A).

Relationships between the mineralisation and the presence of red spots

Microscopic observations of sections cut from samples with red spots and samples taken from the vicinity of oxidized zones revealed that Cu sulphides generally occur in trace amounts. Larger accumulations of sulphides and their intergrowths appear rather in grey and brownish-grey rocks from these zones. Under the reflected light and at crossed nicols numerous, red internal reflexions can be observed, caused by the presence of Fe oxides (Fig. 24), first of all hematite.

Apart from ore minerals typical of the Polkowice-Sieroszowice deposit, aggregates and single crystals of native Au and electrum were observed in rocks with red spots. Microscopic studies under the reflected light at crossed nicols revealed that native phases of precious metals appear in intensively red-colored rocks (Fig. 24B, D). Most commonly native Au and electrum were noticed in the red sandstone, in the Boundary Dolomite and in the Kupferschiefer. In the spotted carbonates these phases (especially native Au) are rare.

GEOCHEMISTRY OF HOST-ROCKS FROM THE SECONDARY OXIDIZED ZONES

Jadwiga Pieczonka, Adam Piestrzyński, Maciej Kotarba & Dariusz Więcław

Geochemical studies were based upon the results of chemical analyses of 36 samples collected from the secondary oxidized zone of Cu deposit in the Polkowice-Sieroszowice area. For comparative purposes the analyzed set included also 3 samples of typical Kupferschiefer (No. RG-1 and RG-2 from the Rudna Mine and No. L-PS/89 from the Lubin Mine). Additionally, were analyzed also 2 samples of the Boundary Dolomite from the Polkowice West Field, 5 samples from the sandstones, 14 samples from the grey Kupferschiefer variety collected in the transitional zone and 12 samples of the red Kupferchiefer. All these samples (totally 33) represent the Au-bearing zone.

GEOCHEMISTRY OF THE SANDSTONES

Chemical composition of the sandstones together with basic statistical parameters was listed in Table 8. Analyzed samples were collected from the top of the sandstone, but

Table 8

Chemical composition of sandstone from SOS zone (pulp rock analyses)

	Unit	N/III/5	N/III/6	N/III/6	N/IV/6	SZ12-238/ 116	Average	σ	V	W	M
SiO_2	%	74.58	69.31	70.19	64.63	52.56	**66.25**	8.43	12.73	71.079	69.31
Al_2O_3	%	2.98	3.30	2.89	4.08	2.80	**3.21**	0.52	16.25	0.272	2.98
Fe_2O_3	%	0.38	-0.01	2.97	-0.01	-0.01	**0.66**	1.30	195.80	1.690	-0.01
FeO	%	0.35	1.08	0.35	0.71	0.44	**0.59**	0.31	53.43	0.098	0.44
TOC	%	0.00	0.00	0.00	0.05	0.03	**0.02**	0.02	143.89	0.001	0.00
MnO	%	0.024	0.119	0.023	0.295	0.289	**0.15**	0.14	90.25	0.018	0.12
MgO	%	0.16	0.19	0.17	0.37	6.50	**1.48**	2.81	190.03	7.889	0.19
CaO	%	7.30	11.64	7.96	15.22	16.32	**11.69**	4.10	35.04	16.771	11.64
Na_2O	%	0.16	0.15	0.18	0.31	0.03	**0.17**	0.10	60.03	0.010	0.16
K_2O	%	1.12	1.15	1.06	1.63	0.68	**1.13**	0.34	29.99	0.114	1.12
TiO_2	%	0.07	0.07	0.07	0.12	0.11	**0.09**	0.02	27.64	0.001	0.07
P_2O_5	%	0.09	0.04	0.05	0.07	0.06	**0.06**	0.02	31.02	0.000	0.06
S	%	3.74	3.47	4.05	0.36	0.07	**2.34**	1.95	83.47	3.809	3.47
Au	**ppb**	**7240.0**	**2270.0**	**1970.0**	**872.0**	**2900.0**	**3050.4**	2454.4	80.46	6024270	2270
As	ppm	3.00	-2.00	6.00	6.00	10.00	**4.60**	4.45	96.73	19.80	6.00
Br	ppm	3.00	2.00	3.00	8.00	1.00	**3.40**	2.70	79.47	7.30	3.00
Co	ppm	1.00	1.00	1.00	2.00	4.00	**1.40**	1.82	129.76	3.30	1.00
Cr	ppm	11.00	13.00	21.00	27.00	21.00	**18.60**	6.54	35.17	42.80	21.00
Cs	ppm	3.1	3.0	4.1	4.7	2.1	**3.40**	1.01	29.85	1.03	3.10
Hf	ppm	1.60	1.30	2.00	1.90	2.20	**1.80**	0.35	19.64	0.13	1.90
Ir	ppm	-5.0	-5.0	-5.0	-5.0	-5.0					
Mo	ppm	-5.00	-5.00	9.00	12.00	-5.00	**1.20**	8.56	712.9	73.20	-5.00
Rb	ppm	40.00	42.00	47.00	55.00	21.00	**41.00**	12.59	30.71	158.5	42.00
Sb	ppm	0.20	0.20	0.40	0.60	0.20	**0.32**	0.18	55.9	0.03	0.20
Sc	ppm	1.30	2.50	1.70	4.60	2.70	**2.56**	1.28	49.84	1.63	2.50
Se	ppm	-3.00	4.00	-3.00	-3.00	-3.00					-1
Ta	ppm	-1	-1	-1	-1	-1					
Th	ppm	1.5	1.5	1.4	2.2	1.9	**1.70**	0.34	19.9	0.12	1.50
U	ppm	2.4	-0.5	5.4	15.4	6.5	**5.84**	6.00	102.7	36.01	5.40
La	ppm	6.90	9.30	7.30	14.30	10.60	**9.68**	2.99	30.87	8.93	9.30
Ce	ppm	14.00	22.00	15.00	37.00	24.00	**22.40**	9.24	41.23	85.30	22.00
Nd	ppm	7.00	19.00	8.00	40.00	17.00	**18.20**	13.29	73.04	176.70	17.00
Sm	ppm	1.70	6.00	2.40	12.80	5.00	**5.58**	4.41	79.04	19.45	5.00
Eu	ppm	0.40	1.60	0.60	3.40	1.50	**1.50**	1.19	79.16	1.41	1.50
Tb	ppm	-0.5	0.6	-0.5	1.1	0.7	**0.28**	0.74	262.93	0.54	0.60
Yb	ppm	0.50	1.20	0.60	3.00	1.50	**1.36**	1.01	74.01	1.01	1.20
Lu	ppm	0.09	0.20	0.10	0.50	0.23	**0.21**	0.15	67.93	0.02	0.20
Ba	ppm	367.00	432.00	825.00	325.00	372.00	**464.20**	205.27	44.22	42134.70	372.00
Sr	ppm	417.00	409.00	757.00	88.00	85.00	**351.20**	279.50	79.58	78120.20	409.00
Y	ppm	8.00	18.00	8.00	42.00	20.00	**19.20**	13.90	72.39	193.20	18.00
Zr	ppm	39.00	48.00	54.00	78.00	71.00	**58.00**	16.17	27.88	261.50	54.00
Ag	ppm	1.20	-0.30	-0.30	6.20	0.80	**1.53**	2.72	176.99	7.38	0.83
Cd	ppm	-0.3	-0.3	1.2	0.8	0.8	**0.43**	0.69	159.65	0.47	0.75
Cu	ppm	324	53	77	1747	66	**453.43**	731.78	161.39	535503.20	77.31
Ni	ppm	1	6	-1	12	6	**4.97**	4.98	100.23	24.77	6.49
Pb	ppm	67	30	22	26	-3	**28.37**	24.97	88.03	623.50	25.97
Zn	ppm	46	12	19	59	22	**31.60**	19.80	62.73	392.00	21.93
Bi	ppm	-2	-2	3	-2	-2					-2.00

– standard deviation, V– coefficient of variability [%], W – variance, M – median, SOS – secondary oxidized system

only the last two samples from this list show typical composition: high and diversified CaO content (up to 16.32 wt.%) and high content of MgO (in one sample, 6.50 wt.%). In the remaining samples MgO contents are lower that those from the typical sandstone and correspond rather to values known from the unchanged Rotliegend sandstones (Mayer & Piestrzyński, 1982).

The analyzed sandstones are characterized by low organic carbon (TOC) and high Au contents (the latter up to 7.24 ppm, Tab. 8). Only two samples derived from the top layer of the sandstone contain traces of organic carbon. Typical Cu-bearing sandstone contains 0.40 wt.% TOC in average whereas the barren sandstone shows only 0.08 wt.% TOC (for n = 80 and 16, respectively) (Mayer & Piestrzyński, 1982). On the contrary, in samples from the topmost sandstone layer much higher values of the TOC were detected (up to even several wt.%). High contents of Au and, simultaneously, low contents of Ag indicate high purity of gold, typical of the zone of secondary oxidation (Piestrzyński *et al.*, 2002).

Three analyzed samples contain significant amounts of total sulphur (S_c), which is presumably the sulphate sulphur, as sulphides were not observed. Contents of FeO are similar to those of the Cu-bearing sandstones whereas Fe_2O_3 ones are lower than those analyzed in the typical red sandstone (except for a single sample) (Piestrzyński *et al.*, 2002). Contents of trace elements: Cu, Ni, Co, Mo, Sb, As, U, Th, Pb and Zn are low and comparable with those typical of the barren sandstones (Tab. 8) (Mayer & Piestrzyński, 1982) whereas Ba and Sr contents are high (average values: 464 and 351 ppm, respectively) (Tab. 8). Such contents are much higher than those observed in both the grey and the red Kupferschiefer varieties (see Tab. 9, 10). Among the REE only La and Ce occur in higher amounts.

GEOCHEMISTRY OF THE GREY AND THE TYPICAL KUPFERSCHIEFER VARIETIES

Chemical composition of the Kupferschiefer samples is shown in Table 9. Average values of main components – SiO_2 and Al_2O_3 are higher than those for the typical Kupferschiefer (36.04 and 12.34 wt.%, respectively).

Average contents of Fe_2O_3 and FeO are 0.74 and 1.30 wt.%, respectively (Tab. 9). FeO values in the studied samples are more than two times higher than those for typical Kupferschiefer, for which average FeO content is 0.55 wt.% whereas Fe_2O_3 values are somewhat lower than average for the black Kupferschiefer variety from the Rudna Mine (0.98 wt.% for dla n = 82) (Mayer & Piestrzyński, 1982). Variability coefficients for these values are also high (Tab. 9) and reflect the true variability (see Fig. 25).

Contents of two components: MgO and CaO, which represent the carbonatization degree of the rocks are diversified. Samples from the transitional oxidation zone reveal CaO values about 2 wt.% higher and MgO values about 0.7 wt.% lower than average (see Tab. 9 and Tab. 6 in Mayer & Piestrzyński, 1982).

The TOC content is low (4.33 wt.%) even if typical, organic-carbon-rich Kupferschiefer samples were included. For comparison, the average TOC content in the Kupferschiefer from the Rudna Mine is 7.32 wt.% (Mayer & Piestrzyński, 1982). In the cumulative diagram (Fig. 26) the TOC values for the black Kupferschiefer variety clearly shift from those representing the samples from secondary oxidation zone.

Average Cu content in the grey Kupferschiefer variety is 2.36 wt.% (Tab. 9) but this value is affected by three samples originating from the Cu deposit where metal contents exceed 10 wt.%. If peak samples are excluded, average Cu content in the grey Kupferschiefer is 0.72 wt.%, which corresponds to values encountered in the Kupferschiefer from the transitional zone (Piestrzyński *et al.*, 2002).

Au contents in analyzed samples are lower than those found in typical grey Kupferschiefer described by Piestrzyński *et al.* (2002). It can be explained by the obvious influence of three negative samples with Au contents below the detection limit (Tab. 9). If these results are eliminated the average Au content is 2.43 ppm, i.e. it is about 1,000 times higher than those found in the typical Kupferschiefer (see chapter "*Geochemistry of Au and PGE*") (Fig. 27). On the contrary, Ag content in the grey Kupferschiefer is only 4 times lower than that of typical Kupferschiefer, which clearly indicates geochemical fractionation of these metals in the copper zone and in the secondary oxidation zone (Fig. 28).

Contents of U and Th (Tab. 9) correspond to those cited by Piestrzyński (1990), except for a single sample which rises the average value by 10 times as U content in it is 1,630 ppm (Tab. 9). This sample shows also high Se value (1,660 ppm, Tab. 9). Coexistence of these two elements in hydrothermal deposits is a normal feature.

Average Ba and Sr contents are 227 and 139 ppm, respectively, being distinctly lower than those quoted from the red sandstones (Tab. 8) and somewhat lower than found in the red Kupferschiefer variety (Tab. 10).

The REE contents exceed 2–4 times those in the sandstone. This difference results from both the depositional environment and qualitative composition of main minerals. Average La and Ce contents (34.55 and 44.82 ppm, respectively) (Tab. 9) are higher than those presented by Janczyszyn *et al.* (1986).

Contents of main metals is shown in Figs 29–31.

GEOCHEMISTRY OF THE RED KUPFERSCHIEFER VARIETY

Chemical composition of the red Kupferschiefer shown in Tab. 10 demonstrates differences in contents of both the main components and the trace elements in comparison with the grey Kupferschiefer (see Tab. 9 and 10). The red Kupferscheifer shows lower contents of SiO_2, Al_2O_3, TOC, Cu, Ag and S, as well as apparently higher contents of Au (see Fig. 27), MgO, CaO and Fe_2O_3 (Fig. 25).

Variability of main components results from differences in mineralogical composition. The red Kupferschiefer variety is distinctly lower in carbonates and resembles rather a marl. Average Fe_2O_3 content is about 5 times higher than that in the grey Kupferschiefer (Fig. 25).

Table 11

Contents of main trace elements in selected samples from the zone of secondary oxidation [in ppm] (samples No. PZ/G-31-1 to -3 after Piestrzyński *et al.*, 2002)

	N-III/6 red sandstone	P-Z-J6 red Kupferschiefer	G-125,d red Kupferschiefer	Pz/G-31/1 red sandstone	Pz/G-31/2 red Kupferschiefer	Pz/G-31/3 grey Kupferschiefer
Au	16.305	50.786	2.342	14.30	0.043	1.470
Ag	1.545	31.013	3.9807	n.a.	n.a.	n.a.
Cu	11.843	59.528	31.1434	76.000	2,264	573
V	22.569	133.313	1,347.990	48.000	435	1,461
As	18.536	29.035	43.4759	n.a.	n.a.	n.a.
Se	25.573	10.095	4.7612	≤3.0	5.000	42.000
Te	0.0	0.039	0.0	n.a.	n.a.	n.a.
Pt	0.163	0.208	0.5307	≤0.227	0.609	0.750
Pd	1.613	1.145	1.795	0.400	0.389	0.250
Ru	0.163	0.072	0.0343	≤0.050	≤0.005	0.011
Rh	0.049	0.016	0.0179	0.0037	0.0006	≤0.001
Os	0.214	0.104	0.0686	≤0.020	≤0.002	≤0.002
Ir	0.0326	0.0094	0.0093	≤0.001	0.0009	0.002
Re	0.0	0.0228	0.1483	n.a.	n.a.	n.a.
Pb	9.9546	9.5744	17.0937	n.a.	n.a.	n.a.
Bi	0.2574	0.7076	1.1708	n.a.	n.a.	n.a.

n.a. – not analyzed

The average TOC content in the red Kupferschiefer is about 10 times lower than that in the black Kupferschiefer (Mayer & Piestrzyński, 1982) and about 5 times lower than that in the grey Kupferschiefer (see Tabs. 9 and 10). Such differences are an effect of secondary oxidation of the organic matter. In the central parts of oxidized zones, which represent extreme conditions, the TOC contents drop down to even below 0.01 wt.% (Piestrzyński *et al.* 2002). It is confirmed by negative TOC/Au correlation observed in all sample populations (Tab. 12). The oxidation of organic matter is described in details in the following chapter as, in author's opinion, this is the key to the understanding of processes operating in the oxidized zones.

Average Cu content is 1,070 ppm at variability coefficient 81% (Tab. 10). The grey Kupferschiefer contains 3 times higher contents of Cu and its variability coefficient is 2 times higher, which points out to quantitative changes during the leaching of copper when secondary oxidation of deposit proceeded (Pieczonka 1998; Piestrzyński *et. al.*, 2002). Thus, low Cu and TOC values can be indicative for oxidizing environment and, consequently, can be good exploration guides to zones enriched in precious metals.

Average Au content in the red Kupferschiefer (15.419 ppm, Tab. 10) is much higher than that for the grey Kupferschiefer (Tab. 9). Comparison of metal contents in samples from the oxidized zones reveal high variability of Au values in the red Kupferschiefer (e.g., samples No P-Z-J6 and G-125 d; Tab. 11), which may change from a few ppm to over 100 ppm (Piestrzyński *et al.*, 2002). Sample No. G-125 d (G-125 exploratory well, No. G-12 mining sector, the Polkowice West Field) was collected in the barren (Cu-free) zone. Negative Cu-Au correlation supports the hypothesis on the introduction of gold into the red Kupferschiefer during the leaching of copper (Piestrzyński & Pieczonka, 1998).

Average U and Th contents in the red Kupferschiefer remain at the same level as are the average values for the whole deposit (see Piestrzyński, 1990). Therefore, it is concluded that uranium and its radiation do not influence the enrichment in precious metals. Catalytical role of U was described in many papers (e.g., Kucha & Przybyłowicz, 1999). In authors opinion, U may play only a marginal role

Table 12

Linear correlation coefficients of Au with selected compounds and elements

	Full population n = 36	Red Kupferschiefer n = 14	Grey and black Kupferschiefer n = 17
	Au	Au	Au
Cu	-0.1528		
Ag	-0.1292	0.1367	-0.2553
FeO	0.05809	-0.0010	0.0035
Fe_2O_3	0.24805	0.00716	0.00523
TOC	-0.1991	-0.1380	-0.1369
As	-0.1391		
Th	-0.0321		
U	0.02073	-0.3522	0.53585

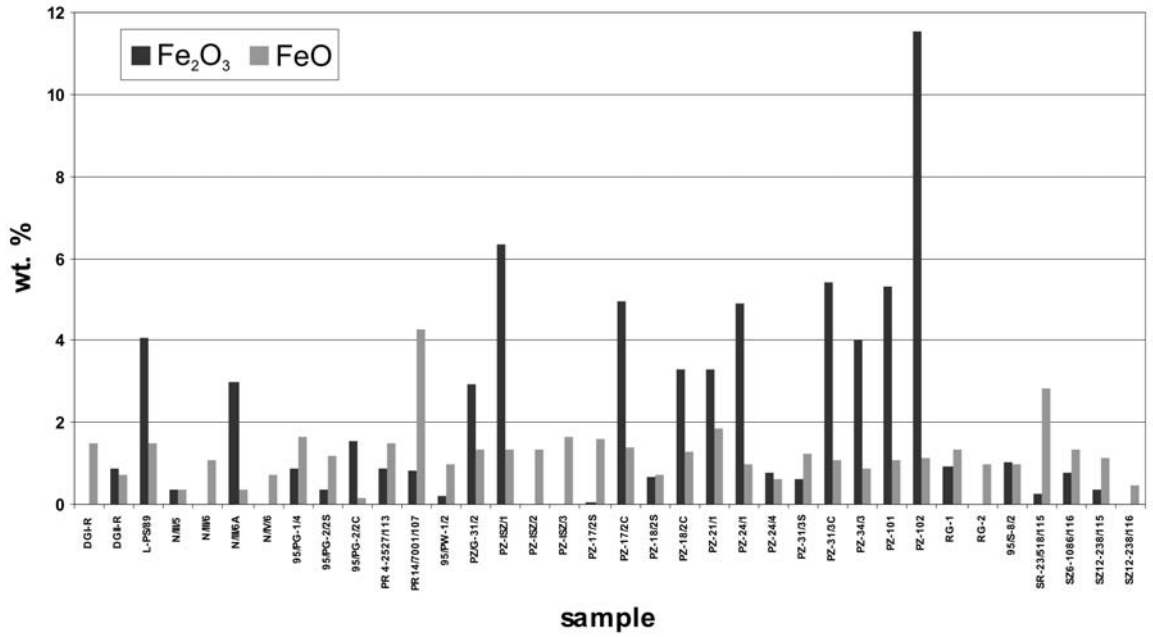

Fig. 25. Comparison of Fe_2O_3 and FeO contents in some investigated samples

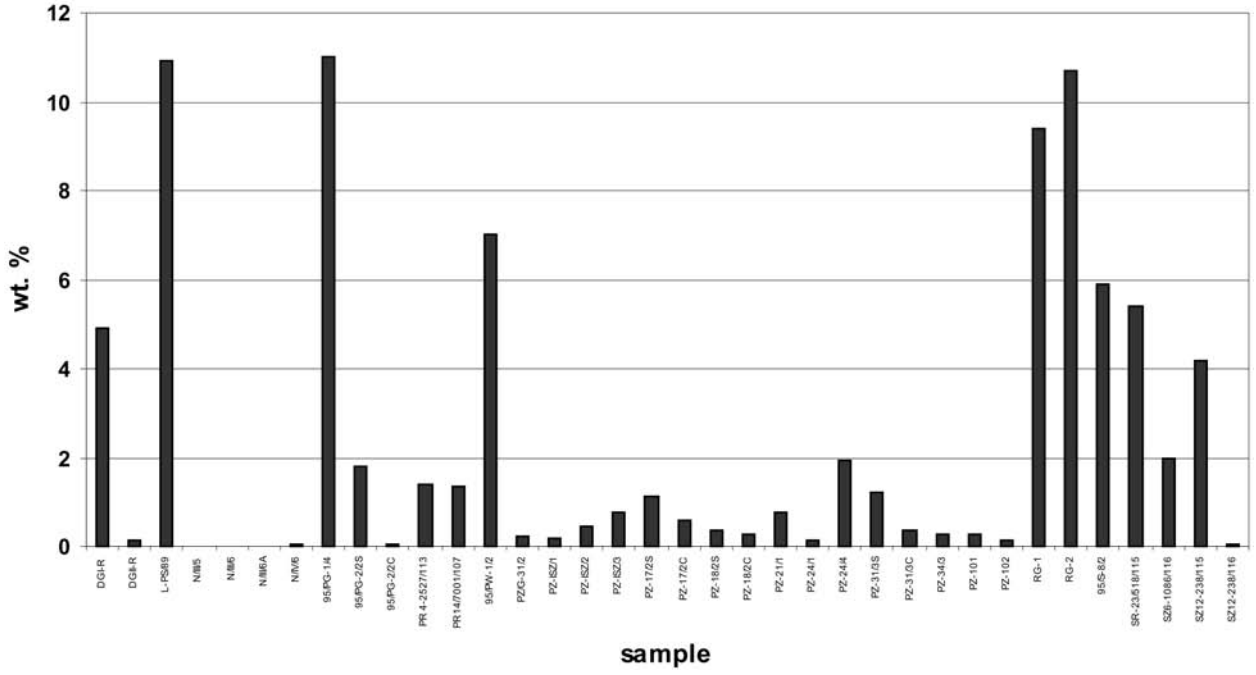

Fig. 26. Total organic matter content in the investigated samples

in Au accumulation in the transitional zone and at the contact with the Cu deposit (from the side of Cu orebody). The important U-Au correlation was found in only a few samples from the grey Kupferschiefer variety (Tab. 12). In the oxidized zone U forms the uranyl ion, which is extremely mobile compound.

Average Ba and Sr contents in the red Kupferschiefer variety are comparable with those from the grey one. It is suggested that both elements, which are presumably concentrated in two minerals: barite and strontianite (as demonstrated by the EDS analyses) either do not participated in hydrothermal processes or have crystallized as early phases.

The studied red Kupferschiefer samples contain increased amounts of La and Ce in comparison to the grey Kupferschiefer (Tab. 10). The presence of REE can be attributed to diagenetic phosphates.

Average contents of Pt and Pd in the economic-grade Au-bearing zone (cut-off grade 0.5 ppm, Piestrzyński *et. al.*, 2002) are 0.132 and 0.056 ppm, respectively. However, in a few samples Pt values up to 6 ppm were noticed. Contents

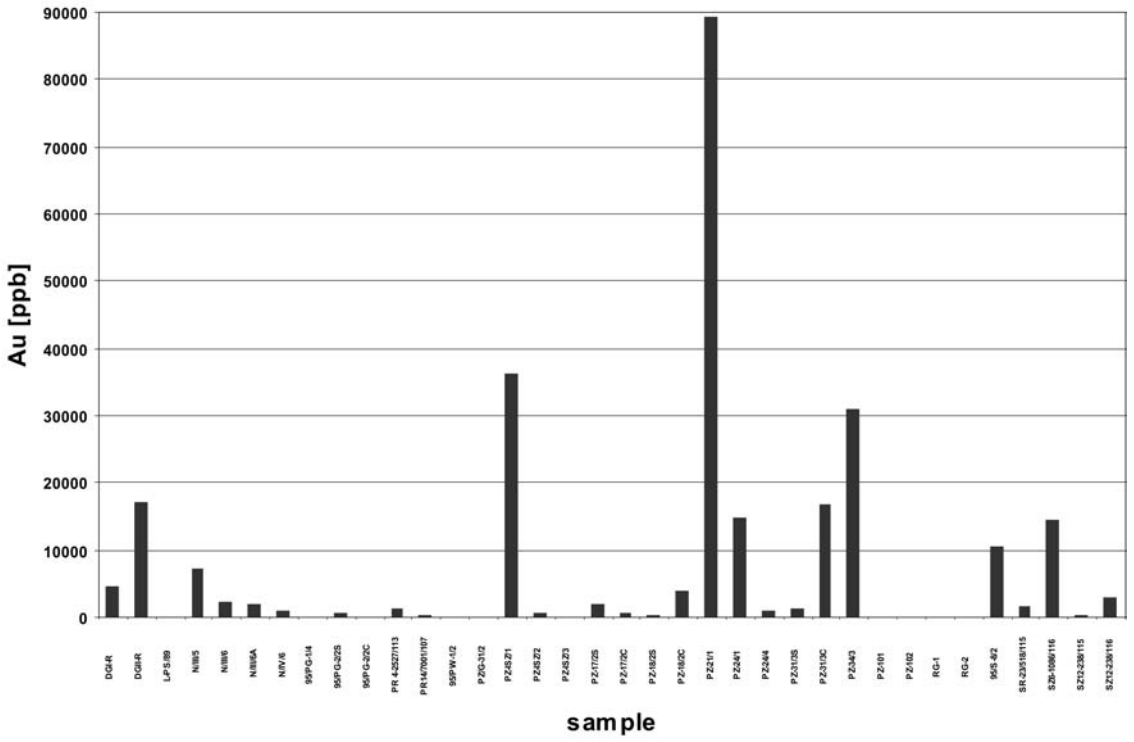

Fig. 27. Gold content in the investigated samples

of all PGE and Au were referred to concentrations of other elements (see Tab. 11). The obtained values differ significantly from those quoted for the so called "precious-metals-rich Kupferschiefer" (see Kucha, 1982a, b). The studied samples originate exclusively from the zone of secondary oxidation of the deposit. It is evident that concentrations of precious metals are related to the top part of the sandstone and to the red Kupferschiefer (see also chapter "*Distribution...*"). The Pd minerals (mostly arsenides) were identified and described in details by Kucha (1982a, b) and in chapter "*Mineralogy and geochemistry...*" of this paper. These disseminated minerals are presumably responsible for Pd concentration. On the contrary, Pt form mostly substitutions in other minerals whereas its own phases are rare (see chapter "*Mineralogy and geochemistry...*"). However, Pt contents are higher than Pd ones, which may suggest that the main Pt carriers have not been identified, as yet (e.g. hydroxides, Oberthür *et al.*, 2003).

GEOCHEMICAL CHARACTERIZATION OF ORGANIC MATTER FROM THE KUPFERSCHIEFER

Organic geochemical studies were carried out on 45 samples (Tab. 13) in order to determine content, genetic type and maturity of dispersed organic matter as well as to identify secondary processes operating in sampled horizons (oxidation, water washing, biodegradation, etc.). Results of wide-range applied analyses are presented in Tables 13 to 18. The values of geochemical indices from routine Rock-Eval pyrolysis vary as follows (Tab. 13): total organic carbon (TOC) from 0.00 to 12.7 wt.%, S_2/S_3 ratio from 0.1 to 103, production index (PI) from 0.05 to 0.67, hydrogen index (HI) from 4 to 408 mg HC/g TOC, oxygen index (OI) from 4 to 462 mg CO_2/g TOC, T_{max} temperature from 434 to 488°C. These values show to a large variability of dispersed organic matter properties in the investigated strata. Samples were classified to the three oxidation zones based on criteria proposed by Więcław *et al.* (2007): reduced (7

Table 14

Content of inorganic sulphur forms

Sample code	Lithology	Zone	Sulphur content (wt. %)		
			elemental	sulphate	pyritic
95/PG-1/4	black shale	R	0.0	0.1	0.5
PZ-Isz/3	drawer-type shale (black)	T	0.0	0.04	traces
RG-2	pitch	T	0.0	0.5	0.7
JB-3 ł cz	red shale	O	0.0	traces	0.06
JB-3 ł sz	grey shale	O	0.0	0.07	traces
PZ-Isz/1 AP5	drawer-type shale (red)	O	0.0	0.07	0.06

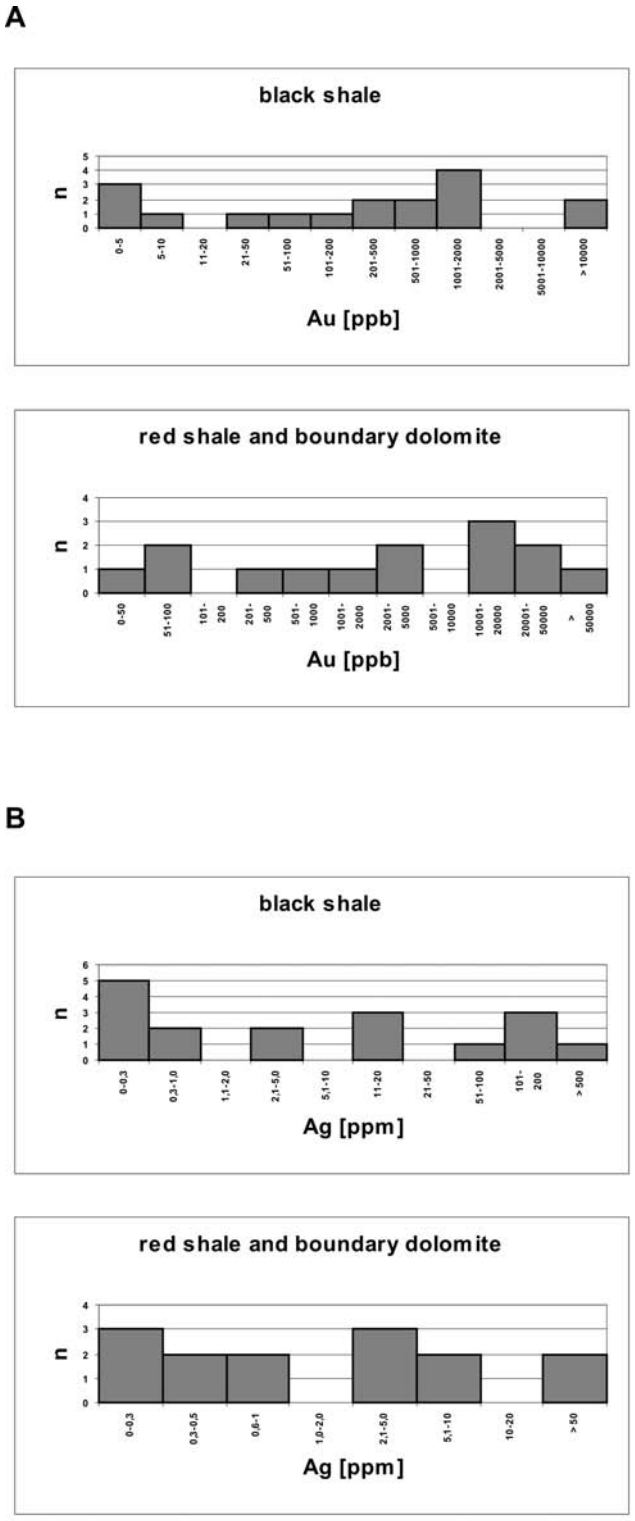

Fig. 28. Histograms showing distribution of Au (**A**) and Ag (**B**) in black shales and red shales and red boundary dolomites, respectively

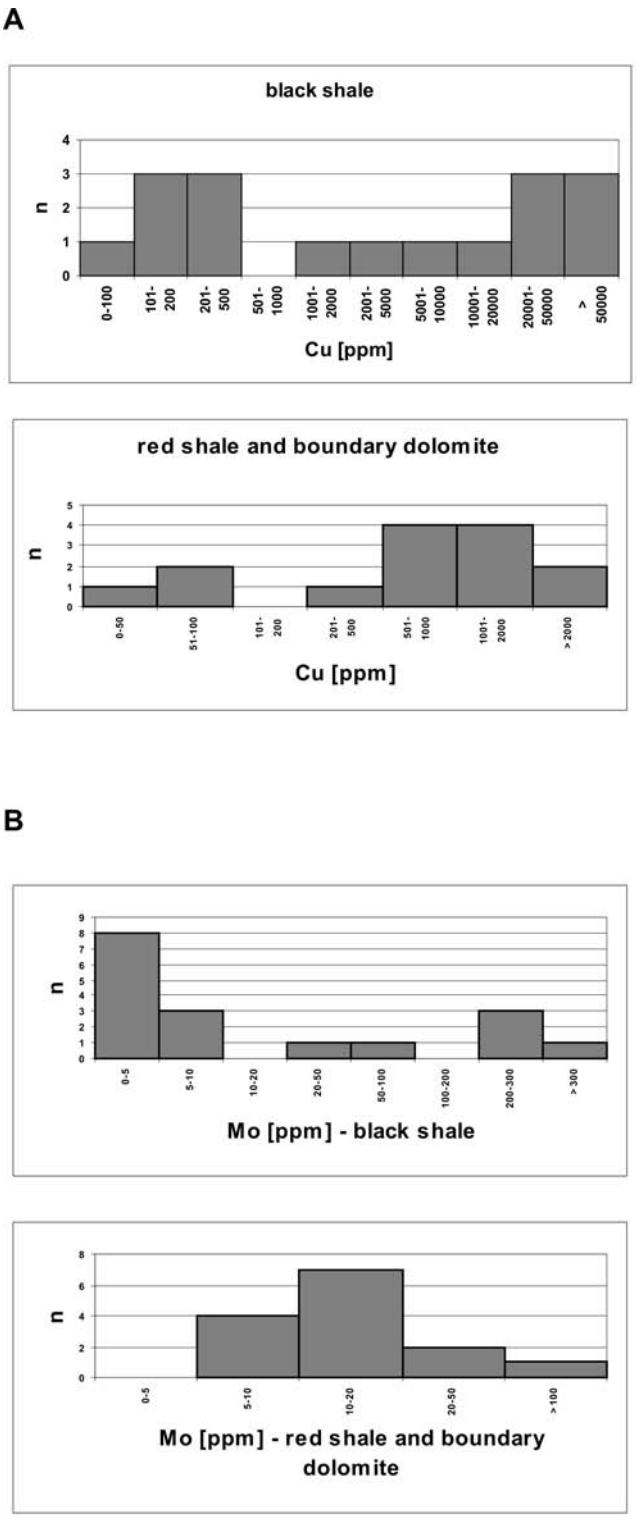

Fig. 29. Histograms showing distribution of Cu (**A**) and Mo (**B**) in black shales and red shales and red boundary dolomites, respectively

samples), transitional (12 samples) and oxidized (26 samples) (Tab. 13).

The studied Kupferschiefer strata reveal variable contents of the TOC – from horizons lean in organic carbon to those containing up to 12.7 wt.% (sample No. RG-2, Tab. 13, Figs 32 and 33). Generally, the low values prevail (below 1 wt.%). The low TOC values are characteristic of secondary oxidized copper-bearing rocks and red-colored strata indicative of the oxidizing environment (Więcław *et al.*, 2007; Piestrzyński *et al.*, 2002). Free hydrocarbons

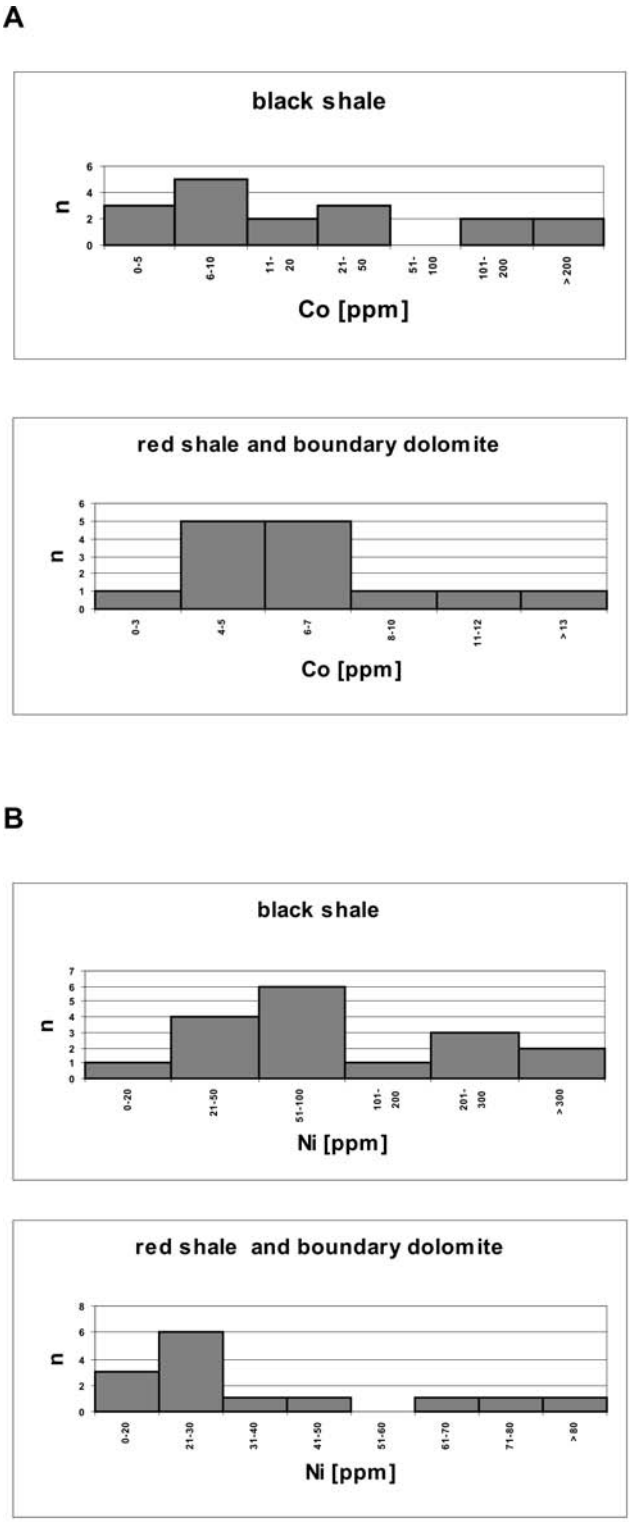

Fig. 30. Histograms showing distribution of Co (**A**) and Ni (**B**) in black shales and red shales and red boundary dolomites, respectively

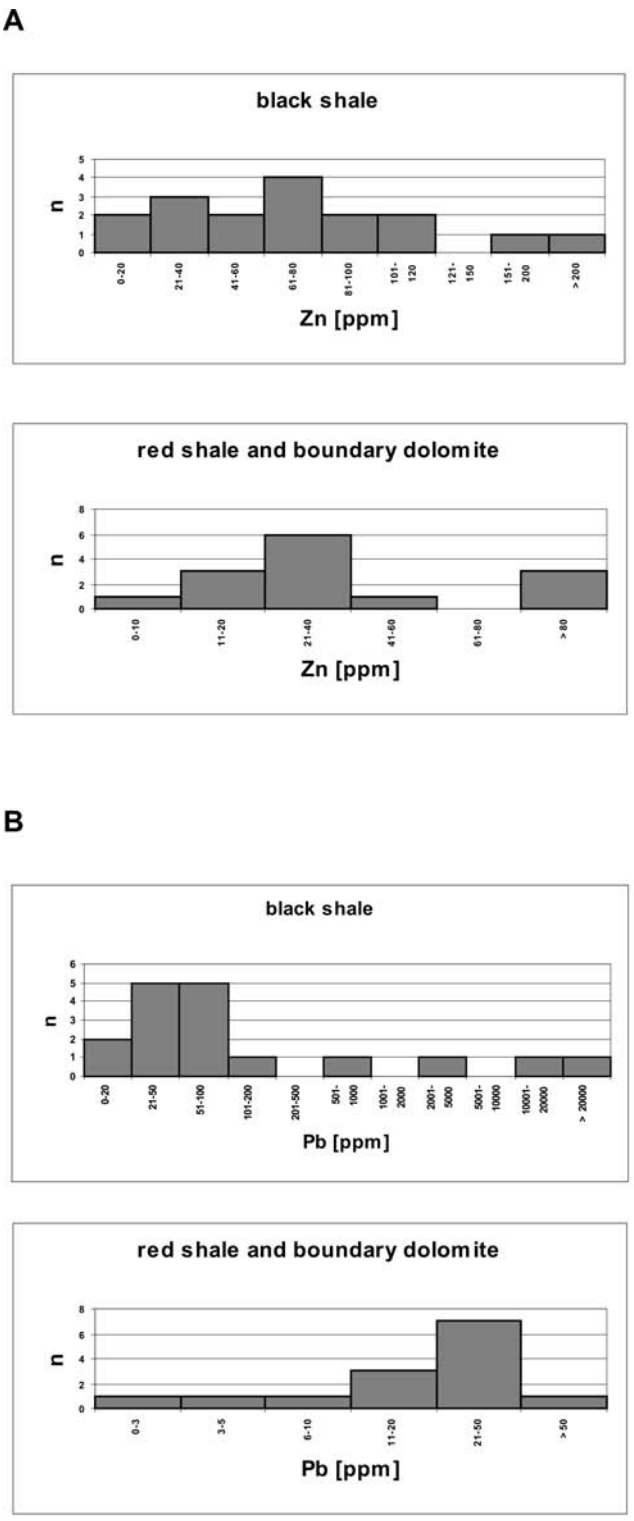

Fig. 31. Histograms showing distribution of Zn (**A**) and Pb (**B**) in black shales and red shales and red boundary dolomites, respectively

present in the rock are syngenetic with the kerogen, although samples W/IV/6 and DgI-R contain some of epigenetic hydrocarbons (Fig. 32) which is confirmed by a high value of production index (Fig. 33A). Correlation of the hydrogen index HI versus the TOC content (Fig. 34A) indicates that the highest HI values (over 200 mg HC/g TOC) correspond to the highest TOC values (samples Nos. DgI-R, L-PS/89, 95/PG-1/4, RG-1 and 95/PW-1/2), whereas the lowest HI values are connected with the samples poor in organic carbon. The samples cited above (DgI-R, L-PS/89,

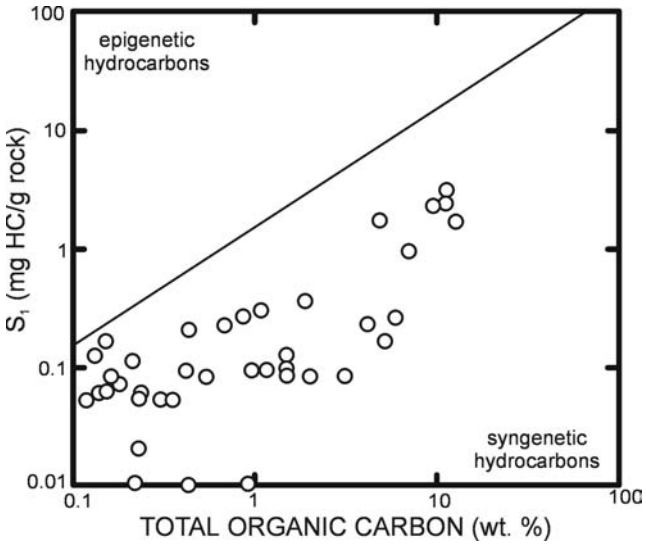

Fig. 32. Identification of epigenetic hydrocarbons in terms of S_1 and total organic carbon. Position of the genetic boundary after Smyth (1994)

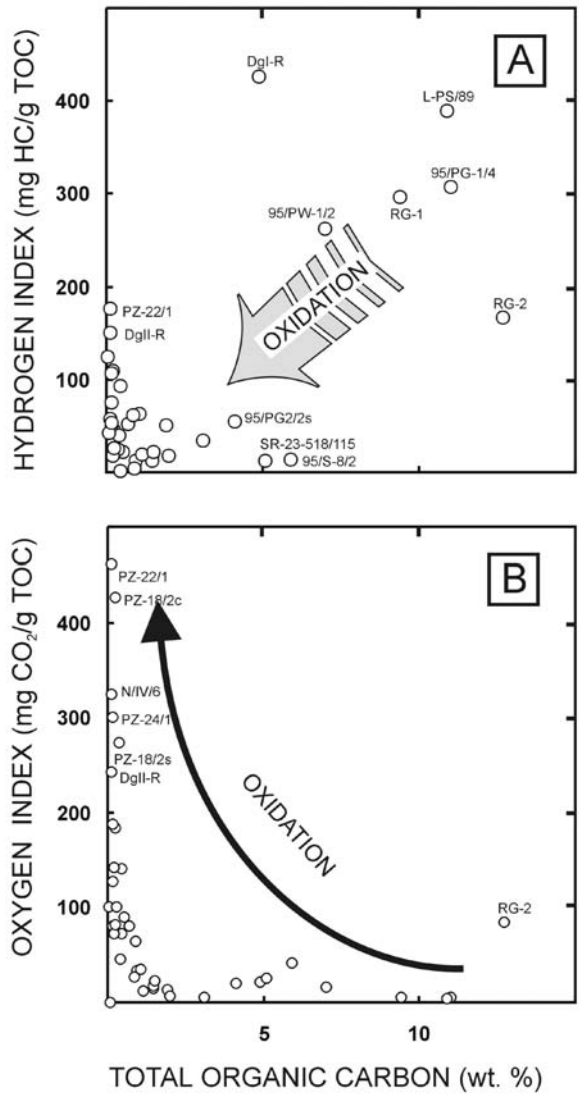

Fig. 33. **A** – hydrogen index; **B** – oxygen index vs. total organic carbon

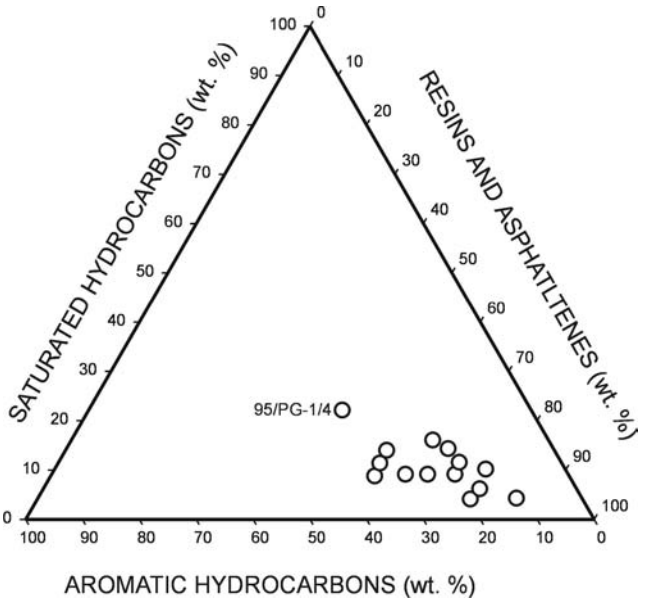

Fig. 34. Ternary diagram of bitumen composition of Kupferschiefer shales

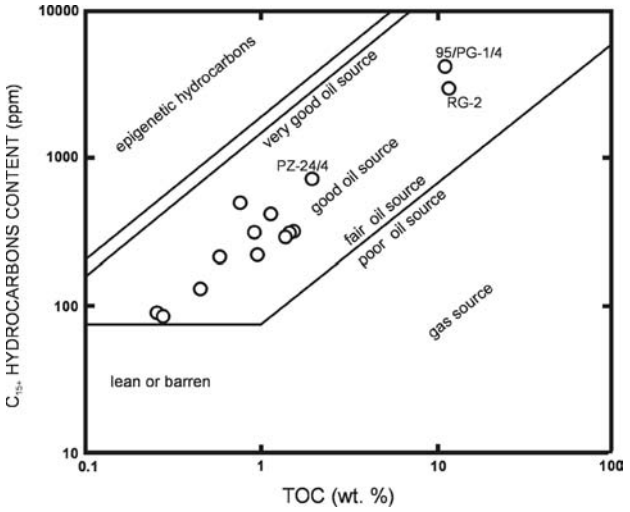

Fig. 35. Source possibility of Kupferschiefer shales in terms of hydrocarbons and TOC content according to the categories after Hunt (1979) and Leenheer (1984)

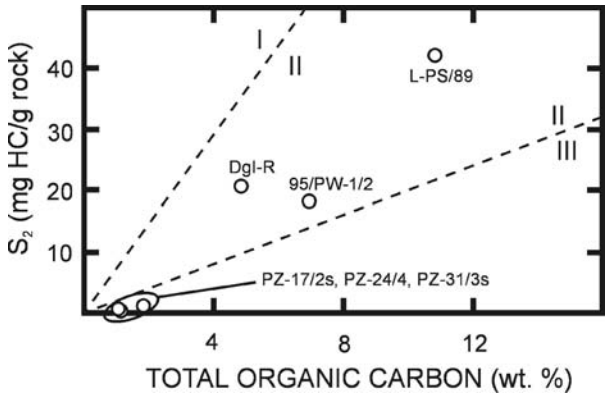

Fig. 36. Kerogen type in terms of residual hydrocarbon potential (S2) and total organic carbon according to the categories of Langford and Blanc-Valleron (1990)

Table 15

Distribution of n-alkanes and isoprenoids

Sample code	95/PG-1/4	PR14/7001/107	PZ-17/2s	PZ-I sz/3	RG-2	JB-2	JB-3 ≤ cz	JB-3 ≤ sz	PZ-101	PZ-17/2c	PZ-I sz/1 AP5
Zone	R	T	T	T	T	O	O	O	O	O	O
n-C_{13}	0.17	0.00	0.00	0.00	0.00	0.00	0.00	0.00	0.00	0.00	0.00
n-C_{14}	2.55	0.00	0.00	0.00	0.11	0.00	0.00	0.00	0.00	0.00	0.00
n-C_{15}	8.18	0.06	0.09	0.11	2.10	0.03	0.04	0.77	0.21	0.05	0.02
n-C_{16}	10.53	1.12	0.11	0.09	7.04	0.16	0.05	3.95	3.80	0.09	0.84
n-C_{17}	11.39	6.08	2.53	0.29	10.77	1.03	0.09	6.40	10.59	2.44	5.23
n-C_{18}	9.33	14.58	16.28	2.59	10.94	3.35	1.04	8.87	14.76	15.48	8.84
n-C_{19}	7.32	9.70	13.11	6.46	9.73	6.97	3.75	8.77	10.55	13.20	8.29
n-C_{20}	5.13	10.04	8.91	9.44	6.85	7.98	8.56	6.67	5.42	6.95	6.93
n-C_{21}	3.68	7.28	7.31	12.07	5.25	9.46	11.73	5.45	2.89	5.64	6.73
n-C_{22}	3.17	5.30	5.08	11.05	4.53	8.27	8.76	5.07	3.32	4.42	5.42
n-C_{23}	2.64	4.61	4.11	9.44	3.62	6.75	7.59	5.43	4.71	4.11	4.55
n-C_{24}	2.21	3.82	3.63	7.14	2.67	5.60	6.86	4.90	3.16	4.25	3.74
n-C_{25}	1.80	3.30	3.28	4.69	2.20	6.27	6.04	4.36	4.06	4.25	3.32
n-C_{26}	1.67	3.93	4.53	6.14	2.14	6.70	6.54	4.11	3.02	5.20	3.49
n-C_{27}	1.61	3.19	5.13	8.03	1.66	6.71	9.83	2.39	1.93	6.09	4.34
n-C_{28}	1.37	3.67	2.43	3.97	1.26	4.83	5.21	2.78	2.52	3.68	3.36
n-C_{29}	1.01	4.62	5.13	7.92	0.97	6.06	8.09	2.03	2.41	5.02	4.69
n-C_{30}	0.95	2.21	1.70	1.89	0.75	4.94	3.18	4.32	1.35	2.19	3.61
n-C_{31}	1.22	4.38	3.73	5.55	1.62	6.71	7.06	5.58	3.78	3.06	5.17
n-C_{32}	1.36	0.67	1.45	1.44	0.47	2.19	2.10	5.02	1.83	1.00	2.84
n-C_{33}	0.38	1.01	0.00	0.00	0.39	3.43	3.09	1.20	0.86	1.38	3.58
n-C_{34}	0.61	0.00	0.00	0.00	0.26	0.00	0.00	1.58	0.00	0.00	3.53
n-C_{35}	0.00	0.00	0.00	0.00	0.22	0.00	0.00	0.00	0.00	0.00	1.37
n-C_{36}	0.00	0.00	0.00	0.00	0.00	0.00	0.00	0.00	0.00	0.00	1.85
n-C_{37}	0.00	0.00	0.00	0.00	0.00	0.00	0.00	0.00	0.00	0.00	1.52
i-C_{15}	0.30	0.00	0.00	0.00	0.00	0.00	0.00	0.00	0.00	0.00	0.00
i-C_{16}	2.42	0.00	0.00	0.00	0.39	0.00	0.00	0.00	0.00	0.00	0.00
i-C_{18} (Norpristane)	4.96	0.00	0.00	0.00	5.77	0.00	0.00	1.62	2.17	0.00	0.52
i-C_{19} (Pristane)	8.48	2.64	1.97	0.16	11.56	0.42	0.04	3.48	5.95	2.15	2.25
i-C_{20} (Phytane)	5.54	7.78	9.49	1.50	6.73	2.14	0.37	5.30	10.72	9.35	3.97
Ratios											
$CPI_{(Total)}$	1.02	0.87	0.97	1.22	1.02	1.11	1.26	0.94	1.01	0.97	1.05
$CPI_{(17-23)}$	1.02	0.75	0.78	1.01	0.99	1.04	1.05	0.98	0.90	0.82	0.94
$CPI_{(25-31)}$	1.04	1.19	1.59	1.75	1.10	1.17	1.64	0.84	1.20	1.33	1.27
i-C_{19}/i-C_{20}	1.53	0.34	0.21	0.11	1.72	0.20	0.11	0.66	0.55	0.23	0.57
i-C_{19}/n-C_{17}	0.74	0.43	0.78	0.56	1.07	0.41	0.42	0.54	0.56	0.88	0.43
i-C_{20}/n-C_{18}	0.59	0.53	0.58	0.58	0.62	0.64	0.36	0.60	0.73	0.60	0.45

R – reduced; T – transitional; O – oxidized;
CPI(Total) = [(n-C17+n-C19+...+n-C27+n-C29)+(n-C19+n-C21+...+n-C29+n-C31)]/2*(n-C18+n-C20+...+n-C28+n-C30);
CPI(17-23) = [(n-C17+n-C19+n-C21)+(n-C19+n-C21+n-C23)]/2*(n-C18+n-C20+n-C22);
CPI(25-31) = (n-C25+n-C27+n-C29)+(n-C27+n-C29+n-C31)/2*(n-C26+n-C28+n-C30)

Table 16

Elemental composition of kerogen

Sample code	Zone	S Total (wt. %)	Fe Total (wt. %)	Elemental composition (wt. %, daf)					Atomic ratios			
				C	H	O	N	S	H/C	O/C	N/C	S/C
PZ-Isz/3	T	3.3	0.5	77.7	3.4	8.1	7.3	3.5	0.53	0.08	0.080	0.017
RG-2	T	5.4	0.1	79.6	5.4	7.7	1.4	5.9	0.82	0.07	0.015	0.028
PZ-Isz/1 AP5	O	6.6	2.1	77.4	3.2	11.7	3.1	4.7	0.50	0.11	0.034	0.023

daf - dry ash-free basis, T - transitional, O - oxidized

Table 17

Maturity of bitumens calculated from distribution of methylphenantrenes

Sample code	Lithology	Zone	P	3-MP	2-MP	9-MP	1-MP	MPI 1	MPR	Rcal.(MPI)
			(sum = 100%)							(%)
95/PG-1/4	black shale	R	33.8	11.1	16.0	23.2	15.9	0.6	1.0	0.7
PR14/7001/107	dark brown shale	T	56.5	20.0	12.5	6.0	5.0	0.7	2.5	0.8
PZ-17/2s	dolomitic shale (grey)	T	31.4	10.0	21.4	21.2	16.0	0.7	1.3	0.8
PZ-Isz/3	drawer-type shale (black)	T	41.9	13.8	23.4	11.0	9.9	0.9	2.4	0.9
RG-2	pitch shale	T	53.8	7.1	12.6	15.5	10.9	0.4	1.2	0.6
JB-2	grey shale	O	39.0	31.5	14.6	9.2	5.6	1.3	2.6	1.1
JB-3 ≤ cz	red shale	O	61.0	12.9	13.1	7.3	5.8	0.5	2.3	0.7
JB-3 ≤ sz	grey shale	O	69.0	11.4	10.3	4.9	4.3	0.4	2.4	0.6
PZ-101	red pitch shale	O	62.9	7.3	13.0	9.6	7.1	0.4	1.8	0.6
PZ-17/2c	dolomitic shale (red)	O	28.8	12.1	21.3	21.3	16.5	0.8	1.3	0.8
PZ-Isz/1 AP5	drawer-type shale (red)	O	74.0	5.4	8.7	6.8	5.2	0.2	1.7	0.5

P – phenantrene; 3-MP – 3-methylphenantrene; 2-MP – 2-methylphenantrene; 9-MP – 9-methylphenantrene; 1-MP – 1-methylphenantrene; MPI 1 (Metylphenantrene Index 1) = 1.5(2-MP+3-MP)/(P+1-MP+9-MP); MPR (Metylphenantrene Ratio) = 2-MP/1-MP; Rcal.(MPI) = 0.60MPI 1 + 0.37 for MPR<2.65; Rcal.(MPI) = -0.59*MPI 1 + 2.59 for MPR>2.65 (Radke 1988); R – reduced; T – transitional; O – oxidized

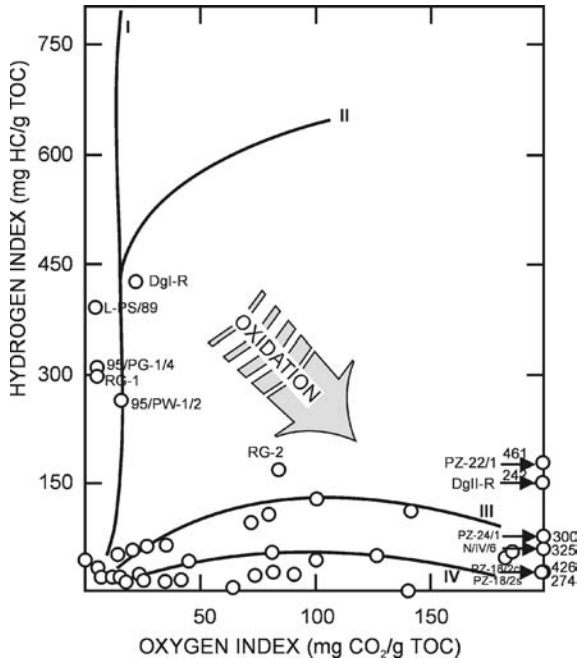

Fig. 37. Hydrogen index vs. oxygen index. Maturation paths for kerogens after Espitalié *et al.* (1985)

95/PG-1/4, RG-1 and 95/PW-1/2) represent the reduced zone and should be regarded as reference samples for identification of the genetic type of dispersed organic matter of Kupferschiefer strata in the study area, as this organic matter remained there unaffected by any secondary processes. Low values of indices obtained for majority of analyzed samples result from oxidation processes or from high maturity of the organic matter. It is supported by Fig. 34B, where the highest values of oxygen index OI (reflecting the oxidized organic matter) correspond to samples with the lowest TOC contents. Of particular importance is sample No. RG-2, in which very high TOC coincides with the low HI

Table 18

Maturity of bitumens calculated from distribution of methyldibenzotiophenes

Sample code	Lithology	Zone	DBT	4-MDBT	2+3-MDBT	1-MDBT	MDR	$R_{cal.(DBT)}$ (%)	$T_{max(DBT)}$ (°C)
			(sum = 100 %)						
95/PG-1/4	black shale	R	47.9	30.7	9.9	11.5	2.7	0.7	437
PR14/7001/107	dark brown shale	T	69.5	17.7	4.4	8.4	2.1	0.7	434
PZ-17/2s	dolomitic shale (grey)	T	28.0	31.9	23.4	16.7	1.9	0.6	433
PZ-Isz/3	drawer-type shale (black)	T	36.3	24.6	19.3	19.8	1.2	0.6	429
RG-2	pitch shale	T	75.6	11.5	4.8	8.0	1.4	0.6	430
JB-2	grey shale	O	47.1	28.8	13.6	10.6	2.7	0.7	437
JB-3 ≤ cz	red shale	O	65.5	15.9	5.1	13.5	1.2	0.6	429
JB-3 ≤ sz	grey shale	O	88.6	6.1	1.8	3.4	1.8	0.6	432
PZ-101	red pitch shale	O	42.8	30.0	12.2	15.0	2.0	0.7	433
PZ-17/2c	dolomitic shale (red)	O	33.8	26.4	18.9	20.8	1.3	0.6	429
PZ-Isz/1 AP5	drawer-type shale (red)	O	86.7	7.1	3.7	2.5	2.8	0.7	437

DBT – dibenzotiophene; 4-MDBT – 4-methyldibenzotiophene; 1-MDBT – 1-methyldibenzotiphene; 2+3-MDBT – 2-methyldibenzotiophene + 3-methyldibenzotiophene; MDR=4-MDBT/1-MDBT; $R_{cal.(DBT)} = 0.51 + 0.073*MDR$ (Radke 1988); $T_{max(DBT)} = 423+5.1*MDR$ (Radke 1988); R – reduced; T – transitional; O – oxidized

value (HI = 166 mg HC/g TOC, Tab. 13, Fig. 34A). The low HI value is likely caused by partial oxidation of organic matter, as confirmed by high content of oxide compounds reflected in the high OI value (Fig. 34B) and high content of sulphate sulphur (Tab. 14). The highest oxidation degree of organic matter (OI over 200 mg CO_2/g TOC) was found in samples Nos. PZ-22/1, PZ-18/2c, N/IV/6, PZ-24/1, PZ-18/2s and DgII-R (Fig. 34B). Moreover, apart from the decrease of the TOC content, the oxidation process causes an increase of TE/TOC values (Tab. 13, Fig. 33B). The extracted bitumens show the dominance of resins and asphaltenes (Tab. 13, Fig. 35).

The Kupferschiefer strata from the reduced zone contain type II kerogen (marine, oil-prone), as revealed by the Rock-Eval data (Tab. 13, Figs 36–38), distribution of *n*- alkanes and isoprenoids (Tab. 15, Fig. 39) and stable carbon isotope composition of bitumens, their fractions and kerogen (Tab. 13, Figs 40–42). These results correspond with the published data (e.g., Speczik & Püttmann, 1987; Rospondek *et al.*, 1993, Sawłowicz *et al.*, 2000; Nowak *et al.*, 2001; Kotarba *et al.*, 2006; Więcław *et al.*, 2007). Determination of the genetic type of organic matter from elemental composition (Tab. 16, Figs 43, 44) may lead to erroneous conclusions due to the oxidation processes affecting the organic matter in the studied samples. Kerogen in all analyzed samples presumably originated from transformation of the same type of marine kerogen, as indicated by narrow range of its isotopic composition (Figs 40, 41). Significant differences in isotopic composition of saturated hydrocarbons (Fig. 41) result from secondary processes (e.g., oxidation,

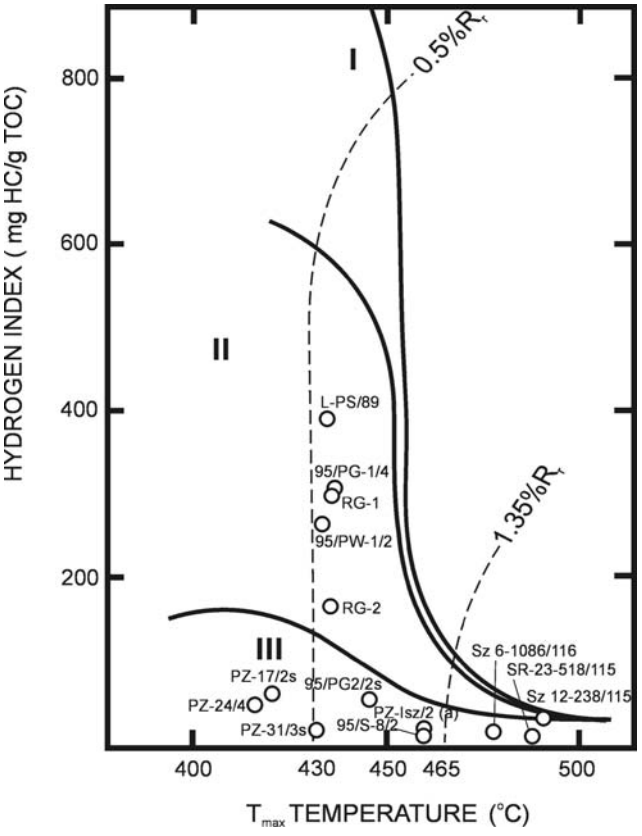

Fig. 38. Hydrogen index vs. T_{max} temperature for Kupferschiefer shales. Maturation paths for kerogens after Espitalie *et al.* (1985)

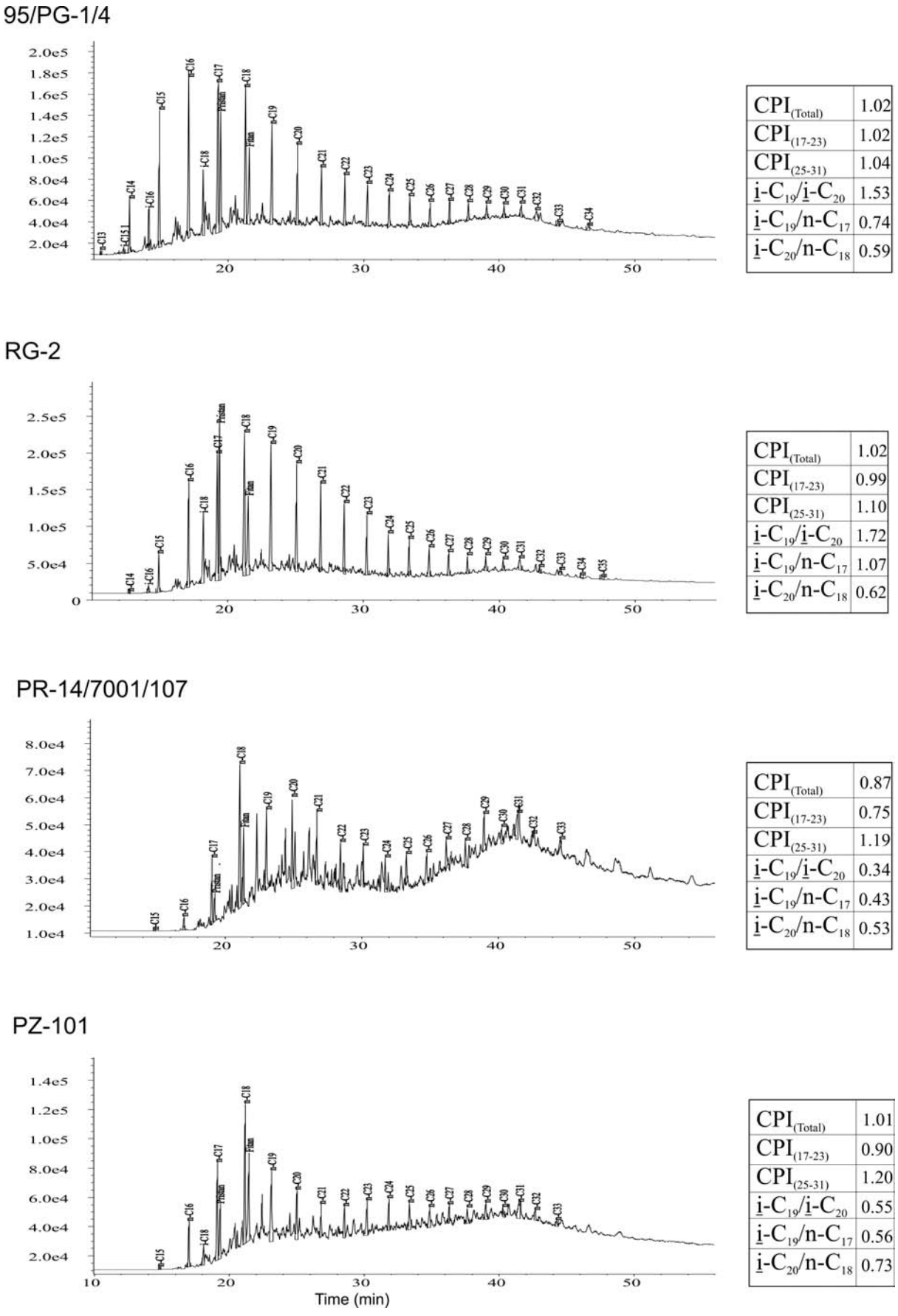

95/PG-1/4	
$CPI_{(Total)}$	1.02
$CPI_{(17-23)}$	1.02
$CPI_{(25-31)}$	1.04
$\underline{i}\text{-}C_{19}/\underline{i}\text{-}C_{20}$	1.53
$\underline{i}\text{-}C_{19}/n\text{-}C_{17}$	0.74
$\underline{i}\text{-}C_{20}/n\text{-}C_{18}$	0.59

RG-2	
$CPI_{(Total)}$	1.02
$CPI_{(17-23)}$	0.99
$CPI_{(25-31)}$	1.10
$\underline{i}\text{-}C_{19}/\underline{i}\text{-}C_{20}$	1.72
$\underline{i}\text{-}C_{19}/n\text{-}C_{17}$	1.07
$\underline{i}\text{-}C_{20}/n\text{-}C_{18}$	0.62

PR-14/7001/107	
$CPI_{(Total)}$	0.87
$CPI_{(17-23)}$	0.75
$CPI_{(25-31)}$	1.19
$\underline{i}\text{-}C_{19}/\underline{i}\text{-}C_{20}$	0.34
$\underline{i}\text{-}C_{19}/n\text{-}C_{17}$	0.43
$\underline{i}\text{-}C_{20}/n\text{-}C_{18}$	0.53

PZ-101	
$CPI_{(Total)}$	1.01
$CPI_{(17-23)}$	0.90
$CPI_{(25-31)}$	1.20
$\underline{i}\text{-}C_{19}/\underline{i}\text{-}C_{20}$	0.55
$\underline{i}\text{-}C_{19}/n\text{-}C_{17}$	0.56
$\underline{i}\text{-}C_{20}/n\text{-}C_{18}$	0.73

Fig. 39. Distribution of *n*-alkanes and isoprenoids in bitumen from Kupferschiefer

PZ-lsz/1

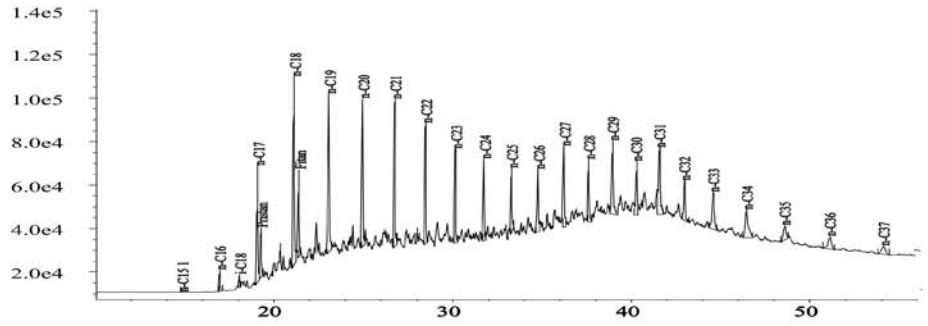

$CPI_{(Total)}$	1.05
$CPI_{(17-23)}$	0.94
$CPI_{(25-31)}$	1.27
$\underline{i}\text{-}C_{19}/\underline{i}\text{-}C_{20}$	0.57
$\underline{i}\text{-}C_{19}/n\text{-}C_{17}$	0.43
$\underline{i}\text{-}C_{20}/n\text{-}C_{18}$	0.45

PZ-lsz/3

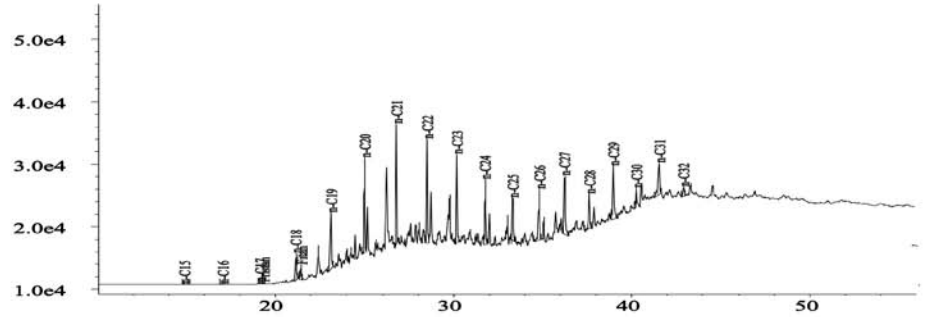

$CPI_{(Total)}$	1.22
$CPI_{(17-23)}$	1.01
$CPI_{(25-31)}$	1.75
$\underline{i}\text{-}C_{19}/\underline{i}\text{-}C_{20}$	0.11
$\underline{i}\text{-}C_{19}/n\text{-}C_{17}$	0.56
$\underline{i}\text{-}C_{20}/n\text{-}C_{18}$	0.58

PZ-17/2c

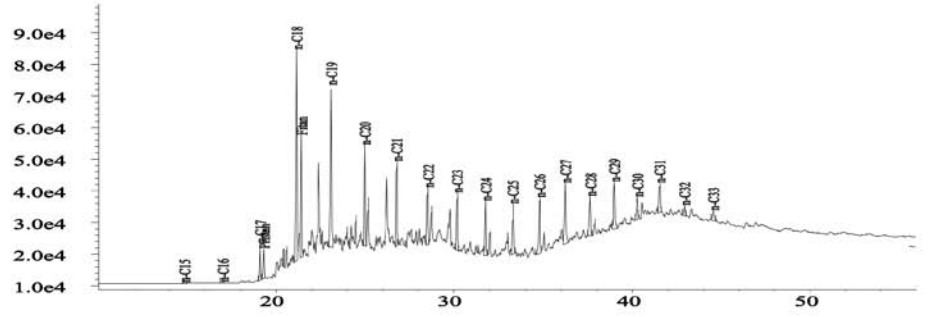

$CPI_{(Total)}$	0.97
$CPI_{(17-23)}$	0.82
$CPI_{(25-31)}$	1.33
$\underline{i}\text{-}C_{19}/\underline{i}\text{-}C_{20}$	0.23
$\underline{i}\text{-}C_{19}/n\text{-}C_{17}$	0.88
$\underline{i}\text{-}C_{20}/n\text{-}C_{18}$	0.60

PZ-17/2s

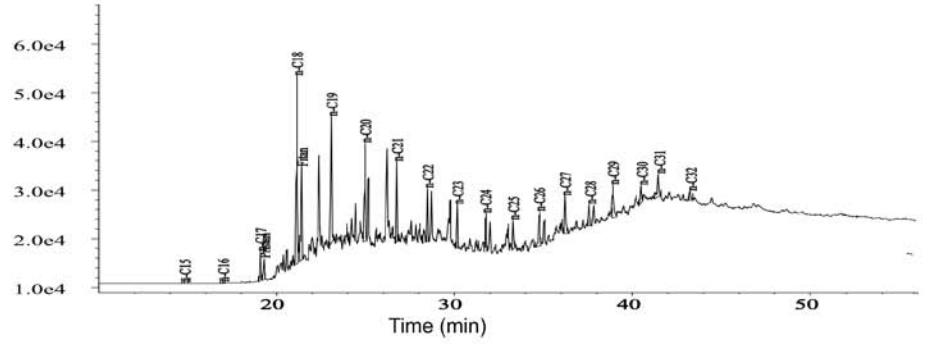

$CPI_{(Total)}$	0.97
$CPI_{(17-23)}$	0.78
$CPI_{(25-31)}$	1.59
$\underline{i}\text{-}C_{19}/\underline{i}\text{-}C_{20}$	0.21
$\underline{i}\text{-}C_{19}/n\text{-}C_{17}$	0.78
$\underline{i}\text{-}C_{20}/n\text{-}C_{18}$	0.58

Fig. 39. continued

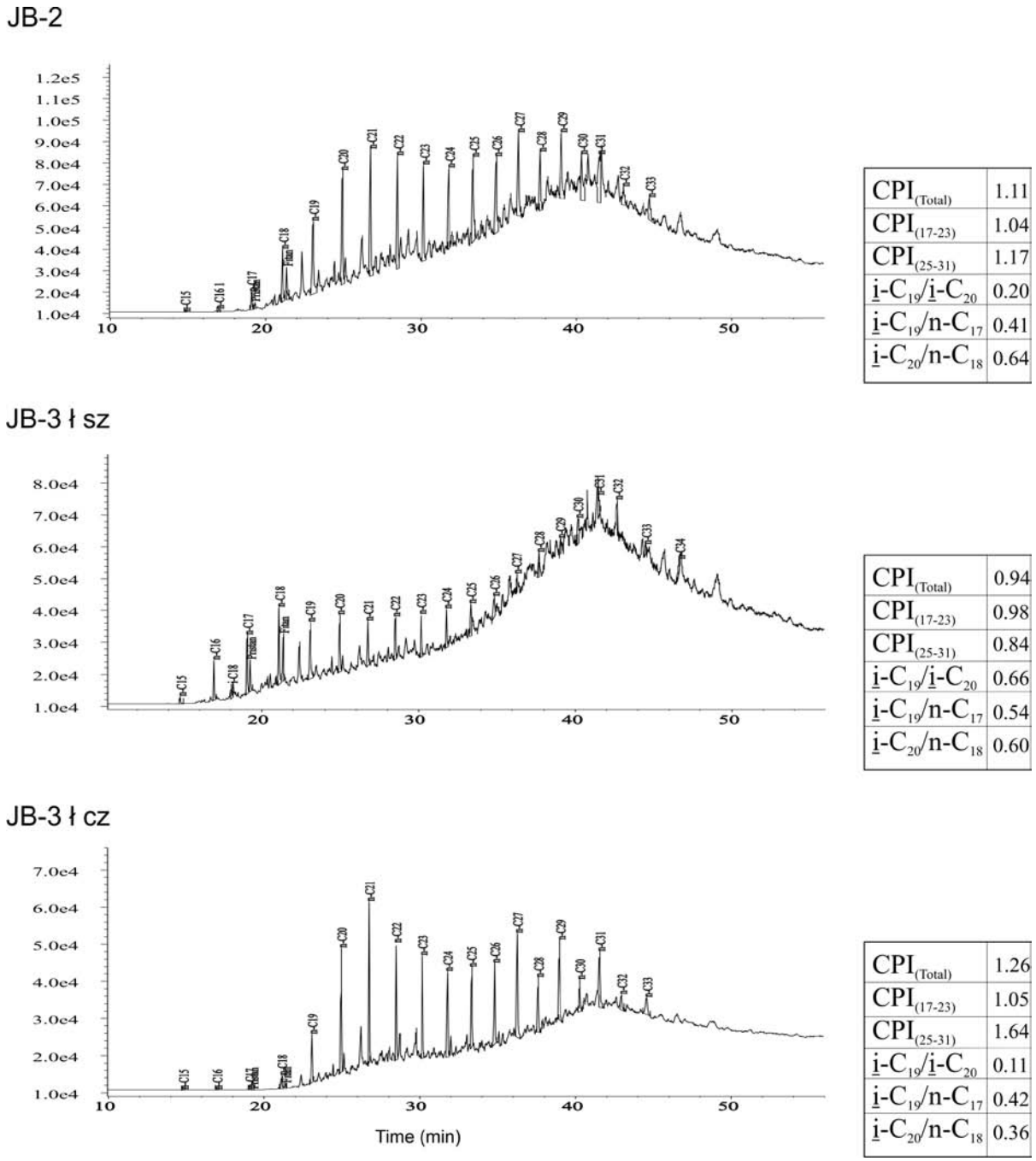

$CPI_{(Total)}$	1.11
$CPI_{(17-23)}$	1.04
$CPI_{(25-31)}$	1.17
$\underline{i}\text{-}C_{19}/\underline{i}\text{-}C_{20}$	0.20
$\underline{i}\text{-}C_{19}/n\text{-}C_{17}$	0.41
$\underline{i}\text{-}C_{20}/n\text{-}C_{18}$	0.64

$CPI_{(Total)}$	0.94
$CPI_{(17-23)}$	0.98
$CPI_{(25-31)}$	0.84
$\underline{i}\text{-}C_{19}/\underline{i}\text{-}C_{20}$	0.66
$\underline{i}\text{-}C_{19}/n\text{-}C_{17}$	0.54
$\underline{i}\text{-}C_{20}/n\text{-}C_{18}$	0.60

$CPI_{(Total)}$	1.26
$CPI_{(17-23)}$	1.05
$CPI_{(25-31)}$	1.64
$\underline{i}\text{-}C_{19}/\underline{i}\text{-}C_{20}$	0.11
$\underline{i}\text{-}C_{19}/n\text{-}C_{17}$	0.42
$\underline{i}\text{-}C_{20}/n\text{-}C_{18}$	0.36

Fig. 39. continued

water washing). This phenomenon was earlier noted by Kotarba *et al.* (2006).

The maturity of organic matter dispersed in the studied rocks determined by the Rock-Eval pyrolysis (Tab. 13), the distribution of methylphenanthrenes (Tab. 17) and methyldibenzothiophenes (Tab. 18) is highly variable. The results of kerogen elemental analysis (Tab. 16, Fig. 43) cannot be trusted due to reasons mentioned above. Most of the studied samples reveal organic matter maturity at the initial phase of the low-temperature thermogenic process ("oil-window"), corresponding to the vitrinite reflectance level of R_r = 0.6–0.8% (Tabs 13, 17, 18, Fig. 38). The increased maturity (1.1–1.2% in vitrinite reflectance scale) was observed in samples Nos. PZ-Isz/2(a), Sz12-238/115 and 95/S-8/2 (Tab. 13, Fig. 38). The highest maturity (T_{max} = 488°C; corresponding to R_r over 1.5%) was observed in the sample No. SR-23-518/115 (Tab. 13, Fig. 38). A very low T_{max} value (360°C) for the sample No. DgI-R suggests a very low maturity (R_r about 0.4%). It can be also explained by a higher content of epigenetic hydrocarbons component (Fig. 32).

Summary

The study results clearly demonstrate the variable contents of most analyzed elements, particularly precious met-

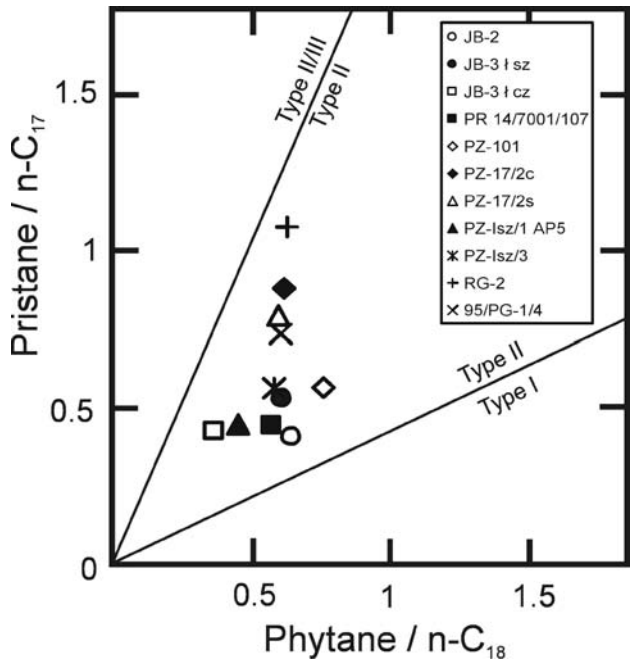

Fig. 40. Genetic characterization of bitumens from Kupferschiefer shales in terms of pristane/*n*-C_{17} and phytane/*n*-C_{18} according to the categories of Obermajer *et al.* (1999)

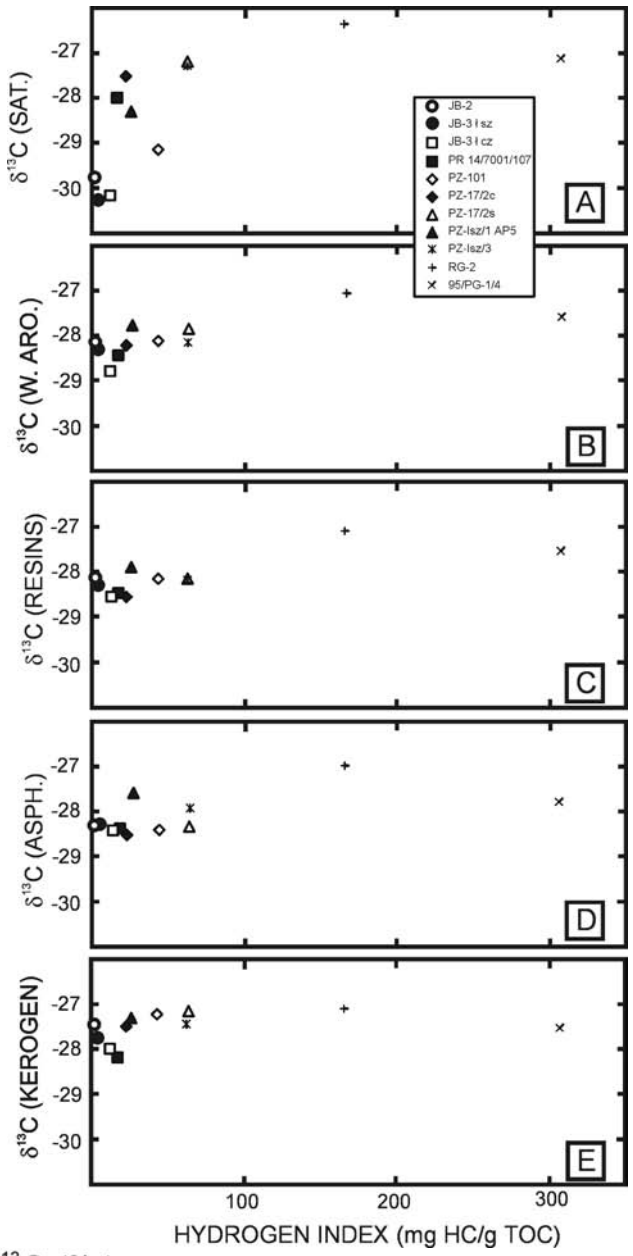

Fig. 42. Correlation of stable carbon isotope composition in: **A** – saturated hydrocarbons; **B** –aromatic hydrocarbons; **C** – resins; **D** – asphaltenes; **E** – kerogen, with hydrogen index for Kupferschiefer shales

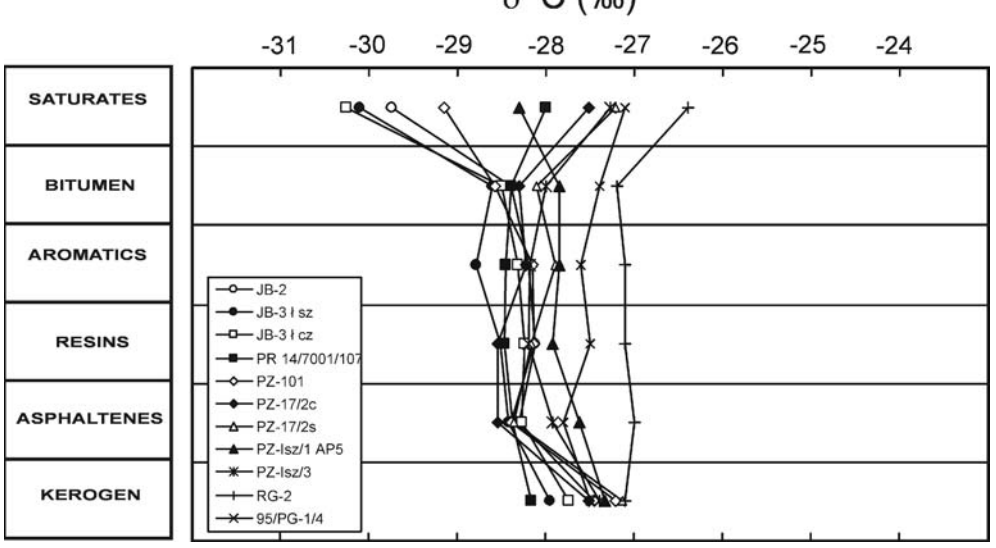

Fig. 41. Stable carbon isotope composition of bitumens, their individual fractions and kerogen from Kupferschiefer shales

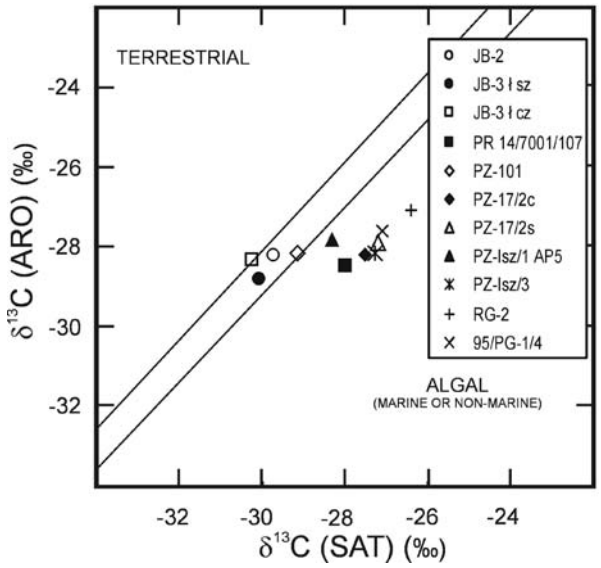

Fig. 43. Genetic characterization of bitumens in terms of $\delta^{13}C$ (aromatic hydrocarbons) and $\delta^{13}C$ (saturated hydrocarbons) from Kupferschiefer shales according to the categories of Sofer (1984)

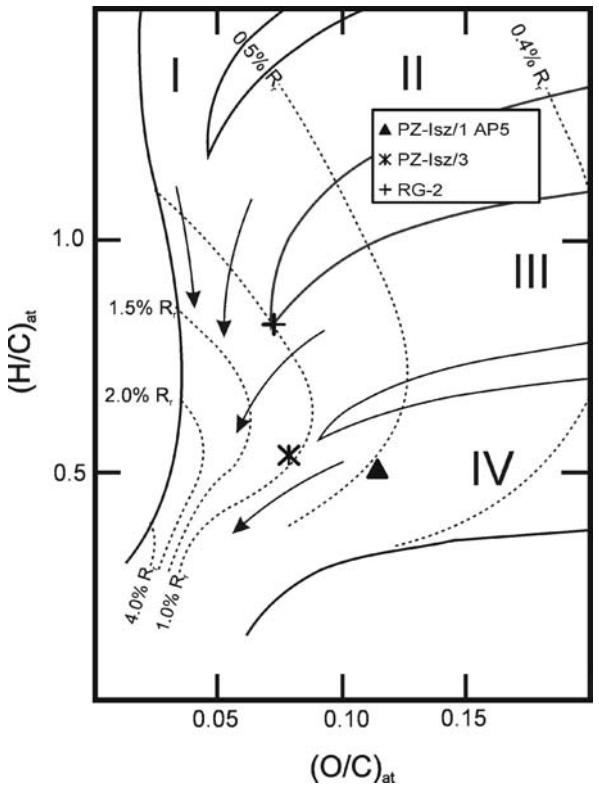

Fig. 44. Genetic characteristics of organic matter of Kupferschiefer shales. Maturation paths for kerogens after Hunt (1996)

als (Fig. 28) and main metals (Figs 29, 30, 31). Contents of all these elements reveal random distributions. Metal concentrations vary from 1,000 times for Au through 5 times for Ag (Fig. 28), 5–50 times for Cu (Fig. 29), 10–15 times for Mo (Fig. 29), 5–45 times for Co (Fig. 30) to 1–2 times for Zn and 6–40 times for Pb. The lowest differences were found for Ni (1–3 times, Fig. 30). These figures point out to the presence of secondary, hydrothermal processes leaching the metals from the system.

The results of organic geochemical studies revealed that the organic matter – one of the major components of the Kupferschiefer – was oxidized in zones where hot brines migrated from sandstone complex. It is documented by variable organic carbon content from 0 to 12.7 wt.%, quantity of organic oxygen compounds (OI vary from 4 to 462 mg CO_2/g TOC) and maturity which suggests local overheating of the system (up to 1.5% in vitrinite reflectance scale). Variable isotopic composition of saturated hydrocarbons, may suggest leaching of organic matter components by water. All these arguments advocate the contribution of active hydrothermal processes causing oxidation and simultaneous water washing of hydrocarbons.

MINERALOGY AND GEOCHEMISTRY OF ORE MINERALS FROM SECONDARY OXIDIZED ZONES

Jadwiga Pieczonka & Adam Piestrzyński

MINERALOGICAL STUDIES

In previous years over 140 ore minerals have been described from the Cu deposits in the Fore-Sudetic Monocline. The earliest identified minerals were those forming the bulk of mineralization: chalcocite, digenite, bornite, chalcopyrite, covellite and accompanying pyrite, marcasite, sphalerite, galena, tenorite, cuprite, native Ag and native Cu. Additionally, a large group of trace-element minerals of Ag, Au, Pt, Pd, Ni, Re, Co, Mo, Zn, Pb, Se, Sb, Bi and V was described, from which only a few metals are recovered (Ag, Au, Pt, Pd, Ni, Re). Detailed list of minerals encountered in the deposit together with the names of authors who made the first discoveries can be found in Piestrzyński (1996a).

Distribution of ore minerals in the deposit is diversified. Cu sulphides are hosted in three rocks, forming three lithologic types of ore: sandstone, shale (Kupferschiefer) and carbonates. In particular parts of the deposit metals concentrations in specific rocks are variable. In the Lubin area, the ore zone includes the sandstones, the Kupferschiefer and the carbonates. In the Rudna area, copper deposit is hosted mostly in the sandstone and the Kupferschiefer whereas in the Polkowice-Sieroszowice area ore-bearing are the Kupferschiefer and the carbonates.

Mineralogical studies on the selected parts of the Polkowice-Sieroszowice area, which are reported on in this chapter, could have commenced not earlier than in 1990-ties when the company has started the development of this part of copper deposit (Report AGH 1996, 1997; Piestrzyński *et al.*, 1996a; Piestrzyński & Pieczonka, 1997a, b).

At the first stage of the research project, the sampling sites for mineralogical and geochemical studies were located in all the operating mining sectors. The results of initial examinations led to the second stage of the project when sampling grid was densified chiefly in the Polkowice West Field, which appeared to be the most perspective for the oc-

currence of precious metals. Moreover, samples were collected also from poorly recognized zones in the Polkowice East Field and in the Sieroszowice Field.

General characterization of ore mineralization

Mineralogical studies were carried on 202 samples derived from 35 sequences. Microscopic observations under the reflected light enabled the authors to identify ore minerals and their structures. Results of observations were plotted separately for each sequence. This led to the distinguishing of several types of ore mineralization, representing various distributions of ore minerals:

Type 1 – copper mineralization is hosted in the Kupferschiefer and in the carbonates or only in the Kupferschiefer, whereas the top part of the sandstone contains only traces of ore minerals. This type was found in the sequences No. Sz02-3056 (Fig. 4), Sz07-0027 (Fig. 6), Sz07-0054, Sz08-0991 (Polkowice East Field), Po17-2125, Po17-2289 (Polkowice Main Field), Pr18-0331 (Polkowice West Field), Sr19-2428 (Fig. 17), Sr19-0802, Ra14-0505 and Ra19-0011 (Sieroszowice Field). In some sequences, mostly collected from the southern part of the Sieroszowice Field, native Au was encountered in the topmost part of the sandstone with red spots (sequences No. N/III, Fig. 18, N/IV, Fig. 19, N/V, Fig. 20, Sr20-0822, Ra14-0274). In No. Sz08-0936 sequences (Polkowice East Field) native gold was found in the Kupferschiefer.

Type 2 – copper mineralization occurs in the Kupferschiefer and in the carbonates, but the lower boundary of ore zone is located in the upper part of the Kupferschiefer layer or at the bottom of the carbonates, whereas the lower part of the Kupferschiefer hosts precious metals association. Such distribution was found in sequences No. Sz02-2700 (Polkowice East Field) and Pr18-0367 (Polkowice West Field).

Type 3 – copper mineralization is hosted only in the carbonates whereas the Kupferschiefer is barren (sequence No. Sr18-0061"s" from the Sieroszowice Field).

Type 4 – copper mineralization is located in the sandstone, in the Boundary Dolomite and, occasionally, in the Kupferschiefer, as found in the sequences No. Po23-2399 and Po23-2384 (Polkowice East Field).

Type 5 – copper mineralization includes the sandstone (down to 1.5 m depth from the top) and the carbonates whereas the Kupferschiefer is absent. This was observed in the sequences No. Sz03-2028 and Sz03-2051 (Polkowice East Field).

Type 6 – low-grade copper mineralisation. Red spots appear in each sequence, in one or more samples. Native Au and electrum are present in the top part of the sandstone, in the Kupferschiefer and in the carbonates, as illustrated in the sequences No. Sr18-7002 (Fig. 16) (Sieroszowice Field) and Sz/III (Fig. 14) (Polkowice West Field).

Characterization of ore mineralization in the oxidized zones

The oxidized zones reveal low concentrations of simple copper sulphides with the dominating chalcopyrite accompanied by bornite, pyrite, covellite, galena, clausthalite, chalcocite, digenite, spioncopite, geerite, native Au, electrum, tetraauricupride, naumannite, native Pb, Pd-arsenides and minerals of mixed composition: Au-Ag-Pb-Bi-Se-Te, Au-Ag-Pb-Te, Bi-Cu, Bi-Pd and Pd-As-O. Most of these minerals was indentified under the ore microscope whereas natural alloys were disclosed with the EDS (see next chapter). Most important are natural alloys of precious metals, Pd-arsenides and oxidized phases (mostly Pd ones) which strongly influence the effectiveness of froth flotation. Distribution of ore minerals is highly diversified. High-purity native gold of intensive yellow colour occupies the central part of the oxidized zone whereas electrum dominates in the transitional and peripherial zones.

Native gold in the sandstone

In the study area, the sandstone is rarely sufficiently exposed to ensure detailed recognition of its character and forms of red spots. In many cases the red spots coalesce in its topmost layer, sometimes forming vein-like structures or the whole thickness of the sandstone is red-coloured. Such rocks host the largest accumulations of native Au.

Native Au is located mostly in the carbonate cement of the sandstone. In No. N/III/6 sequence it is even marcoscopically visible (Fig. 45). The common structures are individual aggregates of various size and shape (Figs 46–48) or intergrowths with electrum, sulphides (mostly chalcopyrite) and Pd-arsenides (Fig. 49A, B) sometimes accompanied by Bi minerals (Fig. 49C, D, E). In numerous individual native Au aggregates fine inclusions of Pd-arsenides and naumannite were found (Fig. 50). More complicated intergrowts were observed of native Au and electrum with Cu sulphides (mostly chalcopyrite, bornite and covellite), naumannite and Pd-arsenides (Fig. 51). In the intensively red-coloured rocks native Au is accompanied by haematite (Figs 52, 53A). At crossed nicols its red internal reflections are seen (Fig. 53A). If intergrown with Cu sulphides, native Au shows bright-yellow colour and usually lower content of Au whereas individual grains or intergrowths with haematite are intensively yellow and show higher purity. The occurrence of native gold was described in several papers (see e.g., Piestrzyński *et al.* (1996a, 2002), Piestrzyński and Pieczonka (1997a, b), Pieczonka (1998, 2000), Piestrzyński and Wodzicki (2000).

Native gold in the Boundary Dolomite

In the areas of the Polkowice West and Main Fields the Boundary Dolomite occurs only locally but it is more common in the Polkowice East Field. Three lithological varieties of this rock are known. The Boundary Dolomite encountered in the Polkowice West Field is red-coloured (Pieczonka, 1998). Samples collected for this project did not contain native Au whereas electrum was found in only a single sample (No. Pr18-0367 from the Polkowice West Field).

Studies completed up to date (Report AGH 1996, 1997; Piestrzyński & Pieczonka, 1997b; Pieczonka, 1998, 2000) revealed that native Au and electrum occur in most examined sections from the Boundary Dolomite. Both minerals form disseminated structures in the whole rock, in epigenetic sparite veinlets cutting the dolomite, at dolomite/

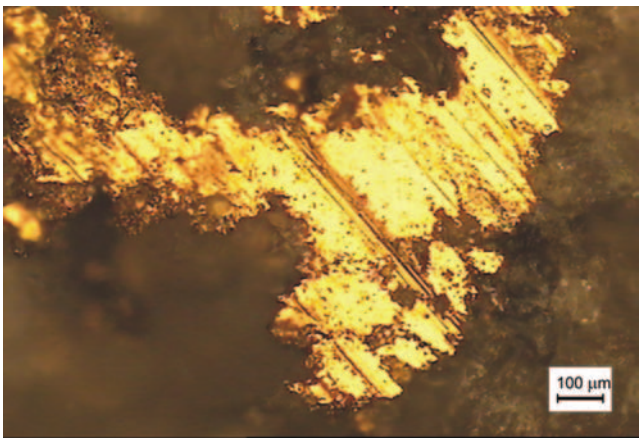

Fig. 45. Video picture of native gold from the secondary oxidized Weissliegende sandstone, Polkowice Mine, West Field

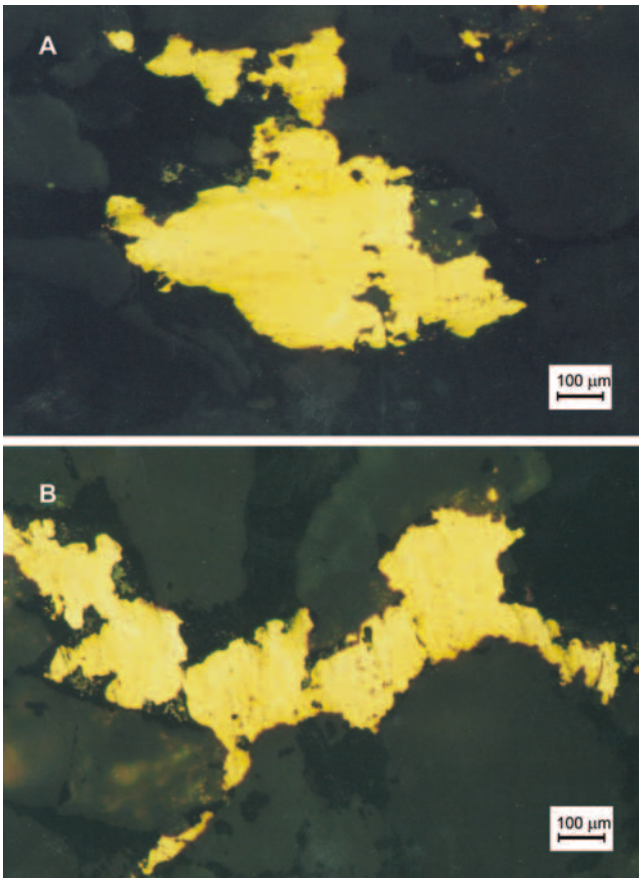

Fig. 46. Gold aggregates in sandstone matrix, reflected light, Polkowice Mine. **A** – nest type structure, sample N/III/5; **B** – veinlets type of structure, sample N/III/5

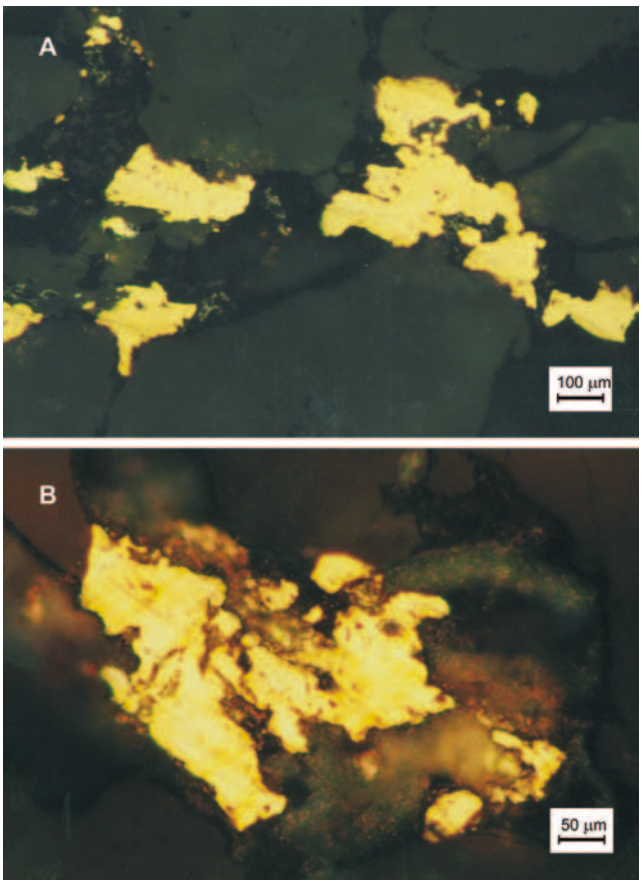

Fig. 47. A–B. Gold aggregates in sandstone matrix, nest type of structure, reflected light, sample N/III/5, Polkowice Mine

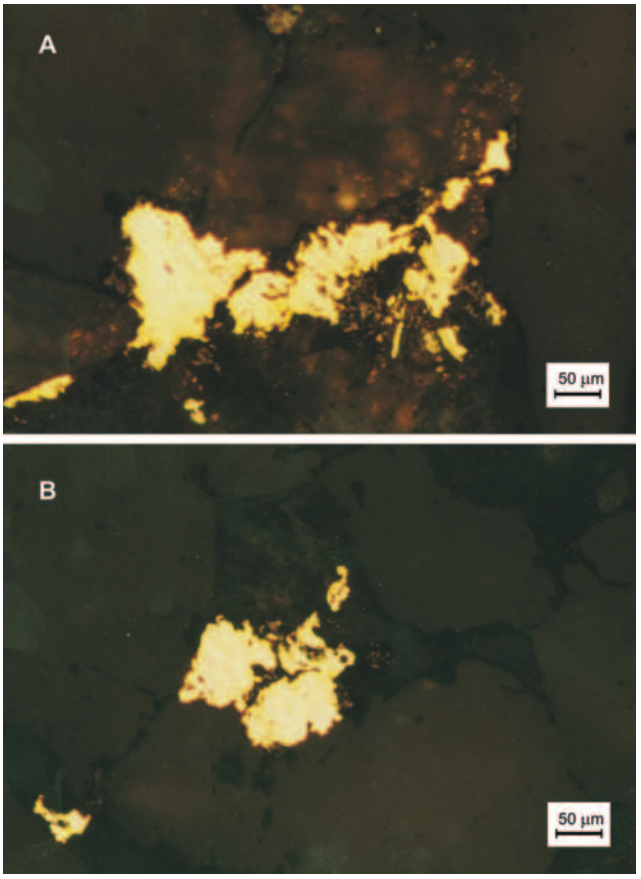

Fig. 48. Gold aggregates in sandstone matrix, reflected light, Polkowice Mine. **A** – nest type structure, internal reflection in the sandstone matrix show much bigger size of the gold nugget, sample N/III/5; **B** – nest type of structure, sample N/III/5

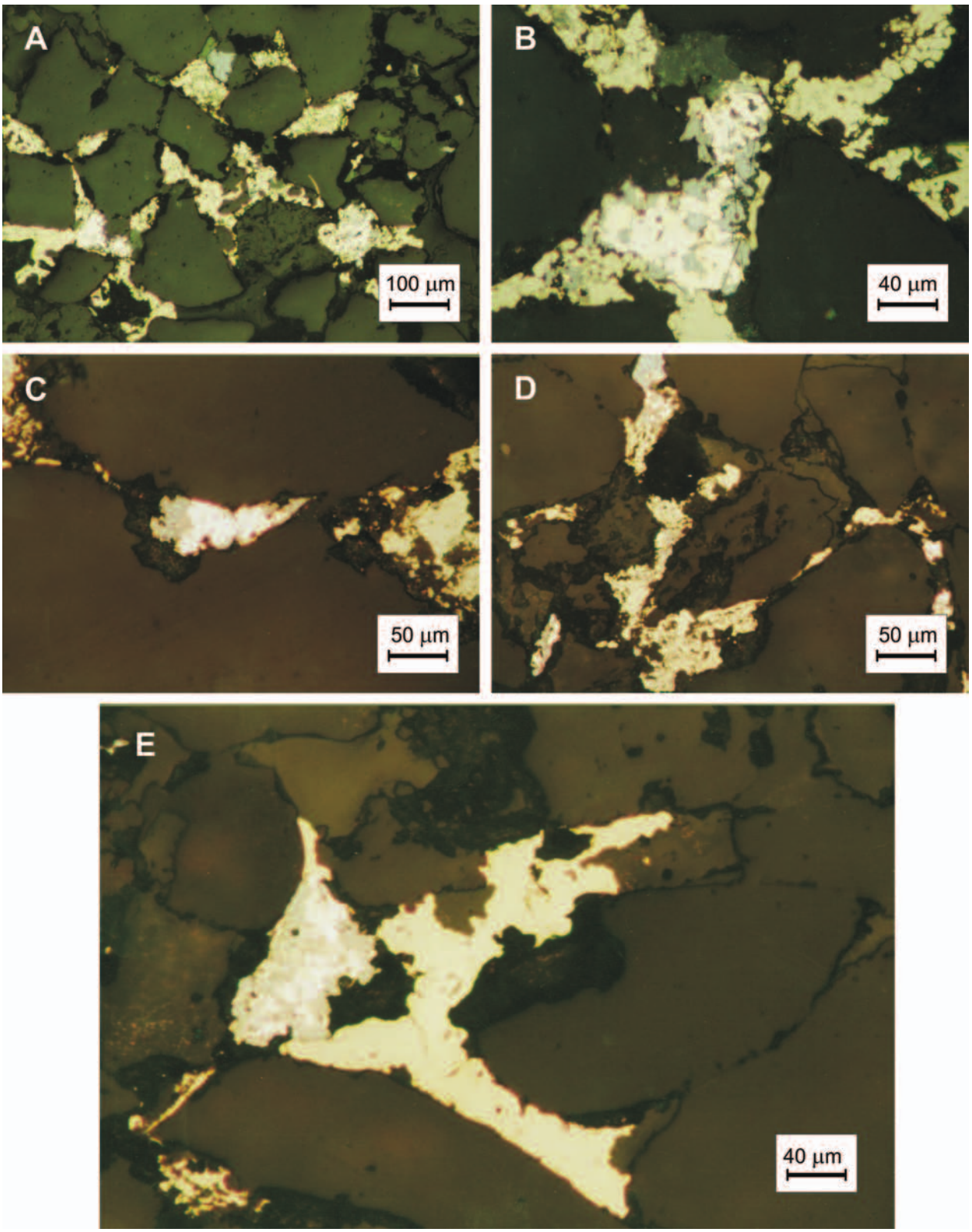

Fig. 49. Gold aggregates and their intergrowths in sandstone matrix, reflected light, Polkowice Mine. **A** – intergrowth of electrum (white-yellow) with Pd-arsenides (pale grey) and chalcopyrite (yellow), sample N/IV/6; **B** – intergrowth of electrum (white-yellow) with Pd-arsenides (pale grey), chalcopyrite (yellow) and sphalerite (dark grey), sample N/IV/6; **C** – intergrowth of electrum (white-yellow), Bi and Pd minerals (grey), sample N/IV/5; **D** – intergrowth of electrum with Pd-arsenides and Bi-alloys (pale grey), sample N/IV/6; **E** – intergrowth of electrum (white) and Pd-arsenides (pale grey), sample N/IV/5

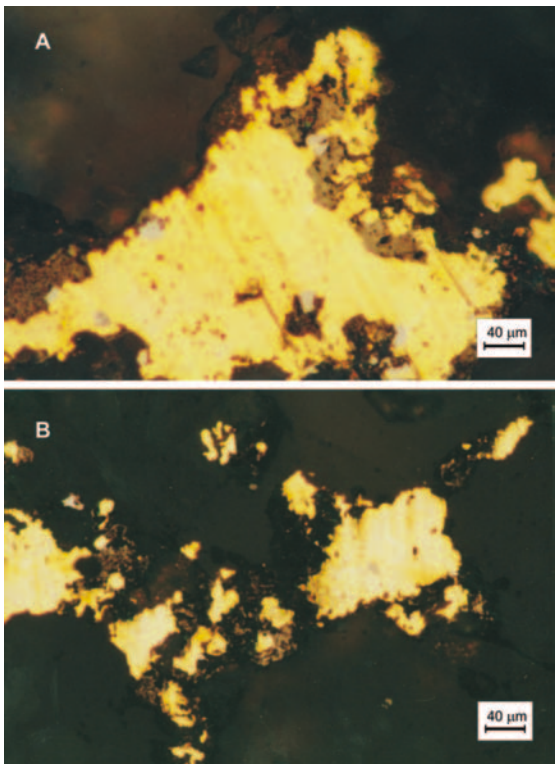

Fig. 50. Gold aggregates and their intergrowths with other ore minerals in sandstone matrix, reflected light, Polkowice Mine. **A** – inclusions of naumannite (pale grey) and Pd-arsenides (dark brown) in gold grain (yellow), sample N/III/5; **B** – small inclusions of selenides and Pd-arsenides in high purity of gold grain (yellow), sample N/III/5

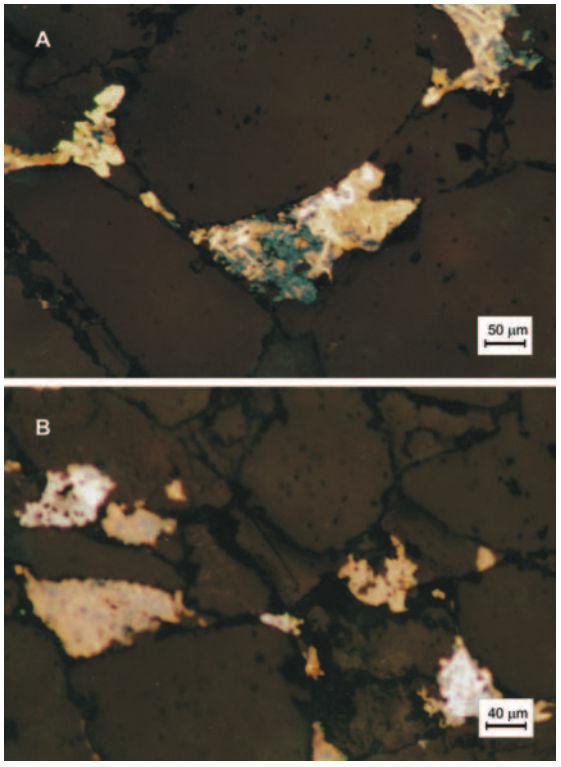

Fig. 51. Intergrowth of electrum (white) with naumannite (pale grey), bornite (dark orange) and covellite (blue) in sandstone matrix. Reflected light, sample N/IV/6, Polkowice Mine

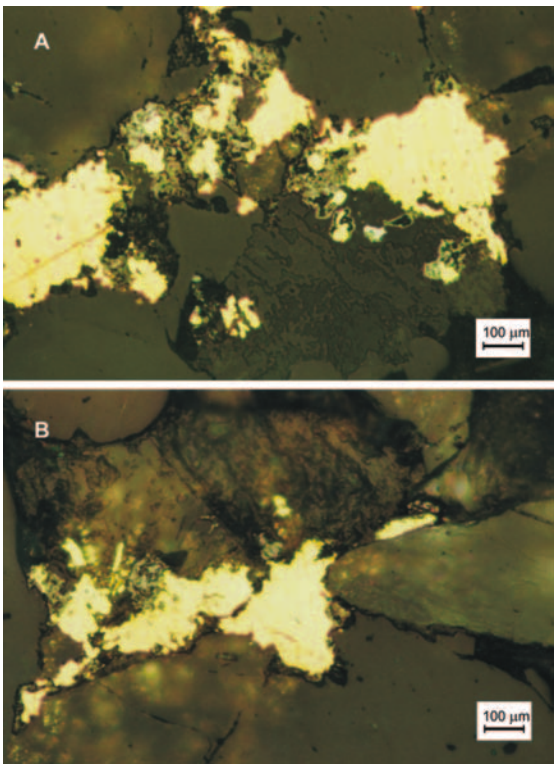

Fig. 52. A–B. Intergrowths of gold (yellow) with hematite (grey) in sandstone matrix, reflected light, sample N/III/6, Polkowice Mine

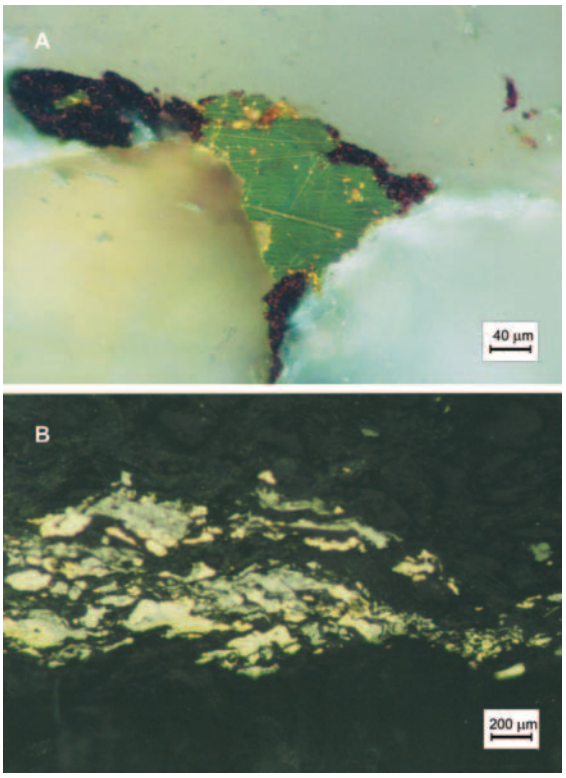

Fig. 53. A – position of gold aggregate (green) and hematite showing maroon tint of internal reflection in sandstone matrix, reflected light, XN, sample N/III/6, Polkowice mine; **B** – reach concentration of native gold (pale yellow) and intergrowth of Pd-arsenides and Cu-sulphides in lowermost part of Kupferschiefer, reflected light, sample PG-1/3, Polkowice Mine

Kupferschiefer boundary and in the underlying shale. Native Au forms intergrowths with and inclusions in Cu sulphides (mostly chalcocite, bornite and digenite) as well as individual grains in the vicinity of Cu sulphides. Disseminated native Au grains were noticed in carbonate nests and veinlets of usually less intensive red colour than the Boundary Dolomite itself. The size of native Au crystals varies from 0.1 to 0.3 mm but some grains are macroscopically visible (Report AGH 1996, 1997; Piestrzyński *et al.*, 1996a, 2002; Pieczonka, 1998, 2000).

Native gold in the Kupferschiefer

Native Au accumulates in both the red and grey Kupferschiefer varieties observed in the southern part of the Polkowice Mine and in the Radwanice area. Usually, the grey Kupferschiefer is Cu-barren.

Microscopic observations under crossed nicols revealed the presence of red internal reflections and various shades of red colour in the rocks. Red colour results from the occurrence of fine hematite disseminated in rock matrix and from coarse-crystalline hematite intergrown with native Au, bornite and chalcopyrite (Piestrzyński & Pieczonka, 1997a, b; Pieczonka, 1998, 2000; Piestrzyński *et al.*, 2002).

Both the native Au and electrum were found in all varieties of the Kupferschiefer. In the pitchy variety elongated intergrowths of native Au with chalcocite and Pd-arsenides were found, arranged parallelly to lamination (Figs 53B, 54A). In the clayey variety native Au was encountered in only a few specimens, as fine inclusions in chalcopyrite accompanied by clausthalite (Fig. 54B). Numerous native Au grains were observed at the boundary between clayey and dolomitic Kupferschiefer varieties where it forms individual grains as well as intergrowths with chalcopyrite (Fig. 55A, B) and digenite (Fig. 55C, D, E). In some crystals inclusions of Pd-arsenides were noticed. In the dolomitic Kupferschiefer variety structures of native Au are more diversified. It forms: (i) very fine, individual crystals disseminated in the host-rock; (ii) larger, also disseminated crystals (Figs 55F, 56A, B, C) or clusters of several smaller, densly packed individuals (Figs 55F, 56A, B, C) or larger crystals (Fig. 56D); (iii) numerous, closely packed crystals forming "veinlets" (Fig. 56E and F), sporadically intergrown with Pd-arsenides; (iv) veinlets 57A, B). Common are intergrowths of native Au with: (i) Pd-arsenides (Fig. 57C, D, E); (ii) chalcocite and digenite (Figs 57F, 58A); (iii) chalcocite and covellite (Fig. 58B, C, E); (iv) chalcocite, covellite, bornite and haematite (Fig. 58 D); (v) chalcopyrite (Fig. 58F).

Native Au in the carbonates

Native Au occurs in carbonates which host red spots and in which Cu mineralization is uneconomic. Under the microscope samples from such rocks revealed the presence of chalcocite, half-bornite, covellite, tennantite, gersdorffite, rammelsbergite, clausthalite and hematite (Report AGH 1996, 1997; Piestrzyński *et al.*, 1996a, b, 2002; Pieczonka, 1998).

In dolomite samples collected for the following project, native Au was found only in the Streaky Dolomite with numerous red spots. In one of the studied sequences intergrowths of native Au with bornite and clausthalite were noticed (Fig. 59A) and in another one intergrowths with digenite, clausthalite and haematite were found (Fig. 59B).

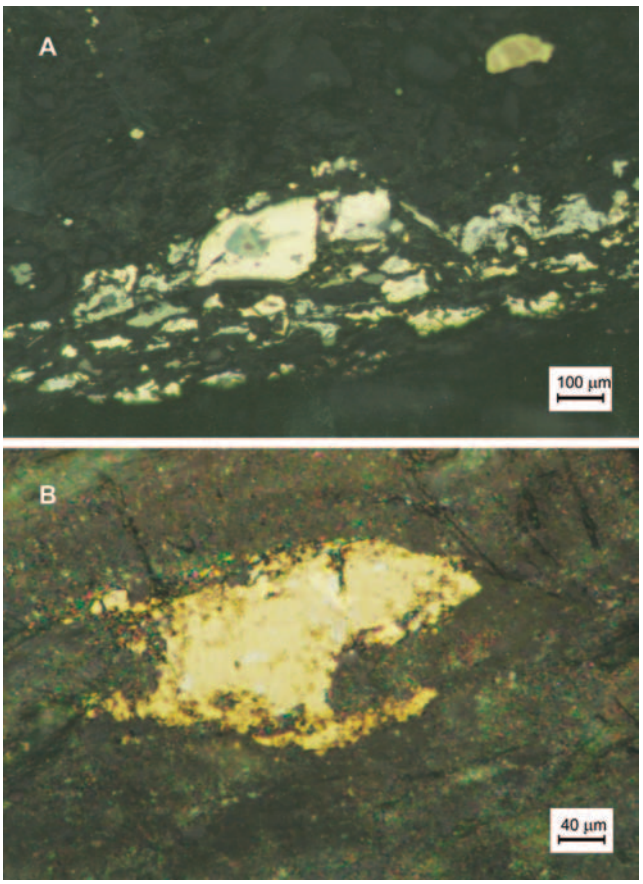

Fig. 54. **A** – intergrowths of native gold (pale yellow) with Pd-arsenides (grey) and chalcocite (blue) in lowermost part of Kupferschiefer, reflected light, sample PG-1/3, Polkowice Mine; **B** – inclusions of gold (pale yellow) at chalcopyrite (yellow) in pitchy shale, reflected light, sample Sz/III/1, Polkowice Mine

Size distribution of native gold and electrum crystals

During the studies run in the years 1995–1998 size distribution of native Au and electrum crystals was analyzed. Data obtained in the years 1997–1998 enabled to draw histograms of size distribution separately for the sandstone (Fig. 60A), the Boundary Dolomite and the Kupferschiefer (Fig. 60B) and the carbonates (Fig. 60C). At that stage of research samples were collected also from the sandstone, down to 1 m depth from the top surface. Hence, the histograms representing various lithologic types of rocks could be compared. The last histogram (Fig. 60D) illustrates the overall native Au and electrum crystal size distribution in gold-bearing rocks, despite their lithology. It was based upon the grain-size measurements made in the years 1995–1998 for both the individual minerals and their intergrowths with various accompanying phases (Pieczonka, 1998).

Analysis of histograms clearly demonstrates that, despite the lithology of the host-rocks, the relative percentage of size classes <50 µm exceeds 90%. Dominating are small crystals (0–5 µm) for which the relative percentage is 50.3%, as demonstrated by the cumulative histogram. Also

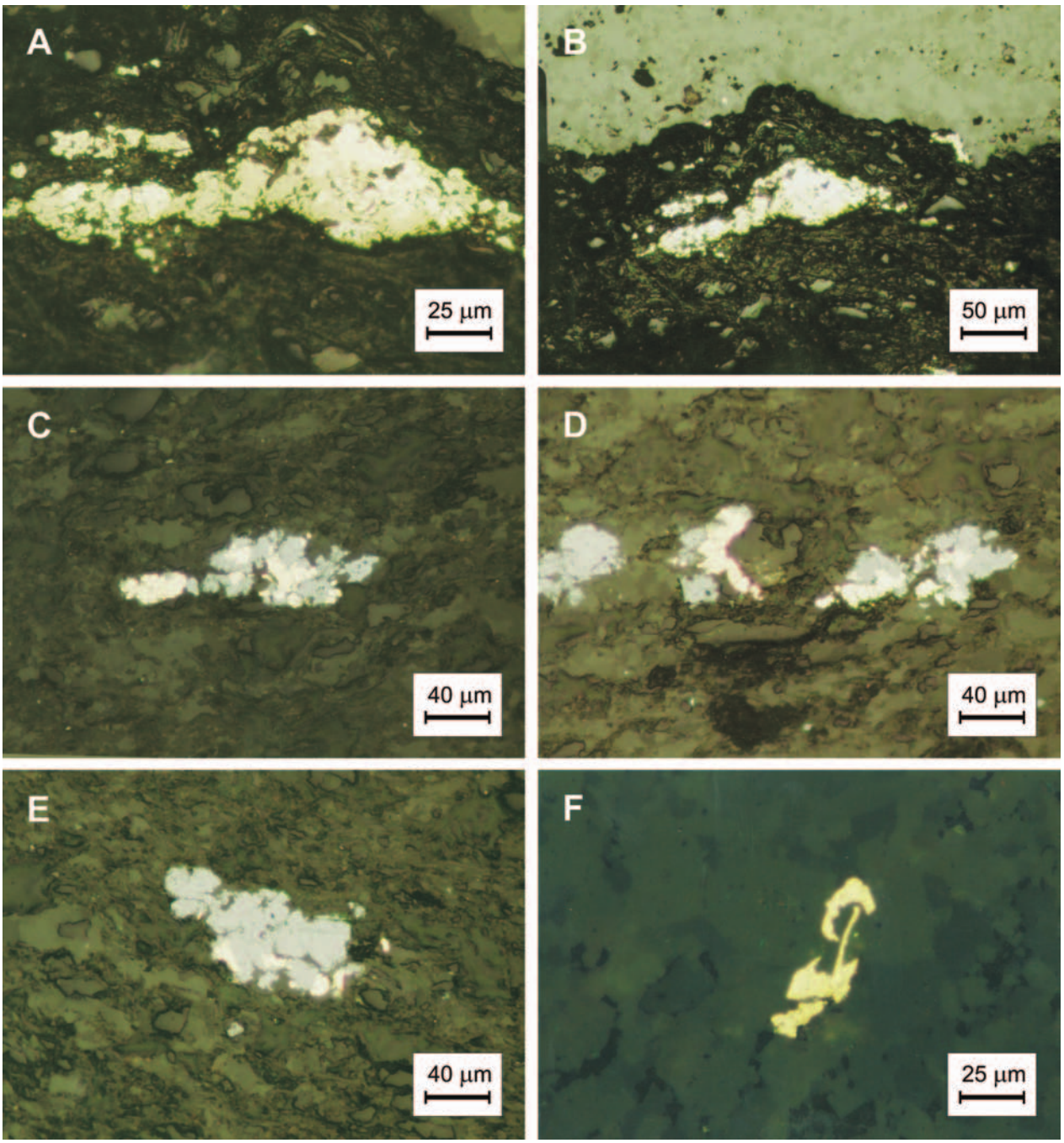

Fig. 55. Gold aggregates and their intergrowths in Kupferschiefer, reflected light, Polkowice Mine. **A** – intergrowth of gold and chalcopyrite in pitchy shale, sample PZ-J-5; **B** – the same picture like on phot. A, but showing structural position of gold-chalcopyrite aggregate in the relation to the boundary dolomite; **C–E** – intergrowths of gold and digenite (pale blue), sample PZ-J-3; **F** – different textures of gold grain in the calcareous shale, sample PZ-J-7

percentages of the next two classes: 5–10 and 10–15 µm are high (20.6 and 11.2%, respectively), whereas the percentages of larger crystals are apparently lower and decrease to below 1% for the class 40–45 µm. Large (over 80 µm) native Au and electrum crystals are rare.

Percentage of fine fractions is very high but the importance of this observation must be analyzed with criticism. Although large crystals of native Au are rare, each crystal is a spatial form and, thus, a single crystal of size above 50 µm may have larger mass than a number of small crystals of size 0–5 µm. The economic importance of particular crystal-size class of gold minerals will depend on its successful beneficiation, i.e., on ore processing technology (Pieczonka, 1998).

GEOCHEMISTRY OF Au IN THE SECONDARY OXIDATION ZONE

The world literature provides immense information on Au and PGE minerals. Gold mostly forms native phases,

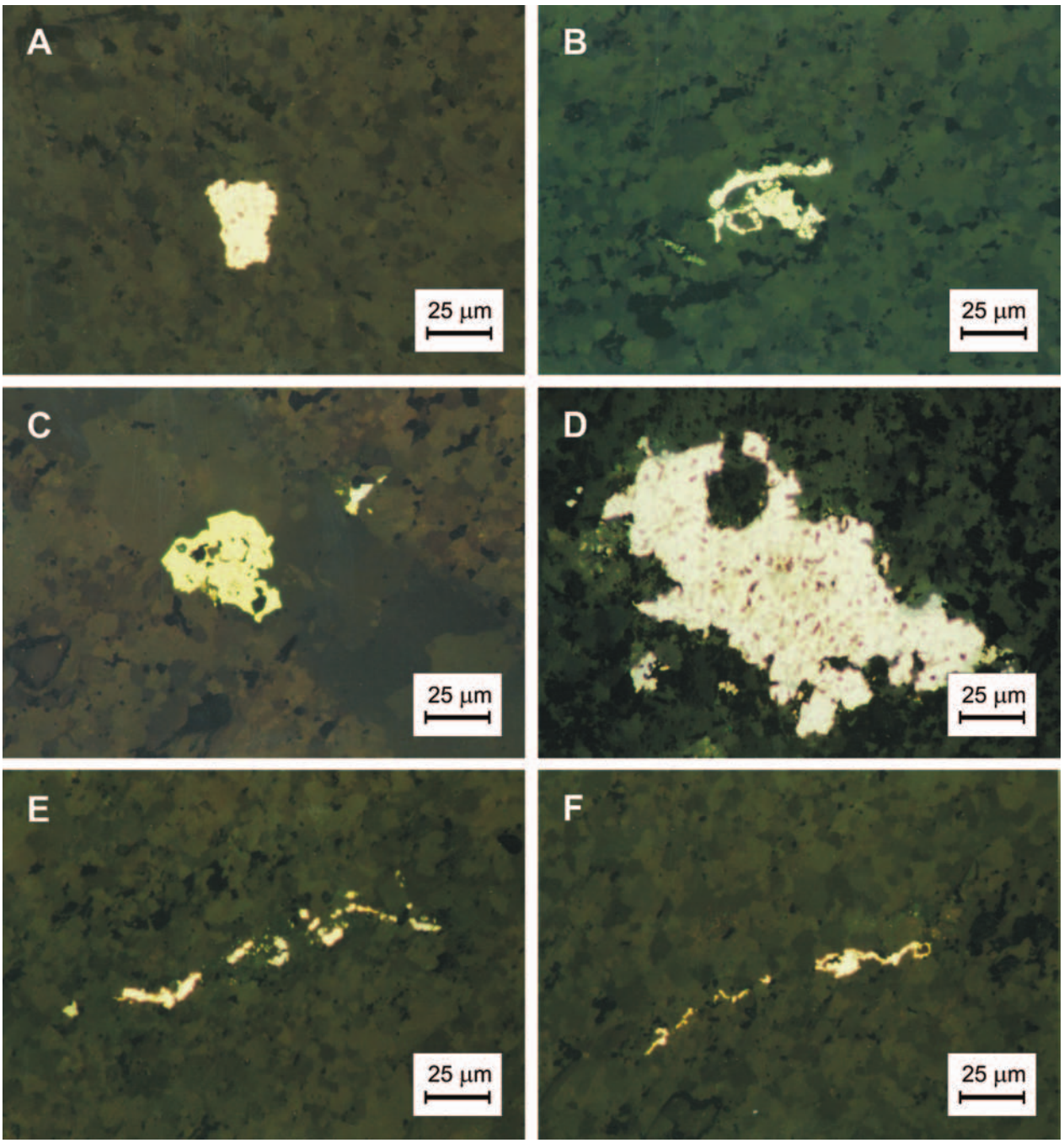

Fig. 56. Gold aggregates and their intergrowths in calcareous variety of Kupferschiefer, reflected light, Polkowice Mine. **A** – nest type structure of native gold, sample PZ-J-7; **B** – nest type structure of native gold, sample PZ-J-6; **C** – nest type structure of native gold on the edge of diagenetic calcite nest, sample PZ-J-7; **D** – big aggregate of native gold, sample PZ-J-7; **E–F** – vein type of native gold structure, sample PZ-J-6

natural alloys with Bi, Cu, Pd and Pb, tellurides, Cu-Au-thiosulphates (Kucha *et al.*, 1997) and silicates (Kucha & Plimer, 2001). The number of Au minerals approved by the International Mimeralogical Association (IMA) reaches several tens. The number of PGE minerals approved by the IMA exceeds 90 (Daltry & Wilson, 1997) but over 500 unidentified and unnamed phases were reported in the literature, which demonstrates the importance of further mineralogical studies. The PGE minerals form two principal genetic types of deposits: (i) layered mafic intrusions (LMI) and (ii) massive sulphides hosted in these intrusions. In last years the rising interest has been observed in studies on unconventional precious metals deposits. The new research projects brought data on new compounds, e.g. Pt-Pd-oxides/hydroxides (Oberthür *et al.*, 2003). The new phases were found also in the secondary oxidation zone of Cu deposit in the Fore-Sudetic Monocline. This zone covers the area of about 40 km^2 between the Polkowice East Field and

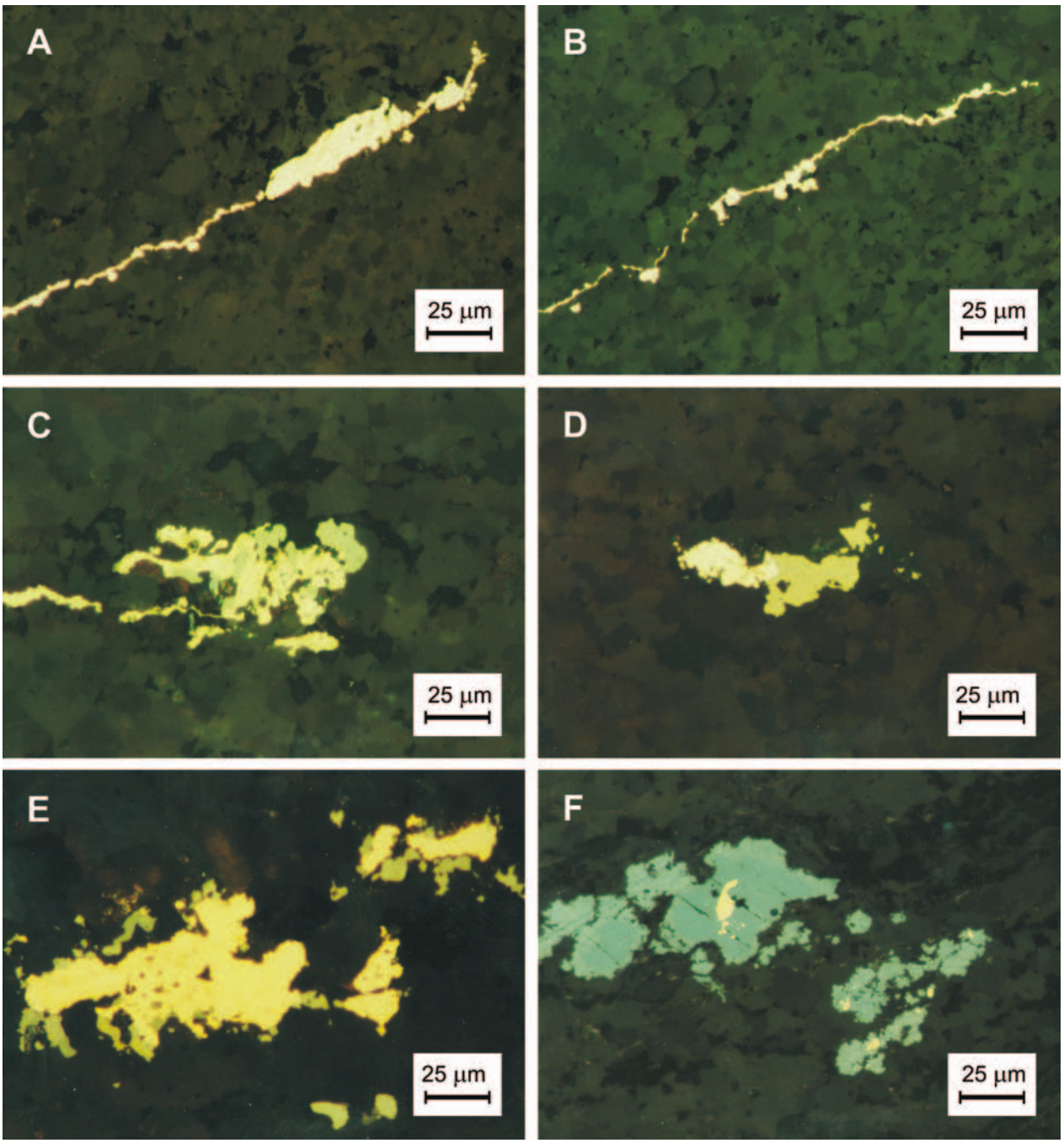

Fig. 57. Gold aggregates and their intergrowths in calcareous variety of the Kupferschiefer, reflected light, Polkowice Mine. **A–B** – vein type of native gold structure, sample PZ-J-6; **C** – nest type structure of native gold (yellow) forming intergrowth with Pd-arsenides (pale grey), sample PZ-J-6; **D** – intergrowth of native gold and chalcopyrite (yellow), sample PZ-J-6; **E** – nest type structure of native gold (yellow) forming intergrowth with Pd-arsenides (pale grey), sample PZ-J-6; **F** – inclusions of native gold (white yellow) in digenite (blue) and chalcocite (pale blue), sample PZ-31/3

the Sieroszowice Mine. The results of 10-years-long studies revealed the zonality of metals distribution: in the marginal zone electrum dominates over high-purity native Au. Minerals from the marginal zone were described e.g., by Kucha (1981) although his genetic model did not relate the Au mineralization to the vast, secondary oxidation zones, as described in later publications (Piestrzyński *et al.*, 1996a, 2002; Pieczonka, 1998, 2000; Piestrzyński & Pieczonka, 1998, 2000; Piestrzyński & Wodzicki, 2000; Pieczonka & Piestrzyński, 2000).

Native gold and electrum

Both the native Au and electrum are rare phases in the Cu deposit. Before the end of the 1990-ties high concentrations of precious metals were encountered only at the Lubin Mine, in so-called "Kupferschiefer with noble metals" (Kucha, 1976a, b, 1982a, b). In 1993, native Au and electrum were identified in samples collected from the Polkowice West Field, from zones of subeconomic copper ore (Report AGH 1996, 1997; Piestrzyński 1996a; Piestrzyński *et al.*, 1996a; Piestrzyński & Pieczonka, 1997a, b).

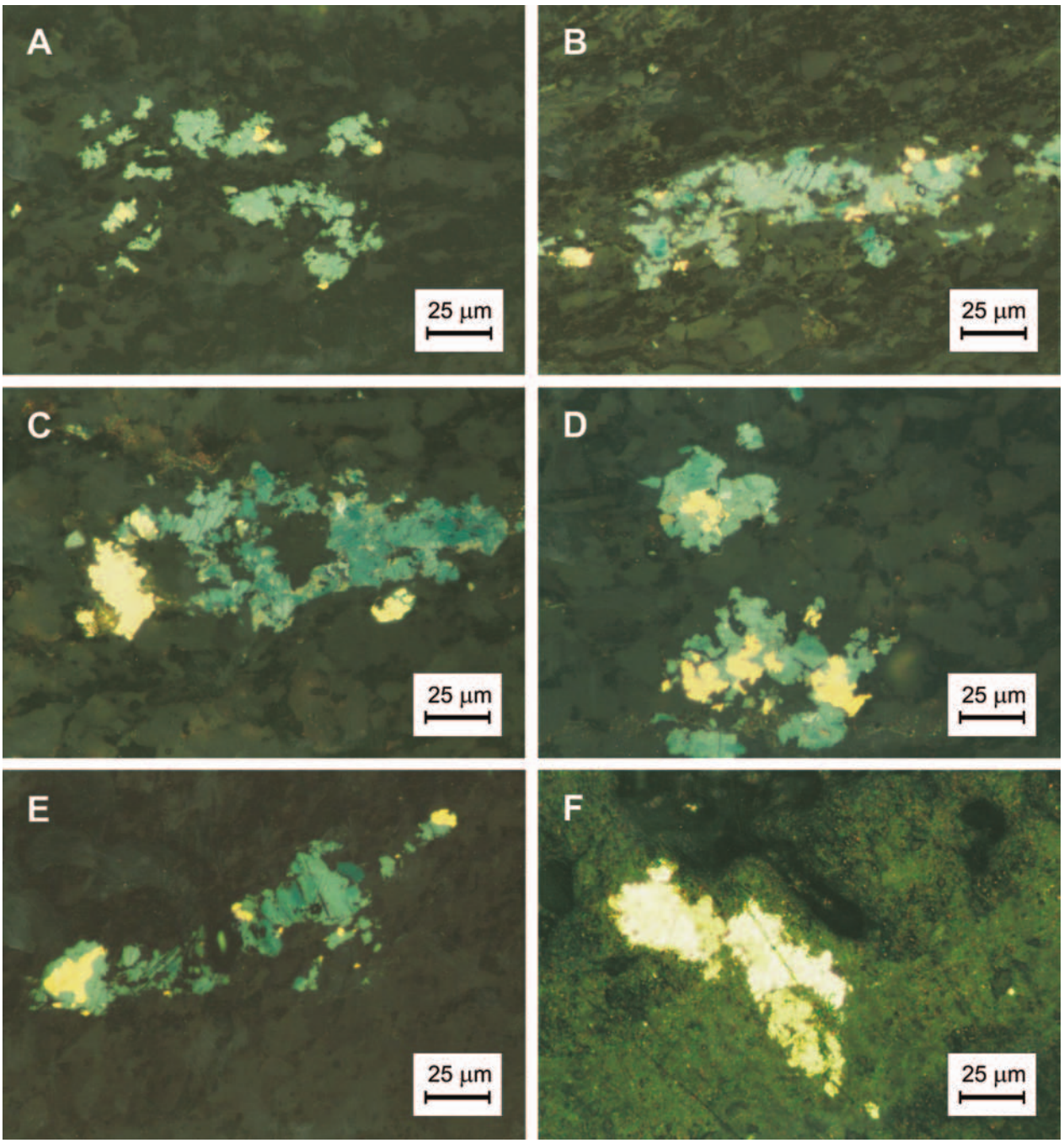

Fig. 58. Gold aggregates and their intergrowths in calcareous variety of the Kupferschiefer, reflected light, Polkowice Mine. **A** – intergrowths of native gold (white-yellow) with chalcocite (pale blue), sample PZ-31/3; **B** – intergrowth of native gold (white-yellow) with chalcocite (pale blue) and covellite (blue), sample PZ-31/3; **C** – nest structure and intergrowth of native gold (white-yellow) with chalcocite (pale blue), and covellite (blue), sample PZ-34/2; **D** – intergrowths of native gold (white-yellow) with chalcocite (pale blue), covellite (blue), and hematite (grey), sample PZ-34/2; **E** – intergrowth of native gold (white-yellow) with chalcocite (pale blue) and covellite (blue), sample PZ-31/3; **F** – intergrowth of native gold (white-yellow) with chalcopyrite (pale yellow), sample PZ-J-17

Precious metals form several parageneses:

1. clausthalite – native Pb – electrum – $AuPb_2$ (Kucha, 1982a, b),

2. Pt-native Au – native Pd – sobolevskite – native Pb (Kucha, 1981; Kucha & Pocheć, 1983),

3. native Au – hematite – bornite – minerals of covellite-chalcocite group (Piestrzyński, 1996a; Piestrzyński *et al.*, 1996a),

4. electrum – tetraauricupride – chalcocite (Piestrzyński & Pieczonka, 1998),

5. electrum – Pd-arsenides – tellurides – selenides – BiPd and CuBi natural alloys – Pd-oxides.

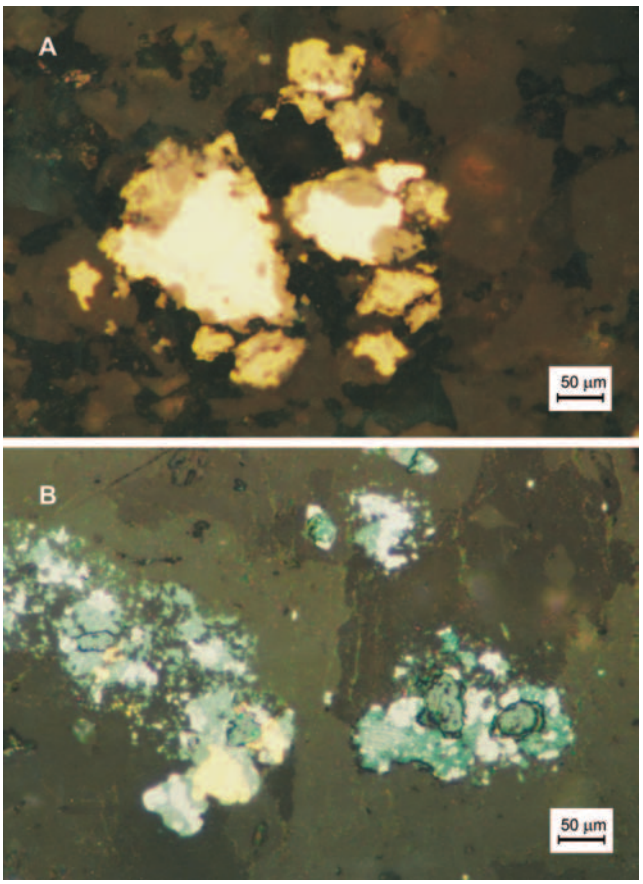

Fig. 59. **A** – intergrowth of native gold (pale yellow) with bornite (orange-brown) and chalcopyrite (grey-yellow) in streaky dolomite, reflected light, sample Sz/III/2, Polkowice Mine; **B** – intergrowths of native gold (pale yellow) with clausthalite (white), digenite (pale blue), covellite (blue) and hematite (grey) in calcite nest, streaky dolomite, reflected light, sample Sz/III/2, Polkowice Mine

The native Au and electrum described in this paper belong to parageneses presented by Piestrzyński (1996a) and Piestrzyński *et al.* (1996a), as well as the native Au – electrum – chalcopyrite – bornite – Pd-arsenides – selenides – natural alloys – oxides paragenesis.

In samples collected from the zones of red spots occurrence a diversified assemblage of ore minerals was found. These zones are out of economic value due to low Cu grade, but precious metals phases, particularly native Au and electrum, form accumulations which may be of industrial interest. Therefore, the further studies (also geochemical) ones were focused on these elements.

Analyses of native Au revealed diversified chemical composition, which depends on the position of particular sample in vertical sequence and in relation to red spots. Native Au from the secondary oxidation zones reveals highest Au contents whereas in the peripheries of these zones and in the areas adjacent to the copper deposit electrum predominates. Chemical analyses allowed the authors distinguish:

– native Au containing over 85 wt.% Au (Tabs 19, 20, 21),

– electrum containing from 50 to 85 wt.% Au (Tabs 21–26),

– tetraauricupride (AuCu) containing from 71 to 76 wt.% Au (Tabs 26, 27).

High-purity native Au forms intergrowths mostly with chalcopyrite, covellite and hematite in the Kupferschiefer and in the sandstones. Electrum usually coexists with Pd-arsenides, selenides, tellurides, chalcocite and digenite, rarely with tetraauricupride in the Kupferschiefer and in the carbonates.

High-purity native Au was encountered in brownish-red Kupferschiefer from the southern part of the Polkowice West Field. From 46 microprobe analyses 39 revealed Au contents over 90 wt.% (90.22–98.2 wt.%), (Tabs 19, 20). In the remaining grains Au contents varied from 86.05 to

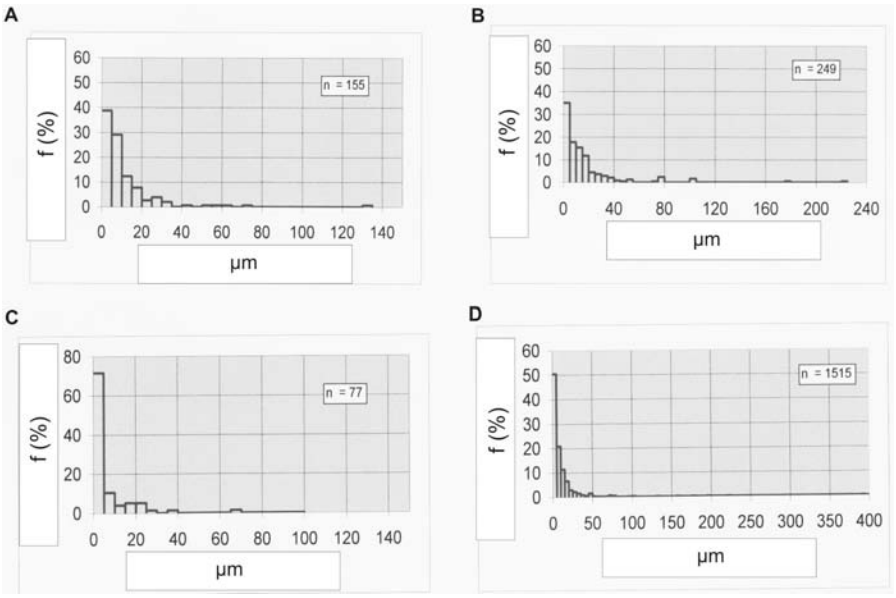

Fig. 60. Histograms showing size of gold and electrum grains. **A** – in sandstone; **B** – in the boundary dolomite and maroon shale; **C** – in dolomite; **D** – in the ore

Table 19

Microprobe composition of native gold and electrum from the Kupferschiefer, mining section G-31, Polkowice West Field (after Piestrzyński & Pieczonka. 1997a) (upper figure – wt.%; lower figure – atomic proportions)

Sample	Au Lα	Ag Lα	Bi Lα	Hg Lα	Cu Kα	Fe Kα	Pt Lα	Pd Lα	As Kα	S Kα	Total
283A/1	96.72	3.62	0.24	1.28	0.95	0.17	≤0.08	0.13	≤0.10	≤0.10	103.11
	0.4910	0.0336	0.0011	0.0064	0.0149	0.0030		0.0012			
283A/2	94.52	4.15	≤0.08	1.63	0.68	0.12	≤0.08	0.14	0.13	≤0.10	101.37
	0.4799	0.0385		0.0081	0.0107	0.0021		0.0013	0.0017		
283A/3	97.84	2.72	≤0.08	0.92	0.53	0.06	≤0.08	≤0.08	0.14	≤0.10	102.21
	0.4967	0.0252		0.0046	0.0083	0.0011			0.0019		
283A/4	98.52	2.12	≤0.08	1.09	0.57	≤0.05	≤0.08	≤0.08	0.21	≤0.10	102.51
	0.5002	0.0197		0.0054	0.0090				0.0028		
283A/5	95.79	2.43	0.52	1.28	0.58	≤0.05	≤0.08	0.15	0.16	≤0.10	100.91
	0.4863	0.0225	0.0025	0.0064	0.0091			0.0014	0.0021		
283A/6	96.95	2.89	0.09	0.96	0.54	≤0.05	0.10	0.12	0.11	≤0.10	102.76
	0.4922	0.0268	0.0004	0.0048	0.0085		0.0005	0.0011	0.0015		
283A/7	97.87	2.76	≤0.08	1.12	0.66	≤0.05	≤0.08	≤0.08	0.11	≤0.10	102.52
	0.4969	0.0256		0.0056	0.0104				0.0015		
283A/8	95.34	2.86	≤0.08	0.84	0.33	≤0.05	0.10	≤0.08	≤0.10	≤0.10	99.47
	0.4840	0.0265		0.0042	0.0052		0.0005				
283A/9	97.71	3.07	≤0.08	1.41	0.39	≤0.05	≤0.08	0.10	0.13	≤0.10	102.81
	0.4961	0.0285		0.0070	0.0061			0.0009	0.0017		
283A/10	93.68	3.19	≤0.08	1.02	0.45	≤0.05	≤0.08	0.21	0.15	≤0.10	98.70
	0.4756	0.0296		0.0051	0.0071			0.0020	0.0020		
283A/11	96.94	3.42	0.49	1.34	0.41	≤0.05	≤0.08	0.17	0.13	≤0.10	102.90
	0.4922	0.0317	0.0023	0.0067	0.0065			0.0016	0.0017		
283A/12	97.24	3.21	≤0.08	1.11	0.32	≤0.05	0.19	0.23	0.19	≤0.10	102.49
	0.4937	0.0298		0.0055	0.0050		0.0010	0.0022	0.0025		
283A/13	92.79	5.64	≤0.08	1.82	0.39	≤0.05	≤0.08	≤0.08	0.18	≤0.10	100.82
	0.4711	0.0523		0.0091	0.0061				0.0024		
283A/15	96.83	3.52	≤0.08	1.01	0.35	≤0.05	≤0.08	0.10	0.11	≤0.10	101.92
	0.4916	0.0326		0.0050	0.0055			0.0009	0.0015		
283B/1	94.75	4.75	≤0.08	1.01	0.08	0.19	≤0.08	0.13	0.11	≤0.10	101.02
	0.4810	0.0440		0.0050	0.0013	0.0034		0.0012	0.0015		
283B/2	96.97	2.58	≤0.08	1.20	≤0.07	0.06	≤0.08	≤0.08	0.14	≤0.10	100.95
	0.4923	0.0239		0.0060		0.0011			0.0019		
283B/3	96.70	4.10	0.38	0.92	0.15	≤0.05	≤0.08	≤0.08	0.13	≤0.10	102.38
	0.4909	0.0380	0.0018	0.0046	0.0024				0.0017		
283B/4	95.52	4.30	0.12	1.28	0.13	≤0.05	≤0.08	≤0.08	0.13	≤0.10	101.48
	0.4850	0.0399	0.0006	0.0064	0.0020				0.0017		
283B/5	86.05	13.39	≤0.08	1.73	≤0.07	≤0.05	≤0.08	≤0.08	0.15	≤0.10	101.32
	0.4369	0.1241		0.0086					0.0020		
283B/6	96.30	4.57	≤0.08	1.20	≤0.07	0.07	≤0.08	0.08	0.11	≤0.10	102.18
	0.4889	0.0424		0.0060		0.0013		0.0008	0.0015		
283B/7	78.70	18.61	0.24	1.53	≤0.07	≤0.05	0.14	≤0.08	0.18	≤0.10	99.40
	0.3996	0.1725	0.0011	0.0076			0.0007		0.0024		
283B/8	88.67	9.42	≤0.08	1.26	≤0.07	0.05	≤0.08	≤0.08	0.12	≤0.10	99.52
	0.4502	0.0873		0.0063		0.0009			0.0016		
283C/1	91.00	11.01	≤0.08	1.57	≤0.07	0.06	≤0.08	≤0.08	0.11	≤0.10	103.75
	0.4620	0.1021		0.0078		0.0011			0.0015		

Table 19 continued

Sample	Au Lα	Ag Lα	Bi Lα	Hg Lα	Cu Kα	Fe Kα	Pt Lα	Pd Lα	As Kα	S Kα	Total
283C/2	93.94	6.47	≤0.08	0.71	0.08	≤0.05	0.09	≤0.08	≤0.10	0.15	101.44
	0.4769	0.0600		0.0035	0.0013		0.0005			0.0047	
283C/3	90.22	6.50	≤0.08	1.31	≤0.07	≤0.05	≤0.08	≤0.08	0.15	≤0.10	98.18
	0.4580	0.0603		0.0065					0.0020		
283C/4	93.60	4.24	≤0.08	0.99	0.08	0.08	≤0.08	≤0.08	0.14	≤0.10	99.13
	0.4752	0.0393		0.0049	0.0013	0.0014			0.0019		
283C/5	87.43	12.35	≤0.08	1.37	≤0.07	0.08	≤0.08	≤0.08	≤0.10	≤0.10	101.23
	0.4439	0.1145		0.0068		0.0014					
283C/6	93.27	5.89	≤0.08	1.43	≤0.07	0.08	≤0.08	≤0.08	≤0.10	≤0.10	100.67
	0.4735	0.0546		0.0071		0.0014					
283C/7	86.90	9.74	≤0.08	1.58	0.07	0.10	≤0.08	≤0.08	0.18	0.15	98.72
	0.4412	0.0903		0.0079	0.0011	0.0018			0.0024	0.0047	
283C/8	95.57	4.84	≤0.08	1.49	0.12	0.06	≤0.08	0.23	≤0.10	≤0.10	102.31
	0.4852	0.4487		0.0074	0.0019	0.0011		0.0022			
283C/9	96.07	3.60	≤0.08	1.13	0.75	0.06	0.13	0.18	0.16	≤0.10	102.08
	0.4877	0.0334		0.0056	0.0118	0.0011	0.0007	0.0017	0.0021		
283C/10	97.23	3.75	0.12	1.05	0.29	0.06	≤0.08	≤0.08	0.21	≤0.10	102.71
	0.4936	0.0348	0.0006	0.0052	0.0046	0.0011			0.0028		
283D/1	92.48	5.79	≤0.08	1.39	0.23	0.38	≤0.08	0.08	0.13	≤0.10	100.48
	0.4695	0.0537		0.0069	0.0036	0.0068		0.0008	0.0017		
283D/2	96.61	3.12	0.10	1.03	0.25	0.19	≤0.08	0.44	0.12	0.11	101.97
	0.4905	0.0289	0.0005	0.0051	0.0039	0.0034		0.0041	0.0016	0.0034	
283D/3	97.25	2.76	≤0.08	1.33	0.11	0.28	≤0.08	≤0.08	0.10	≤0.10	101.83
	0.4937	0.0256		0.0066	0.0017	0.0050			0.0013		
283D/4	94.43	3.64	≤0.08	1.33	0.25	0.57	≤0.08	≤0.08	0.18	≤0.10	100.40
	0.4794	0.0337		0.0066	0.0039	0.0102			0.0024		
283D/5	92.45	7.84	≤0.08	1.37	0.39	0.45	0.19	≤0.08	0.13	≤0.10	102.82
	0.4694	0.0727		0.0068	0.0061	0.0081	0.0010		0.0017		

88.67 wt.%. Only a single grain of electrum was found, of composition 78.70 wt.% Au and 18.61 wt.% Ag. Even this grain showed Au content close to the upper limit of weight proportions. High-purity native Au contains admixtures of Ag (usually below 10 wt.%) as well as Hg (0.71–1.82 wt.%), Cu (0.58–2.9 wt.%), Pd (0.1–0.44 wt.%), Pt (up to 0.23 wt.%) and As (up to 0.24 wt.%) (Pieczonka, 1998). This variety of native Au was identified also in the red-coloured sandstone from the same area. Preliminary results of analyses were published by Piestrzyński *et al.* (1996a). These analyses document the presence of native Au containing over 90 wt.% of metal (90.15–94.79 wt.%). Other analyzed crystals contained from 81.26 to 88.6 wt.% Au. Native Au from the red-spotted sandstone contains from 5.08 to 15.93 wt.% Ag and from 0.21 to 1.08 wt.% Hg.

Analyses of native Au originating from the grey Kupferschiefer revealed the presence of Au in only its dolomitic variety. Accompanying electrum usually contains over 80 wt.% Au (Tab. 21). The presence of high-purity Au phases in grey and black Kupferschiefer is a rarity although it should be noticed that the sandstone at the bottom and the dolomite at the top of this Kupferschiefer were red-coloured. Native Au has the admixtures of: Ag (12.36–15.37 wt.%), Hg (0.80–1.28 wt.%), Cu (0.63–1.16 wt.%) and As (0.16–0.29 wt.%). Electrum contains the same admixtures in similar quantities: Hg (0.21–1.07 wt.%), Cu (0.15–1.75 wt.%), As (0.06–0.24 wt.%) and Fe (0.04–0.77 wt.%).

Microprobe analyses indicated the presence of two groups of natural alloys in the clayey and dolomitic varieties of the grey Kupferschiefer. In the first group Ag contents are low (16–22 wt.%, Tab. 21). Such electrum usually forms paragenesis with native Au. The second group includes alloys containing up to 63 wt.% Ag. These minerals can be regarded as members of küstelite group (15–50 wt.% Au), (Tab. 22–26). Highest variability in electrum composition was observed in the transitional zone of oxidized area (TZ) which is usually located in the grey Kupferschiefer. Contents of both Ag and Au cover the full range of values possible in this mineral (Tabs 22, 23). The most common admixtures in electrum are: Se (up to 6.09 wt.%), Te (up to 4.57 wt.%) and Hg (up to 4.38 wt.%) (Tabs 22, 23). Occassionally, Pb, Pt, Pd and Fe were detected (Tab. 22).

Table 20

Microprobe composition of native gold and electrum from the Kupferschiefer (clayey variety), mining section G-31, Polkowice West Field (after Pieczonka 1998), sequence No. PZ-21/1, (upper figure – wt.%; lower figure – atomic proportions)

Sample	As Kα	Bi Lα	Hg Lα	Au Lα	Cu Kα	Fe Kα	Pt Lα	S Kα	Pd Lα	Ag Lα	Total
286/B1	0.21	0.16	0.77	95.68	1.61	0.10	≤0.07	≤0.15	0.16	3.28	101.97
	0.0028	0.0008	0.0038	0.4858	0.0253	0.0018			0.0015	0.0304	
286/B1	0.18	≤0.10	1.24	94.44	1.56	0.15	≤0.07	≤0.15	0.42	359	101.58
	0.0024		0.0062	0.4795	0.0245	0.0027			0.0039	0.0333	
286/B2	0.10	≤0.10	1.78	92.65	1.43	0.13	≤0.07	≤0.15	0.23	4.74	101.06
	0.0013		0.0089	0.4704	0.0225	0.0023			0.0022	0.0439	
286/B3	0.11	≤0.10	1.27	95.12	1.32	0.16	0.14	≤0.15	0.06	3.78	101.96
	0.0015		0.0063	0.4829	0.0208	0.0029	0.0007		0.0006	0.0350	
286/B4	0.12	≤0.10	1.03	95.83	0.54	0.34	≤0.07	≤0.15	0.08	2.79	101.73
	0.0016		0.0051	0.4865	0.0242	0.0061			0.0008	0.0259	
286/B5	≤0.10	≤0.10	0.97	94.43	1.45	0.17	≤0.07	≤0.15	≤0.05	3.36	100.38
			0.0048	0.4794	0.0228	0.0030				0.0311	
286/A6	0.16	≤0.10	1.39	94.34	1.14	0.08	≤0.07	≤0.15	0.13	3.15	100.39
	0.0021		0.0069	0.4790	0.0179	0.0014			0.0012	0.0292	
286/A7	0.10	0.15	0.96	94.60	2.69	0.23	0.23	≤.15	0.30	3.57	102.83
	0.0013	0.0007	0.0048	0.4803	0.0423	0.0041	0.0012		0.0028	0.0331	
286/C8	0.24	0.16	1.42	94.06	0.58	0.08	≤0.07	≤0.15	≤0.05	3.37	99.91
	0.0032	0.0008	0.0071	0.4775	0.0091	0.0014				0.0312	

Electrum from the grey, clayey Kupferschiefer sampled at the Polkowice West Field shows significant variability of Au (49.80–80.14 wt.%) and Ag (19.01–46.57 wt.%) contents. Moreover, admixtures of Hg (1.10–3.69 wt.%), Cu (0.13–1.03wt.%) and As (0.09–0.23 wt.%) were detected. The results point out to the presence of küstelite, which may contain 40.18–49.48 wt.% Au and 47.97–55.66 wt.% Ag, and high admixtures of Hg (2.53–4.38 wt.%) as well as traces of Cu and As (Tab. 23). In a similar Kupferschiefer variety from the Polkowice Main Field electrum of more stable chemical composition was found (57.33–68.61 wt.% Au, 27.49–40.28 wt.% Ag, 1.29–2.31 wt.% Hg and 0.35–0.58 wt.% Cu (Tab. 24).

Both electrum and küstelite were found also in the grey Kupferschiefer (Tab. 25). Electrum contains from 50.86 to 71.17 wt.% Au and from 26.39 do 46.73 wt.% Ag as well as admixtures of Hg (1.23–3.60 wt.%), Cu (0.52–1.21 wt.%) and As (0.06–0.19 wt.%). Au contents in küstelite vary from 25.98 to 48.59 wt.% and Ag from 48.19 to 67.51 wt.% Characteristic are high admixtures of Hg – from 3.91 to 6.34 wt.%.

In the red-colored Boundary Dolomite from the Polkowice West Field (Tab. 26), küstelite is the main Au phase. Its contents change from 36.49 to 46.66 wt.% whereas those of Ag – from 45.80 to 54.80 wt.%. Most important trace elements are: Hg (5.34–7.36 wt.%), Cu (0.09–3.96 wt.%) and As (0.05–0.26 wt.%). Electrum from this Boundary Dolomite has from 58.49 to 77.66 wt.% Au and from 21.45 to 35.89 wt.% Ag. Contents of Hg are much lower than in küstelite: from 1.02 to 2.03 wt.%. Other admixtures are Cu (0.16–2.43 wt.%) and As (0.17–0.24 wt.%) (Pieczonka, 1998).

Three results (Tab. 26) indicate the presence of high-Au/high-Cu variety of electrum of composition: Au (78.44–76.52 wt.%), Cu (23.36–21.56 wt.%) with small amounts of Ag (0.18–0.21 wt.%), Hg (0.55–0.88 wt.%), As and Bi. Calculated chemical formulae of this mineral are: $Au_{1.0413}Cu_{1,0000}$ for measurement point A/10, $Au_{1.0168}Cu_{1,0000}$ for measurement point A/11 (Piestrzyński & Pieczonka, 1998) and $Au_{1.1734}Cu_{1.0000}$ for the third point. This phase was identified as tetraauricupride. It was described for the first time from the Fore-Sudetic Monocline deposit by Piestrzyński and Pieczonka (1998). Tetraauricupride forms intergrowths with high-Hg electrum (Tab. 26) and Cu-sulphides, Pd-arsenides and selenides. The presence of tetraauricupride in this deposit is very interesting as it has already been known mostly from ultramafic intrusions (Piestrzyński & Pieczonka, 1998).

Chemical composition of studied tetraauricupride is close to that described by Tarkian *et al.* (1992) from the Skyros Island: 73.3–75.1 wt.% Au, 23.7–24.2 wt.% Cu and 0.4–1.6 wt.% Fe. The difference between tetraauricupride from ophiolitic and ultramafic complexes, and from reducing sediments (i.e. from the Polkowice deposit) appears in trace elements set.

The results of microprobe analyses support the microscopic observations that Au minerals from the central part of secondary oxidation zone differ in parageneses from those described from the so-called "Kupferschiefer with noble metals" (Kucha, 1975, 1982a, b; Salamon, 1979; Pie-

Table 21

Microprobe composition of native gold and electrum from the Kupferschiefer (dolomitic variety), mining section G-31, Polkowice West Field (after Piestrzyński & Pieczonka, 1997a), sequence No. PR 18-0188, (upper figure – wt.%; lower figure – atomic proportions)

Sample	As Kα	Bi Lα	Hg Lα	Au Lα	Cu Kα	Fe Kα	Pt Lα	S Kα	Pd Lα	Ag Lα	Total
I/18	0.19	0.39	0.90	83.58	0.79	≤0.03	≤0.03	≤0.05	≤0.05	14.60	100.45
	0.0025	0.0019	0.0045	0.4243	0.0124					0.1354	
I/18b	0.09	0.20	0.61	82.45	0.41	0.14	0.07	≤0.05	≤0.05	19.32	103.29
	0.0012	0.0010	0.0030	0.4186	0.0065	0.0025	0.0004			0.1791	
I/19	0.11	≤0.05	0.85	83.28	0.63	≤0.03	≤0.03	≤0.05	≤0.05	15.52	100.39
	0.0015		0.0042	0.4228	0.0099					0.1439	
I/20	0.23	0.32	0.76	80.60	0.25	0.04	0.08	≤0.05	≤0.05	17.93	100.21
	0.0031	0.0015	0.0038	0.4092	0.0039	0.0007	0.0004			0.1662	
I/21	0.08	≤0.05	0.73	74.76	0.20	≤0.03	≤0.03	≤0.05	≤0.05	22.93	98.70
	0.0011		0.0036	0.3796	0.0031					0.2126	
I/22	0.16	≤0.05	1.19	85.04	1.13	0.11	≤0.03	≤0.05	≤0.05	13.84	101.47
	0.0021		0.0059	0.4317	0.0178	0.0020				0.1283	
I/23	0.22	≤0.05	0.56	82.29	1.33	0.27	≤0.03	≤0.05	≤0.05	16.91	101.58
	0.0029		0.0028	0.4178	0.0209	0.0048				0.1568	
$\bar{x}$	**0.15**	**0.13**	**0.80**	**81.71**	**0.68**	**0.09**				**17.30**	
	0.0020	0.0006	0.0040	0.4148	0.0107	0.0016				0.1604	
III/49	0.19	≤0.05	0.50	80.01	1.75	0.76	0.10	≤0.05	≤0.05	17.25	100.56
	0.0025		0.0025	0.4062	0.0275	0.0136	0.0005			0.1599	
III/50	0.21	≤0.05	0.92	80.92	1.72	0.77	≤0.03	0.11	≤0.05	17.46	102.11
	0.0028		0.0046	0.4108	0.0271	0.0138		0.0034		0.1619	
III/51	0.21	0.29	0.96	80.12	1.29	0.65	0.05	0.14	≤0.05	16.24	99.95
	0.0028	0.0014	0.0048	0.4068	0.0203	0.0116	0.0003	0.0044		0.1506	
III/53	0.06	≤0.05	0.68	82.07	1.44	0.56	≤0.03	≤0.05	≤0.05	16.10	100.91
	0.0008		0.0034	0.4167	0.0227	0.0100				0.1493	
III/54	0.16	0.25	0.21	83.98	1.62	0.63	≤0.03	≤0.05	≤0.05	16.94	103.79
	0.0021	0.0012	0.0010	0.4264	0.0256	0.0113				0.1570	
III/55	0.14	≤0.05	0.35	80.30	0.83	0.37	≤0.03	≤0.05	≤0.05	17.07	99.06
	0.0019		0.0017	0.4077	0.0131	0.0066				0.1582	
III/56	0.15	≤0.05	0.83	78.03	1.21	0.63	≤0.03	0.44	≤0.05	17.61	98.90
	0.0020		0.0041	0.3962	0.0190	0.0113		0.0137		0.1633	
$\bar{x}$	**0.16**	**0.08**	**0.69**	**80.72**	**1.41**	**0.62**		**0.17**		**16.96**	
	0.0021	0.0004	0.0034	0.4098	0.0222	0.0111		0.0053		0.1572	
I/14	0.32	≤0.05	0.80	85.50	0.63	≤0.03	≤0.03	≤0.05	≤0.05	14.94	102.19
	0.0043		0.0040	0.4341	0.0099					0.1385	
I/15	0.14	≤0.05	0.31	83.94	0.15	0.04	≤0.03	≤0.05	≤0.05	18.10	102.68
	0.0019		0.0015	0.4262	0.0024	0.0007				0.1678	
I/16	0.29	≤0.05	1.28	86.77	0.80	≤0.03	0.16	≤0.05	≤0.05	12.36	101.66
	0.0039		0.0064	0.4405	0.0126		0.0008			0.1146	
I/17	0.17	≤0.05	1.05	85.92	1.16	0.17	≤0.03	≤0.05	≤0.05	12.79	101.26
	0.0023		0.0052	0.4362	0.0183	0.0030				0.1202	
$\bar{x}$	**0.23**		**0.86**	**85.53**	**0.69**					**14.55**	
	0.0031		0.0043	0.4342	0.0108	0.13				0.1353	
II/1	0.23	≤0.005	1.15	84.79	0.99	0.0023	≤0.03	0.05	≤0.05	15.37	102.71
	0.0031		0.0057	0.4305	0.0156	0.24		0.0016		0.1425	
II/2	0.13	0.28	0.91	82.20	0.86	0.0043	≤0.03	≤0.05	≤0.05	17.76	102.38
	0.0017	0.0013	0.0045	0.4173	0.0135					0.1646	

Table 21 continued

Sample	As Kα	Bi Lα	Hg Lα	Au Lα	Cu Kα	Fe Kα	Pt Lα	S Kα	Pd Lα	Ag Lα	Total
II/3	0.22	0.05	0.48	83.87	0.93	0.26	≤0.03	0.05	≤0.05	16.52	102.38
	0.0029	0.0002	0.0024	0.4258	0.0146	0.0047		0.0016		0.1531	
II/4	0.24	≤0.05	0.67	83.89	1.19	0.61	≤0.03	0.33	≤0.05	11.97	98.57
	0.0032		0.0033	0.4259	0.0187	0.0109		0.0103		0.1110	
II/5	0.17	0.07	0.63	83.73	1.01	0.29	≤0.03	0.05	≤0.05	15.47	101.37
	0.0023	0.0003	0.0031	0.4251	0.0159	0.0052		0.0016		0.1434	
II/6	0.24	≤0.05	0.47	84.35	0.94	0.23	≤0.03	≤0.05	≤0.05	16.08	102.31
	0.0032		0.0023	0.4282	0.0148	0.0041				0.1491	
II/7	0.08	≤0.05	1.07	83.12	0.95	0.29	0.05	≤0.05	≤0.05	16.25	101.81
	0.0011		0.0053	0.4220	0.0149	0.0052	0.0003			0.1506	
$\bar{x}$	**0.19**	**0.13**	**0.77**	**83.71**	**0.98**	**0.29**		**0.12**		**15.63**	
	0.0025	0.0006	0.0038	0.4250	0.0154	0.0052		0.0038		0.1448	

Table 22

EDS composition of electrum from the Kupferschiefer (dolomitic variety), Polkowice West Field [wt.%]

Sample	Ag Lα	Au Lα	Pb Lα	Se Kα	Pd Lα	Pt Lα	As Kα	Te Lα	Fe Kα	Total
PZ-J7-9a/10	19.18	79.56	≤0.3	1.20	≤0.05	≤0.15	≤0.2	≤0.1	≤0.05	99.94
PZ-J7-9a/13	16.04	76.46	≤0.3	3.59	≤0.05	≤0.15	1.20	2.57	0.14	100.00
PZ-J7-9a/14	31.34	61.41	1.14	0.60	0.16	≤0.15	0.40	4.57	0.38	100.00
PZ-J7-9/1	25.29	66.05	≤0.3	6.09	≤0.05	1.22	0.47	0.89	n.a.	100.00
PZ-J7-10/1	24.42	74.37	≤0.3	n.a.	≤0.05	0.16	0.26	0.79	n.a.	100.00
PZ-J7-4/1	58.74	41.26	≤0.3	n.a.	≤0.05	≤0.15	≤0.2	≤0.1	n.a.	100.00
PZ-J7-4/2	62.79	36.86	0.35	n.a.	≤0.05	≤0.15	≤0.2	≤0.1	n.a.	100.00
PZ-J7-4/3	25.62	74.38	≤0.3	n.a.	≤0.05	≤0.15	≤0.2	≤0.1	n.a.	100.00
PZ-J7-4/4	28.87	71.13	≤0.3	n.a.	≤0.05	≤0.15	≤0.2	≤0.1	n.a.	100.00
PZ-J7-2/2	25.15	73.96	≤0.3	n.a.	0.89	≤0.15	≤0.2	≤0.1	n.a.	100.00
PZ-J7-3/3	25.03	74.52	≤0.3	n.a.	≤0.05	0.45	≤0.2	≤0.1	n.a.	100.00
PZ-J7-3/2	25.49	74.51	≤0.3	n.a.	≤0.05	≤0.15	≤0.2	≤0.1	n.a.	100.00
PZ-J7-3/1	24.81	74.83	≤0.3	n.a.	0.36	≤0.15	≤0.2	≤0.1	n.a.	100.00
PZ-J7-5/3	34.06	65.94	≤0.3	n.a.	≤0.05	≤0.15	≤0.2	≤0.1	n.a.	100.00
PZ-J7-5/2	27.28	72.76	≤0.3	n.a.	0.05	≤0.15	≤0.2	≤0.1	n.a.	100.00
PZ-J7-5/1	31.51	68.49	≤0.3	n.a.	≤0.05	≤0.15	≤0.2	≤0.1	n.a.	100.00
PZ-J7-14/1	27.63	72.37	≤0.3	n.a.	≤0.05	≤0.15	≤0.2	≤0.1	n.a.	100.00
PZ-J7-14/2	24.76	74.94	≤0.3	n.a.	≤0.05	≤0.15	≤0.2	≤0.1	n.a.	100.00
PZ-J7-14/3	61.06	38.94	≤0.3	n.a.	≤0.05	≤0.15	≤0.2	≤0.1	n.a.	100.00
PZ-J7-14/4	63.33	36.67	≤0.3	n.a.	≤0.05	≤0.15	≤0.2	≤0.1	n.a.	100.00
PZ-J7-16/5	30.55	69.28	≤0.3	n.a.	≤0.05	≤0.15	≤0.2	≤0.1	n.a.	100.00
PZ-J7-19/1	18.10	81.90	≤0.3	n.a.	≤0.05	≤0.15	≤0.2	≤0.1	n.a.	100.00
PZ-J7-19/3	45.72	47.95	2.00	0.31	≤0.05	≤0.15	≤0.2	4.02	n.a.	100.00
PZ-J7-19/9	26.98	73.02	≤0.3	n.a.	≤0.05	≤0.15	≤0.2	≤0.1	n.a.	100.00
PZ-J7-19/12	25.66	74.34	≤0.3	n.a.	≤0.05	≤0.15	≤0.2	≤0.1	n.a.	100.00
PZ-J7-19/13	72.45	27.55	≤0.3	n.a.	≤0.05	≤0.15	≤0.2	≤0.1	n.a.	100.00
PZ-J7-19/14	25.84	74.16	≤0.3	n.a.	≤0.05	≤0.15	≤0.2	≤0.1	n.a.	100.00
AP-291/3-7/1	32.60	67.40	≤0.3	n.a.	≤0.05	≤0.15	≤0.2	≤0.1	n.a.	100.00
AP-291/3-7/2	42.30	54.76	≤0.3	n.a.	≤0.05	2.95	≤0.2	≤0.1	n.a.	100.00

Table 22 continued

Sample	Ag Lα	Au Lα	Pb Lα	Se Kα	Pd Lα	Pt Lα	As Kα	Te Lα	Fe Kα	Total
AP-291/3-7/3	30.79	69.21	≤0.3	n.a.	≤0.05	≤0.15	≤0.2	≤0.1	n.a.	100.00
AP-291/3-7/4	33.92	66.08	≤0.3	n.a.	≤0.05	≤0.15	≤0.2	≤0.1	n.a.	100.00
AP-291/3-7/5	40.36	59.64	≤0.3	n.a.	≤0.05	≤0.15	≤0.2	≤0.1	n.a.	100.00
AP-291/3-7/6	34.92	64.07	≤0.3	n.a.	≤0.05	1.02	≤0.2	≤0.1	n.a.	100.00
AP-291/3-3-2	38.70	61.30	≤0.3	n.a.	≤0.05	≤0.15	≤0.2	≤0.1	n.a.	100.00
AP-291/3-2-4	37.63	56.84	≤0.3	n.a.	≤0.05	1.39	2.43	≤0.1	Ni = 0.72	100.00
P2J7-5-3	34.00	65.94	n.a.	n.a.	n.a.	n.a.	n.a.	n.a.	n.a.	100.00
P2J7-5-2	27.28	72.66	n.a.	n.a.	n.a.	n.a.	n.a.	n.a.	n.a.	100.00
P2J7-5-1	31.51	68.49	n.a.	n.a.	n.a.	n.a.	n.a.	n.a.	n.a.	100.00

strzyński, 1996a). Phases described by Kucha (1982a, b) contain usually from 50 to 75 wt.% Au and are enriched in Hg (up to 6.30 wt.%) as well as in Pt and Pd, rarely in Pb (Kucha & Mayer, 1996). Phases described in the following paper, particularly originating from the brownish-red Kupferschiefer and sandstone commonly show over 85 wt.% Au (Tabs 19–21). On the other hand, electrum reveals lower amounts of Au (50–85 wt.%) and much lower admixtures of Hg (maximum about 3 wt.%) in comparison with results published by Kucha (1976a, b). Higher contents of Hg (over 6 wt.%) appear in küstelite. Analyses did not show significant contents of Pt and Pd as well as did not detected Pb.

Table 23

Microprobe composition of electrum from the Kupferschiefer (clayey variety), mining section G-31, Polkowice West Field (after Pieczonka, 1998), sequence No. PZ-25/2 (upper figure – wt.%; lower figure – atomic proportions)

Sample	As Kα	Bi Lα	Hg Lα	Au Lα	Cu Kα	Fe Kα	Pt Lα	S Kα	Pd Lα	Ag Lα	Total
287/C1	0.11	0.11	1.10	77.36	0.72	≤0.05	≤0.05	≤0.15	≤0.05	19.82	99.22
	0.0015	0.0005	0.0055	0.3928	0.0113					0.1837	
287/C2	0.18	≤0.10	1.68	61.29	0.13	≤0.05	≤0.05	≤0.15	0.07	34.95	98.30
	0.0024		0.0084	0.3112	0.0020				0.0007	0.3240	
287/C3	0.14	≤0.10	2.70	53.88	0.42	≤0.05	≤0.05	≤0.15	≤0.05	41.52	98.66
	0.0019		0.0135	0.2735	0.0066					0.3849	
287/A4	0.19	0.43	4.38	42.07	0.10	≤0.05	≤0.05	≤0.15	≤0.05	52.82	99.99
	0.0025	0.0021	0.0218	0.2136	0.0016					0.4897	
287/A5	0.17	≤0.10	2.53	49.48	0.12	≤0.05	≤0.05	≤0.15	0.15	47.97	100.42
	0.0023		0.0126	0.2512	0.0019				0.0014	0.4447	
287/A6	0.13	≤0.10	2.13	54.85	≤0.08	≤0.05	≤0.05	≤0.15	≤0.05	43.06	100.15
	0.0017		0.0106	0.2785						0.3992	
287/A7	0.14	0.34	3.69	51.16	0.25	≤0.05	≤0.05	≤0.15	≤0.05	45.36	100.94
	0.0019	0.0016	0.0184	0.2597	0.0039					0.4205	
287/A8	0.09	0.32	3.52	49.80	0.47	≤0.05	≤0.05	≤0.15	≤0.05	46.57	100.77
	0.0012	0.0015	0.0175	0.2528	0.0074					0.4317	
287/B9	0.14	≤0.10	1.58	80.14	1.03	≤0.05	≤0.05	≤0.15	≤0.05	19.01	101.90
	0.0019		0.0079	0.4069	0.0162					0.1762	
287/B10	0.23	≤0.10	2.41	56.26	≤0.08	≤0.05	≤0.05	≤0.15	≤0.05	41.14	100.04
	0.0031		0.0120	0.2856						0.3814	
287/B11	0.10	≤0.10	3.30	42.90	0.58	≤0.05	≤0.05	≤0.15	≤0.05	54.47	101.35
	0.0013		0.0165	0.2178	0.0091					0.5050	
287/B12	0.15	≤0.10	3.18	40.18	0.14	≤0.05	0.10	≤0.15	≤0.05	55.66	99.41
	0.0020		0.0159	0.2040	0.0022		0.0005			0.5160	

Table 24

EDS composition of electrum, pitchy Kupferchiefer variety, mining section PG-1/3, Polkowice Main Field (after Pieczonka, 1998) (upper figure – wt.%; lower figure – atomic proportions)

Sample	As Kα	Bi Lα	Hg Lα	Au Lα	Cu Kα	Fe Kα	Pt Lα	S Kα	Pd Lα	Ag Lα	Total
291/A2	0.14	≤0.10	1.96	62.05	0.35	≤0.05	≤0.07	≤0.15	≤0.5	35.41	99.91
	0.0019		0.0098	0.3150	0.0055					0.3283	
291/A3	0.11	≤0.10	2.14	58.15	0.58	≤0.05	≤0.07	≤0.15	≤0.05	37.66	98.64
	0.0015		0.0107	0.2952	0.0091					0.3491	
291/A4	0.19	0.30	1.29	67.10	0.50	≤0.05	≤0.07	≤0.15	≤0.05	31.18	100.56
	0.0025	0.0014	0.0064	0.3407	0.0079					0.2891	
291/A5	0.09	≤0.10	1.30	67.99	0.46	≤0.05	≤0.07	≤0.15	≤0.05	28.80	98.64
	0.0012		0.0065	0.3452	0.0072					0.2670	
291/A6	0.14	≤0.10	1.46	68.61	0.55	≤0.05	0.16	≤0.15	≤0.05	27.49	98.41
	0.0019		0.0073	0.3483	0.0087		0.0008			0.2548	
291/A6	0.20	0.14	2.31	57.33	0.36	≤0.05	≤0.07	≤0.15	≤0.05	40.28	100.62
	0.0027	0.0007	0.0115	0.2911	0.0057					0.3734	

The results of microprobe analyses point out to the presence of natural alloys of very diversified compositions (Tab. 27). The main admixture is Pb. Its atomic proportions preclude the presence of clausthalite inclusion in electrum whereas the presence of Te suggests the existence of mixed phases for which atomic proportions are difficult to be determined (Tab. 27). Such alloys form intergrowths with many minerals, usually with electrum and naumannite. The crystal size (5–10 μm) and the presence of bright fields in the BSE images (indicating the heavy elements e.g., Pb) confirm the correctness of obtained results. Atomic proportions suggest the presence of the following phases: $Au_2(AgPbSeTe)_1$, $Ag_3(AuPbSeTe)_1$ and $Au_2(AgPbSeAsTe)_3$ (Tab. 27). Such minerals can be identified as Pb-Se-

Table 25

Microprobe composition of electrum from the Kupferschiefer (dolomitic variety), mining section G-31, Polkowice West Field (after Pieczonka, 1998) , sequence PZ-20/3, (upper figure – wt.%; lower figure – atomic proportions)

Sample	As Kα	Bi Lα	Hg Lα	Au Lα	Cu Kα	Fe Kα	S Kα	Pd Lα	Ag Lα	Total
288/B1	0.13	≤0.10	1.62	70.44	0.52	≤0.05	≤0.15	≤0.05	26.39	99.10
	0.0017		0.0081	0.3576	0.0082				0.2447	
288/B2	0.06	≤0.10	1.34	68.53	1.21	≤0.05	0.16	≤0.05	27.68	98.98
	0.0008		0.0067	0.3479	0.0190		0.0050		0.2566	
288/B3	0.09	≤0.10	5.41	35.01	0.39	≤0.05	≤0.15	≤0.05	57.49	98.39
	0.0012		0.0270	0.1777	0.0061				0.5330	
288/B4	0.21	≤0.10	6.34	25.98	0.61	≤0.05	≤0.15	≤0.05	67.51	100.65
	0.0028		0.0316	0.1319	0.0096				0.6259	
288/C10	0.08	≤0.10	2.79	54.37	0.38	≤0.05	≤0.15	0.09	42.37	100.08
	0.0011		0.0139	0.2760	0.0060			0.0008	0.3928	
288/C11	0.11	0.14	4.41	41.59	0.72	0.10	≤0.15	≤0.05	52.57	99.64
	0.0015	0.0007	0.0220	0.2112	0.0113	0.0018			0.4874	
288/D13	0.13	0.10	3.60	50.86	0.43	≤0.05	≤0.15	0.21	46.73	102.06
	0.0017	0.0005	0.0179	0.2582	0.0068			0.0020	0.4332	
288/D14	0.18	≤0.10	1.30	71.01	0.65	≤0.05	≤0.15	≤0.05	28.81	101.95
	0.0024		0.0065	0.3605	0.0102				0.2671	
288/A15	0.12	≤0.10	3.91	48.59	0.14	≤0.05	≤0.15	≤0.05	48.19	100.95
	0.0016		0.0195	0.2467	0.0022				0.4467	
288/A16	0.19	≤0.10	1.23	71.17	0.35	≤0.05	≤0.15	0.06	27.30	100.30
	0.0025		0.0061	0.3613	0.0055			0.0006	0.2531	

Table 26

Microprobe composition of tetrauricupride and electrum from the Kupferschiefer, mining section G-31, Polkowice West Field, sequence G-31/294 A (upper figure – wt.%; lower figure – atomic proportions)

Sample	As Kα	Bi Lα	Hg Lα	Au Lα	Cu Kα	Fe Kα	Pt Lα	S Kα	Pd Lα	Ag Lα	Total
A/1	0.16	≤0.05	5.41	44.68	0.09	≤0.04	≤0.03	≤0.05	≤0.05	47.25	97.59
	0.0021		0.0270	0.2268	0.0014					0.4380	
A/2	0. 17	≤0.05	1.02	77.51	0.42	≤0.04	≤0.03	≤0.05	0.05	22.88	102.10
	0.0023		0.0051	0.3935	0.0066				0.0005	0.2121	
A/3	0.16	≤0.05	5.82	44.53	0.09	≤0.04	≤0.03	≤0.05	≤0.05	50.58	100.98
	0.0021		0.0290	0.2261	0.0014					0.4689	
A/4	0.24	≤0.05	2.03	58.49	0.16	≤0.04	0.04	0.06	0.09	35.89	97.00
	0.0032		0.0101	0.2970	0.0025		0.0002	0.0019	0.0008	0.3327	
A/5	0.15	≤0.05	6.51	40.65	0.25	≤0.04	0.24	≤0.05	≤0.05	52.63	100.43
	0.0020		0.0325	0.2064	0.0039		0.0012			0.4879	
A/6	0.05	0.23	5.34	46.54	0.41	≤0.04	≤0.03	≤0.05	≤0.05	46.86	99.43
	0.0007	0.0011	0.0266	0.2363	0.0065					0.4344	
A/7	0.09	≤0.05	5.51	42.30	0.83	≤0.04	≤0.03	≤0.05	≤0.05	48.68	97.41
	0.0012		0.0275	0.2148	0.0131					0.4513	
A/8	0.13	≤0.05	6.24	46.66	3.09	≤0.04	≤0.03	≤0.05	≤0.05	45.80	101.92
	0.0017		0.0311	0.2369	0.0486					0.4246	
A/9	0.26	0.19	6.60	41.02	0.14	≤0.04	≤0.03	≤0.05	≤0.05	53.63	101.84
	0.0035	0.0009	0.0329	0.2083	0.0022					0.4972	
A/10	0.23	0.53	0.88	76.52	23.71	≤0.04	≤0.03	≤0.05	≤0.05	0.21	102.08
	0.0083	0.0067	0.0118	1.0413	1.0000					0.0051	
A/11	0.14	0.08	0.55	73.63	23.36	≤0.04	≤0.03	≤0.05	0.14	0.18	98.08
	0.0051	0.0011	0.0073	1.0168	1.0000				0.0035	0.0046	
PZ-J7-16/4	≤0.05	≤0.05	≤0.05	78.44	21.56	≤0.04	≤0.03	≤0.05	≤0.05	≤0.15	100.00
				1.1734	1.0000						
A/12	0.19	≤0.05	1.08	77.66	0.59	≤0.04	≤0.03	≤0.05	≤0.05	23.38	102.90
	0.0025		0.0054	0.3943	0.0093					0.2167	
A/13	0.20	≤0.05	1.04	75.87	2.43	≤0.04	≤0.03	≤0.05	≤0.05	21.45	100.99
	0.0027		0.0052	0.3852	0.0382					0.1989	
A/14	0.22	0.56	7.36	36.49	3.96	≤0.04	0.14	≤0.05	≤0.05	54.04	102.63
	0.0029	0.0027	0.0367	0.1853	0.0623		0.0007			0.5010	
A/15	0.17	≤0.05	6.95	37.47	3.36	≤0.04	≤0.03	≤0.05	0.15	54.80	102.90
	0.0023		0.0346	0.1902	0.0529				0.0014	0.5080	

Table 27

EDS composition of native alloys from the Kupferschiefer, mining section G-31, Polkowice West Field (upper figure – wt.%; lower figure – atomic proportions)

Sample	Ag Lα	Au Lα	Pb Lα	Se Kα	Pd Lα	Pt Lα	As Kα	Te Lα	Composition
PZ-J7-10/14	13.56	69.96	10.24	3.53	≤0.05	≤0.15	0.39	2.33	$Au_{1.0000}Ag_{0.3539}Pb_{0.1486}Se_{0.033}Te_{0.0515}$
	0.3539	1.0000	0.1486	0.1258			0.0146	0.0515	
PZ-J7-11/9	58.39	25.02	9.33	1.41	≤0.05	≤0.15	0.79	5.07	$Ag_{1.0000}Au_{0.2346}Pb_{0.0831}Se_{0.0033}Te_{0.0733}$
	1.0000	0.2346	0.0831	0.0033			0.0194	0.0733	
PZ-J7-11/11	24.88	53.66	12.30	2.26	≤0.05	≤0.15	3.28	3.62	$Au_{1.0000}Ag_{0.8469}Pb_{0.2181}Se_{0.1377}As_{0.1949}Te_{0.1043}$
	0.8469	1.0000	0.2181	0.1377			0.1949	0.1043	

Te-electrum, as Se, Pb and Te are permanent and important components.

TELLURIDES

Microscopic observations revealed the presence of several phases which optical properties did not provide undoubtful identification. Unfortunately, microprobe analyses did not resolve identification doubts as most of these phases showed diversified compositions (por. Tabs 28, 29). The most common mineral was identified as naumannite (see also next chapter "*Selenides*"). Its crystals are usually rimmed by a grey zone of similar reflectance (probably reaction zone). The BSE images clearly demonstrate the presence of a new phase of distinctly different chemical composition because, apart from Se, significant amounts of Te (6.43–14.42 wt.%) and Bi (up to 20.30 wt.%) were detected (Tab. 28). Such composition points out to the presence of two phases showing different Te and Se proportions, precisely, the highest contents of Te correspond to high contents of Se and to low ones of Te (Tab. 28). Atomic proportions indicate the new minerals of compositions: $Me_3Se_2(TeAs)_1$, $Me_2(SeTe)_1$, $Me_5Se_4(TeAs)_1$, $Me_2(SeTeAs)_1$ and $Me_3(SeTeAs)_2$, where Me = Ag+Au+Pb+Bi (Tab. 28, 29). Moreover, a small amounts of Pt was detected (up to 2.7 wt.%, Tab. 28). The new phases require further studies as minerals of such compositions have not been described in the literature. Analyses for Te can be affected by analytical error (see chapter "*Geochemistry of Au and PGE*"). Detailed microprobe analyses (Figs 61, 62), particularly the BSE images, revealed the presence of grey fields of various intensity, which is an effect different mass numbers of elements. Intensive, white dots in Te map located outside the contours of ore minerals (Fig. 61) originate from CaKα line whereas white dots within the ore minerals reflect TeLα.

Paragenesis of high-Te and high-Se minerals includes phases of compositions close to $(Pb_{1.3371}Ag_{0.9591}Au_{0.3651})Te_{0.5896}Se_{0.4104}$ and $(Pd_{0.4822}Ag_{0.3109}Au_{0.0949}Pb_{0.0231})As_{0.8825}Te_{0.1175}$ (Tab. 29). Hence, the general formula roughly corresponds to $Me_5(TeSe)_2$ and Me(AsTe). The latter phase can be proposed as a new, uknown PdAs mineral with high admixtures of Au, Ag and Te. Similar phase, although Te-free, was described by Kucha (1975) in paragenesis with other arsenides. Its formula can also be calculated as $Pb_{5.0348}Bi_{2.0828}Au_{1.0638}Ag_{0.833}Se_{2.1836}Te_{2.0000}$ (Tab. 28, analysis PZ-J7-11/10).

Tellurium was detected in many other minerals from the precious metals association. Highest contents were found in naumannite (up to 9.19 wt.%, Tab. 30, analysis Pz-J7-11/7, i.e. 1/2 content of Se). This phase can also be a new mineral. Significant amounts of Te (up to 5.07 wt.%) were detected in Pb-native Au (Tab. 27). Diadochous substitutions of Te were found in nonstoichiometric Pb-selenides (Tab. 31).

SELENIDES

Clausthalite is a common mineral in the Cu deposit of the Fore-Sudetic Monocline. It was identified quite early in the Cu-bearing zone (Harańczyk, 1972) as well as in the "Kupferschiefer with noble metals" (Kucha, 1981, 1982a,

Table 28

EDS composition of Ag-Au-Pb-Bi-Te-Se minerals, Polkowice West Field
(upper figure – wt.%; lower figure – atomic proportions)

Sample	Ag Lα	Au Lα	Pb Mα	Se Kα	Pd Lα	Pt Lα	As Kα	Te Lα	Bi Mα
PZ-J7-11/4	2.28	1.79	58.73	18.77	≤0.3	2.32	0.83	14.38	1.27
	0.0888	0.0383	1.1923	1.0000		0.0500	0.0467	0.4741	0.0256
PZ-J7-11/3	1.23	1.21	58.47	21.22	≤0.3	0.79	0.13	7.38	9.51
	0.0424	0.0227	1.0502	1.0000		0.0149	0.0063	0.2151	0.1693
PZ-J7-11/2	16.58	≤0.2	49.73	13.29	≤0.3	≤0.3	0.93	6.83	12.65
	0.6563		1.0248	0.7186			0.0529	0.2284	0.2583
PZ-J7-11/1	5.11	0.24	51.51	14.16	≤0.3	0.34	0.58	7.76	20.30
	0.1913	0.0048	1.0032	0.7236		0.0069	0.0311	0.2453	0.3918
PZ-J7-11/10	4.01	9.32	46.98	7.70		0.19	0.95	11.40	19.45
	0.1995	0.2536	1.2155	0.5227		0.0009	0.0676	0.4772	0.4986
PZ-J7-11/12	4.10	4.97	53.83	18.39	≤0.3	2.73	1.57	14.42	≤0.3
	0.1632	0.1082	1.1155	1.0000		0.0601	0.0902	0.4852	
PZ-J7-11/13	6.47	14.01	44.72	8.04	≤0.3	≤0.3	0.27	6.43	20.06
	0.3851	0.4564	1.3851	0.6534			0.0231	0.3235	0.6162
PZ-J7-19/2	18.48	12.84	49.47	5.79	≤0.3	≤0.3	≤0.3	13.43	≤0.3
	0.9591	0.3651	1.3371	0.4104				0.5896	
PZ-J7-19/7	17.70	9.87	2.53	≤0.2	27.08	≤0.3	34.90	7.91	≤0.3
	0.3109	0.0949	0.0231		0.4822		0.8825	0.1175	

Table 29

Atomic proportions calculated for chemical compositions given in Table 28

Sample	Total/atomic proportions	Formula
PZ-J7-11/4	100.00 $(Pb_{2.3846}Ag_{0.1776}Au_{0.0766}Bi_{0.0512})Se_{2.0000}Te_{0.9482}As_{0.0942}$	$Me_3Se_2(TeAs)_1$
PZ-J7-11/3	100.00 $(Pb_{4.2008}Bi_{0.6772}Pt_{0.0596}Au_{0.0908}Ag_{0.1696})Se_{4.0000}Te_{0.8604}As_{0.0232}$	$Me_5Se_4(TeAs)_1$
PZ-J7-11/2	100.00 $(Pb_{1.0248}Bi_{0.2583}Ag_{0.6563})Se_{0.7186}Te_{0.2285}As_{0.0529}$	$Me_2(SeTeAs)_1$
PZ-J7-11/1	100.00 $(Pb_{1.0032}Bi_{0.3918}Ag_{0.1913}Au_{0.0048}Pt_{0.0069})Se_{0.7236}Te_{0.2453}As_{0.0311}$	$Me_3(SeTeAs)_2$
PZ-J7-11/10	100.00 $(Pb_{1.2155}Bi_{0.4986}Au_{0.2536}Ag_{0.1995})(Se_{0.5227}Te_{0.4772})$	$Me_2(SeTe)_1$
PZ-J7-11/12	100.00 $(Pb_{2.2310}Au_{0.2164}Ag_{0.3264}Pt_{0.1202})Se_{2.0000}Te_{0.9704}As_{0.1804}$	$Me_3Se_2(TeAs)_1$
PZ-J7-11/13	100.00 $(Pb_{1.3851}Bi_{0.6162}Au_{0.4564}Ag_{0.3851})Se_{0.6534}Te_{0.4852}As_{0.0902}$	$Me_3(SeTeAs)_1$
PZ-J7-19/2	100.00 $(Pb_{1.3371}Ag_{0.9591}Au_{0.3651})Te_{0.5896}Se_{0.4104}$	$Me_5(TeSe)_2$
PZ-J7-19/7	100.00 $(Pd_{0.4822}Ag_{0.3109}Au_{0.0949}Pb_{0.0231})As_{0.8825}Te_{0.1175}$	$Me(AsTe)_1$

b) and in the zone of secondary oxidation of the copper deposit (Pieczonka, 1998; Piestrzyński *et al.*, 2002).

In the secondary oxidation zone, clausthalite was observed in almost all polished sections containing electrum and, less commonly, in samples with high-purity native Au. It forms intergrowths with precious metals alloys, native Pb, Pd-arsenides, Cu-sulphides and other selenides (naumannite) including those containing Te.

In the zone of secondary oxidation, naumannite occurs in paragenesis with native Au, electrum and native Pb. Optical properties indicate high-temperature variety of pseudofluorite structure (Schröcke & Weiner, 1981), which crystallizes above 135°C, although Karakaya and Thompson (1990) suggest lower transformation temperature, i.e. 130°C.

Microscopic observations of fine intergrowths are less accurate than the SEM studies. The BSE images enable the authors to distinguish specific phases and demonstrate the differences in mineral composition in terms of grey scale dependent on atomic weights of elements (Figs 63–71). Results of these studies also indicate the presence of minerals of approximated Pb_3Se_2 composition (Tab. 31), which contain significant admixtures of other metals: Ag – up to 16.17 wt.%, Au – up to 11.16 wt.% and Pt – up to 0.71 wt.%. (Tab. 31). Some grains contained also Te – up to 4.81 wt.% (Tab. 31) and, rarely, small amounts of sulphur (Tab. 30). High contents of Ag correlate with low contents of Au and *vice versa* (see Tab. 31). Therefore, these are not physical mixtures of selenides and electrum but reaction zones of these minerals, of variable chemical composition. Such reaction zones are visible in the BSE images (Figs 63, 66 and 68). Microprobe analyses revealed significant admixtures of Ag and Au in clausthalites, even up to 20 wt.% (see Tab. 30).

Detailed studies on naumannites indicate the presence of several varieties (Tab. 30). Most common are phases with up to 10 wt.% Pb and several wt.% Au (Tab. 30). However, many analyzed grains contain too much Ag and Au to be classified as Au-Ag-naumannites (see Tab. 30). These are presumably new minerals of Me_2Se composition containing up to 40 wt.% Au and up to 49 wt.% Ag (Tab. 30). Emission spectra of selenides demonstrated various intensities of Se, Ag and Pb lines, which points to variable composition of these minerals, as supported by quantitative analyses (Tab. 30, 31). The minerals show admixtures of Pt (up to 2.18 wt.%), As (up to 1.36 wt.%), Bi (up to 1.32 wt.%) and Te (up to 9.19 wt.%) (Tab. 30, 31). These are also the only phases in which admixtures of other PGE were detected: Rh up to 1.3 wt.% (Tab. 30).

Microprobe analyses revealed the presence of a selenide of $AgSe_2$ composition (Tab. 30). Minerals containing two Se anions are: bohdanowiczite ($AgBiSe_2$), krutaite ($CuSe_2$) and some Fe-, Co- and $NiSe_2$ phases but $AgSe_2$ is unknown (Karakaya & Thompson, 1990).

Pd AND Pt MINERALS

The presence of Pd minerals in the copper deposit of the Fore-Sudetic Monocline has been known since the early paper by Kucha (1975). Further publications (Kucha, 1981, 1982a, b; Kucha & Pocheć, 1983; Kucha & Przybyłowicz, 1999) brought new data on other Pd minerals and compounds. Up to date the following Pd phases were indentified: PdAs, $PdAs_2$, Pd_3As_5, Pd_2As_3, Pd_5As_2, Pd_8As_2S, Pd_3As (vincentite), $(NiPd)_3As_3$, $PdCu(As,S)_6$ and $Pd_8As_6S_3$ (Kucha, 1975, 1984).

In the secondary oxidation zone somewhat different Pd-arsenides assemblage was discovered. Their chemical compositions are listed in Table 32. Apart from already known vincentite, 14 new minerals were identified: $PdAs_7$, Pd_2As, Pd_4As, Pd_9As_2, Pd_5As, $Me_{13}As_2$ (where Me = Pd,

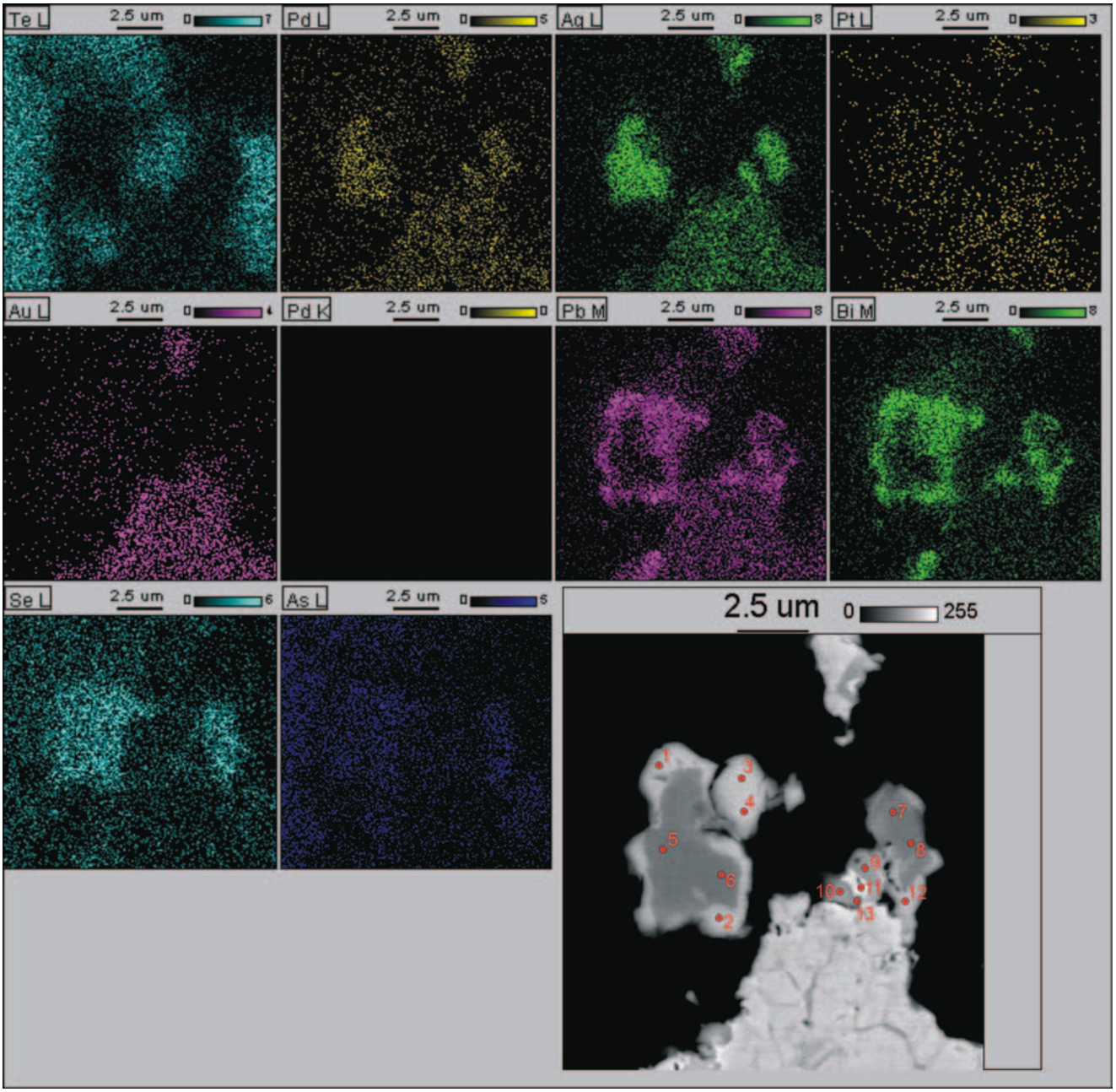

Fig. 61. Single element scans and BSE image (bottom right), red circles show position of quantitative measurements, sample PZ-J7-11

Pt, Au and Ag), Me_8As_3 (where Me = Pd, Ag and Pt), $Pd(NiFe)_2As_{3.5}S_{0.5}$ or Me_4As_7S, $(PdPtNi)As_7$, $(PdNi)As_7$, $(PdAuNi)_3As$ and $PdAs_3$ (Tab. 32, Figs 72–76). The most interesting is the mineral of composition $Pd_{9.1588}Pt_{1.102}(Au_{2.2148}Ag_{0.5694})As_{2.0000}$, which contains 11.70 wt.% Pt (Tab. 32), which is the highest concentration of this metal in all phases indentified up to date. Such mineral has not been found even in a comprehensive list of 600 Pt-bearing phases published by Daltry and Wilson (1997). In metallurgical literature (e.g., Okamoto, 1990) 18 high-temperature phases were mentioned of various atomic proportions and crystal structures. Five minerals identified in the Fore-Sudetic Monocline deposit: Pd_2As, $PdAs_2$, Pd_5As, Pd_8As_3 and Pd_3As reveal stoichiometries similar to those described by Okamoto (1990). The noticable difference is the presence of numerous and significant substitutions of trace elements in natural phases.

The atomic proportions of Me_8As_3 phase resemble Pd_8As_2S mineral described by Kucha (1984) but other phases (excluding five Pd-arsenides mentioned above) have no equivalents in the literature (Daltry & Wilson, 1997; Okamoto, 1990). Analyzed arsenides occasionally contain significant admixtures of: Ag (up to 12.57 wt.%), Au (up to 5.96 wt.%), Ni (up to 3.76 wt.%) and Pt (up to 1.39 wt.%). In several crystals contents of Cu (up to 0.9 wt.%) and Pb (up to 7.09 wt.%) were detected. In a single analytical point 7.32 wt.% Bi was found and in another one 0.32 wt.% Fe and 2.24 wt.% S were indicated (Tab. 32).

Less common Pd mineral is sobolevskite, PdBi (Fig. 77) described for the first time by Kucha (1975). It coexists

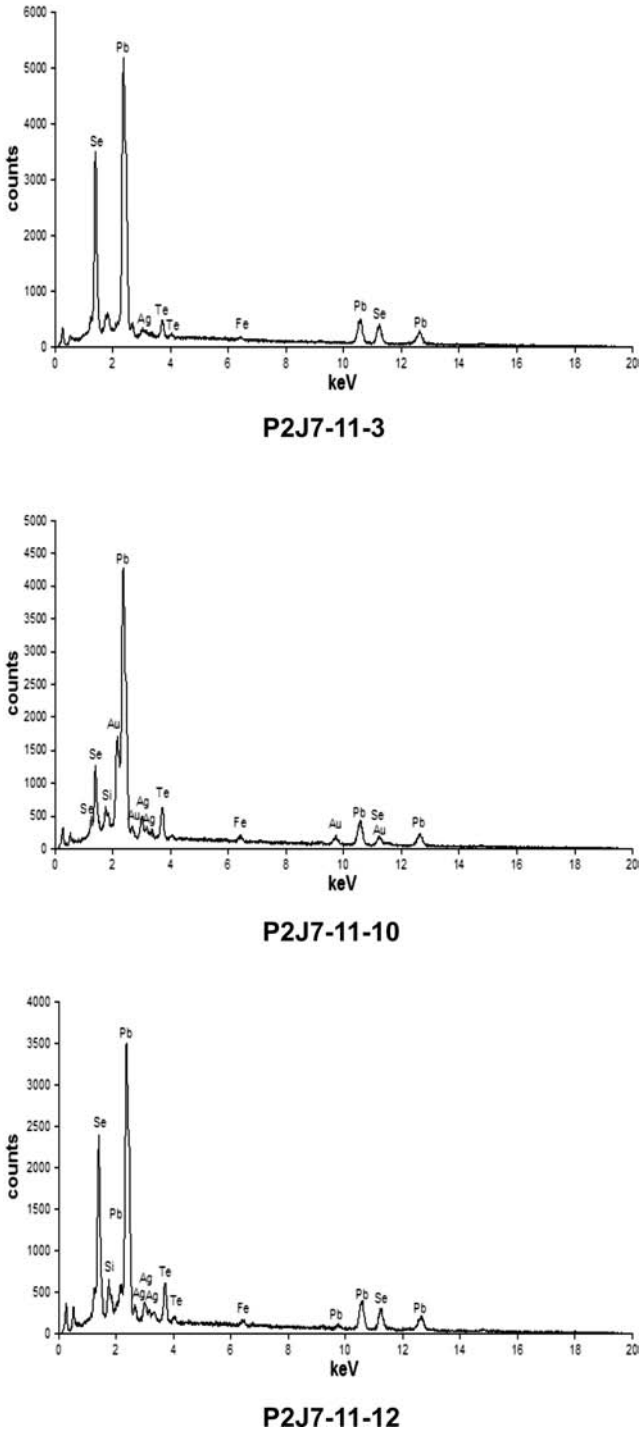

Fig. 62. EDS spectra of Pb-Ag-Au-Te-Se minerals, sample PZ-J7-11

usually with Pd-arsenides (Fig. 75, sample 291-3/1-1), native Pb, Cu-sulphides, Bi-sulphides, electrum and Bi-Cu alloys. Its composition is listed in Table 33. Apart from small amounts of Hg, sobolevskite contains also significant admixtures of Au. New data revealed the presence of naumannite (Tab. 30) and Bi-Cu alloys (Tab. 34) in this para-ge nesis. The α-BiPd phase is stable up to 210°C and β-BiPd is stable in temperature range 210–380°C (Okamoto, 1990). Phases of other atomic proportions formed in other temperature ranges may also exist (Okamoto, 1990).

Microprobe analyses demonstrated the presence of two new minerals of compositions: BiCu and Bi_2Cu (Tab. 34), which contain 18.37 and 13.68 wt.% Cu, respectively. Important admixtures are Pd, Au and S. Such minerals have not been known from the Fore-Sudetic deposit. In the available literature metastable phase of Cu_5Bi_2 composition is mentioned, which exists at temperature below 300°C (Chakrabarti & Laughlin, 1990). However, phases from the Fore-Sudetic deposit contain much higher admixtures of Bi.

OXIDIZED As COMPOUNDS

The presence of oxidized As compounds was communicated by Kucha and Przybyłowicz (1999) who found Pd_2AsO_4, in clay-organic matrix of the Kupferschiefer, in paragenesis with castaingite, electrum, covellite, Pd-arsenide (Pd_3As_5), Ni- and Co-arsenides and Bi-sulphides. Similar paragenesis, although without arsenates, was mentioned in some earlier papers (Kucha, 1981, 1982a, b). New data revealed seven new minerals of general Pd-As-O composition (Tab. 35): $PdAsO_2$, Pd_2AsO_2, $Pd_4As_2O_3$ (Fig. 76), $Pd_3As_2O_4$, $Pd_5As_4O_8$, $Pd_6As_4O_7$ (Fig. 77) and $Pd_8As_4O_7$ (Fig. 77). Studied compounds usually include variable amounts of Pd (from 43.55 to 64.06 wt.%) and As (22–34 wt.%), as well as admixtures of Au (up to 3.9 wt.%), Bi (up to 2.94 wt.%), Hg (up to 0.75 wt.% in single analysis), Cu (up to 6.64 wt.%) and Ni (up to 8.51 wt.%) (Tab. 35).

Pt MINERALS

Up to date, only a few minerals containing Pt admixtures were found although contents of this element in analyzed samples is higher than that of Pd. Highest content (2.5 wt.%) was reported from Pt-native Au (Kucha & Mayer, 1996). Increased amounts (up to 0.21 wt.%) were detected in thucholite and in arsenates (up to 0.73 wt.%) (Kucha & Przybyłowicz, 1999).

The new Pt mineral can be the phase of approximate composition $Pd_{9.1588}Pt_{1.102}(Au_{2.2148}Ag_{0.5694})As_{2.0000}$, which contains 11.70 wt.% Pt (Tab. 32) and over 53 wt.% Pd, and 23.75 wt.% Au (Tab. 32). This is the only high-Pt mineral found in the studied polished sections.

Electrum which coexists with Pd-bismuthides and Pd-arsenides usually contains some Pt (up to 4.0 wt.%, Tab. 34), which is simultaneously the highest admixture of Pt in electrum derived from the secondary oxidized zones. Normally, Pt contents in electrum do not exceed 1.2 wt.% (Tabs 19–27). Platinum was found in larger number of analytical points than palladium, which may explain its higher contents in analyzed rock samples. Admixtures of Pt were detected also in Pb-selenides of usually nonstoichiometric compositions (Tab. 31). Newly discovered Ag-selenides with Au (naumannite) contain also significant amounts of Pt (up to even 2.18 wt.%, Tab. 30). In these selenides Rh was detected, as well (Tab. 30). High amounts of Pt were found in new tellurides – up to 2.73 wt.% Pt in phases low in Bi and high in Te. These minerals contain also Ag and Au (Tab. 28).

Tabela 30

EDS and microprobe composition of Ag-Au-Pb-Se minerals, Polkowice-Sieroszowice Mine
(upper figure - wt.%.; lower figure – atomic proportions)

Sample	Ag Lα	Au Lα	Pb Lα	Se Kα	Pd Lα	Pt Lα	As Kα	Te Lα	Total
PZ-J7-9a/1	1.28	17.30	69.90	11.92	≤0.2	≤0.3	≤0.2	≤0.2	100.00
	0.0788	0.5815	2.2337	1.0000					$Pb_{2.2337}Au_{0.5815}Ag_{0.0788}Se_{1.0000}$
PZ-J7-9a/2	1.79	23.22	57.87	14.02	≤0.2	≤0.3	3.10	≤0.2	100.00
	0.0758	0.5384	1.2753	0.8109			0.1891		$Pb_{1.2753}Au_{0.5384}Ag_{0.0758}Se_{0.8109}As_{0.1891}$
PZ-J7-9a/5	34.87	≤0.3	2.16	61.01	≤0.2	≤0.3	≤0.2	1.96	100.00
	0.4102		0.0132	0.9805				0.0195	$Ag_{0.8204}Pb_{0.0264}Se_{1.9610}Te_{0.0390}$
PZ-J7-9a/6	33.86	≤0.3	6.17	59.88	0.09	≤0.3	≤0.2	≤0.2	100.00
	0.4139		0.0393	1.0000	0.0011				$Ag_{0.8278}Pb_{0.0518}Pd_{0.0022}Se_{2.0000}$
PZ-J7-9a/7	38.90	≤0.3	1.23	59.87	≤0.2	≤0.3	≤0.2	≤0.2	$AgSe_2$ 100.00
	0.4756		0.078	1.0000					$Ag_{0.9512}Pb_{0.0156}Se_{2.0000}$
PZ-J7-9a/8	4.64	≤0.3	78.74	16.62	≤0.2	≤0.3	≤0.2	≤0.2	Ag-clausthalite 100.00
	0.2042		1.8052	1.0000					$Pb_{1.8052}Ag_{0.2042}Se_{1.0000}$
PZ-J7-9a/9	1.05	≤0.3	91.24	5.17	S=1.6	Fe=0.9	≤0.2	≤0.2	Pb-native 100.00
PZ-J7-9a/15	47.22	21.75	4.41	23.03	≤0.2	≤0.3	≤0.2	3.59	Au-naumannite 100.00
	1.3687	0.3452	0.0666	0.9121				0.0879	$(Ag_{1.3687}Au_{0.3452}Pb_{0.0666})Se_{0.9121}Te_{0.0879}$
PZ-J7-9a/16	37.66	24.41	14.78	17.18	≤0.2	≤0.3	≤0.2	5.97	Au-Pb-naumannite 100.00
	1.3203	0.4686	0.2697	0.8230				0.1770	$(Ag_{1.3203}Au_{0.4686}Pb_{0.2697})Se_{0.8230}Te_{0.1770}$
PZ-J7-9a/17	20.31	40.31	22.85	10.86	≤0.2	≤0.3	0.74	4.94	Au-naumannite 100.00
	1.0113	1.0999	0.5927	0.7389			0.0532	0.2079	$(Ag_{1.0113}Au_{1.0999}Pb_{0.5927})Se_{0.7389}Te_{0.2079}As_{0.0532}$
PZ-J7-9/2	55.62	21.04	≤0.3	19.46	0.22	0.59	0.70	2.38	Au-naumannite 100.00
	1.8783	0.3891		0.8980	0.0077	0.0109	0.0338	0.0681	$(Ag_{1.8783}Au_{0.3891}Pd_{0.0077}Pt_{0.0109})Se_{0.8980}Te_{0.0681}As_{0.0338}$
PZ-J7-9/3	49.09	24.09	0.30	21.71	≤0.2	1.83	0.81	2.17	Au-naumannite 100.00
	1.5035	0.4040	0.0046	0.9082		0.0311	0.0357	0.0561	$(Ag_{1.5035}Au_{0.4040}Pt_{0.0311}Pb_{0.0046})Se_{0.9082}Te_{0.0561}As_{0.0357}$
PZ-J7-9/4	42.17	36.72	0.50	17.62	≤0.2	2.18	0.23	0.58	Au-naumannite 100.00
	1.6937	0.8076	0.0407	0.9671		0.0485	0.0134	0.0195	$(Ag_{1.6937}Au_{0.4040}Pt_{0.0485}Pb_{0.0407})Se_{0.9671}Te_{0.0195}As_{0.0134}$
PZ-J7-9/5	58.84	6.99	6.55	20.74	≤0.2	0.74	0.92	5.22	naumannite 100.00
	1.7268	0.1124	0.1000	0.8316		0.0120	0.0389	0.1295	$(Ag_{1.7268}Au_{0.1124}Pb_{0.1000}Pt_{0.0120})Se_{0.8316}Te_{0.1295}As_{0.0389}$
PZ-J7-9/6	73.13	0.30	0.22	23.34	≤0.2	≤0.3	0.87	2.14	naumannite 100.00
	2.0923	0.0046	0.0034	0.9123			0.0358	0.0519	$(Ag_{2.0923}Au_{0.0046}Pb_{0.0034})Se_{0.9123}Te_{0.0519}As_{0.0358}$
PZ-J7-9/7	72.68	1.03	≤0.3	21.52	≤0.2	0.85	1.36	2.56	naumannite 100.00
	2.1679	0.0167		0.8768		0.0142	0.0586	0.0646	$(Ag_{2.1679}Au_{0.0167}Pt_{0.0142})Se_{0.8768}Te_{0.0646}As_{0.0586}$
PZ-J7-9/8	71.72	1.27	≤0.3	25.18	≤0.2	≤0.3	0.84	0.60	naumannite 99.77
	1.9859	0.0191		0.9525			0.0335	0.0140	$(Ag_{1.9859}Au_{0.0191})Se_{0.9525}Te_{0.0140}As_{0.0335}$
PZ-J7-9/9	68.41	0.71	6.01	20.58	≤0.2	≤0.3	1.15	3.14	naumannite 100.00
	2.1105	0.0120	0.0965	0.8672			0.0509	0.0819	$(Ag_{2.1105}Pb_{0.0965}Au_{0.0120})Se_{0.8672}Te_{0.0819}As_{0.0509}$
PZ-J7-10/2	64.27	1.12	7.55	21.89	≤0.2	≤0.3	1.10	4.04	Pb-naumannite 100.00
	1.8412	0.0176	0.1125	0.8566			0.0454	0.0980	$(Ag_{1.8412}Pb_{0.1125}Au_{0.0176})Se_{0.8566}Te_{0.0980}As_{0.0454}$
PZ-J7-10/3	63.69	2.27	6.44	24.35	≤0.2	0.84	≤0.2	2.41	naumannite 100.00
	1.8044	0.0351	0.0950	0.9422		0.0131		0.0578	$(Ag_{1.8044}Pb_{0.0950}Au_{0.0351}Pt0.0131)_{Se0.9422}Te_{0.0578}$
PZ-J7-10/4	62.98	0.47	9.93	22.44	≤0.2	0.52	0.71	2.95	Pb-naumannite 100.00
	1.8431	0.0076	0.1512	0.8971		0.0085	0.0299	0.0730	$(Ag_{1.8431}Pb_{0.1512}Au_{0.0076}Pt_{0.0085})Se_{0.8971}Te_{0.0725}As_{0.0299}$
PZ-J7-10/5	68.07	1.51	3.81	22.54	≤0.2	≤0.3	1.23	2.84	naumannite 100.00
	1.9463	0.0237	0.0567	0.8806			0.0506	0.0688	$(Ag_{1.9463}Pb_{0.0567}Au_{0.0237})Se_{0.8806}Te_{0.0688}As_{0.0506}$
PZ-J7-10/6	72.45	1.36	≤0.3	22.46	≤0.2	0.48	1.18	2.07	naumannite 100.00
	2.1226	0.0218		0.8989		0.0079	0.0512	0.0500	$(Ag_{2.1226}Au_{0.0218}Pt_{0.0079})Se_{0.8989}Te_{0.0500}As_{0.0512}$

Table 30 continued

Sample	Ag Lα	Au Lα	Pb Lα	Se Kα	Pd Lα	Pt Lα	As Kα	Te Lα	Total
PZ-J7-10/7	49.94	27.61	0.65	18.63	Bi=0.05	0.42	0.63	2.08	Au-naumannite 100.00
	1.7767	0.5379	0.0119	0.9052		0.0084	0.0322	0.0625	$(Ag_{1.7767}Au_{0.5379}Pb_{0.0119}Pt_{0.0084})Se_{0.9052}Te_{0.0625}As_{0.0322}$
PZ-J7-10/8	47.73	27.82	≤0.3	19.80	1.13	Rh=1.3	0.40	1.81	Au-Rh-naumannite 100.00
	1.6371	0.5224		0.9279	0.0392	0.0725	0.0196	0.0525	$(Ag_{1.6371}Au_{0.5224}Pd_{0.0392}Rh_{0.0725})Se_{0.9279}Te_{0.0525}As_{0.0196}$
PZ-J7-10/12	57.00	15.54	3.35	20.23	Rh=0.18	1.11	0.57	2.01	Au-Rh-naumannite 100.00
	1.8898	0.2822	0.0579	0.9163	0.0061	0.0204	0.0272	0.0565	$(Ag_{1.8898}Au_{0.2822}Pb_{0.0579}Pt_{0.0204}Rh_{0.0061})Se_{0.9163}Te_{0.0565}As_{0.0272}$
PZ-J7-10/13	49.26	11.99	9.24	25.35	Bi=0.83	0.75	0.43	2.15	Au-naumannite 100.00
	1.3295	0.1773	0.1298	0.9345	0.0116	0.0111	0.0166	0.0489	$(Ag_{1.3295}Au_{0.1773}Pb_{0.1298}Bi_{0.0116}Pt_{0.0111})Se_{0.9345}Te_{0.0489}As_{0.0166}$
PZ-J7-11/5	69.11	0.82	3.84	21.93	≤0.2	≤0.3	1.12	3.18	naumannite 100.00
	2.0179	0.0132	0.0583	0.8746			0.0469	0.0784	$(Ag_{2.0179}Pb_{0.0583}Au_{0.0132})Se_{0.8746}Te_{0.0784}As_{0.0469}$
PZ-J7-11/6	64.78	0.70	5.49	22.92	Bi=0.95	0.34	1.07	3.76	naumannite 100.00
	1.7974	0.0108	0.0793	0.8689	0.0135	0.0051	0.0428	0.0883	$(Ag_{1.7974}Pb_{0.0793}Au_{0.0108}Bi_{0.0135}Pt_{0.0051})Se_{0.8689}Te_{0.0883}As_{0.0428}$
PZ-J7-11/7	62.95	0.94	4.85	22.07	≤0.2	≤0.3	≤0.2	9.19	naumannite 100.00
	1.6603	0.0137	0.0666	0.7952				0.2048	$(Ag_{1.6603}Au_{0.0137}Pb_{0.0666})Se_{0.7952}Te_{0.2048}$
PZ-J7-11/8	61.25	1.27	8.86	19.10	≤0.2	0.43	0.85	8.24	Pb-naumannite 100.00
	1.7867	0.0201	0.1347	0.7612		0.0069	0.0356	0.2033	$(Ag_{1.7867}Pb_{0.1347}Au_{0.0201}Pt_{0.0069})Se_{0.7612}Te_{0.2033}As_{0.0356}$
PZ-J7-16/6	4.08	20.12	57.33	18.47	≤0.2	≤0.3	≤0.2	≤0.2	Au-clausthalit 100.00
	0.1616	0.4365	1.1830	1.0000					$Pb_{1.1830}Au_{0.4365}Ag_{0.1616}Se_{1.0000}$
PZ-J7-16/7	8.65	16.22	61.00	16.76	≤0.2	≤0.3	≤0.2	≤0.2	Au-Ag-clausthalite 100.00
	0.3778	0.3877	1.3867	1.0000					$Pb_{1.3867}Au_{0.3877}Ag_{0.3778}Se_{1.0000}$
PZ-J7-19/5	6.44	9.58	59.39	18.41	Th=3.3	≤0.3	2.85	≤0.2	96.70
	0.2201	0.1792	1.0568	0.8599			0.1629		$Pb_{1.0568}Ag_{0.2201}Au_{0.1792}Se_{0.8599}As_{0.1401}$
PZ-J7-19/8	57.30	≤0.2	17.84	24.86	≤0.2	≤0.3	≤0.2	≤0.2	Pb-naumannite 100.00
	1.6874		0.2735	1.0000					$Ag_{1.6874}Pb_{0.2735}Se_{1.0000}$

Table 31

EDS composition of Pb-selenides from the Polkowice-Sieroszowice Mine
(upper figure – wt.%; lower figure – atomic proportions)

Sample	Ag Lα	Au Lα	Pb Mα	Se Kα	Pt Lα	As Kα	Te Lα	Bi Mα	Total/atomic proportions
PZ-J7-9a/3	1.13	0.61	78.54	19.65	≤0.15	0.06	≤0.2	≤0.3	100.00
	0.0418	0.0124	1.5233	1.0000		0.0032			$Pb_{3.0466}Se_{2.0000}$
PZ-J7-9a/4	2.25	0.80	77.87	19.01	≤0.15	0.07	≤0.2	≤0.3	100.00
	0.0864	0.0170	1.5613	1.0000		0.0037			$Pb_{3.1226}Se_{2.0000}$
PZ-J7-10/9	7.01	3.40	67.63	16.59	0.71	0.37	2.69	1.32	99.72
	0.1551	0.0413	0.7798	0.5021	0.0086	0.0150	0.0504	0.0150	$Pb_{2.3394}Ag_{0.4653}Au_{0.1239}Bi_{0.0450}(Se_{1.5063}Te_{0.1513})$
PZ-J7-10/10	13.96	3.75	59.26	19.96	0.03	0.42	2.62	≤0.3	100.00
	0.4736	0.0695	1.0531	0.9250	0.0002	0.0056	0.0750		$(Pb_{2.1062}Ag_{0.9472}Au_{0.1390})_{3.1924}(Se_{1.8500}Te_{0.1500})_{2.0000}$
PZ-J7-10/11	16.17	1.64	60.08	16.75	0.30	0.26	4.81	≤0.3	100.00
	0.6000	0.0332	1.1605	0.8491	0.0015	0.0035	0.1509		$Pb_{1.1605}Ag_{0.6000}Au_{0.0332}(Se_{0.8491}Te_{0.1509})$
PZ-J7-20/2	≤0.2	≤0.2	75.28	24.72	≤0.15	≤0.07	≤0.2	≤0.3	100.00
			1.0000	0.8615					$Pb_{1.0000}Se_{0.8615}$
PZ-J7-20/3	≤0.2	≤0.2	78.44	21.56	≤0.15	≤0.07	≤0.2	≤0.3	100.00
			1.0000	0.7213					$Pb_{1.0000}Se_{0.7231}$

Table 31 continued

Sample	Ag Lα	Au Lα	Pb Mα	Se Kα	Pt Lα	As Kα	Te Lα	Bi Mα	Total/atomic proportions
PZ-J7-20/4	≤0.2	≤0.2	73.78	26.22	≤0.15	≤0.07	≤0.2	≤0.3	100.00
			1.0000	0.9329					$Pb_{1.0000}Se_{0.9329}$
PZ-J7-20/5	≤0.2	≤0.2	74.62	25.38	≤0.15	≤0.07	≤0.2	≤0.3	100.00
			1.0000	0.8925					$Pb_{1.0000}Se_{0.8925}$
PZ-J7-19/10	≤0.2	≤0.2	79.10	20.90	≤0.15	≤0.07	≤0.2	≤0.3	100.00
			1.0000	0.6146					$Pb_{3.0000}Se_{1.8438}$
PZ-J7-19/11	5.04	11.16	62.91	20.89	≤0.15	≤0.07	≤0.2	≤0.3	100.00
	0.1147	0.1391	0.7461	0.6500					$(Pb_{0.7461}Au_{0.1391}Ag_{0.1147})_{3.0000}Se_{1.9501}$
PZ-J7-19/15	≤0.2	≤0.2	77.53	22.47	≤0.15	≤0.07	≤0.2	≤0.3	100.00
			1.0000	0.7605					$Pb_{3.0000}Se_{2.2950}$
PZ-J7-19/16	≤0.2	≤0.2	76.17	23.83	≤0.15	≤0.07	≤0.2	≤0.3	100.00
			1.0000	0.8210					$Pb_{1.0000}Se_{0.8210}$
PZ-J7-17/2	≤0.2	≤0.2	75.20	24.49	S- 0.31	≤0.07	≤0.2	≤0.3	100.00
			1.0000	0.8548	0.0267				$Pb_{1.0000}Se_{0.8548}S_{0.0267}$
PZ-J7-17/3	≤0.2	≤0.2	74.23	25.77	≤15	≤0.07	≤0.2	≤0.3	100.00
			1.0000	0.9109					$Pb_{1.0000}Se_{0.9109}$

Table 32

EDS and WDS compositions of Pd-arsenides from the Polkowice-Sieroszowice Mine
(upper figure – wt.%; lower figure – atomic proportions)

Sample	As Kα	Ag Lα	Au Lα	Pd Lα	Pt Lα	Bi Mα	Ni Kα	Formula, total and atomic proportions
AP-291/2-6	13.22	1.77	3.41	81.60	≤ 0.3	≤ 0.2	≤ 0.2	Me_9As_2 100.00
	1.0000	0.0929	0.0980	4.3450				$(Pd_{8.6900}Au_{0.1960}Ag_{0.1858})As_{2.0000}$
AP-291/3-5	11.40	4.24	5.84	70.68	0.53	7.32	≤ 0.2	Me_5As_2 100.00
	1.0000	0.2582	0.1945	4.3646	0.0177	0.2299		$(Pd_{4.3646}Bi_{0.2299}Au_{0.1945}Ag_{0.2582})As_{1.0000}$
AP-19/3-5-2	27.75	≤ 0.2	≤ 0.3	72.25	≤ 0.3	≤ 0.3	≤ 0.2	Pd_2As 100.00
	1.0000			1.8329				$Pd_{1.8329}As_{1.0000}$
AP-19/3-5-1	26.77	≤ 0.2	2.34	70.89	≤ 0.3	≤ 0.3	≤ 0.2	Me_2As 100.00
	1.0000		0.0333	1.8643				$Pd_{1.8329}Au_{0.0333}As_{1.0000}$
AP-291/3-4	8.16	3.34	23.75	53.06	11.70	≤ 0.2	≤ 0.2	$Me_{13}As_3$ 100.00
	1.0000	0.2847	1.1074	4.5794	0.5510			$Pd_{9.1588}Pt_{1.102}(Au_{2.2148}Ag_{0.5694})As_{2.0000}$
AP-291/3-3	17.04	5.23	≤ 0.3	76.34	1.39	≤ 0.2	≤ 0.2	Me_8As_3 100.00
	0.2941	0.0677		0.9281	0.0092			$(Pd_{0.9281}Ag_{0.0677}Pt_{0.0092})_{4.0000}As_{1.1764}$
AP-291/3-2	16.06	6.33	≤ 0.3	77.57	≤ 0.3	≤ 0.2	≤ 0.2	Pd_4As 99.96
	0.2722	0.0745		0.9255				$(Pd_{0.9255}Ag_{0.0745})_{4.0000}As_{1.0887}$
AP-91/3-2-2	58.08	≤ 0.2	≤ 0.3	27.07	S=2.24	Fe=0.32	11.41	Me_4As_7S 99.12
	0.8942			0.2935	0.1058	0.0066	0.2242	$Pd_{1.174}Ni_{0.8968}Fe_{0.0198}As_{3.5768}S_{0.4232}$
AP-291/2-3c	82.02	≤ 0.2	≤ 0.3	15.84	0.47	≤ 0.3	1.67	$PdAs_7$ 99.70
	1.0000			0.1360	0.0022		0.0260	$Pd_{0.9520}Pt_{0.0154}Ni_{0.1820}As_{7.0000}$
AP-291/2-3b	80.44	≤ 0.2	≤ 0.3	16.25	1.38	≤ 0.3	1.92	$PdAs_7$ 99.94
	1.0000			0.1422	0.0066		0.0305	$Pd_{0.9954}Pt_{0.0046}Ni_{0.2135}As_{7.0000}$
AP-291/2-3	81.83	≤ 0.2	≤ 0.3	17.05	≤ 0.3	≤ 0.3	1.12	$PdAs_7$ 100.00
	1.0000			0.1467			0.0175	$Pd_{1.0269}Ni_{0.1225}As_{7.0000}$
AP-91/3-3-1	16.86	≤ 0.2	5.53	70.90	≤ 0.3	Cu=0.83	0.72	Pd_3As 94.84
	1.0000		0.1249	2.9618		0.0582	0.0546	$Pd_{2.9618}Au_{0.1249}Cu_{0.0582}Ni_{0.0546}As_{1.0000}$

Table 32 continued

Sample	As Kα	Ag Lα	Au Lα	Pd Lα	Pt Lα	Bi Mα	Ni Kα	Formula, total and atomic proportions
AP-91/3-3-1	16.86	≤ 0.2	5.53	70.90	≤ 0.3	Cu=0.83	0.72	Pd_3As 94.84
	1.0000		0.1249	2.9618		0.0582	0.0546	$Pd_{2.9618}Au_{0.1249}Cu_{0.0582}Ni_{0.0546}As_{1.0000}$
AP-1/3-3-1b	18.20	≤ 0.2	5.96	74.17	≤ 0.3	Cu=0.90	0.77	Me_3As 100.00
	1.0000		0.1247	2.8691		0.0585	0.0539	$Pd_{2.8691}Au_{0.1247}Cu_{0.0585}Ni_{0.0539}As_{1.0000}$
AP-91/3-1-1	55.16	≤ 0.2	0.50	39.14	≤ 0.3	Pb=1.75	2.63	$PdAs_2$ 99.18
	1.0000		0.0034	0.4997		0.0114	0.0608	$Pd_{0.999}4Au_{0.0064}Pb_{0.0114}Ni_{0.0608}As_{2.0000}$
AP-91/ 3-1-1b	61.92	≤ 0.2	0.21	30.94	≤ 0.3	Pb=0.71	3.76	$PdAs_3$ 97.54
	1.0000		0.0014	0.3518		0.0034	0.0775	$Pd_{1.0554}Au_{0.0042}Pb_{0.0123}Ni_{0.2325}As_{3.0000}$
AP-91/ 3-1-1c	55.29	≤ 0.2	0.99	39.34	≤ 0.3	Pb=1.75	2.63	$PdAs_2$ 100.00
	1.0000		0.0068	0.5010		0.0114	0.0607	$Pd_{1.0020}Au_{0.0116}Pb_{0.0228}Ni_{0.1214}As_{2.0000}$
PZ-J7-9/6	45.72	12.57	≤ 0.3	34.62	≤ 0.3	Pb=7.09	≤ 0.2	Pd_3As_4 100.00
	1.0000	0.1909		0.5331		0.0560		$Pd_{2.1324}Ag_{0.7636}Pb_{0.2240}As_{4.0000}$
AP-91/3-6-6	25.45	≤ 0.2	≤ 0.3	72.66	≤ 0.3	≤ 0.3	1.89	Pd_2As 100.00
	1.0000			2.0100			0.0947	$Pd_{2.0100}Ni_{0.0947}As_{1.0000}$

Table 33

EDS compositions of Bi-Pd minerals from the Polkowice West Field
(upper figure – wt.%; lower figure – atomic proportions)

Sample	Bi Mα	Pd Lα	Au Lα	Hg Lα	Total/atomic proportions
PZ-J7-16/1	62.72	35.31	0.88	1.09	100.00
	1.0000	1.1056	0.0149	0.179	$Bi_{1.0000}Pd_{1.1056}$
	0.9852	1.0893	0.0148	0.0177	$(Bi_{0.9852}Au_{0.0148})Pd_{1.0893}$
PZ-J7-16/2	63.16	35.46	1.12	0.26	100.00
	1.0000	1.1026	0.0188	0.0043	$Bi_{1.0000}Pd_{1.1026}$
	0.9815	1.0822	0.0185	0.0042	$(Bi_{0.9815}Au_{0.0185})Pd_{1.0822}$
PZ-J7-16/3	59.99	34.71	4.72	0.58	100.00
	1.0000	1.13618	0.0832	0.0101	$Bi_{1.0000}Pd_{1.13618}$
	0.9231	1.0488	0.0769	0.0093	$(Bi_{0.9231}Au_{0.0769})Pd_{1.0488}$

Table 34

EDS compositions of Pd-bearing minerals from the Polkowice Main Field
(upper figure – wt.%; lower figure – atomic proportions)

Sample	As Lα	S Kα	Ag Lα	Au Lα	Pd Lα	Pt Lα	Bi Mα	Cu Kα	Total/atomic proportions
AP-291/3-1	1.55	≤ 0.2	14.94	74.54	4.91	4.05	≤ 0.2	≤ 0.05	100.00
AP-291/1-3		≤ 0.2	15.36	83.16	0.27	1.21	≤ 0.2	≤ 0.05	100.00
AP-291/3-2-4	2.43	≤ 0.2	37.63	56.84		1.39	≤ 0.2	Ni-0.72	100.00
Ap-291/1-4	≤ 0.2	2.42	1.07	2.98	0.83	≤ 0.2	74.33	18.37	100.00
		0.2122	0.0278	0.0424	0.0219		1.0000	0.8127	$Bi_{1.00}Pd_{0.0219}Cu_{0.8127}Ag_{0.2122}Au_{0.0424}$ $(Bi_{0.9395}Au_{0.0399}Pd_{0.0206})$
		0.1994	0.0261	0.0399	0.0206		0.9395	0.7636	$Cu_{0.7636}Ag_{0.0261}S_{0.1994}$
AP-291/1-1	≤ 0.2	2.22	1.09	≤ 0.2	1.41	≤ 0.2	81.59	13.68	100.00
		0.1714	0.0250		0.0329		0.9671	0.5333	$(Bi_{0.9671}Pd_{0.0329})$ $Cu_{0.5333}Ag_{0.0250}S_{0.1714}$

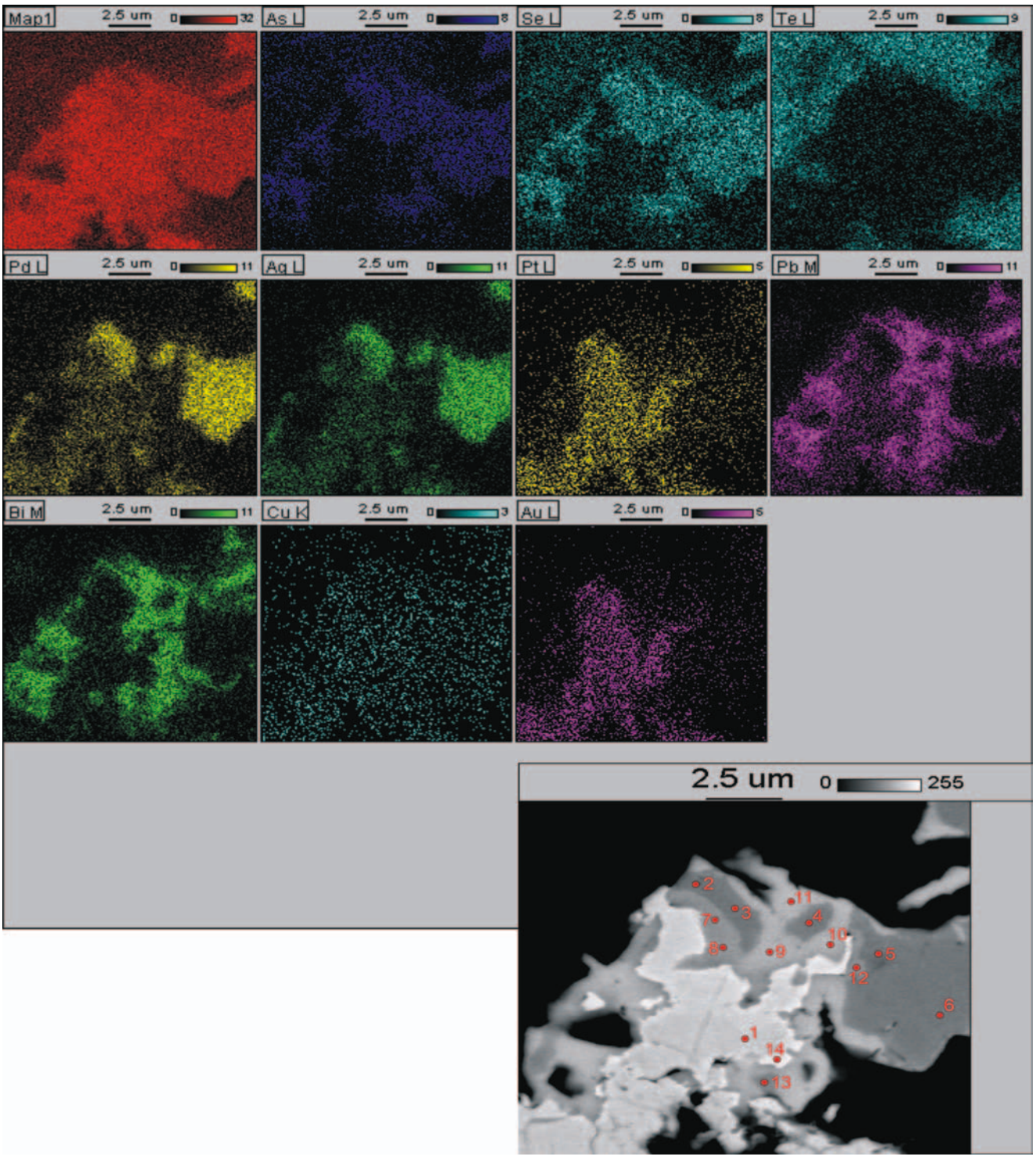

Fig. 63. Single element scans and BSE image (bottom right), red circles show position of quantitative measurements, sample PZ-J7-10

The thucholitic substance provides a separate problem. In the secondary oxidized zones this compound has not been found. Thucholite (or rather "ucholite", see Piestrzyński, 1989) occurs in the Kupferschiefer from the reducing zone. Microprobe analyses of ucholite aggregates revealed significant amounts of Pt (up to 0.88 wt.%, Tab. 36). Highest contents were observed in analytical points of highest U values. In ucholites studied under the microscope inclusions of noble metals phases and uraninite have not been found. The presence of uraninite crystals points out to the progessing ordering of ucholite structure and to the destruction of organometallic compounds. In such grains small amounts of U and Pt were observed (Tab. 36). Studied ucholites do not contain Au and/or Ag over detection limits but variable amounts of Fe, Cu and S were indicated (Tab. 36). Solution of the problem of precious metals occurrence in the organic

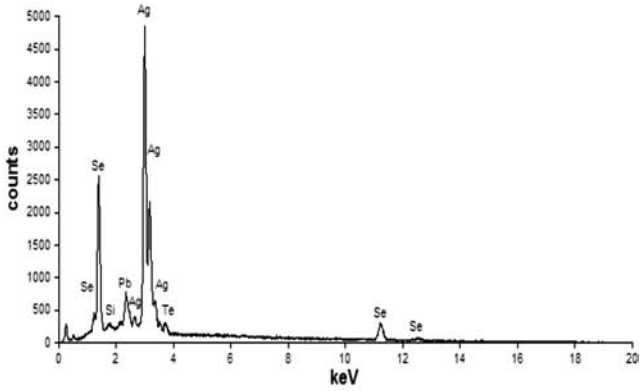

P2J7-10-2

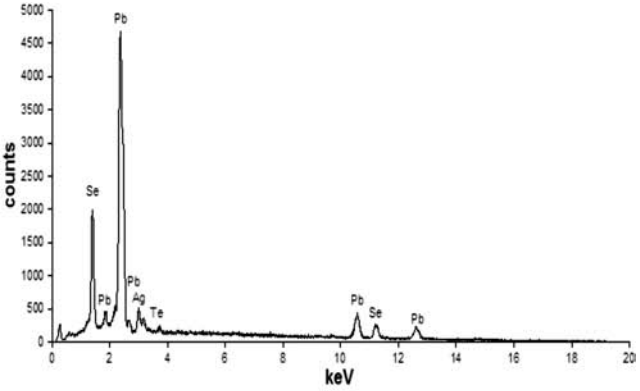

P2J7-10-9

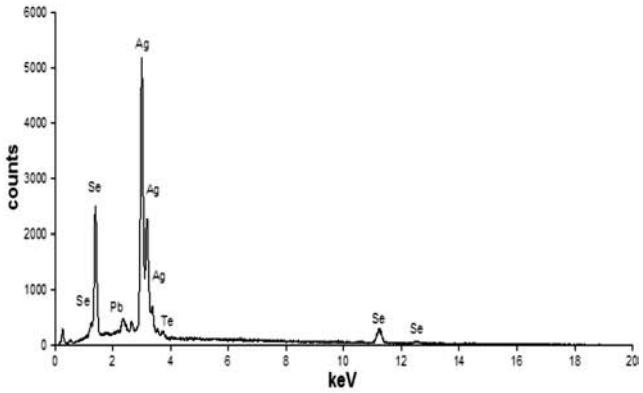

P2J7-10-5

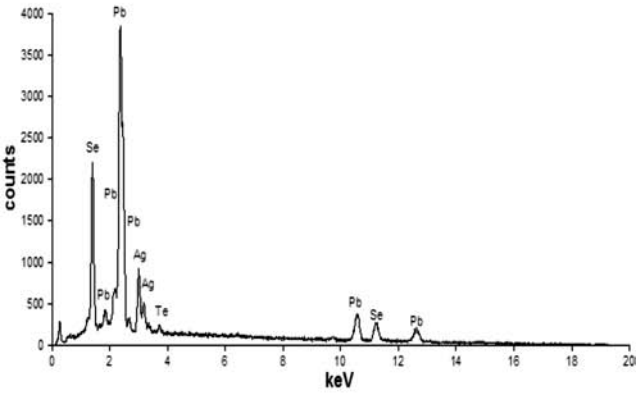

P2J7-10-10

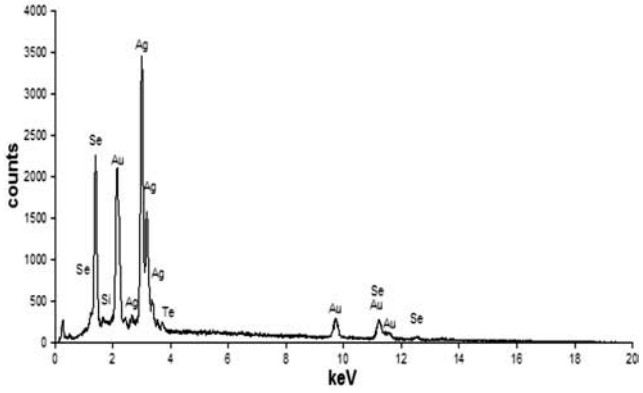

P2J7-10-7

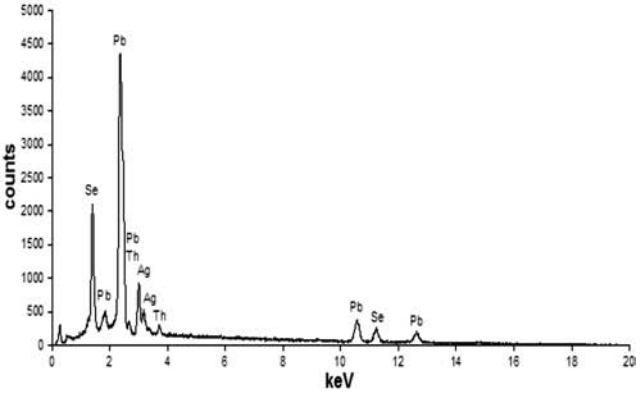

P2J7-10-11

Fig. 64. EDS spectra of different selenides, sample PZ-J7-10

Fig. 65. EDS spectra of different selenides, sample PZ-J7-10

matter requires further studies. Obviously, the organic compounds concentrate the precious metals (Kucha, 1982a, b; Kucha & Przybyłowicz, 1999). However, accumulation of these metals is possible only in the so-called "transitional zone" (Piestrzyński *et al.*, 1996a, 2002) where thucholitic substance could precipitate and where precious metals content in solution was still high. It is the fact that the whole organic matter in the secondary oxidized zones was oxidized and that these zones concentrated precious metals 1,000 times more that rocks from the reducing zone, which are rich in organic matter (Report AGH, 1996, 1997; Piestrzyński, 1996a; Piestrzyński *et al.*, 1996a, 2002; Pieczonka, 1998, 2000; Piestrzyński & Pieczonka, 1998). Therefore, it is suggested that the main stage of precious metals concentration took place in the secondary oxidation zone. Dispersed charater of Pt in studied samples point out

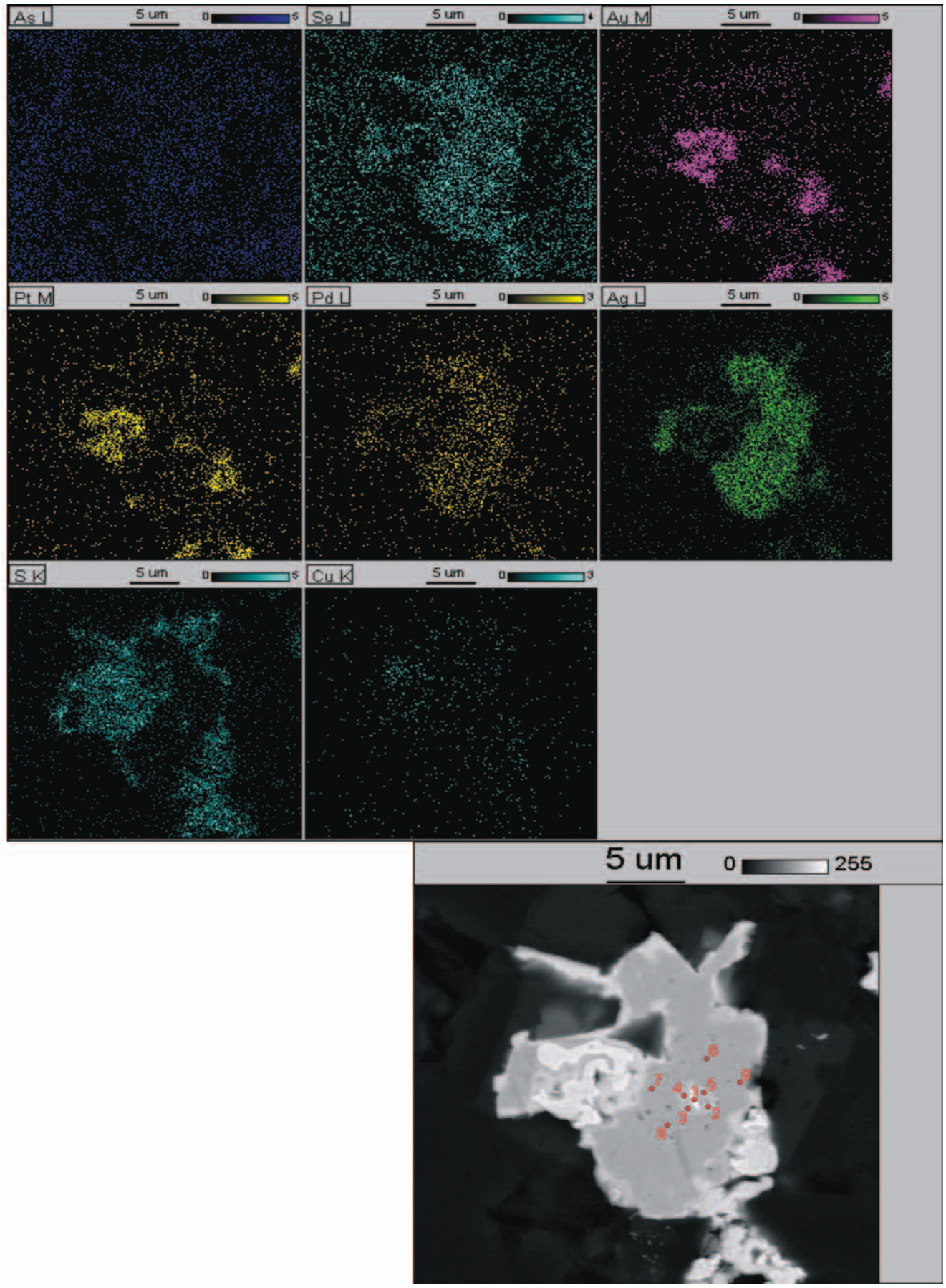

Fig. 66. Single element scans and BSE image (bottom right), red circles show position of quantitative measurements, sample PZ-J7-9

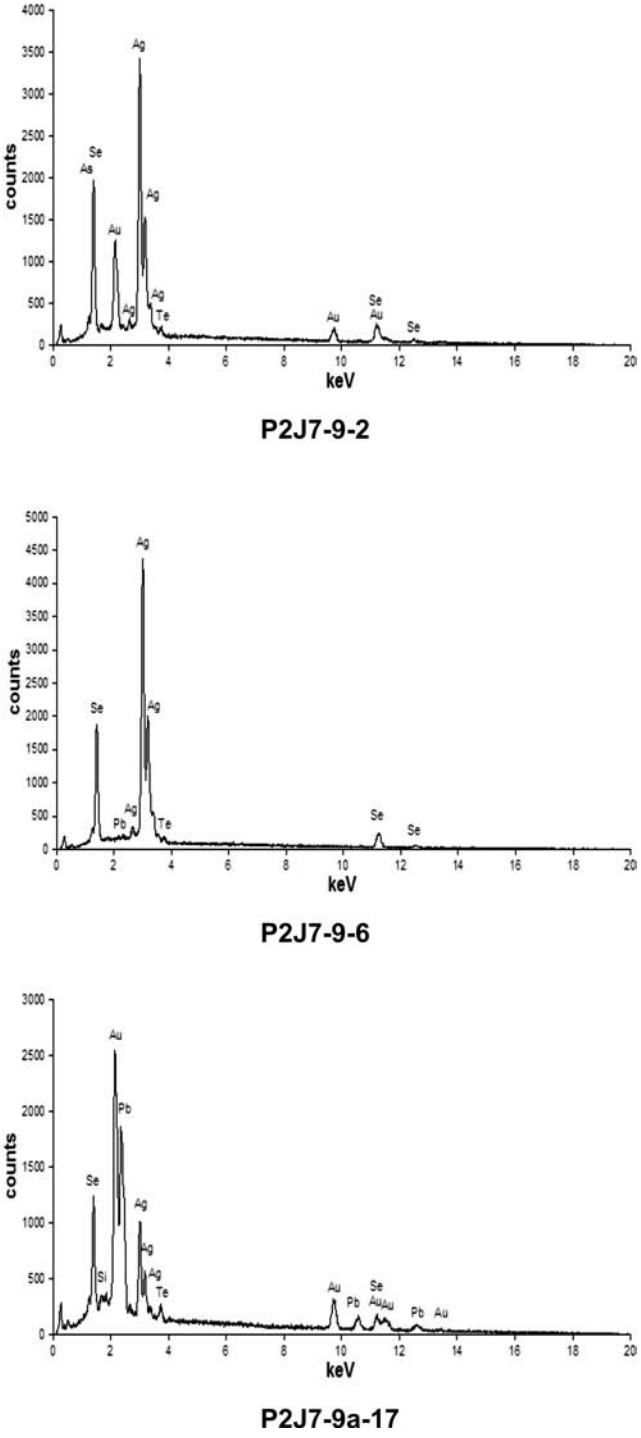

Fig. 67. EDS spectra of different selenides, sample PZ-J7-9 and PZ-J7-9a

that, apart from precious metals and arsenides, the carriers of Pt can be also oxidized Fe compounds, e.g., hematite or Fe-hydroxides (Oberthür *et al.*, 2003). These are the only minerals occurring in sufficient amounts and in dispersion, which can adsorb fine particles of Pt or Pt-Fe-alloys.

The organic matter with increased amounts of PGE occurs between the oxidized and the reducing zones. This zone, together with the U-bearing organic matter, were formed contemporaneously with the progressing oxidation of the Cu deposit. The organic matter might have played the role of a sorbent of precious metals. Such mechanism is confirmed by significant admixtures of Fe, Cu and S in the organic matter from this zone (Tab. 36). Large amounts of organic matter, including the thucholitic compounds, which occur in the Cu deposit do not concentrate precious metals (see chapter "*Geochemistry of Au and PGE*").

Studies on distribution of Pd and Pt evidence the concentration of Pd in zones enriched in As, and, simultaneously, the lack of As in the vicinity of Pt (Figs 72, 73). Distribution of metals shown in Fig. 72 suggests some spatial correlations of Pd with Au, Pd with Ag (Fig. 73) and Pd–Ag–Au (Fig. 74) whereas Pt is spatially correlated with Bi (Fig. 73). Disseminated character of Pt results in low recovery of this metal during ore processing, in comparison with Au (Mączka *et al.*, 2003).

GEOCHEMISTRY OF OTHER ORE MINERALS

Apart from precious metals, the secondary oxidation zone hosts a number of sulphides, arsenides and oxides of transitional metals. These minerals occur in trace amounts, larger concentrations were found of chalcopyrite, bornite, covellite, digenite and chalcocite (Report AGH, 1996, 1997; Piestrzyński, 1996a; Pieczonka, 1998, 2000; Piestrzyński & Pieczonka, 1998). In the zones of oxidizing leaching the microprobe analyses indicated the presence of spionkopite, yarrowite and geerite (Piestrzyński & Pieczonka, 1998).

Chalcopyrite

Chalcopyrite belongs to minerals which chemical composition is difficult to determine with the microprobe analyser due to the lack of relevant standards. In such analyses the contents of Fe and S are usually underestimated and, consequemtly, the total falls below 100%.

Analyzed were chalcopyrites intergrown with native Au and bornite, derived from the grey Kupferschiefer variety in the profile PR 18-0188 (Tab. 37). Because all analyses (except one) indicate underestimated values of Fe and variable values of S (presumably resulting from an analytical error), the calculations were based on Cu contents. Hence, chemical composition of the first chalcopyrite corresponds to $Cu_{1.0000}Fe_{0.9260\text{-}0.9718}S_{1.8837\text{-}1.9142}$ and that of the second one to: $Cu_{1.0000}Fe_{0.9370\text{-}1.0221}S_{2.0122\text{-}2.0159}$. These chalcopyrites contain small amounts of Au, As, Hg and Bi from which Au and Bi probably substitute for Cu. Taking into account these admixtures, compositions of chalcopyrites are (Pieczonka, 1998):

$Cu_{1.0000}Au_{0.0011\text{-}0.0022}Bi_{0.0004\text{-}0.0010}\ Hg_{0.0005\text{-}0.0029}$
$Fe_{0.9260\text{-}0.9718}S_{1.8837\text{-}1.9142}$

and

$Cu_{1.0000}Au_{0.0004\text{-}0.0009}\ Bi_{0.0004\text{-}0.0022}\ Hg_{0.0011\text{-}\ 0.0013}$
$Fe_{0.9370\text{-}1.0221}S_{2.0122\text{-}2.0159}$.

Apart from typical chalcopyrite, microprobe analyses revealed the presence of chalcopyrite with mosaic structure (called "marbled structure", Pieczonka, 1998). This variety is enriched in Se (<1 wt.%) and Ca. The presence of Ca may suggest metasomatic origin of this sulphide, in which relics

Table 35

EDS composition of Pd-As-O minerals
(upper figure – wt.%; lower figure – atomic proportions)

Sample	Au Lα	As Λα	Hg Mα	Pd Lα	O Kα	Cu Kα	Ni Kα	Assumed formula/total/atomic proportions
AP-291/3-7a-1	0.83	23.21	≤0.1	64.06	8.37	1.46	2.05	Pd_4As2O_3 100.00
	0.0136	1.0000		1.9435	1.6885	0.0742	0.0113	$(Pd_{3.8870}Au_{0.0271}Ni_{0.0225}Cu_{0.1484})As_{2.0000}O_{3.377}$
AP-291/3-7a	Bi=2.94	22.41	0.75	62.72	8.29	0.94	1.96	Pd_2AsO_2 100.00
	0.0471	1.0000	0.0124	1.9709	1.7322	0.0495	0.1117	$Pd_{1.9709}Ni_{0.1117}Bi_{0.0471}Cu_{0.0495}As_{1.0000}O_{1.7322}$
AP-291/3-7-5	0.66	25.38	≤0.1	52.10	10.96	6.64	4.25	Pd_2AsO_2 100.00
	0.0100	1.0000		1.4454	2.0218	0.3084	0.2137	$Pd_{1.4454}Cu_{0.3084}Ni_{0.2137}Au_{0.0100}As_{1.0000}O_{2.0218}$
AP-291/3-7a-2	3.90	28.00	≤0.1	51.93	10.47	2.51	3.19	$Pd_6As_4O_7$ 100.00
	0.0530	1.0000		1.3061	1.7511	0.1057	0.1456	$Pd_{1.3061}Ni_{0.1456}Cu_{0.1057}Au_{0.0530}As_{1.0000}O_{1.7511}$
AP-291/3-7-3	≤0.2	23.81	≤0.1	62.36	8.96	≤0.1	4.87	$Pd_8As_4O_7$ 100.00
		1.0000		1.8442	1.7621		0.2612	$Pd_{1.8442}Ni_{0.2612}As_{1.0000}O_{1.7621}$
AP-291/3-7a-4	≤0.2	24.55	≤0.1	62.76	8.88	1.07	2.74	$Pd_4As_2O_3$ 100.00
		1.0000		1.7998	1.6936	0.0513	0.1425	$Pd_{1.7998}Ni_{0.1425}Cu_{0.0513}As1.0000O_{1.6936}$
AP-291/3-6-7	≤0.2	32.33	≤0.1	45.14	12.93	2.26	7.35	$Pd_5As_4O_7$ 100.00
		1.0000		0.9831	1.8728	0.0825	0.2902	$Pd_{0.9831}Ni_{0.2902}Cu_{0.0825}As_{1.0000}O_{1.8728}$
AP-291/3-6-5	≤0.2	23.87	≤0.1	62.30	8.95	1.06	3.81	$Pd_8As_4O_7$ 100.00
		1.0000		1.8377	1.7558	0.0052	0.2040	$Pd_{1.8377}Ni_{0.2040}Cu_{0.0052}As_{1.0000}O_{1.7558}$
AP-291/3-6-4	≤0.2	28.34	≤0.1	50.40	11.66	1.70	7.91	$Pd_5As_4O_8$ 100.00
		1.0000		1.2522	1.9265	0.0701	0.3563	$Pd_{1.2522}Ni_{0.3563}Cu_{0.0701}As_{1.0000}O_{1.9265}$
AP-291/3-6-3	≤0.2	28.23	≤0.1	51.64	11.44	≤0.1	8.09	$Pd_3As_2O_4$ 100.00
		1.0000		1.2879	1.8976		0.3657	$Pd_{1.2879}Ni_{0.3657}As_{1.0000}O_{1.8976}$
AP-291/3-5-3	≤0.2	34.55	≤0.1	43.55	13.39	≤0.1	8.51	$PdAsO_2$ 100.00
		1.0000		0.8875	1.8146		0.2489	$Pd_{0.8875}Ni_{0.2489}As_{1.0000}O_{1.8146}$
AP-291/3-6-1	≤0.2	28.84	≤0.1	53.33	11.08	≤0.1	6.74	$Pd_3As_2O_4$ 100.00
		1.0000		1.3026	1.7992		0.2983	$Pd_{1.3026}Ni_{0.2983}As_{1.0000}O_{1.7992}$
AP-291/3-5-4	3.73	23.33	≤0.1	59.44	8.97	1.38	1.65	Pd_2AsO_2 100.00
	0.0607	1.0000		1.7938	1.8003	0.0697	0.0902	$Pd_{1.7938}Au_{0.0607}Ni_{0.0902}Cu_{0.0697}As_{1.0000}O_{1.8003}$

Table 36

WDS composition of thucholitic substances from the Kupferschiefer (pitchy variety) from transitional zone, sequence No. 95-S-8/2, Sieroszowice Mine [wt.%]

Sample	Al	Si	S	Ca	Fe	Cu	Pd	Pt	Au	Pb	Th	U
291/1	0.03	0.26	1.73	0.57	2.65	2.17	≤0.05	0.18	≤0.05	0.60	0.13	17.94
291/2	0.15	0.30	0.96	0.64	1.23	0.97	≤0.05	≤0.05	≤0.05	≤0.05	≤0.10	22.90
291/3	0.17	0.14	0.70	0.50	0.61	0.69	≤0.05	0.10	≤0.05	≤0.05	≤0.10	21.02
291/4	0.17	0.18	3.43	0.58	4.15	4.53	0.14	0.23	≤0.05	0.34	0.26	13.12
291/5	≤0.03	0.08	1.34	0.62	1.05	0.77	≤0.05	0.14	≤0.05	0.22	≤0.10	21.06
291/6	0.18	0.38	4.47	0.83	3.89	3.46	≤0.05	0.26	≤0.05	0.36	≤0.10	24.70
291/7	≤0.03	0.22	5.03	0.91	5.25	4.88	≤0.05	≤0.05	≤0.05	0.48	≤0.10	23.68
291/8	≤0.03	0.19	2.43	0.59	1.88	2.25	0.07	0.28	≤0.05	≤0.05	≤0.10	9.74
291/11	0.18	0.13	1.20	0.55	1.01	1.18	≤0.05	≤0.05	≤0.05	28.30	≤0.10	4.89
291/12	≤0.03	0.26	3.81	1.09	3.51	3.15	≤0.05	0.79	≤0.05	0.41	≤0.10	43.85
291/13	0.20	0.40	2.22	1.55	2.28	2.10	≤0.05	0.53	≤0.05	0.32	0.77	53.42
291/14	≤0.03	0.30	1.13	1.62	1.84	1.98	≤0.05	0.58	≤0.05	≤0.05	0.10	68.41
291/15	0.09	0.51	1.49	1.77	2.53	2.19	0.13	0.88	≤0.05	≤0.05	0.80	65.35
291/16	0.15	0.29	13.92	0.64	15.38	15.71	0.17	0.41	≤0.05	1.07	≤0.10	19.90
291/18	0.21	0.22	0.65	0.46	0.66	0.75	0.05	0.13	≤0.05	≤0.05	≤0.10	6.54

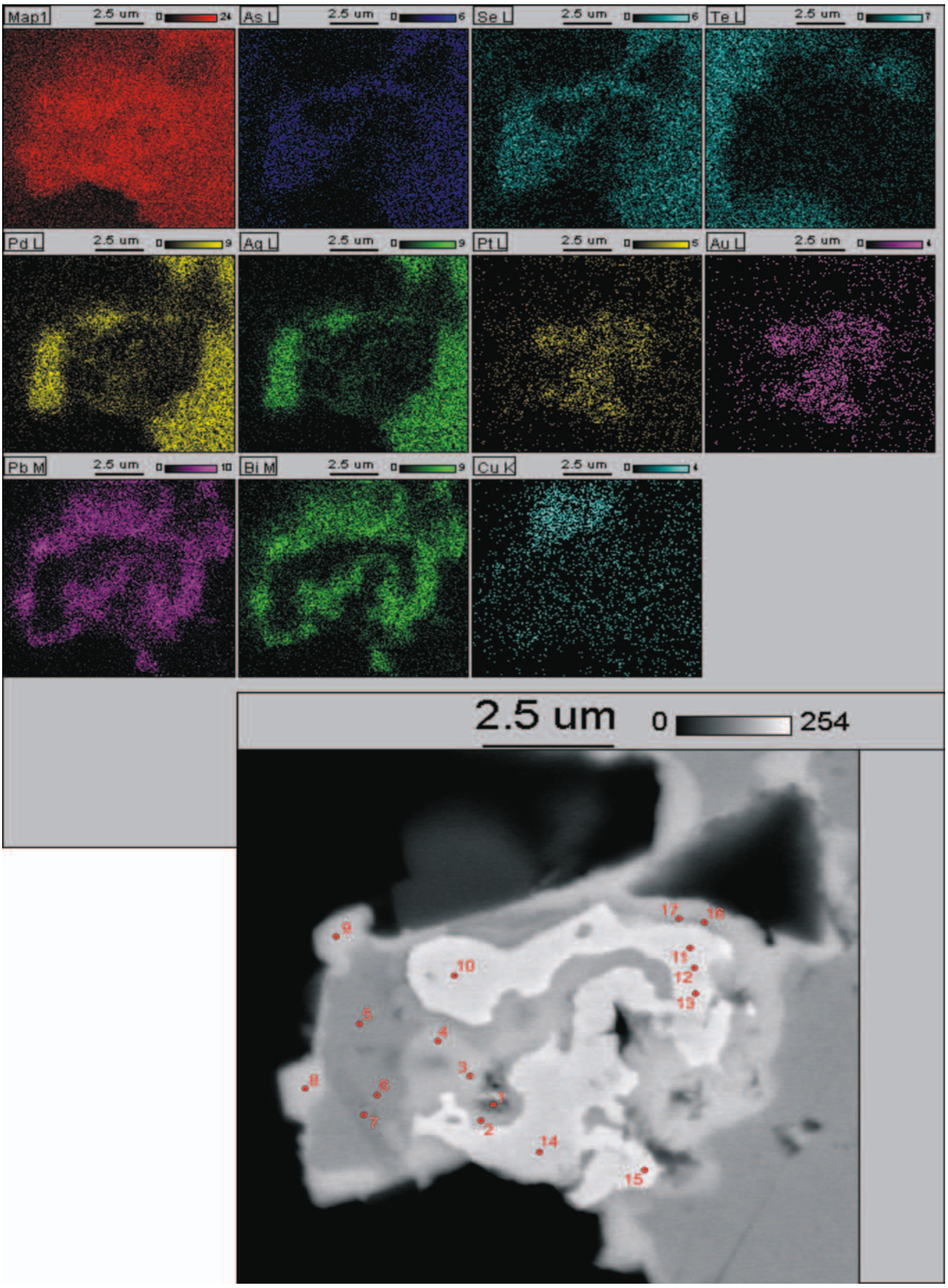

Fig. 68. Single element scans and BSE image (bottom right), red circles show position of quantitative measurements, sample PZ-J7-9a

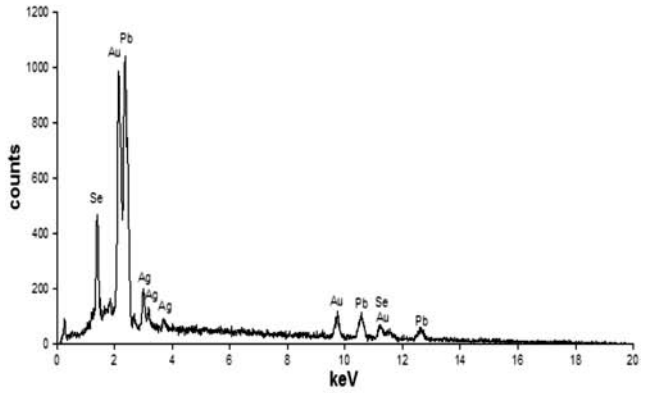

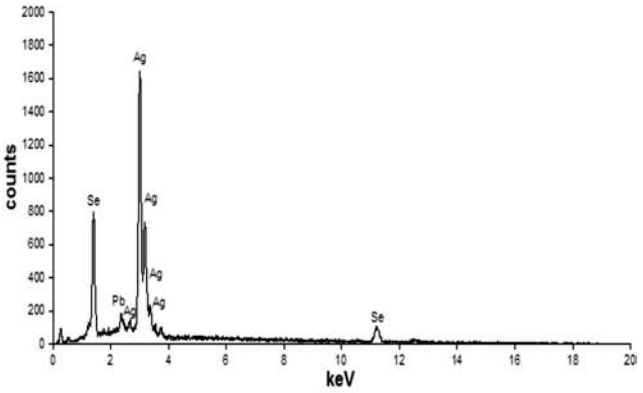

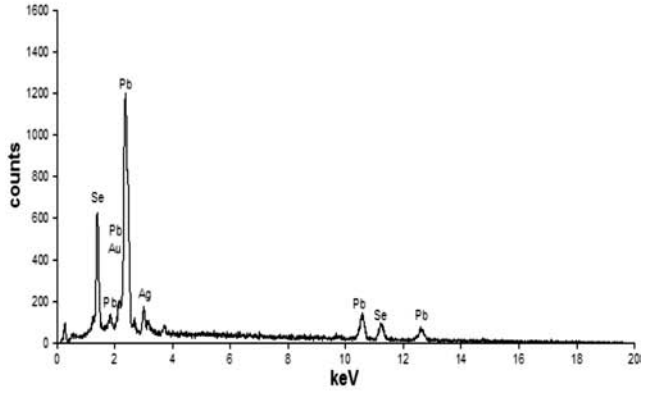

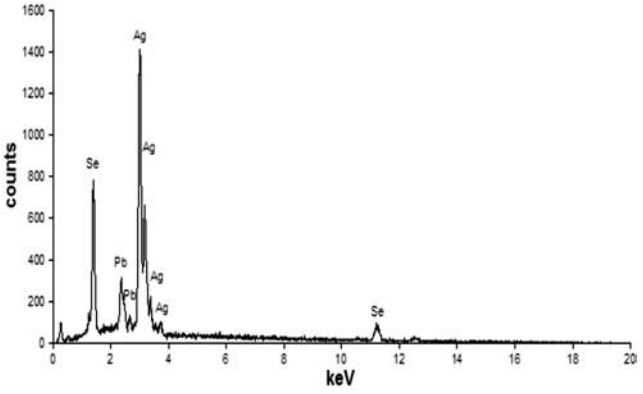

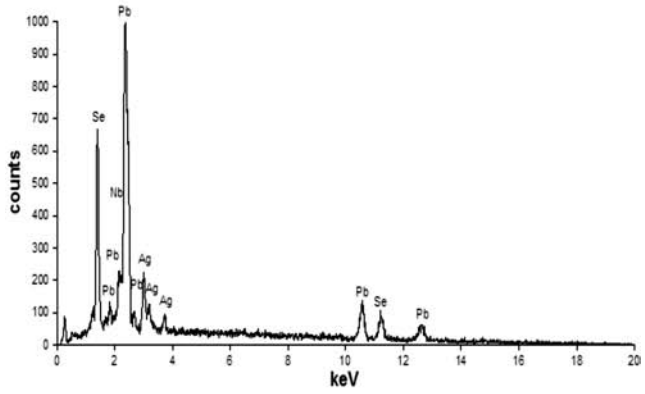

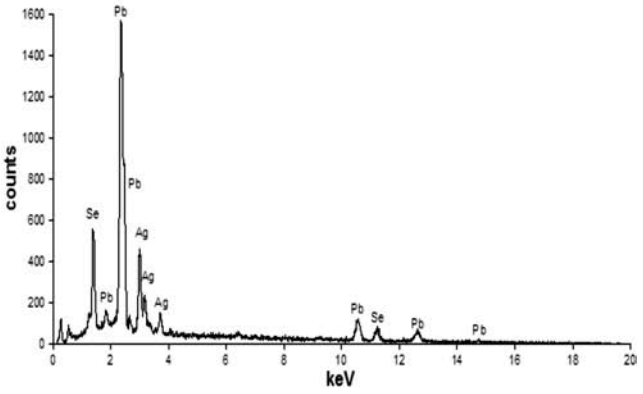

Fig. 69. EDS spectra of different selenides, sample PZ-J7-9a

Fig. 70. EDS spectra of different selenides, sample PZ-J7-9a

of carbonates are still preserved. The "marbled" chalcopyrites show high contents of Au (0.39–1.08 wt.%) and even higher admixtures of Ag (1.02–1.55 wt.%) (Pieczonka, 1998). However, it must be emphasized that the analyzed chalcopyrites form intergrowths with native Au and electrum. Moreover, enrichments in As (0.17–0.20 wt.%), Hg (0.09–0.30 wt.%), Pt (up to 0.16 wt.%) and Pd (up to 0.09 wt.%) were detected. Under the microscope the "marbled" chalcopyrites show brass-yellow colour (Pieczonka, 1998). Chalcopyrites of different chemical composition (containing Ag), were described from the Rücken-type hydrothermal veins (Piestrzyński *et al.*, 2000).

Chalcopyrites from the black Kupferschiefer variety enriched in Ag (0.13–0.31 wt.%) and intergrown with thiosulphates, plattnerite, galena, covellite, bornite and carbonates were described by Kucha and Piestrzyński (1991). These phases contain also significant admixtures of Pb (3.52 wt.%), on the contrary to those described above. High

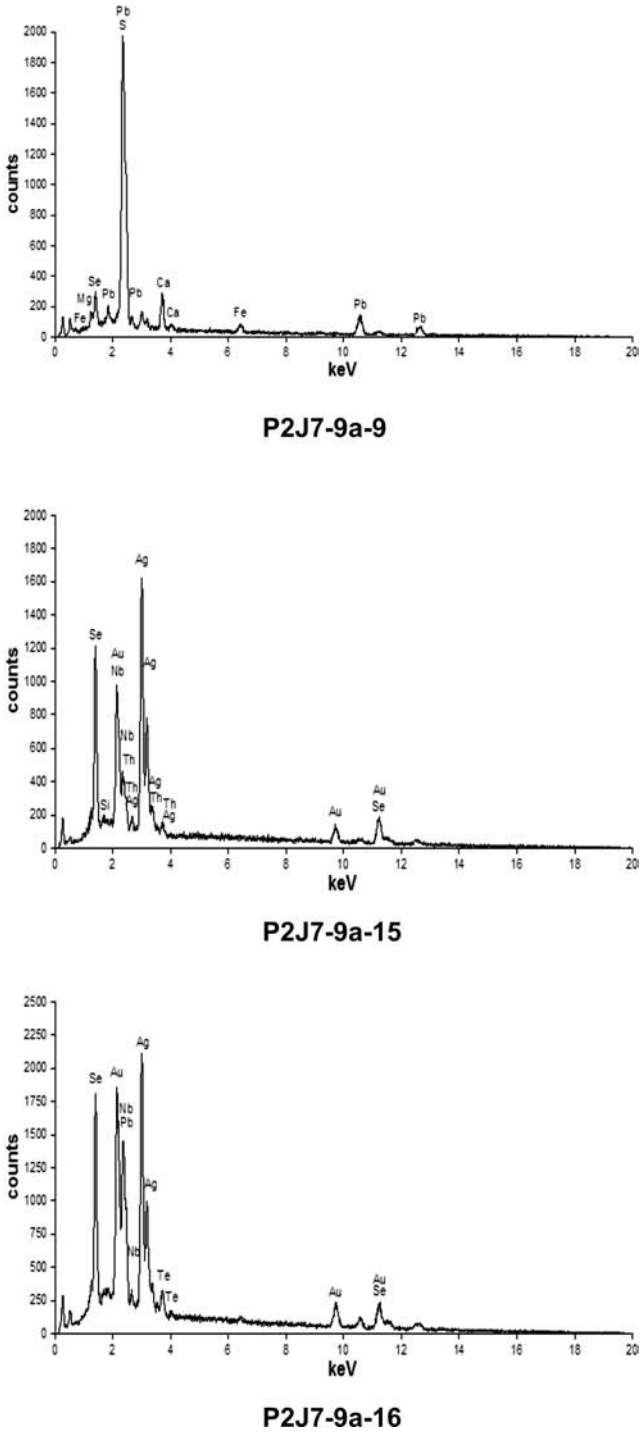

Fig. 71. EDS spectra of different selenides, sample PZ-J7-9a

Au admixtures are not casual feature. In the earlier studies 1.36 wt.% Au was detected in chalcopyrite coexisting with thucholite in the black Kupferschiefer (Piestrzyński, 1989). This variety was not enriched in Pb, Mo and Ni as well as in U and Th (due to the presence of thucholite). In the literature only a single example of such high-Au chalcopyrite (0.05–0.65 wt.% Au) was described by Piestrzyński *et al.*, (1991) from a porphyry copper deposit in the Philippines. In all cases the high content of Au in chalcopyrite is explained in terms of the presence of a dispersed Au-Ag solid phase of crystal size below the resolution of optical microscope. Results of chalcopyrite analyses from the other parts of copper deposit did not reveal Au contents detectable with the WDS method (Salamon, 1976). Therefore, it can be assumed that the presence of native Au is typical of chalcopyrites forming intergrowts with native Au and/or electrum.

Bornite

Microprobe analyses of bornites from the secondary oxidation zones revealed highly variable chemical composition of this sulphide. Taking into account Fe contents, several varieties were distinguished: (i) typical bornites (samples No. 286/A1, 286/A7, 286/A8, 286/C13 from the red and grey Kupferschiefer varieties), (ii) "half-bornites" (samples No. 286/A2, 286/A3, 286/A4 and 286/C12) and (iii) "quarter-bornites" (samples No. 286/B10 and 286/B11) (Tabs 38, 39). The terms "half-bornite" and "quarter-bornite" were introduced to the literature by Kucha *et al.*, (1981) for bornites containing respectively 50% and 25% of stoichiometric Fe content together with increased amounts of Cu.

In the analyzed typical bornites Cu contents vary from 58.05 to 63.38 wt.%, and those of Fe – from 9.79 to 13.97 wt.%. Such values clearly shift from the stoichiometric composition. Most of analyzed bornites show deficit of Cu in relation to Fe and their composition can be expressed as $Cu_{4.1579\text{-}5.0228}\ Fe_{0.8828\text{-}1.1461}\ S_{40000}$. These minerals are enriched in Au (0.04–1.20 wt.%), Ag (0.03–0.26 wt.%), Hg (0.08–0.57 wt.%), As (0.10–0.29 wt.%), Bi (0.30–0.48 wt.%), Pt (up to 0.21 wt.%) and Pd (up to 0.11 wt.%) (Tab. 38, 39). Such bornites were observed in both the red and the grey Kupferschiefer varieties. Contents of Ag are low, and the Ag-rich, pinkish-lillac and pinkish-crème bornite varieties described by Salamon (1979) from the eastern part of the Fore-Sudetic deposit are absent. According to Salamon (1979), the pinkish-lillac bornites contained up to 15.5 wt.% Ag whereas very rare, pinkish-crème variety forming intergrowths with electrum in thucholite contained 10.3 wt.% Ag and 4.0 wt.% Au. Silver contents in some samples from the red and the grey Kupferschiefer varieties are close to the lower level of its concentration in pinkish-grey bornite (0.14–0.62 wt.% Ag), (Salamon, 1979). The highest known amount of Ag in bornite (49.63 wt.%) was reported by Kucha and Mayer (1996).

"Half-bornites" show high contents of Cu – from 67.59 to 70.24 wt.% and Fe contents from 4.31 to 5.79 wt.%, i.e., about a half of stoichiometric value. Thus, their composition corresponds to $Cu_{5.7198\text{-}6.0300}Fe_{0.4212\text{-}0,5577}S_{4.0000}$. Half-bornites reveal very high amounts of Au (0.46–1.27 wt.%) as well as admixtures of Hg (0.31–0.56 wt.%), Bi (up to 0.47 wt.%), Ag (0.17–0.37 wt.%), As (up to 0.17 wt.%), Pt (up to 0.09 wt.%) and Pd (up to 0.14 wt.%) (Tab. 38) (Pieczonka, 1998).

"Quarter-bornites" contain up to 3.46 wt.% Fe and 70.91 wt.% Cu. The deficiency of Fe is presumably compensated by the excess of Cu. Composition of such bornites corresponds to $Cu_{6.0548\text{-}6.1267}Fe_{0.3011\text{-}0.3445}S_{4.0000}$. This variety also contains high amounts of Au (from 0.22 to 0.99 wt.%) as well as admixtures of Ag (0.15–0.17 wt.%), Hg (0.25–0.47 wt.%), Bi (0.30 wt.%) and As (0.11 wt.%) (Tab. 38) (Pieczonka, 1998).

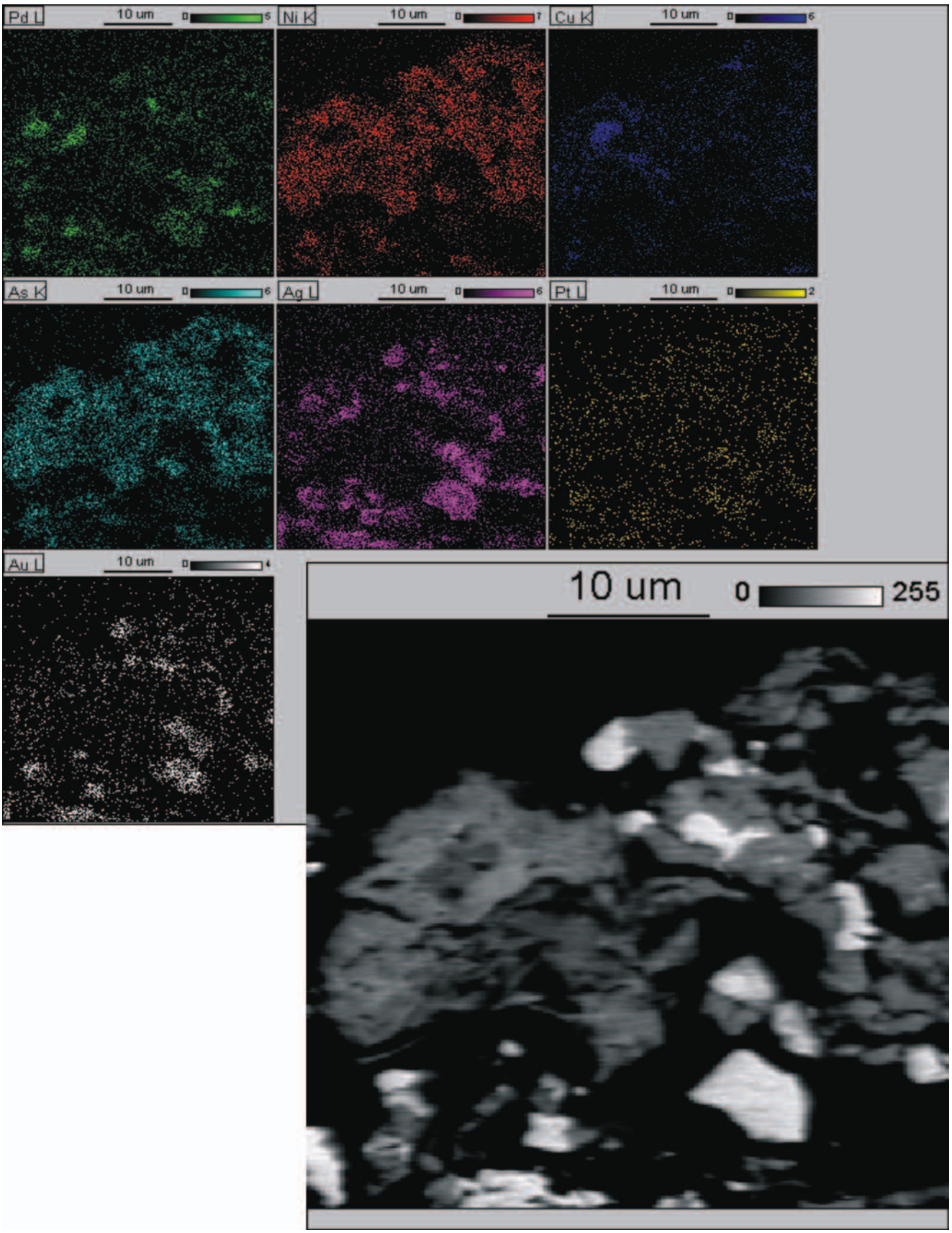

Fig. 72. Single element scans and BSE image (bottom right), red circles show position of quantitative measurements, sample 291-3/2

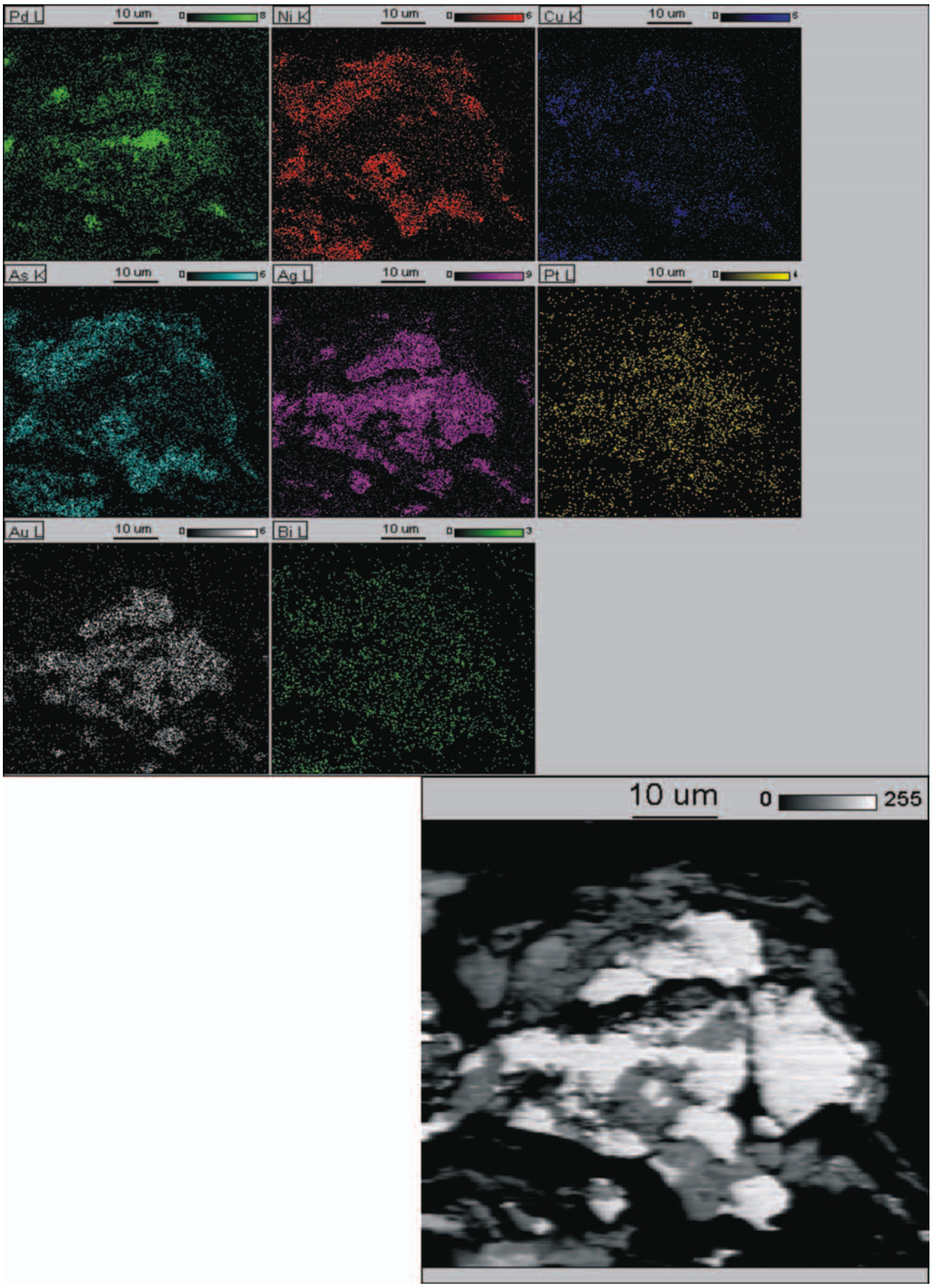

Fig. 73. Single element scans and BSE image (bottom right), red circles show position of quantitative measurements, sample 291-3/3

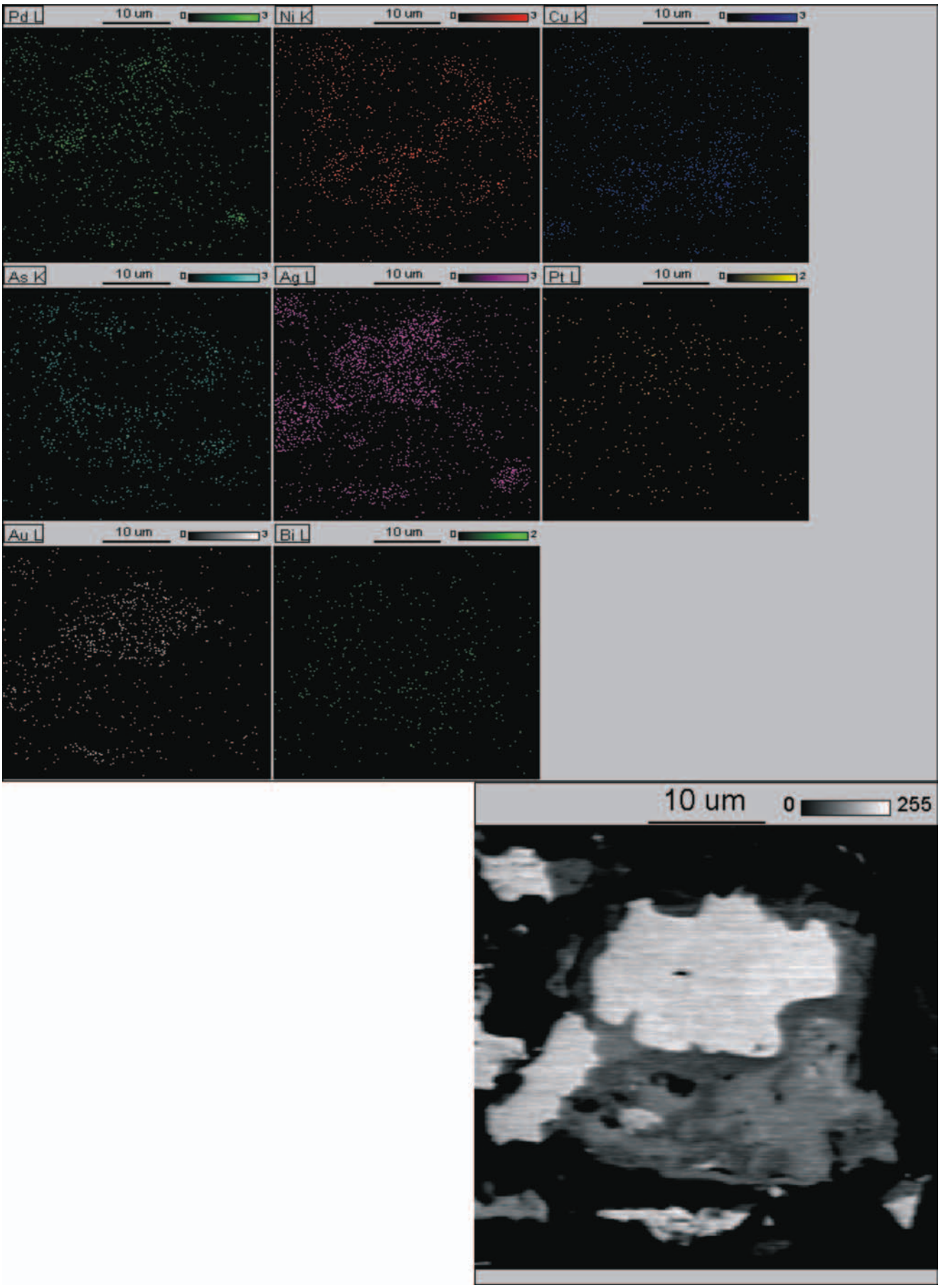

Fig. 74. Single element scans and BSE image (bottom right), red circles show position of quantitative measurements, sample 291-3/1

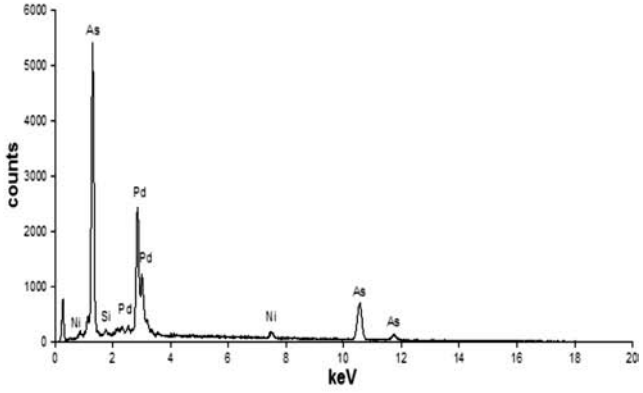

291-3-1-1

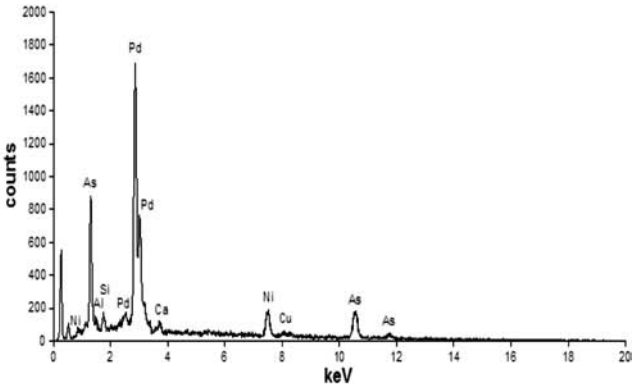

291-3-6-4

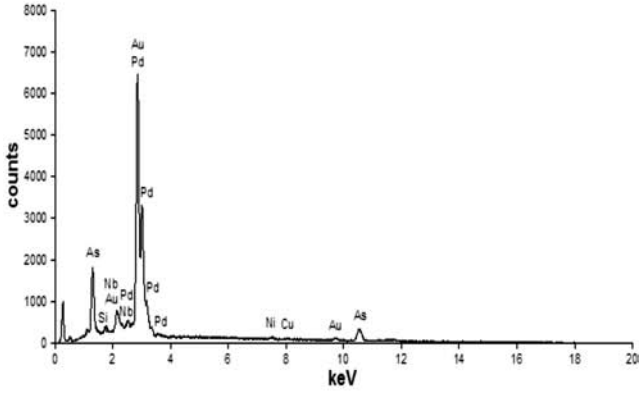

291-3-3-1

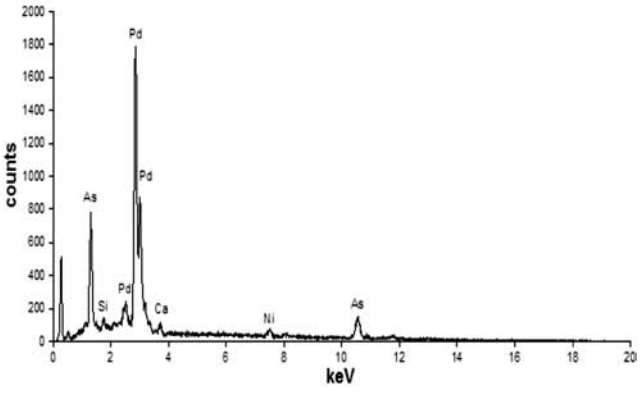

291-3-7-1a

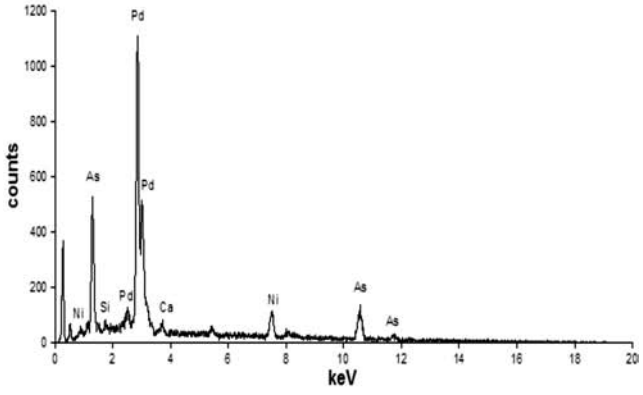

291-3-6-1

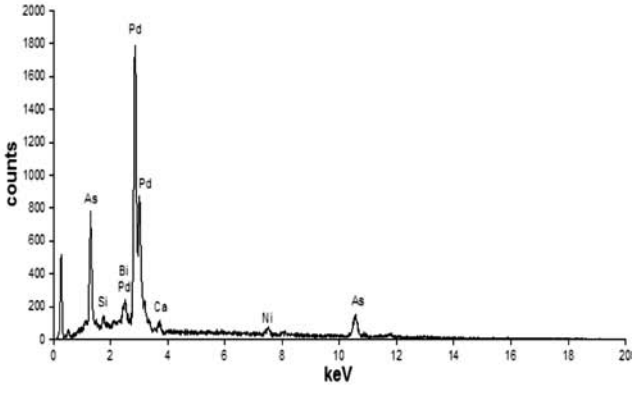

291-3-7a-1a

Fig. 75. EDS spectra of different Pd-arsenides, sample 291-3

Fig. 76. EDS spectra of different Pd-arsenides, sample 291-3

Both the "half-bornites" and the "quarter-bornites" analyzed in the following project differ somewhat from those described by Kucha *et al.*, (1981), which corresponded to the formulae $Cu_{5.5}Fe_{0.5}S_4$ and $Cu_{5.75}Fe_{0.25}S_{4.0000}$, respectively. Moreover, these bornites did not contain admixtures of precious metals due to different localization. New studies carried on the porphyry copper deposits revealed the existence of other Cu-Fe-S phases, e.g. nukundamite – $Cu_{3.38}Fe_{0.62}S_4$ (Inan & Einaudi, 2002), which clearly demonstrates that the knowledge of Cu-Fe-S system has not been completed.

Minerals of CuS-Cu$_2$S and Cu-Ag-S systems

Minerals encountered in various rocks and identified under the microscope as chalcocite, digenite, djurleite, anilite and covellite show highly diversified chemical compo-

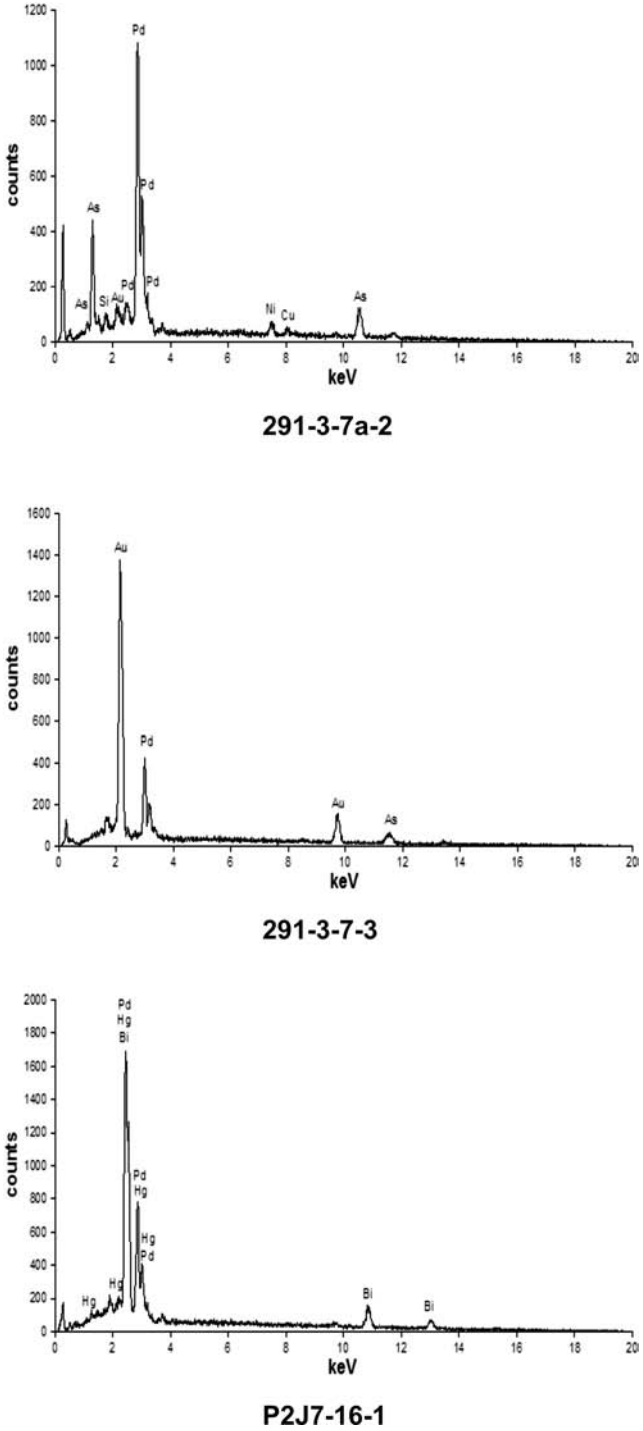

Fig. 77. EDS spectra of different Pd-arsenides and alloys, sample 291-3, and PZ-J7-16

sitions when analyzed with the microprobe. The CuS-Cu_2S system includes the following minerals: covellite (CuS), yarrowite ($Cu_{1.12}S$), spionkopite ($Cu_{1.40}S$), geerite ($Cu_{1.60}S$), anilite ($Cu_{1.75}S$), digenite ($Cu_{1.80}S$), djurleite ($Cu_{1.97}S$) and chalcocite (Cu_2S), (Goble, 1981). Chemical compositions of analyzed minerals documented the presence of almost all members of CuS-Cu_2S system. These phases form intergrowths with native Au, electrum, Pd-arsenides, selenides and native Ag. Hence, the main trace elements are Ag, Au, Se and Hg with high variability of the contents of the two first elements. High Hg contents were noticed in all analyzed members of the CuS-Cu_2S system, despite their host-rocks whereas Se was found mostly in the covellite group. During calculations of formulae these trace elements were taken into consideration as compensators of Cu deficit. Iron admixtures, typical of the members of CuS-Cu_2S system are low (up to 0.12 wt.%). Detection limits of Pt and Pd precludes their credible quantitative determinations in studied sulphides.

Chemical composition of minerals found in the clayey variety of the Kupferschiefer corresponds to the formula $Cu_{1.8209\text{-}1.9100}S_{1.0000}$ (Tab. 40). Highest admixtures of Ag (0.15–7.11 wt.%) and Au (0.14–2.78 wt.%) indicate possible participation of these minerals in crystallization of native Au and electrum. Important trace element is also Hg (0.20–0.69 wt.%). If Ag, Au and Hg are included, the composition of end-members with minimum and maximum Cu contents are:$Cu_{1.8209}Ag_{0.0195}Au_{0.0094}Hg_{0.0042}S_{1.0000}$ and $Cu_{1.9100}Ag_{0.0152}$ $Au_{0.0225}Hg_{0.0043}S_{1.0000}$. This composition is closest to that of djurleite.

The members of CuS-Cu_2S system found in the dolomitic Kupferschiefer variety (Tab. 41) show slightly lower Cu contents (74.59–76.19 wt.%) and much less Ag (up to 0.09 wt.%) and Au (up to 0.26 wt.%). The admixture of Pb (up to 0.39 wt.%) is an effect of clausthalite inclusions (Pieczonka, 1998). When the most important trace elements are included, chemical composition of these phases changes from $Cu_{1.6530}Au_{0.0014}Hg_{0.0032}S_{1.0000}$ to $Cu_{1.6990}Au_{0.0007}$ $Hg_{0.0035}S_{1.}0000$, which roughly corresponds to that of anilite. Among covellite analyses only those selected as correct were listed in Table 42. Significant differences in the results were caused by technical problems. Analyzed minerals represent typical covellite ($Cu_{1.0669}S_{1.0000}$) as well as the "blue-remaining covellite" I i II (Goble, 1980) recently named spionkopite ($Cu_{1.3103}S_{1.0000}$) and yarrowite ($Cu_{1.1705}S_{1.0000}$). Covellites contain admixtures of Se (up to 1.11 wt.%) and Te (up to 0.14 wt.%) (Pieczonka, 1998) related to the intergrowths with selenides and tellurides.

In the boundary dolomite CuS-Cu_2S-system minerals of compositions corresponding to chalcocite ($Cu_{2.0893}$ $S_{1.0000}$) and djurleite ($Cu_{1.8833}S_{1.0000}$) were observed (Tab. 43). The admixtures of Au (up to 0.37 wt.%), Ag (up to 0.24 wt.%) and Hg (up to 0.39 wt.%) were detected (Pieczonka, 1998).

Minerals forming intergrowths with native Ag in nests encountered in the clayey dolomite show variable compositions (Tab. 44). Microscopic studies indentified chalcocite and digenite accompanied by members of Cu-Ag-S system: Cu-stromeyerite described earlier by Jarosz (1966), Harańczyk and Jarosz (1966), and Harańczyk and Bryniarska (1967), mckinstryite found by Salamon (1976, 1979) and stromeyerite (Harańczyk & Jarosz, 1966). Chalcocites ($Cu_{1.8883\text{-}2.1955}S_{1.0000}$) and digenites ($Cu_{1.8335\text{-}1.8619}$ $S_{1.0000}$) reveal high contents of Ag (0.21–3.47 wt.%). Other trace element is Hg (0.20–0.38 wt.%) and, in a few samples, also Pt (0.04–0.16 wt.%). The remaining trace elements contents are low. The Cu-stromeyerites ($Cu_{1.4336\text{-}1.4904}$ $Ag_{0..5757\text{-}0.7842}S_{1.0000}$) are apparently enriched in Cu at the expense of Ag. Similar process, although less pronounced,

Table 37

WDS compositions of chalcopyrites from the Kupferschiefer (grey variety), profile PR 18-0188/4, mining section G-31, Polkowice West Field (after Pieczonka, 1998) upper figure – wt.%; lower figure – atomic proportions)

Sample	As Kα	Bi Mα	Hg Lα	Au Lα	Cu Kα	Fe Kα	Pt Lα	S Kα	Pd Lα	Ag Lα	Total
I/28	0.17	0.11	0.32	0.11	35.04	29.40	≤0.03	33.47	≤0.03	0.03	98.65
	0.0042	0.0009	0.0029	0.0011	1.0000	0.9547		1.8930		0.0005	
I/29	0.08	≤0.04	0.33	0.14	34.76	29.69	≤0.03	33.04	0.11	≤0.03	98.19
	0.0020		0.0029	0.0013	1.0000	0.9718		1.8837	0.0018		
I/30	0.16	0.09	0.07	0.21	35.31	28.74	≤0.03	34.11	≤0.03	0.07	98.76
	0.0038	0.0007	0.0005	0,0020	1.0000	0.9260		1.9142		0.0011	
I/31	0.19	0.12	≤0.03	0.23	35.22	29.24	≤0.03	33.70	≤0.03	0.08	98.78
	0.0045	0.0010		0.0022	1.0000	0.9448		1.8964		0.0013	
II/8	0.16	≤0.05	0.15	≤0.03	33.64	30.22	≤0.03	34.22	≤0.03	≤0.03	98.39
	0.0040		0.0013		1.0000	1.0221		2.0159			
II/9	0.11	0.25	0.15	0.09	34.60	29.00	0.16	35.13	0.05	≤0.03	99.54
	0.0028	0.0022	0.0013	0.0009	1.0000	0.9537	0.0015	2.0121	0.0009		
II/10	0.18	≤0.05	0.13	0.10	34.39	28.32	≤0.03	34.92	≤0.03	0.08	98.12
	0.0044		0.0011	0.0009	1.0000	0.9370		2.0122		0.0013	

Table 38

WDS composition of bornites from the Kupferschiefer (red variety), profile PZ-21/1, Polkowice West Field (after Piestrzyński & Pieczonka, 1997a) (upper figure – wt.%; lower figure – atomic proportions)

Sample	As Kα	Bi Mα	Hg Lα	Au Lα	Cu Kα	Fe Kα	Pt Lα	S Kα	Pd Lα	Ag Lα	Total
286/A1	0.18	≤0.05	≤0.10	1.20	63.38	9.79	≤0.05	25.47	≤0.06	0.26	100.28
	0.0121			0.0307	5.0228	0.8828		4.0000		0.0121	
286/A2	0.17	0.47	0.38	0.46	70.24	4.31	0.09	23.51	≤0.06	0.17	99.80
	0.0125	0.0120	0.0104	0.0125	6.0300	0,4212	0.0027	4.0000		0.0087	
286/A3	0.10	≤0.05	0.31	0.98	67.59	5.79	0.09	23.85	≤0.06	0.37	99.08
	0.0070		0.0081	0.0269	5.7198	0.5577	0.0027	4.0000		0.0183	
286/A4	0.08	0.21	0.37	1.27	68.00	5.30	0.06	24.46	≤0.06	0.19	99.94
	0.0058	00.052	0.0094	0.0336	5.6114	0.4976	0.0016	4.0000		0.0094	
286/A7	0.14	≤0.05	0.39	0.29	61.92	10.49	≤0.05	27.00	0.08	0.10	100.41
	0.0090		0.0090	0.0071	4.6290	0.8922		4.0000	0.0038	0.0043	
286/A8	0.19	≤0.05	0.57	0.21	61.76	10.38	0.21	27.59	0.11	0.09	101.11
	0.0116		0.0130	0.0051	4.5184	0.8642	0.0051	4.0000	0.0046	0.0037	
286/B10	0.11	≤0.05	0.47	0.99	70.91	3.10	≤0.05	23.64	0.08	0.15	99.45
	0.0081		0.0125	0.0271	6.0548	0.3011		4.0000	0.0043	0.0076	
286/B11	≤0.07	0.30	0.25	0.22	70.06	3.46	≤0.05	23.08	0.08	0.17	97.67
		0.0078	0.0067	0.0061	6.1267	0.3445		4.0000	0.0044	0.0089	
286/C12	≤0.07	≤0.05	0.56	0.82	69.02	5.01	≤0.05	24.79	0.14	0.18	100.52
			0.0145	0.0217	5.6195	0.4641		4.0000	0.0067	0.0088	
286/C13	0.23	0.19	0.37	0.38	61.17	11.03	0.10	24.58	≤0.05	0.07	98.12
	0.0162	0.0050	0.0094	0.0099	5.0233	1.0306	0.0026	4.0000		0.0031	

Table 39

WDS composition of bornites from the Kupferschiefer (grey variety), profile PR 18-0188, Polkowice West Field (after Pieczonka, 1998) (upper figure – wt.%; lower figure – atomic proportions)

Sample	As Kα	Bi Mα	Hg Lα	Au Lα	Cu Kα	Fe Kα	Pt Lα	S Kα	Pd Lα	Ag Lα	Total
293/60	0.16	≤0.05	0.18	≤0.05	58.05	10.59	≤0.05	28.18	0.07	0.06	97.63
	0.0096		0.0041		4.1579	0.8630		4.0000	0.3186	0.0027	
293/61	0.18	0.41	0.08	≤0.05	59.17	12.13	≤0.05	28.17	0.07	≤0.06	100.21
	0.0109	0.0091	0.0018		4.2395	0.9890		4.0000	0.0032		
293/32	0.29	0.48	0.21	0.04	60.68	11.65	0.12	25.57	0.02	0.03	99.09
	0.0196	0.0115	0.0050	0.0010	4.7901	1.0464	0.0030	4.0000	0.0010	0.0015	
293/33	0.25	≤0.05	0.51	0.15	63.18	10.73	0.14	24.41	0.01	0.08	99.46
	0.0173		0.0131	0.0042	5.2244	1.0095	0.0037	4.0000	0.0005	0.0037	
293/34	0.14	≤0.05	0.38	0.04	57.85	13.97	≤0.05	27.99	≤0.05	0.07	100.44
	0.0087		0.0087	0.0009	4.1718	1.1461		4.0000		0.0027	

can be observed in mckinstryite ($Cu_{1.2510}Ag_{0.8843}S_{1.0000}$), where main admixtures are Hg and Au, occasionally also Bi. Mineral composition close to stromeyerite ($Cu_{1.0162}Ag_{1.1807}S_{1.0000}$) was observed at the contact of native Ag and chalcocite, which may support the concept of the origin of stromeyeyrite from metasomatic processes along such contacts (Salamon, 1976; Mayer & Piestrzyński, 1985). This phase also contains high amounts of Hg (0.45 wt.%). Minerals of Cu-Ag-Hg-S composition described by Mayer and Piestrzyński (1985) from metal-rich Kupferschiefer contained up to 11.2 wt.% Hg. Also Salamon (1979) reported on the occurrence of Hg-rich stromeyerites (0.05–11 wt.% Hg) in association with Ag-amalgams.

Native Ag

Both the macro- and microscopic observations proved the occurrence of native Ag in the study area, in the top part of the Kupferschiefer and in the clayey dolomite. Microprobe analyses were made for native Ag intergrown with simple Cu-sulphides, occasionally also with stromeyerite in the clayey dolomite. Results are shown in Table 45. The analyzed native Ag contains high amounts of Cu (up to 8.16 wt.%) and Hg (up to 6.91 wt.%). According to Salamon (1979), such high Cu contents (over 1 wt.%) can be explained by the presence of native Cu microinclusions. However, native Ag analyzed by this author contained maximum 1.7 wt.% Cu. The high Hg admixtures (about 6 wt.% in sev-

Table 40

WDS composition of the members of CuS-Cu_2S system from the Kupferschiefer (clayey variety), profile PZ-25/2, Polkowice West Field (after Piestrzyński and Pieczonka, 1997a) (upper figure – wt.%; lower figure – atomic proportions)

Sample	As Kα	Bi Mα	Hg Lα	Au Lα	Cu Kα	Fe Kα	Pt Lα	S Kα	Pd Lα	Ag Lα	Total
287/A4	0.24	≤0.05	0.28	0.57	77.61	0.10	≤0.05	20.89	0.09	0.33	100.11
	0.0049		0.0021	0.0045	1.8746	0.0028		1.0000	0.0012	0.0048	
287/A5	0.09	≤0.05	0.20	0.44	77.78	≤0.02	0.08	20.97	≤0.05	0.48	100.04
	0.0018		0.0015	0.0034	1.8716		0.0006	1.0000		0.0067	
287/A6	0.06	≤0.05	0.62	≤0.05	71.26	≤0.02	≤0.05	19.62	≤0.05	7.11	98.67
	0.0013		0.0051		1.8327			1.0000		0.1077	
287/A7	0.28	0.58	0.69	0.14	77.03	≤0.02	≤0.05	21.30	≤0.05	1.21	101.23
	0.0056	0.0042	0.0051	0.0011	1.8248			1.0000		0.0169	
287/B8	0.08	≤0.05	0.56	1.23	76.36	0.07	≤0.05	21.16	0.05	1..39	100.90
	0.0017		0.0042	0.0094	1.8209	0.0020		1.0000	0.0008	0.0195	
287/B9	0.05	0.69	0.60	≤0.05	76.71	0.10	≤0.05	20.62	≤0.05	0.15	98.92
	0.0011	0.0051	0.0047		1.8774	0.0028		1.0000		0.0022	
287/C10	0.17	0.18	0.54	2.78	75.89	0.04	≤0.05	20.05	≤0.05	1.02	100.67
	0.0037	0.0014	0.0043	0.0225	1.9100	0.0011		1.0000		0.0152	

Table 41

WDS composition of the members of CuS-Cu_2S system from the Kupferschiefer (dolomitic variety), profile PZ-20/3, Polkowice West Field (after Pieczonka, 1998) (upper figure – wt.%; lower figure – atomic proportions)

Sample	As Kα	Bi Mα	Hg Lα	Au Lα	Cu Kα	Fe Kα	Pt Lα	S Kα	Pd Lα	Ag Lα	Total
288/B5	0.07	≤0.05	0.51	0.26	74.90	0.11	22.55	0.30	≤0.05	0.09	98.79
	0.0013		0.0036	0.0018	1.6762	0.0028	1.0000	0.0020		0.0011	
288/B6	0.15	0.41	0.54	0.21	74.90	0.10	22.31	0.21	0.05	0.07	98.95
	0.0029	0.0029	0.0039	0.0016	1.6940	0.0026	1.0000	0.0014	0.0007	0.0009	
288/B7	0.13	≤0.05	0.46	0.20	74.59	0.12	22.77	≤0.15	≤0.05	≤0.05	98.27
	0.0024		0.0032	0.0014	1.6530	0.0030	1.0000				
288/B8	0.21	0.51	0.50	0.10	76.19	0.10	22.63	0.39	≤0.05	0.07	100.70
	0.0040	0.0034	0.0035	0.0007	1.6990	0.0026	1.0000	0.0027		0.0009	

Table 42

WDS composition of covellites from the Kupferschiefer, mining section G-31, Polkowice West Field (after Pieczonka, 1998) (upper figure – wt.%; lower figure – atomic proportions)

Sample	Se Kα	Cu Kα	S Kα	Te Lα	Total
283/A3	1.11	70.03	30.19	0.13	101.46
	0.0150	1.1705	1.0000	0.0011	
283/A4	1.01	71.43	27.51	0.07	100.02
	0.0149	1.3103	1.0000	0.0006	
283/A5	0.69	68.31	32.31	0.14	101.45
	0.0086	1.0669	1.0000	0.0011	

eral analyses) suggest that analyzed native Ag occupies relevant position between native Ag and Ag-amalgams, the latter containing over 20 wt.% Hg (Mayer & Piestrzyński, 1985). So high contents of both elements can be explained by: (i) domain-type substitutions of native Ag cells by kolymite (Kucha, 1986), (ii) kolymite inclusions in native Ag, (iii) native Cu inclusions in Ag-Hg-alloy and (iv) combination of all possible processes, including that proposed by Salamon (1979). Analyzed native Ag contains also As (up to 1.68 wt.%), S (up to 0.62 wt.%) and Bi (up to 0.59 wt.%). Results of Pt and Pd analyses are close to detection limits, which precludes their credible determination.

Members of Cu-Bi-S system

In the copper deposit bismuth forms its own minerals and isomorphic substitutions in tetrahedrite, Ni-Co-arsenides and in bornite, chalcocite and niccolite.

Chemical analyses were carried on Bi mineral from the pitchy variety of the Kupferschiefer, encountered in paragenesis with electrum. Its optical properties suggested wittichenite (Cu_3BiS_3). Chemical composition of this phase corresponds to the formula $Cu_{2.7188\text{-}2.7290}Bi_{0.9092\text{-}0.9165}S_{3.0000}$. As all other minerals accompanying the precious metals accumulations, wittichenite also contains high amounts of Au (2.24 wt.%) and Ag (5.5 wt.%), as well as Hg (0.70 wt.%) (Tab. 46). Assuming that Ag substitutes for Cu and Au compensates the deficiency of Bi, composition of this minerals should correspond to: $(Cu+Ag)_{2.9561\text{-}2.9859}(Bi+Au)_{0.9747\text{-}0.9610}S_{3.0000}$.

Wittichenite described earlier by Kijewski and Jarosz (1987) contained much higher amounts of Ag (up to 15 wt.%) but lower admixtures of Au (0.4–0.8 wt.%). Additionally, it contained also Hg (0.5–1.3 wt.%), Mo (up to 1.2

Table 43

WDS composition of the members of CuS-Cu_2S system from the boundary dolomite, mining section G-31, Polkowice West Field (after Pieczonka, 1998) (upper figure – wt.%; lower figure – atomic proportions)

Sample	As Kα	Bi Mα	Hg Lα	Au Lα	Cu Kα	Fe Kα	Pt Lα	S Kα	Pd Lα	Ag Lα	Total
A/1	0.13	≤0.05	0.24	0.35	78.76	≤0.03	0.10	19.02	≤0.05	0.24	98.84
	0.0029		0.0020	0.0030	2.0893		0.0008	1.0000		0.0034	
A/2	0.12	≤0.05	0.39	0.03	79.39	≤0.03	≤0.05	18.51	0.09	0.15	98.68
	0.0038		0.0033	0.0003	2.1644			1.0000	0.0014	0.0024	
A/3	0.17	≤0.05	0.37	0.37	76.58	≤0.03	≤0.05	20.52	≤0.05	0.24	98.25
	0.0036		0.0028	0.0030	1.8833			1.0000		0.0034	

Table 44

WDS composition of the members of CuS-Cu_2S and Cu-Ag-S systems from the clayey dolomite, sequences No. 95-S-5/5 and 95-S-5/6, Sieroszowice Mine (after Pieczonka, 1998) (upper figure – wt.%; lower figure – atomic proportions)

Sample	As Kα	Bi Mα	Hg Lα	Au Lα	Cu Kα	Fe Kα	Pt Lα	S Kα	Pd Lα	Ag Lα	Total
285/A1	0.10	≤0.05	0.36	≤0.04	76.01	0.03	0.04	20.60	0.10	0.82	98.06
	0.0020		0.0028		1.8619	0.0008	0.0003	1.0000	0.0014	0.0118	
285/A3	0.21	≤0.05	0.20	≤0.04	79.42	0.07	0.07	21.22	0.05	0.33	100.57
	0.0042		0.0015		1.8885	0.0020	0.0006	1.0000	0.0008	0.0047	
285/A4	0.11	≤0.05	0.33	0.04	79.05	0.04	≤0.04	21.03	≤0.04	0.28	100.88
	0.0023		0.0024	0.0003	2.1955	0.0011		1.0000		0.0040	
285/B7	0.30	≤0.05	0.29	0.06	78.27	≤0.03	0.11	21.40	≤0.04	0.40	100.83
	0.0060		0.0021	0.0004	1.8455		0.0009	1.0000		0.0055	
285/B8	0.13	0.12	0.38	≤0.04	76.96	≤0.03	0.05	20.82	≤0.04	0.21	98.67
	0.0026	0.0009	0.0029		1.8652		0.0005	1.0000		0.0029	
285/B9	0.19	0.28	0.31	≤0.04	77.79	≤0.03	0.16	21.41	≤0.04	0.28	100.42
	0.0037	0.0019	0.0022		1.8335		0.0012	1.0000		0.0039	
285/D7	0.22	≤0.05	≤0.10	≤0.04	42.84	≤0.03	≤0.05	15.08	0.13	39.78	98.05
	0.0062				1.4336			1.0000	0.0026	0.7842	
285/D8	0.18	≤0.05	0.55	0.18	50.54	≤0.03	≤0.05	17.11	≤0.05	33.14	101.70
	0.0045		0.0051	0.0017	1.4904			1.0000		0.5757	
285/D9	0.22	0.10	0.45	≤0.04	29.02	0.04	≤0.05	14.41	0.09	57.24	101.57
	0.0065	0.0011	0.0049		1.0162	0.0016		1.0000	0.0018	1.1807	
285/D10	0.16	0.20	0.38	0.11	38.48	0.03	≤0.05	15.52	≤0.05	46.17	101.05
	0.0043	0.0021	0.0039	0.0012	1.2510	0.0010		1.0000		0.8843	
285/D11	0.18	≤0.05	0.36	0.22	77.78	≤0.03	≤0.05	21.3 3	≤0.05	1.24	101.11
	0.0036		0.0027	0.0017	1.8400			1.0000		0.0173	
285/D12	0.16	≤0.05	0.25	≤0.05	77.31	≤0.03	≤0.05	20.66	≤0.05	3.47	101.85
	0.0033		0.0019		1.8883			1.0000		0.0500	

wt.%) and Te (up to 0.15 wt.%). Kucha and Piestrzyński (1991) also reported on Bi-sulphides containing increased amounts of Au. Their results indicated up to 7.35 wt.% Au and up to 11.47 wt.% Ag as well as high amounts of Hg (up to 9.68 wt.%), Fe (up to 13.07 wt.%) and As (up to 5.64 wt.%).

Hematite

Hematite is one of the main minerals encountered in the secondary oxidation zone of the copper deposit in the Fore-Sudetic Monocline. It forms intergrowths with native Au and Cu-sulphides observed in all lithological types of host-rocks. Hematite forms disseminated structures responsible for red coloration of the rocks but it also occurs as large (up to 1 mm) aggregates easily recognizable due to their significant hardness in comparison with sulphides and native Au. This hematite variety was described as hydrothermal (Pieczonka, 1998; Piestrzyński *et al.*, 2002).

Results of microprobe analyses of hematites intergrown with native Au confirmed the assumptions that this minerals accumulates high amounts of Au. Contents of Au in analyzed hematites vary from 0.23 to 2.65 wt.% (Tab. 47). Such high admixtures may suggest the presence of submicroscopic-size inclusions of native Au and, consequently, contemporaneous formation of both minerals. Hematites contain also increased amounts of Cu (up to 0.62 wt.%), Hg (up to 0.62 wt.%) and As (up to 0.28 wt.%). In a few samples Bi, Pt, Pd and Ag were detected, as well. Chemical composition reveals deficit of iron in relation to oxygen, presumably compensated at least partly by gold. Moreover, other elements: Al, Ti, Mn and Mg may participate in such compensation. These elements were not analyzed in this project but are known to form significant admixtures in hematite. Taking into account maximum and minium Fe contents, calculated formulae of studied hematites are: $Fe_{1.6509}O_{3.0000}$ – $Fe_{1.8465}O_{3.0000}$ (Piestrzyński & Pieczonka, 1997a, b; Pieczonka, 1998; Piestrzyński *et al.*, 2002).

Galena

Galena is a common mineral, although in the zones of secondary oxidation it occurs in trace amounts. This sulphide has been mentioned in almost all publication on ore mineralogy of the Cu deposit in the Fore-Sudetic Mono-

Table 45

WDS composition of native Ag from the clayey dolomite, profile S-5/5 and S-5/6, Sieroszowice Mine (after Pieczonka, 1998) (upper figure – wt.%; lower figure – atomic proportions)

Sample	As Kα	Bi Mα	Hg Lα	Au Lα	Cu Kα	Fe Kα	Pt Lα	S Kα	Pd Lα	Ag Lα	Total
285/A5	0.16	0.10	5.62	≤0.07	1.38	≤0.05	≤0.05	0.31	0.08	93.88	101.53
	0.0021	0.0005	0.0280		0.0217			0.0097	0.0008	0.8703	
285/A6	0.21	≤0.10	6.70	≤0.07	2.76	≤0.05	≤0.05	0.04	0.10	92.21	102.20
	0.0028		0.0334		0.0434			0.0012	0.0009	0.8548	
285/A7	0.11	≤0.10	0.81	≤0.07	6.05	≤0.05	≤0.05	0.51	0.05	92.13	99.66
	0.0015		0.0040		0.0952			0.0159	0.0005	0.8541	
285/A1	0.15	≤0.10	5.98	≤0.07	3.11	≤0.05	≤0.05	0.12	≤0.04	92.62	101.98
	0.0020		0.0298		0.0489			0.0037		0.8586	
285/A1	0.31	≤0.10	5.95	≤0.07	2.91	≤0.05	≤0.05	0.05	≤0.04	92.73	101.95
	0.0041		0.0297		0.0458			0.0016		0.8397	
285/A2	0.10	0.19	6.91	≤0.07	3.87	≤0.05	≤0.05	0.10	0.11	91.67	102.95
	0.0013	0.0009	0.0344		0.0609			0.0031	0.0010	0.8498	
285/A3	0.25	0.14	0.82	≤0.07	4.95	≤0.05	0.14	0.20	0.07	96.08	102.65
	0.0033	0.0007	0.0041		0.0779		0.0007	0.0062	0.0007	0.8907	
285/B4	0.20	0.19	0.80	≤0.07	0.20	≤0.05	≤0.05	≤0.04	≤0.05	99.30	100.69
	0.0027	0.0009	0.0040		0.0031					0.9206	
285/B5	0.06	≤0.10	0.61	≤0.07	0.12	≤0.05	0.06	≤0.04	≤0.04	99.26	100.11
	0.0008		0.0030		0.0019		0.0003			0.9202	
285/C1	0.11	≤0.10	0.66	0.06	4.31	≤0.05	0.10	0.62	0.12	92.56	98.54
	0.0015		0.0033	0.0003	0.0678		0.0005	0.0193	0.0011	0.8581	
285/C2	0.15	0.10	0.91	≤0.05	5.12	≤0.05	≤0.06	0.44	0.20	91.82	98.74
	0.0020	0.0005	0.0045		0.0806			0.0137	0.0019	0.8512	
285/C3	0.25	≤0.10	0.42	0.27	5.89	≤0.05	0.09	0.54	≤0.05	93.89	101.35
	0.0033		0.0021	0.0014	0.0927		0.0005	0.0168		0.8704	
285/C4	0.13	0.59	0.23	≤0.07	8.16	≤0.05	≤0.06	0.53	0.14	91.74	101.52
	0.0017	0.0028	0.0011		0.1284			0.0165	0.0013	0.8505	
285/C5	0.07	0.22	0.96	≤0.07	6.64	≤0.05	0.07	0.40	0.06	91.10	99.52
	0.0009	0.0011	0.0048		0.1045		0.0004	0.0125	0.0006	0.8445	
285/C6	0.23	0.37	1.10	0.16	5.10	≤0.05	≤0.05	0.42	0.16	93.09	100.63
	0.0031	0.0018	0.0055	0.0008	0.0803			0.0131	0.0015	0.8630	
285/D1	0.13	≤0.10	1.24	≤0.07	2.24	≤0.05	≤0.06	0.20	≤0.05	96.45	100.26
	0.0017		0.0062		0.0353			0.0062		0.8941	
285/D2	0.21	≤0.10	0.46	≤0.07	2.18	0.08	≤0.06	0.37	0.14	94.60	98.04
	0.0028		0.0023		0.0343	0.0014		0.0115	0.0013	0.8770	
285/D3	0.11	0.25	0.43	≤0.07	2.12	≤0.05	0.07	0.26	≤0.05	94.94	98.18
	0.0015	0.0012	0.0021		0.0334		0.0004	0.0081		0.8801	
285/D4	0.14	≤0.10	0.95	≤0.07	1.19	≤0.05	≤0.06	0.10	0.14	98.76	101.28
	0.0019		0.0047		0.0187			0.0031	0.0013	0.9156	
285/E1	1.68	0.41	0.41	≤0.07	1.07	0.05	≤0.06	0.11	0.12	98.53	102.38
	0.0224	0.0020	0.0020		0.0168	0.0009		0.0034	0.0011	0.9134	
285/E2	1.65	0.22	1.20	≤0.07	1.90	0.10	0.09	0.14	0.08	97.50	102.88
	0.0220	0.0011	0.0060		0.0299	0.0018	0.0005	0.0044	0.0008	0.9039	
285/E3	1.47	≤0.10	1.19	0.32	203	0.05	≤0.06	0.17	≤0.05	96.80	102.03
	0.0196		0.0059	0.0016	0.0319	0.0009		0.0053		0.8974	
285/E4	1.53	0.21	0.91	≤0.07	3.07	0.28	0.06	0.47	≤0.05	95.20	101.73
	0.0204	0.0010	0.0045		0.0483	0.0050	0.0003	0.0147		0.8826	

Table 46

WDS composition of the members of Cu-Bi-S system from the Kupferschiefer (pitchy variety), profile PG-1/3, Polkowice Main Field (after Pieczonka, 1998) (upper figure – wt.%; lower figure – atomic proportions)

Sample	As Kα	Bi Mα	Hg Lα	Au Lα	Cu Kα	Fe Kα	Pt Lα	S Kα	Pd Lα	Ag Lα	Total
291/A7	0.07	37.72	0.70	2.02	34.43	≤0.05	≤0.05	19.10	0.04	5.50	99.58
	0.0045	0.9092	0.0176	0.0519	2.7290			3.0000	0.0020	0.2569	
291/A8	0.13	37.53	0.56	2.24	33.86	≤0.05	≤0.05	18.85	≤0.03	5.02	98.19
	0.0087	0.9165	0.0143	0.0582	2.7188			3.0000		0.2373	

Table 47

WDS composition of hematites from the Kupferschiefer (red variety), mining section G-31, Polkowice West Field (after Piestrzyński and Pieczonka, 1997a) (upper figure – wt.%; lower figure – atomic proportions)

Sample	Fe Kα	As Kα	Bi Mα	Hg Lα	Au Lα	Cu Kα	Pt Lα	Pd Lα	Ag Lα	O Kα	Total
283-A/1	67.47	0.28	≤0.08	0.09	0.43	0.26	≤0.05	≤0.05	≤0.07	31.43	100.00
	1.8450	0.0057		0.0006	0.0034	0.0063				3.0000	
283-A/2	66.31	0.14	0.27	0.47	1.00	0.62	0.11	0.05	0.08	31.02	100.00
	1.8373	0.0029	0.0020	0.0036	0.0079	0.0152	0.0009	0.0008	0.0010	3.0000	
283-A/3	67.05	0.14	≤0.08	0.23	0.62	0.17	0.13	≤0.05	≤0.07	31.58	100.00
	1.8248	0.0029		0.0017	0.0047	0.0041	0.0010			3.0000	
283-A/4	66.45	0.23	0.14	0.46	1.13	0.27	≤0.05	≤0.05	≤0.07	31.29	100.00
	1.8253	0.0048	0.0011	0.0035	0.0087	0.0064				3.0000	
283-A/5	66.64	0.20	≤0.08	0.35	0.93	0.46	≤0.05	≤0.05	≤0.07	31.33	100.00
	1.8282	0.0041		0.0026	0.0072	0.0110				3.0000	
283-D/1	66.56	0.11	0.38	0.47	0.66	0.16	≤0.05	≤0.05	≤0.07	31.62	100.00
	1.8091	0.0023	0.0027	0.0035	0.0052	0.0038				3.0000	
283-D/2	64.56	0.21	0.14	0.25	0.86	0.19	0.05	0.13	≤0.07	33.61	100.00
	1.6509	0.0040	0.0010	0.0017	0.0063	0.0043	0.0004	0.0017		3.0000	
283-D/3	66.94	0.15	≤0.08	0.53	0.23	0.14	0.05	0.05	≤0.07	31.90	100.00
	1.8035	0.0030		0.0039	0.0018	0.0033	0.0005	0.0008		3.0000	
283-D/4	66.74	0.13	≤0.08	0.62	0.24	0.18	≤0.05	0.05	≤0.07	31.99	100.00
	1.7932	0.0026		0.0047	0.0018	0.0042		0.0008		3.0000	
283-D/5	66.84	0.13	≤0.08	0.28	1.07	0.27	0.12	≤0.05	≤0.07	31.11	100.00
	1.8465	0.0039		0.0022	0.0083	0.0065	0.0009			3.0000	
283-D/6	64.05	0.16	≤0.08	0.31	2.65	0.19	0.11	0.14	0.75	31.65	100.00
	1.7393	0.0032		0.0023	0.0205	0.0045	0.0009	0.0020	0.0106	3.0000	

cline. It forms polycrystalline intergrowths with other members of hydrothermal association – sulphides, selenides, arsenides, tellurides and precious metals. Chemical composition of galenas from the secondary oxidation zone apparently shifts from the stoichiometric one. Analyzed xenomorphic crystals reveal increased admixtures of Se (up to even 6.97 wt.%) (Tab. 48). Substitutions of Se for S are normal feature in hydrothermal systems (Schröcke & Weiner, 1981). These authors reported on the possible substitutions of PbSe for PbS and even of PbTe for PbS.

Table 48

EDS composition of galena from the Kupferschiefer (red variety) (upper figure – wt.%; lower figure – atomic proportions)

Sample	Pb Lα	Se Kα	S Kα	Total/atomic proportions
PZ-J7-9a/10	83.93	3.09	12.98	100.00
	0.9912	0.0095	0.9905	$Pb_{0.9912}S_{0.9905}Se_{0.0095}$
PZ-J7-17/1	85.61	2.84	11.55	100.00
	1.0432	0.0906	0.9094	$Pb_{1.0432}S_{0.9094}Se_{0.0906}$
PZ-J7-17/4	83.02	6.97	10.01	100.00
	1.0002	0.2205	0.7795	$Pb_{1.0002}S_{0.7795}Se_{0.2205}$
PZ-J7-17/5	86.52	1.52	11.96	100.00
	1.0645	0.0492	0.9508	$Pb_{1.0645}S_{0.9508}Se_{0.0492}$
PZ-J7-17/6	85.70	1.09	13.21	100.00
	0.9713	0.0324	0.9676	$Pb_{0.9713}S_{0.9676}Se_{0.0324}$
PZ-J7-18/1	84.35	2.50	13.15	100.00
	0.9215	0.0718	0.9282	$Pb_{0.9215}S_{0.9282}Se_{0.0718}$
PZ-J7-18/2	86.25	1.24	12.51	100.00
	1.0259	0.0157	0.9613	$Pb_{1.0259}S_{0.9613}Se_{0.0157}$

DISTRIBUTION OF PRECIOUS METALS

Jadwiga Pieczonka, Adam Piestrzyński, Jacek Mucha & Adam Głuszek

DISTRIBUTION OF Au, Pt AND Pd IN COPPER DEPOSIT OF THE FORE-SUDETIC MONOCLINE

The first notices on the presence of Au in the copper deposit of the Fore-Sudetic Monocline were published by Wojciechowska and Serkies (1967), and Harańczyk (1972). In the following years several other publications have appeared: Kucha (1973, 1974, 1976a, b, 1982a, b), Salamon (1976, 1979), Kucha and Pocheć (1983), Banaś and Kijewski (1987), and Czajowski (1987).

According to Wojciechowska and Serkies (1967), and Harańczyk (1972), Au contents in the Kupferschiefer are below 1 ppm and 0.01–0.3 ppm, respectively. However, Kucha (1982b) reported on much higher, maximum contents of precious metals: 3,000 ppm for Au, 340 ppm for Pt and 1,000 ppm for Pd. Such extreme values were attributed by this author to the so-called "Noble-metal Kupferschiefer" variety, only 1 cm thick and located beneath the Kupferschiefer enriched in thucholite. Much lower contents of precious metals were found in another Kupferschiefer varieties: that with thucholite and that with phosphates (Kucha 1982b). These Kupferschiefer varities were observed only in the Lubin West Field. Increased amounts of Au (up to 2.47 ppm), Pt and Pd were reported by Sawłowicz (1993, 1994) from samples collected from the Polkowice West Field. Moreover, Kucha *et al.* (1982) found significant Au contents in the copper deposit of the North-Sudetic Trough. In 1993 native Au was identified in specimens collected from the Kupferschiefer and underlying sandstone in the Polkowice West Field (Report AGH, 1996, 1997; Piestrzyński *et al.*, 1996a, 2002; Piestrzyński & Pieczonka, 1997a, b; Pieczonka 1998, 2000; Piestrzyński & Wodzicki, 2000; Pieczonka & Piestrzyński, 2000).

As revealed by published data, in the Fore-Sudetic copper deposit Au occurs as:

– own minerals: native Au (Kucha, 1974, 1982b; Piestrzyński *et al.*, 1996a; Piestrzyński & Pieczonka 1997a, b); electrum (Kucha, 1976a, b; Salamon 1976; Piestrzyński, 1996a, b; Piestrzyński & Pieczonka, 1997a) and tetraauricuprite (Piestrzyński & Pieczonka, 1998),

– isomorphic substitutions in native Ag (up to about 1 wt.%) (Kucha, 1976a; Salamon, 1976),

– organometallic compounds (Kucha, 1973, 1976a, 1982b),

– isomorphic substitutions in some Cu sulphides, Ag sulphides and Pd arsenides (Kucha 1976b; Kucha & Pocheć, 1983; Salamon, 1979; Kucha & Piestrzyński, 1991; Pieczonka 1998; Piestrzyński *et al.*, 2002).

Percentages of particular Au minerals and compounds in the total amount of Au phases are difficult to determine. It is suggested that Au which forms substitutions in native Ag is of main economic value as this Ag mineral is common in the Cu deposit.

Distribution of Au, Pt and Pd in vertical sequence of ore deposit

Results of chemical analyses of rocks collected from channel samples at the Polkowice-Sieroszowice Mine (Fig. 1) revealed the following regularities in distribution of precious metals.

1. Maximum Au contents are located at various depths beneath the top of the sandstone (from 0 to 100 cm) whereas maximum Pt and Pd contents either follow Au peaks or are somewhat shifted [e.g. profiles No. 95-PZ-40 (Fig. 8), 95-PZ-3, Pr14-1679, Pr09-1368, Po16-1925, Sr24-6895 (Pieczonka, 1998), Sz08-1054 (Fig. 7), Sr18-7002 (Fig. 16), Pr18-0367, N/III (Fig. 18) and N/IV (Fig. 19)].

In these profiles maximum Au contents were observed beneath the red-colored sandstone. Highest values were detected in the sandstone from No. PZ-40 sequence (29.27 ppm) but high Au contents were found also in overlying Kupferschiefer. In the pitchy variety of the Kupferschiefer Au values decreased to below 1 ppm. Maximum Pt (0.78 ppm) and Pd (0.37 ppm) contents were found in the red Kupferschiefer (Pieczonka, 1998; Pieczonka & Piestrzyński, 2000). High Au contents were noticed also in the top sandstone layer, in profiles No. N/III (26.78 ppm) and No. N/IV (11.60 ppm). In the overlying dolomite Au contents abruptly decreased but high contents pf Pt (0.95 ppm) and Pd (0.3 ppm) appeared. In profile No. Sz08-1054 increased amounts of Au were also detected in the dolomite (0.52 ppm) over the top of the sandstone (4.48 ppm).

2. Two peaks of Au contents were identified. The four patterns were distinguished:

a. Both peaks occur in the sandstone: the first was located at depths from 0 to 40 cm and the second – at depths from 40 to 80 cm beneath the top of the sandstone. Contents

of PGE were variable. Representative profiles are Nos.: Sz12-0238, Sz09-0727, Sr14-0672, Pr25-0923 (Pieczonka & Piestrzyński, 2000), Sz02-3056 (Fig. 4), Sz02-0438, Sz07-0027 (Fig. 6), Ra14-0274, Ra14-0505 and N/V (Fig. 20). In the two profiles: No. Sz08-0936 and No. Sz08-0991 both peaks appeared at greater depths – first about 60 cm and second about 1 m beneath the top of the sandstone.

High Au contents (generally above 1 ppm) were observed in both the red-colored and the grey sandstone. In the profile No. Sz07-0027 Au contents of 1.1 ppm occurred twice whereas maximum combined Pt+Pd content in the sandstone was about 0.25 ppm. Maximum contents of precious metals were detected in No. Sz02-3056 profile, where peak Au contents coexist with peak Pt+Pd values and are: 0.58, 0.53 and 0.26 ppm, respectively for the lower maximum and 3.33, 0.52 and 0.21 ppm, respectively for the upper maximum. Increased contents of Pt (0.1–0.25 ppm) and Pd (0.08–0.15 ppm) were noticed in the sandstone from No. Ra14-0274 and Sz08-0991 profiles but these values did not correlate with maximum Au contents.

b. The first peak, which marks high Au contents occurs in the top part of the sandstone, rarely deeper, the second peak is located in the Kupferschiefer [e.g. profiles No. 95-PZ-19 (Fig. 11), 95-PZ-16 (Pieczonka, 1998; Pieczonka & Piestrzyński, 2000), Sz07-0054, Sz07-429, Pr18-0331, Sr19-0802, Ra19-0011].

Such pattern was observed in both the red-colored rocks and in rocks devoid of red stainings. However, in the red-colored rocks contents of precious metals were higher. For instance, in No. 95-PZ-19 profile maximum Au content in the sandstone reached 6.99 ppm and in the pitchy variety of the Kupferschiefer it was 4.14 ppm. Contents over 1 ppm were found in the clayey variety of the Kupferschiefer.

Maximum contents of Pt and Pd (1.15 ppm combined metals) were observed in both the pitchy and clayey varieties of the Kupferschiefer. It must be emphasized, however, that in the previous projects only the Kupferschiefer and the carbonates were analyzed for noble metals, whereas the sandstone could not be effectively sampled because it provides a suitable bottom of mine workings. Thus, it is suggested that in the profiles enriched in precious metals red spots might have occurred also in the lower, unaccessible parts of the sandstone (Pieczonka, 1998; Pieczonka & Piestrzyński, 2000). In the newly collected channel samples highest Au contents (1.6 ppm) were detected in No. Pr18-0331 profile, in the clayey variety of the Kupferschiefer whereas in the remaining samples Au contents were below 0.2 ppm. In these samples highest contents of Pt and Pd followed those of Au but the highest combined Pt+Pd value – 0.12 ppm – was detected in the Boundary Dolomite and in the Kupferschiefer from profile No. Sz07-0429.

c. Both Au peaks occur in the Kupferschiefer [e.g. profiles No. 95-PG-1, PZ-24 (Pieczonka, 1998)].

This pattern includes profiles in which peak contents in the bottom part of the Kupferschiefer were accompanied by another peak values located in the middle or upper parts of the Kupferschiefer bed. In No. 95-PG-1 profile maximum Au content (71.29 ppm) was found in a thin layer of pitchy variety overlying the red variety. Moreover, the pitchy Kupferschiefer contained also Pt (0.80 ppm) and Pd (2.95 ppm). In the overlying, dolomitic Kupferschiefer PGE contents dropped down below detection limit and those of Au varied from 0.032 ppm in the bottom to 0.76 ppm in the top of this bed. In an another profile (No. PZ-24) maximum Au (6.91 ppm) and Pt (0.4 ppm) and Pd (0.4 ppm) contents were observed in the red Kupferschiefer variety.

d. Au peak occurs in the Kupferschiefer whereas second, much lower peak is observed in the carbonates [e.g., profiles No. 95-PZ-11, 95-PZ-13, Sz-6/1, Sz-6/2, (Pieczonka, 1998, 2000)].

This pattern was found in sequences from the Polkowice West and the Polkowice Main fields. Maximum Au content (3.32 ppm) occurred in the clayey Kupferschiefer from the profile No. 95-PZ-11. Combined Pt+Pd content in this variety was 0.64 ppm. Similar Pt+Pd contents (about 0.65 ppm) were detected in adjacent analyzed profiles, in the clayey Kupferschiefer variety. In the carbonates overlying the Kupferschiefer another enrichment in Au was observed, particularly in No. 95-PZ-13 profile (0.39 ppm). In some profiles from this group carbonates revealed also increased contents of Pt and Pd (about 0.01 ppm). No red spots were observed in the analyzed rocks from these profiles.

3. Maximum Au contents occur usually in the top part of the sandstone whereas maximum contents of Pt or Pd are shifted up the sequence, to the Kupferschiefer [e.g, profiles No. 95-PG-7, 95-PW-2, 95-PZ-15, 95-PG-2, Sz-07-0127, Po16-1924, Pr10-2267 (Pieczonka, 1998)].

Profiles representing this pattern were found in the southern parts of the Polkowice East, Main and West Fields. Maximum Au contents were detected in the top part of the sandstone with red spots. Highest Au value (16.46 ppm) was found in the sandstone from No. 95-PG-7 profile. Up the Kupferschiefer sequence Au contents decreased down to the lowest values, as observed in the clayey Kupferschiefer variety from No. 95-PW-2 profile. Where the Kupferschiefer thickness was low, increased Au contents (0.017 ppm) occurred in the bottom part of carbonates (e.g., No. 95-PZ-15 profile).

Maximum Pt and Pd values were reported from various rocks immediately overlying the sandstone: pitchy and clayey varieties of the Kupferschiefer and/or boundary dolomite but Au content in these rocks decreased. Highest contents of Pt (0.58 ppm) and Pd (0.50 ppm) occured in the boundary dolomite from No. 95-PW-2 profile. In carbonate rocks Pt and Pd were present in trace amounts (Pieczonka, 1998; Pieczonka & Piestrzyński, 2000).

4. Maximum Au, Pt and Pd contents overlap. The presence of a single peak for all three precious metals is a most common pattern. It occurs in the bottom part of the Kupferschiefer, rarely in the top part of the sandstone [e.g. profiles No. 95-PW-1, 95-PZ-12, 95-PZ-18 (Fig. 12), 95-PZ-17, 95-PZ-2, 95-PZ-10, 95-PG-9, 95-S-7, 95-PG-4, Sz-1/3, Sr23-0518, Pr4-2527, Sz06-1086, Sr23-0517, Sz06-0407, Pr08-0166, Pr04-2532, Pr04-2528 [(Pieczonka, 1998), Sr18-0061"s", Sr19-2428 (Fig. 17)]. Only in a single profile (Pr04-2527) maximum Pt content was 2 ppm, i.e., more than maximum Au grade and Pt+Pd value was 3 ppm. However, Pt contents about 1 ppm were found in the Kupferschiefer from several profiles.

Depending on lithology of the Kupferschiefer, peak contents of precious metals may occur in various varieties. Usually, beneath the Kupferschiefer the sandstone with red spots was found, locally separated from the shale by a thin layer of the boundary dolomite. Only in 5 profiles red spots were absent in the sandstone, as e.g. in No. Sr19-2428 profile where Au (4.42 ppm), Pt (0.33 ppm) and Pd (0.11 ppm) were detected in the top of this layer.

Maximum contents of Au, Pt and Pd in the Boundary Dolomite were noticed in its thin layer sampled in profiles No. 95-PW-1, 95-PZ-12 and Sr18-0061"s". In No. 95-PW-12 profile Au content was 7.17 ppm and combined Pt+Pd content was about 1 ppm. In No. Sr18-0061"s" profile these values were 2.36 and 0.06 ppm, respectively. Increased amounts of Au were noticed as high in the sequence as in the clayey dolomite. Moreover, Au and PGE were detected also in the red-colored sandstone.

In the second population of profiles, the sandstone (commonly devoid of red spots) is overlain by a thin layer of red, usually dolomitic variety of the Kupferschiefer. This layer hosts the precious metals. Highest Au, Pt and Pd contents were found in No. 95-PZ-18: 14.16, 1.05 and 0.70, respectively. Somewhat lower values were detected in No. 95-PZ-17 profile, whereas in No. 95-PZ-2 one maximum Au content was lower (7.02 ppm) but those of Pt and Pd were higher (1.24 and 0.54 ppm, respectively).

In the profiles where clayey variety of the Kupferschiefer immediately overlies the sandstone precious metals accumulated in the bottom of this variety and their contents decreased up the sequence (as in No. 95-PZ-10) or the PGE concentrated at the bottom of the Kupferschiefer (95-PG-9).

The last population includes profiles, in which maximum contents of precious metals occur in the pitchy variety of the Kupferschiefer, which covers the red-spotted sandstone. Despite the lithology of overlying beds, clayey Kupferschiefer, (No. 95-S-7, 95-PG-4, 95-PG-5 profiles) or carbonates (No. Sz1/3 profile), contents of precious metals distinctly decreased up the sequence (sometimes abruptly, as in No. 95-PG-5 one). Highest contents of Au (11.29 ppm), Pt (1.50 ppm) and Pd (0.61 ppm) were observed in the pitchy variety of the Kupferschiefer 95-PG-4 profile (Pieczonka, 1998; Pieczonka & Piestrzyński, 2000).

a. Among the profiles of the fourth group a population can be distinguished, in which maximum concentrations of precious metals are located in the bottom part of the Kupferschiefer but their peak values do no overlap [No. 95-PZ, 95-PZ-22, PZ-42, 95-PG-3, 95-PZ-23 (Pieczonka, 1998)].

Despite the presence of red Kupferschiefer in most of profiles from this group, only in a few examples peak values of Au and PGE were detected in this variety. In No. 95-PZ-1 profile maximum Au content was 10.93 ppm and that of Pd was 0.34 ppm whereas maximum Pt content (0.93 ppm) was found in the overlying clayey Kupferschiefer. Similar pattern was noticed in No. 95-PZ-22 profile where maximum Au and Pd values (13.31 and 0.72 ppm, respectively) were noticed in the red Kupferschiefer and Pt (0.85 ppm) occurred in the clayey Kupferschiefer. The highest Au content (14.03 ppm) in the dolomitic variety of the Kupferschiefer was detected in No. PZ-42 profile but PGE were concentrated in the underlying, red Kupferschiefer variety (Pt – 1.42 ppm and Pd – 1.50 ppm). It is interesting to note that Pd contents dropped down beneath detection limit in the top part of the Kupferschiefer but those of Au and Pt decreased gradually and were still noticeable in the carbonates.

In No. 95-PG-3 and 95-PZ-23 profiles maximum Au values (5.34 and 2.67 ppm, respectively) occurred in the clayey variety of the Kupferschiefer overlying the red variety. Au contents decreased gradually up the Kupferschiefer sequence (as in No. 95-PG-3 profile) or were still high (over 1 ppm) in the bottom parts of the carbonates. Maximum PGE contents (2.53 ppm) were observed in the red variety which constitutes the bottom of the Kupferschiefer bed or above, in the dolomitic variety (over 1 ppm). In No. 95-PG-3 profile high PGE values were found only in the Kupferschiefer and in No. 95-PZ-23 profile both high Au and PGE values were noticed in the carbonates.

5. There are three or more peak Au contents. At the present stage of studies analysis of this pattern is rather difficult. Several, single examples of Au occurrence in various parts of the ore sequence were disclosed [e.g. in No. 95-PZ-21, PZ-41 and Pr18-0262 sequences (Pieczonka, 1998; Pieczonka & Piestrzyński, 2000), Sz02-2700, Sz03- 1026 (Fig. 5)].

In No. 95-PZ-21 profile the highest Au content (101.0 ppm) was detected in a thin layer of red Kupferschiefer whereas in the overlying clayey Kupferschiefer Au contents first decreased down to 0.63 ppm, then increased in the top of this variety and again decreased distinctly in the dolomitic Kupferschiefer which is the uppermost variety of this bed. The third Au peak (over 1 ppm) was found in the bottom of the carbonates. Simultaneously, peak Pt (1.12 ppm) and Pd (1.62 ppm) values occurred in the red Kupferschiefer, as are the Au values, and apparently decreased up the Kupferschiefer sequence.

Other pattern was noticed in No. PZ-41 profile. The first Au peak (8.13 ppm) occurred in the sandstone, the maximum content (55.99 ppm) was found in the red Kupferschiefer, and the third peak (5.87 ppm) was detected in the overlying pitchy variety of the Kupferschiefer. Au content over 1 ppm was still present in the clayey Kupferschiefer, which forms the top of this bed in that sequence. Significant amounts of Pt (0.84 ppm) and Pd (0.33 ppm) appeared as high in the sequence as in the dolomitic Kupferschiefer, being sandwiched between the red and the pitchy Kupferschiefer varieties but increased amounts of Pt were observed in all other varieties of the Kupferschiefer and those of Pd also in the red-spotted sandstone.

In No. Pr18-0262 profile very high Au content (230 ppm) was disclosed in the red-spotted sandstone, at depth interval 80–100 cm beneath the top of this layer. Unfortunately, this sample was the lowermost in this sequence and the determination of lower contour of such high Au accumulation was impossible. Microscopic observations did not confirm the presence of native Au in this sample but found this mineral in the interval 60–80 cm beneath the top of the sandstone. The second peak of Au contents (4.65 ppm) occurred in the top part of the sandstone and the third one (1.25 ppm) was localized in the top part of the clayey Kupferschiefer. Peaks of Pt and Pd contents (0.03 and 0.30 ppm, respectively) followed that of Au (Pieczonka, 1998). Simi-

lar patter was found in No. Sz02-2700 profile where high values of Au, Pt and Pd occurred at depths 70 cm (2.74, 0.32 and 0.17 ppm, respectively) and 20 cm (1.82, 0.15, 0.08 ppm, respectively) beneath the top of the sandstone as well as in the Kupferschiefer (2.70, 0.12 and 0.05 ppm, respectively).

In No. Sz03-1026 profile all three peaks of Au contents occur in the sandstone: the first (14.88 ppm) at a depth of 1.6 m, the second (0.45 ppm) at 1.1 m and the third (0.17 ppm) at 0.5 m beneath the top of this layer. Small amounts of Pt and Pd coexist with those of Au.

6. Maximum Au contents occur in the carbonates and those of PGE – in the Kupferschiefer [as e.g. in profiles No. PZ-43 (Fig. 9), 95-PZ-14 (Pieczonka 1998; Pieczonka & Piestrzyński, 2000), Sz/III (Fig. 14)] or in the carbonates [No. Sz/IV (Fig. 15) and Pr13-7001 profiles (Fig. 13)].

All the rocks forming No. PZ-43 profile were red-colored. Increased amounts of Au and PGE appeared first in the sandstone but maximum content (1.50 ppm) was localized in the bottom part of the carbonates. Next maximum (0.37 ppm) occurred in the middle part of the streaky dolomite. Highest PGE contents were observed in a thin layer of red Kupferschiefer (the only variety present in this profile). It is suggested that such low thickness of the Kupferschiefer might have caused increased contents of PGE in the overlying carbonates. Pd was accumulated only at the bottom of carbonate sequence whereas Pt occurred also higher in that sequence. Increased amounts of PGE corresponded to decrease in Au contents.

In the second representative profile of this group, maximum Au content (5.37 ppm) was found in the bottom part of the clayey dolomite and some increase was noticed also in the bottom part of the streaky dolomite. Maximum Pt contents (0.98 ppm) were detected in the dolomitic Kupferschiefer and those of Pd (0.66 ppm) – in the red Kupferschiefer.

In profiles Nos. Sz/III, Sz/IV and Pr13-7001 maximum Au contents (11.14, 5.41 and 12.17 ppm, respectively) occurred at the bottom of the Streaky Dolomite with red spots. In No. Sz/IV profile maximum Pt and Pd values were low and corresponded to Au peak. In the remaining profiles PGE occurred immediately beneath the bottom surface of the streaky dolomite, i.e. in the clayey Kupferschiefer variety (No. Sz/III, 1.45 and 1.26 ppm, respectively) or in the clayey dolomite (No. Pr13-7001, 1.05 and 0.83, respectively).

7. This group includes profiles in which no distinct Au, Pt and Pd accumulations were observed. Contents of three elements only sporadically exceed their detection limits [e.g. No. 95-S-3, 95-S-5, 95-PW-3, 95-PW-4 [(Pieczonka, 1998), Po23-2384, Po23-2399, Sz03-2028, Sz03-2051, Sr18-1628, Sr19-1186, Sr20-0822]. In all these profiles maximum Au contents in all the lithologies were at the level of several ppb. The exception is No. 95-S-5 profile where 0.07 ppm Au was detected. No red coloration was observed and all profiles originate from the area in which the Cu deposit shows typical characterization.

Analysis of available data allows us to conclude that the highest Au contents occur in the top part of the sandstone and at the bottom of the Kupferschiefer. Moreover, results of chemical analyses indicate that, possibly, high Au contents exist at greater depths. Boreholes drilled down to 1 m depth beneath the top of the sandstone could not reach the bottom of Au-bearing zone.

Taking into account all analyzed precious metals (Au, Pt and Pd), most common feature is the high Au accumulation in the bottom part of the Kupferschiefer. The Kupferschiefer bed comprises several lithological varieties and an attempt was made to correlate vertical distribution of precious metals with the Kupferschiefer lithology. The results show that contents of precious metals are controlled not by the Kupferschiefer lithology but rather by physical properties: porosity, permeability and position in the sequence. It is valid also for red-colored Kupferschiefer. Precious metals accumulate in the bottom part of the Kupferschiefer bed overlying the sandstone with red spots. If boundary dolomite is present between the Kupferschiefer and the sandstone, the precious metals accumulate in this layer.

Accumulations of precious metals in the carbonates are rare and unimportant in evaluation of their economic value (Pieczonka, 1998; Pieczonka & Piestrzyński, 2000).

Horizontal distribution of Au, Pt and Pd

Gold

Map of Au distribution in the Polkowice-Sieroszowice area was based upon cut-off value 0.5 ppm determined for the assessment of the horizon rich in precious metals and accepted in the mine sampling instruction (Piestrzyński *et al.*, 1996a, c). For map construction analyses of all samples collected for the purposes of research projects run at the AGH-University of Science and Technology in the years 1996 and 1997 were included together with routine samples collected by the geologists from the Polkowice Mine and samples from boreholes investigated by the Polish Geological Institute in 1996. It must be emphasized that exploration of Au deposit is not uniform – the best recognized are the areas of the Polkowice East and Main Fields, hence, interpretation of data from these areas is most credible.

In the prevailing part of the Polkowice-Sieroszowice deposit thickness of Au-bearing horizon contoured by 0.5 ppm cut-off value reaches maximum 0.2 m (Fig. 78). Thicknesses from 0.2 to 0.3 m are rarely observed as irregular zones of various size clustered in the central part of the Polkowice East Field. Westward, towards the Polkowice Main Field, their number distinctly decreases and again increases in the Polkowice West Field. The largest zone is located in the southwestern part of the Polkowice West Field where it covers about 12 km^2. This zone expands as narrow branches into the area of the Sieroszowice Mine. In both the southwestern and southern parts of the Sieroszowice Mine several small, isolated zones were identified, which comprise small parts of Au horizon of thickness 0.3–0.5 m. Thickness above 0.5 m are sporadical. Top thickness – over 0.9 m – were found in a few, small zones, located mostly in the Polkowice East and West Fields, close to the border with the Sieroszowice Mine. Largest such bodies (about 0.5 km^2) were encountered in the latter field.

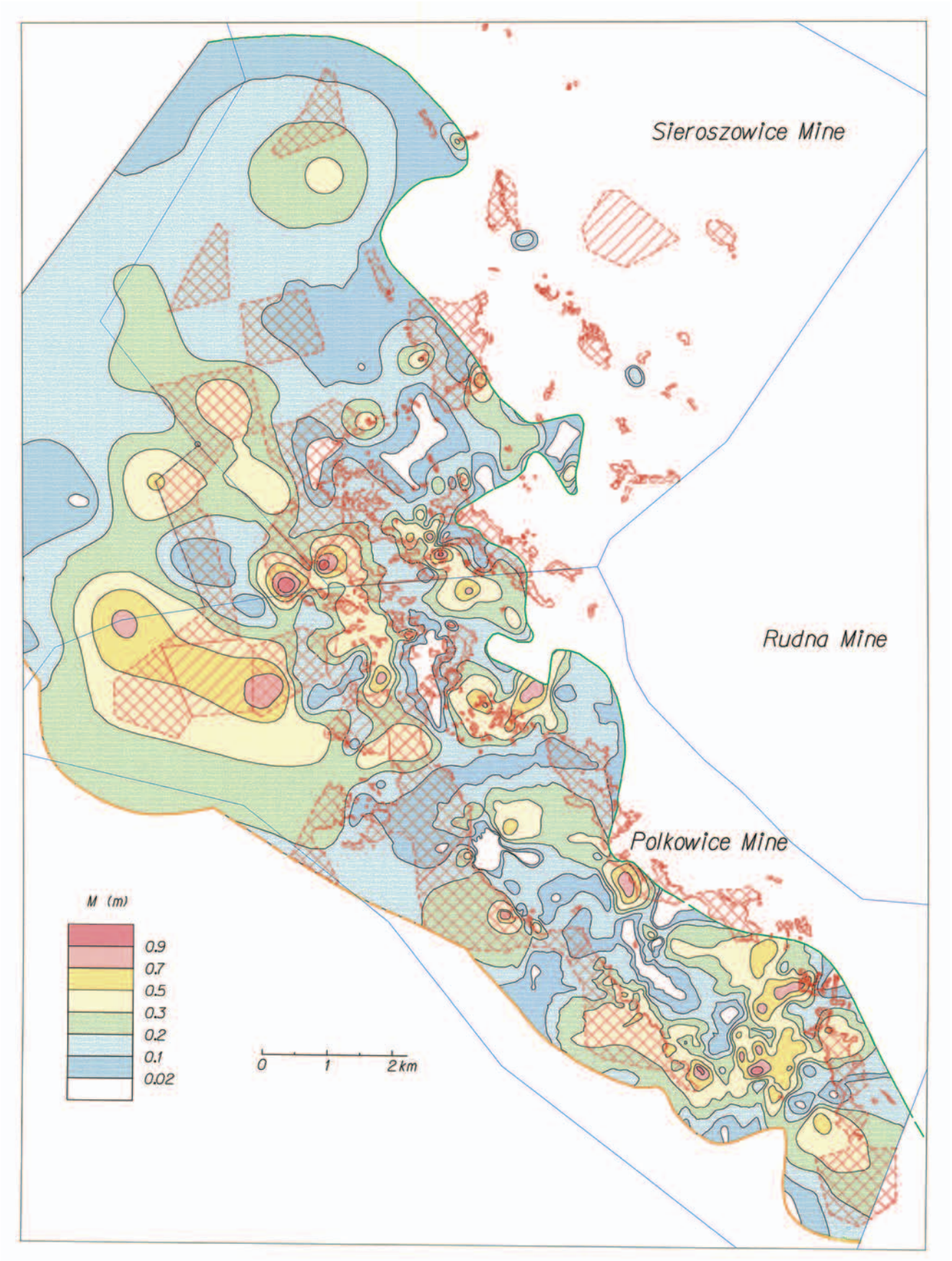

Fig. 78. Contour map of thickness of gold horizon for cat of grade 0.5 ppm, red hatched polygons represent areas without copper mineralisation, polygons with solid line represent areas with sub-economic copper ores, Polkowice – Sieroszowice Mine

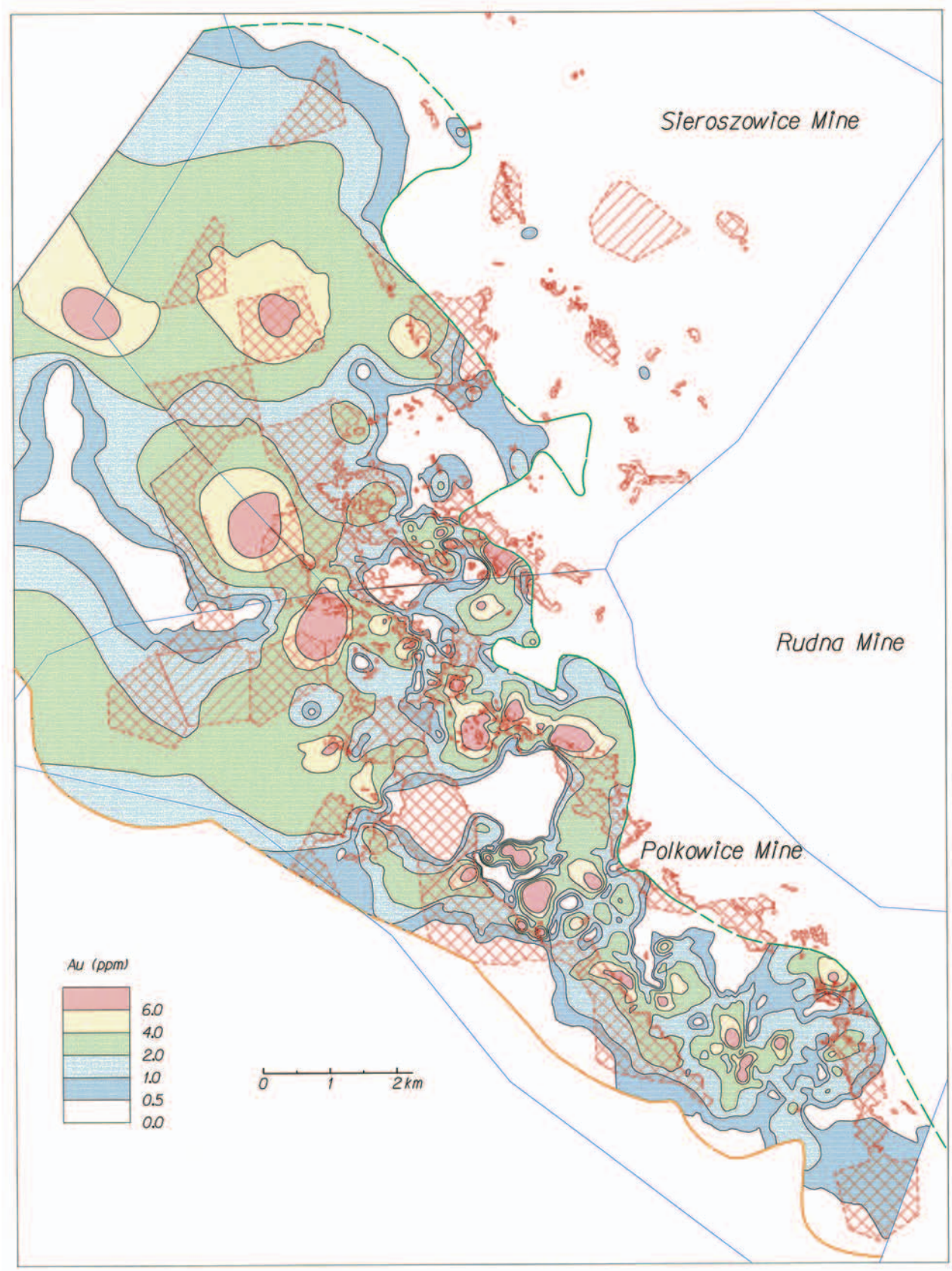

Fig. 79. Contour map of gold concentration for cat of grade 0.5 ppm, red hatched polygons represent areas without copper mineralisation, polygons with solid line represent areas with sub-economic copper ores, Polkowice-Sieroszowice Mine

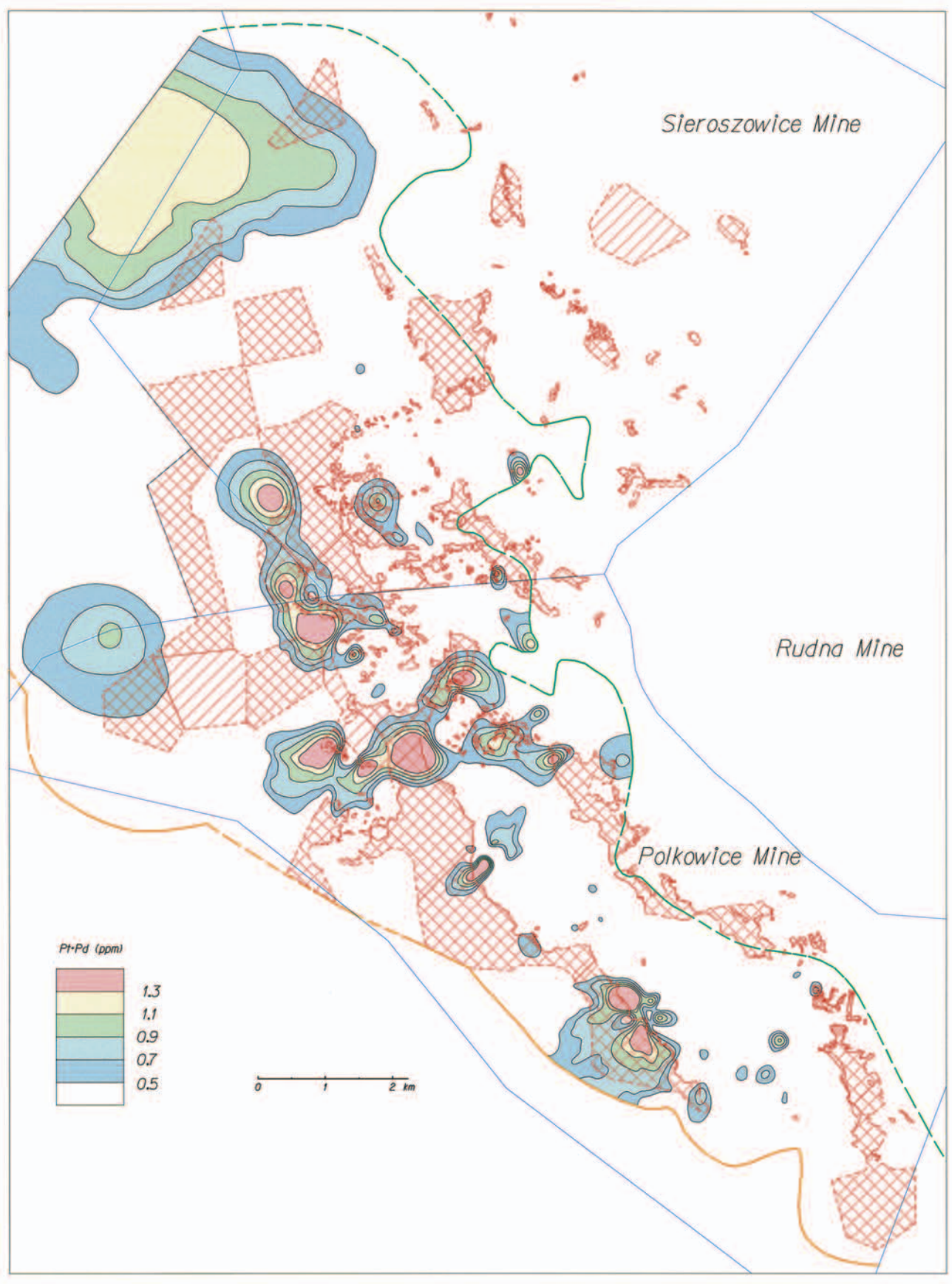

Fig. 80. Contour map of Pt + Pd concentrations for gold interval with cat of grade 0.5 ppm, red hatched polygons represent areas without copper mineralisation, polygons with solid line represent areas with sub-economic copper ores, Polkowice-Sieroszowice Mine

At the Polkowice-Sieroszowice Mine zones of highest Au contents (Fig. 79) do not correlate with the zones of maximum thickness of Au-bearing horizon. Generally, high-Au zones show thickness below 0.2 m. In the Polkowice West Field several, high-Au zones reveal thickness over 0.3 m, sporadically even 0.5 m. The richest Au zones (over 6 ppm) occur at the border between the Polkowice West Field, the Radwanice Prospect and the Sieroszowice Mine reveal thickness from 0.1 to 0.3 m.

The zone of Au grades from 0.5 to 2 ppm forms a northwest-southeast-trending belt, which continues through the central parts of the Polkowice East and Main fields, then expands to the west and covers most part of the Polkowice West Field, and continues through the Radwanice Prospect towards the southwestern and western parts of the Sieroszowice Mine. In the latter area its contours are still poorly recognized and defined mostly by borehole data. The whole belt covers about 80 km^2.

The zone of higher Au grades (2–4 ppm) also shows some continuity. It covers largest area (about 12 km^2) in the southwestern part of the Polkowice West Field and in the Sieroszowice Mine, and a few smaller areas. Such Au contents are of industrial value.

The higher Au grades, from 4 to 6 ppm (i.e. the economic-grade Au deposit), occur as isolated zones arranged in northwest-southeast direction. Within such zones the smaller areas of various size appear where Au grades exceed 6 ppm. The largest such zones (up to 0.8 km^2) were found at the boundary between the Radwanice Prospect and the Sieroszowice Mine, smaller zones occur also at the Polkowice Mine. The zones of highest Au grade are usually surrounded by Cu-barren zones, which have never been sufficiently explored for the presence of precious metals.

At the Polkowice Mine Au-free zones were identified within the Au-bearing belt. These zones are related to the appearance of isolated areas of economic-grade Cu mineralisation. At the Sieroszowice Mine a distinct trend is observed of decreasing Au contents towards the northeast. Outside the Au-bearing belt, in the center of the Mine only three zones of Au grades up to 2 ppm occur. Further northeastward the area is poorly explored.

Platinum and palladium

The zones with Pt and Pd accumulations are rare (Fig. 80). These are irregular zones of variable size scattered within the range of Au-bearing belt. In the Polkowice East Field only small, single zones were encountered of Pt and Pd grades below 0.9 ppm (only one zone shows values over 1.1 ppm). In the Polkowice Main Field there exist several small zones and a single large one located in the southern part of this field in which combined Pt+Pd grade varies from 0.5 to over 1.3 ppm. Zones of similar grade but more variable in shape and size were identified in the central part of the Polkowice West Field and its border with the Radwanice Prospect and the Sieroszowice Mine. Large zone of Pt+Pd grades from 0.5 to 1.1 ppm occurs at the border with the Radwanice Prospect. In the southern part of the Sieroszowice Mine only four small, isolated, high-grade Pt+Pd zones were disclosed. Moreover, in the northwestern part of this mine there is a single, large zone (some 10 km^2) of Pt+Pd grades from 0.5 to 1.3 ppm. It must be noticed that this zone as well as other zones at the border with the Polkowice West Field and the Radwanice Prospect area were interpreted only from borehole data. Their true size can be much smaller and, at present, these zones have only a prognostic importance.

Relationships between precious-metals horizon and Cu deposit

Distribution of Au, Pt and Pd in relation to Cu

Analysis of Au, Pt and Pd distribution in studied profiles reveals some regularities in distribution of their accumulations in relation to Cu deposit.

Despite the sequences in which Au peak values occurs in the top part of the sandstone or in the carbonates, distinct increase in Au grade is observed at the sandstone-Kupferschiefer interface. As Cu grade in the sandstone is low, distinct rise of Cu contents at the bottom of the Kupferschiefer can be observed, as well. Hence, comparison of vertical distribution patterns of metals in the lower part of the Kupferschiefer bed suggests similarities (e.g. No. Pr18-0331, Sr19-0802, Ra14-0274, Sz07-0429 profiles). However, despite a few special cases, contents of Au, Pt and Pd decrease up the Kupferschiefer sequence whereas Cu contents clearly increase in this direction (No. Ra14-0274, Ra19-0011, Sz07-0429 and Pr18-0367 profiles).

In some profiles differences in distribution of precious metals and Cu can be observed in the full thickness of the Kupferschiefer. Au contents are highest in the sandstone and abruptly decrease in the Kupferschiefer whereas Cu contents strongly increase in this bed [No. Ra14-0505, Sz08-0991, Sr19-2428 (Fig. 17) and Sz02-0438 profiles]. If higher Au contents appear in the top part of the sandstone, in the boundary dolomite and in the Kupferschiefer, the first Cu enrichment appears in the overlying dolomites (No. Sr18-0061"s" and Pr18-0367 profiles).

Analysis of these details of metals distribution in the Kupferschiefer clearly demonstrates that similarities between distribution pattern of Au, Pt, Pd and Cu occur only in these sequences, in which Cu contents are low (usually below 0.4%). If Cu grade rises to several percent and more the contents of precious metals decrease. If Cu deposit is located also in the sandstone but the Kupferschiefer is absent, precious metals do not accumulate in the sandstone (No. Sz03-2051 profile). Therefore, the new results confirm the earlier conclusion that in the zones with Au, Pt and Pd accumulations Cu occurs is small amounts. On the contrary, economic-grade Cu zones contain only trace amounts of precious metals (Piestrzyński & Pieczonka, 1997a; Pieczonka, 1998, 2000; Pieczonka & Piestrzynski, 2000).

Au-bearing horizon versus Cu deposit

In order to illustrate the relationships between Cu and Au deposits, five cross-sections were drawn through the Polkowice East and Main fields.

The P2u cross-section (Fig. 81), oriented SW–NE, was located in the Polkowice Main Field where deposit is

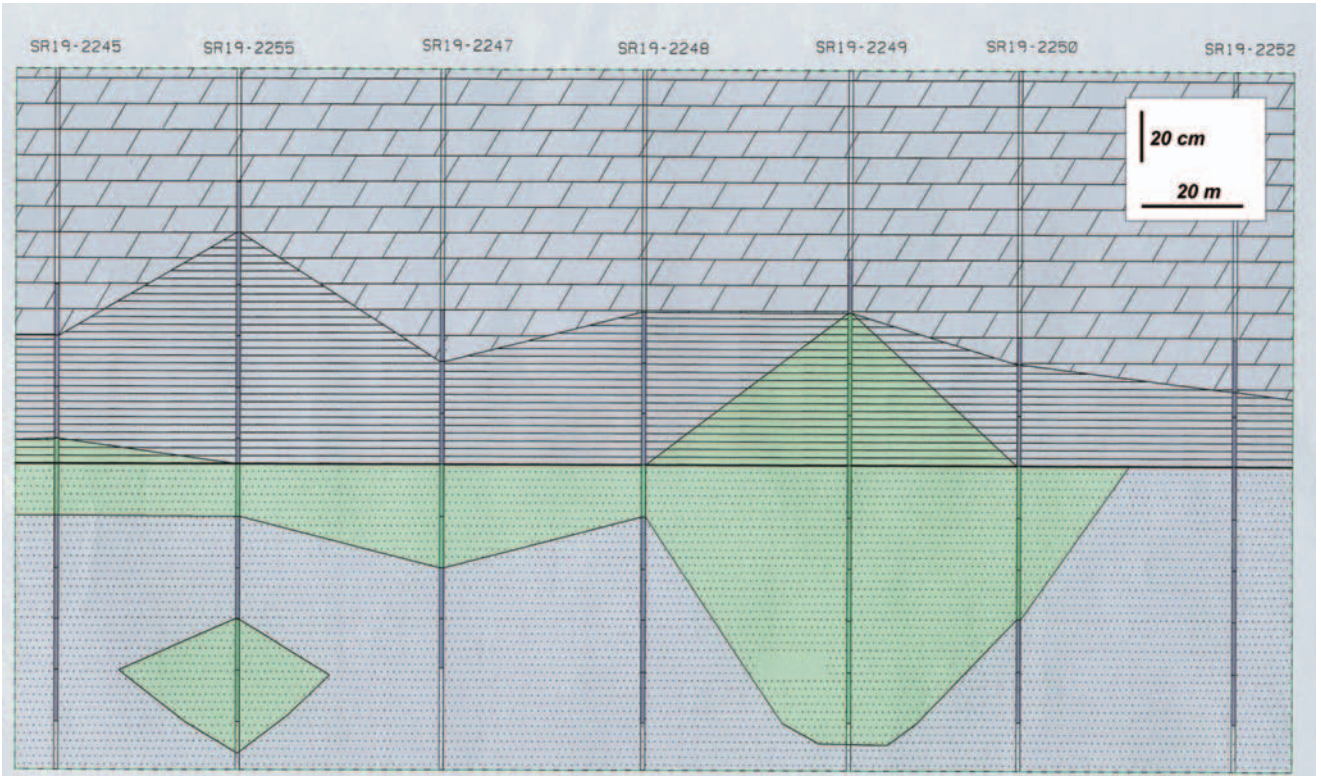

Fig. 86. Vertical model of gold deposit, based on channel sampling e.g. Sr-19-2250, through the southern part of Sieroszowice Mine. Vertical scale 1:20, horizontal scale 1:1000, dashed area represents Kupferschiefer, above is dolomite and below is sandstone, green color show gold horizon for cat of grade 0.5 ppm

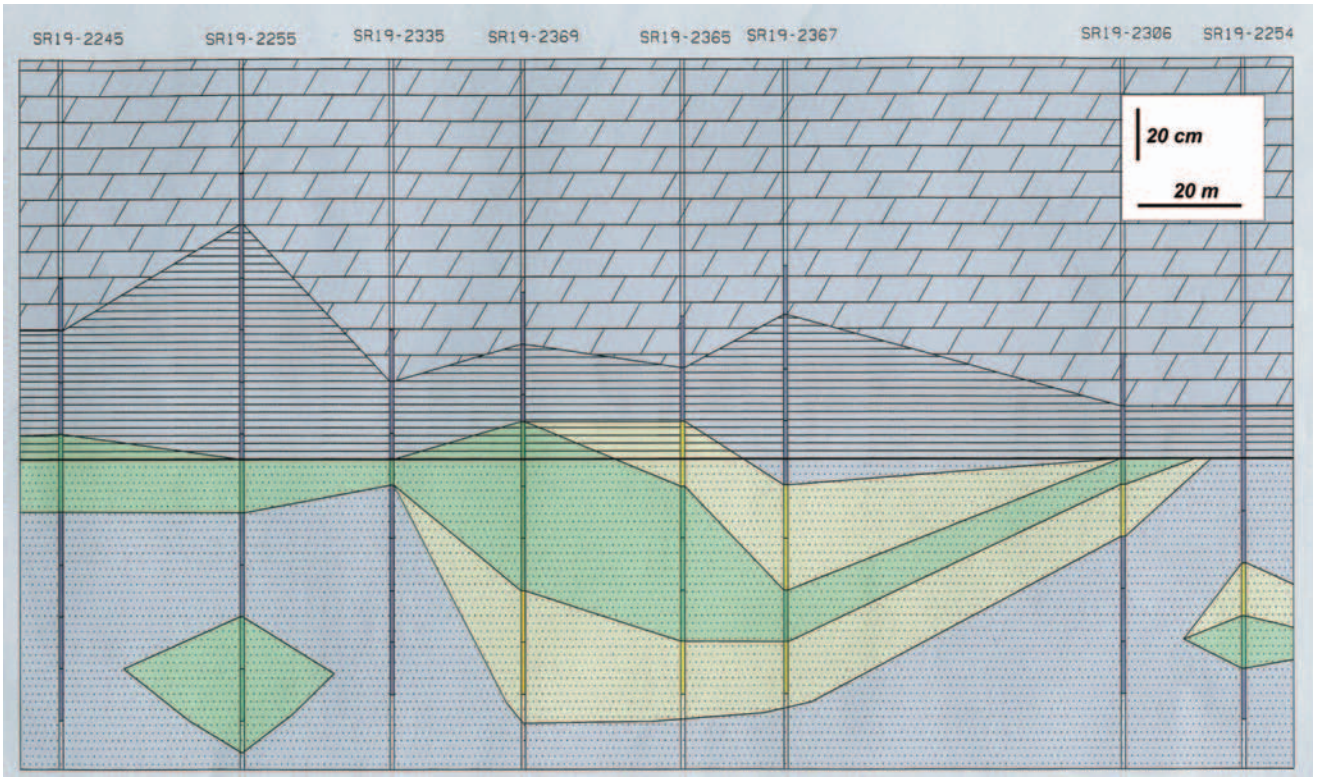

Fig. 87. Vertical model of gold deposit, based on channel sampling e.g. Sr-19-2367, through the southern part of Sieroszowice Mine. Vertical scale 1:20, horizontal scale 1:1000, dashed area represents Kupferschiefer, above is dolomite and below is sandstone, green color show gold horizon for cat of grade 0.5 ppm, yellow color show sub-economic gold horizon 0.2–0.5 ppm

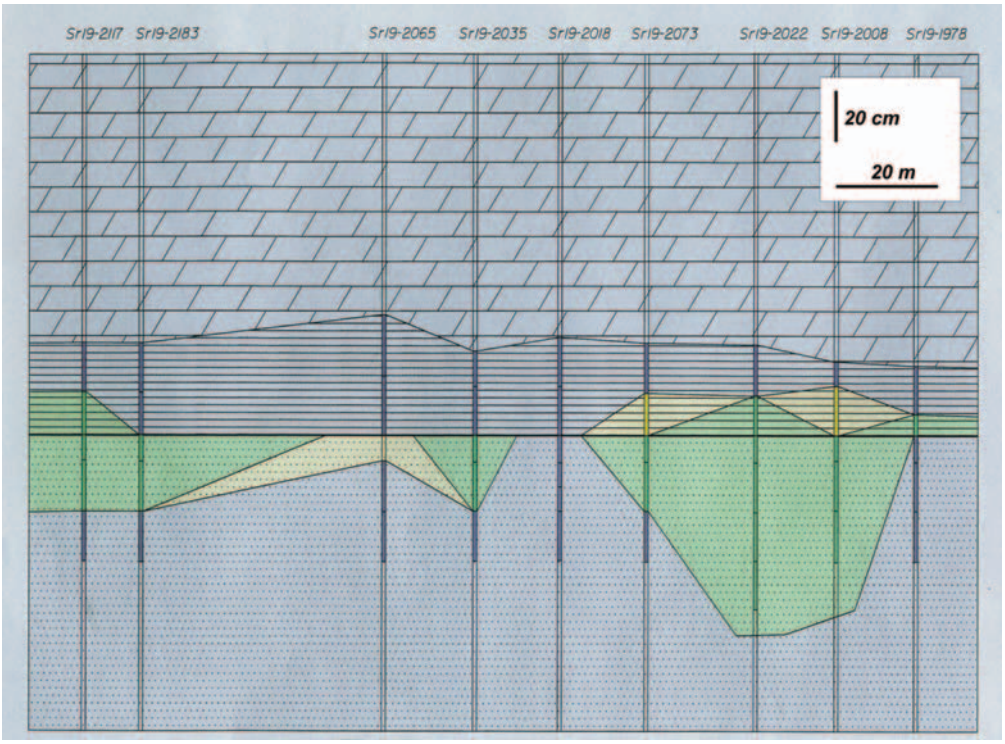

Fig. 88. Vertical model of gold deposit, based on channel sampling e.g. Sr-19-2022, through the southern part of Sieroszowice Mine. Vertical scale 1:20, horizontal scale 1:1000, dashed area represents Kupferschiefer, above is dolomite and below is sandstone, green color show gold horizon for cat of grade 0.5 ppm, yellow color show sub-economic gold horizon 0.2–0.5 ppm

hosted in the Kupferschiefer and in the carbonates. Three faults cut this area. In the southwestern part, bordered by the first fault, Au horizon extends down to 50 cm depth beneath the top part of the sandstone. Au contents generally rise towards the fault (up to 5.97 ppm) but decrease about 30 m from the fault. Instead of Au, Pt and Pd appear in the top part of the sandstone. Close to the fault Au horizon is rather thin and Pt+Pd accumulations are absent. In the footwall block Au horizon expands to the Kupferschiefer bed and its thickness increases to 1 m. About 55 m behind the first fault Au-horizon, about 10 cm thick, occurs only in the Kupferschiefer. Close to and behind the second fault Au horizon is located again in the sandstone and its thickness decreases. About 60 m behind the second fault, Au horizon vanishes and appears again close to the third fault, in the Kupferschiefer. In the footwall block Au contents rise up to 11.29 ppm. Also high are Pt and Pd values, which accumulate in the Kupferschiefer and in the sandstone. About 50 m from the third fault Au horizon once again disappears. Along the full length of this cross-section Au horizon is generally continuous but its thickness is variable.

The P2r cross-section (Fig. 82), oriented NW–SE, is located in the Polkowice Main Field, perpendicularly to the P2u one. Two small faults cut this area, first in the northwestern, second in the southeastern parts of the field. In the vicinity of the first fault and in the southeastern part of the field Cu deposit is absent. In the remaining parts Cu-bearing zone is highly variable and is hosted either in the Kupferschiefer and in the dolomite or only in the dolomite. The cross-section includes 23 sampling profiles, most of them localized in the areas where Cu zone is hosted only in the dolomite, at various heights over the top surface of the sandstone or where Cu deposit is absent. In all these profiles high Au contents were detected (from 2 to 29.90 ppm) and in three profiles high contents of Pt+Pd were observed, as well (up to 5.46 ppm, No. Sz01-1946 sequence). In sequences where Cu deposit is located in both the Kupferschiefer and the dolomites, Au contents were usually below 2 ppm, except for two, in which 6.2 and 11.27 ppm Au were detected. Locally, high contents of Pt+Pd appeared (4.04 ppm in No. Sz01-1661 profile).

In the profiles localized in the northwestern part of the P2r cross-section maximum Au, Pt and Pd contents occur in the Kupferschiefer. Hence, Au-bearing horizon shows low (up to 0.3 m) but stable thickness, even in the vicinity of fault zone. At the distance over 20 m from the first fault, in its hanging-wall block high Au contents appeared also in the sandstone and in the Kupferschiefer Pt+Pd contents reached 4.04 ppm. The Au horizon was found in both the Kupferschiefer and the sandstone, and its thickness increased to 0.5 m. Similarly to the first, the second fault did not affect decisively the position of Au-bearing horizon but significant enrichment was observed in the vicinity of dislocation (up to 29.90 ppm). About 40 m from the fault Au-bearing horizon was found only in the top part of the sandstone and its thickness decreased. In the southeastern part Au horizon occurred alternatively in the Kupferschiefer and in the sandstone or only in the sandstone. In all the profiles from this part of the field increased contents of Pt and Pd were noticed, as well.

It is difficult to recognize regularities in distribution of precious metals. High Au contents were observed: (i) where Cu deposit is absent, (ii) where Cu horizon is located in the carbonates and (iii) where it occurs in both the Kupferschiefer and the carbonates. It seems, however, that in Cu-barren zones Au contents are generally higher. High contents of Pt and Pd appear in both the Cu-barren and the Cu-rich Kupferschiefer. In the southeastern part of the field high Pt and Pd values were detected also in the sandstone. No influence of a fault on Au-bearing horizon has ever been observed, as high Au contents occur close to the fault and at a distance from it.

The P6r, P5u and P5r cross-sections were localized in the central part of the Polkowice. The NW–SE-oriented P6r and P5r cross-sections are roughly parallel and about 0.5 km distant from each other whereas P5u section is perpendicular to those two. In this part of the mining field Cu deposit is hosted in the Kupferschiefer and in the carbonates, except for southeastern fragment of the Pr5r section where the Kupferschiefer pinches out and Cu deposit is absent. In all three cross-sections Au horizon is located at various depths in the sandstone. Au contents do not exceed 2 ppm (locally, two times higher values were detected) but thickness of the horizon is significant. Lower contour of the horizon cannot be determined due to the lack of data. Low contents of Pt and Pd were detected only in a few profiles, in the sandstone.

In the P6r cross-section (Fig. 83) Au-bearing horizon is continuous. Its upper contour is close to or follows the top surface of the sandstone, and its thickness varies from a dozen of centimeters in the southeastern part to about 1 m in the central part of the section. Hence, the lower Au contents are compensated by higher thickness of the horizon. In the southeastern part of the cross-section Au contents are very high (up to 8.57 ppm) but thickness of horizon is lowest. In the northwestern part of the section small, local Au accumulation occurs beneath the main Au horizon. Only in two profiles some enrichment in Pt and Pd has been found.

In the P5r cross-section Au horizon is discontinuous. In the northwestern part it is about 1 m thick and is hosted in the uppermost part of the sandstone. In the central part Au horizon pinches out and precious metals disappear along the distance of some 250 m. It reappears in the vicinity of the only fault present in this area. Behind this fault Au horizon dips into the sandstone down to 1 m depth beneath its top surface (in No. Sz08-0936 profile) and its thickness decreases to about 10 cm. Towards the southeast the Au horizon again shifts to the top of the sandstone. Simultaneously, Cu deposit shifts to higher members of the carbonate series and then disappears. However, high Au contents were detected in No. Sz08-1054 profile (Fig. 7) – the last one in this cross-section, which justifies further exploration towards the southeast.

The P5u cross-section (Fig. 84), oriented SW–NE, includes several faults of throws from 1.5 to 3.5 m. According to current interpretation, these faults can be younger than Au mineralisation. Similarly to P2u and P2r cross-sections, Au anomalies have not been observed in the vicinity of the faults but Au horizon was slightly shifted, as were the host rocks. In the southwestern part Au horizon extends from the top of the sandstone to about 0.4 m beneath. Starting from No. Sz12-0050 profile, towards the first fault, the upper contour of Au horizon dips down to about 0.6 m, its thickness increases to about 1 m and Au content rises to 7.29 ppm. Between the first and the second fault the horizon gradually approaches the top of the sandstone and Au content decreases to below 1 ppm. In the neighborhood of next consecutive faults position of the horizon, its thickness and Au content remain stable. Then, behind this zone, Au horizon shifts deeper into the sandstone, pinches out and terminates. Increased Au content in No. Sz13-0553 profile enables us to contour a small, isolated body close to a fault. Continuous Au horizon reappears about 100 m from the fault but its thickness is much lower, Au contents are below 1 ppm and its upper contour occurs at greater depths within the sandstone. In the northeastern portion of the cross-section Au content increases to 8.37 ppm and thickness of its horizon rises.

The P4u cross-section (Fig. 85), oriented SW–NE, is about 800 m distant from and parallel to the P5u cross-section. Cu deposit is here hosted in the Kupferschiefer and in the carbonates. In the central part of the section the boundary dolomite occurs. In some parts bottom portion of the Kupferschiefer is barren. In the southwestern part a fault occurs of 50 m throw. Close to this reverse fault thickness of the deposit doubles. In the hanging wall of this fault Au horizon is located beneath the top of the sandstone and Au contents are very high (maximum – 13.49 ppm). At the distance of about 30 m to the fault Au horizon terminates but reappears behind the fault and becomes continuous to the end of this cross-section. Its thickness varies from about 20 to 100 cm. The Au horizon is hosted in the top part of the sandstone and in the boundary dolomite (if present). Au contents are high in the whole thickness of the horizon: in its middle part up to 6.60 ppm were detected and in the northeastern part of the section even 15.52 ppm Au were found. The horizon extends northeastwards. Maximum Au contents occur usually in the top part of the sandstone but in some profiles second enrichment was noticed about 1 m beneath the top surface (up to 5.81 ppm in No. Sz07-1045 profile). Pt and Pd were found in three sequences located in the central part of the section (Pt+Pd = 0.5–0.8 ppm) and in two profiles located in its northeastern part (about 0.2 ppm). In the remaining profiles PGE do not accumulate.

Cross-sections presented in Figs 86, 87 and 88 illustrate the position of Au horizon in the southeastern part of the Sieroszowice Mine. This mine is most perspective for Au exploration as the area of worked-out Cu orebody is small. The scale of cross-sections facilitates the recognition of the details of Au horizon. Fig. 86 shows a single, distinct horizon hosted in the top part of the sandstone and, locally, in the Kupferschiefer as well as second, poorly visible horizon located deeper in the sandstone. The sub-economic zone contoured by Au cut-off 0.5–0.2 ppm is absent from this section. Two other cross-sections reveal more diversified patterns (Fig. 87, 88). Locally, thickness of Au horizon reaches even 1 m and nest-like forms appear. In Fig. 87 the sub-economic zone envelops the Au horizon, which is a rare feature as in profiles where the contour of Au horizon is lithological the sub-economic zone is absent (Fig. 86).

Small nests visible in Fig. 87 and located about 1 m beneath the top of the sandstone should be regarded as sub-economic if these do not continue perpendicularly to the cross-section.

Summary

Generally, Au horizon is continuous and located close to the bottom contour of Cu deposit. It includes the top part of the sandstone and extends down, even beneath 1 m from the sandstone top surface. Commonly, the horizon includes also the Kupferschiefer, particularly its bottom part, and the Boundary Dolomite (if present in host-rocks lithology). Hence, in various parts of deposit thickness of Au horizon varies from several centimeters to over 1 m. The lack of data from deeper parts of the sandstone precludes the determination of the lower contour. Rarely, increasing thickness is accompanied by very high Au grade. The richest parts of the horizon are usually about 40 cm thick. High contents of Pt and Pd occur mostly if the Au horizon is hosted in the Kupferschiefer although both PGE were observed also in the sandstone. Small faults marked in the cross-sections do not affect the formation of precious metals accumulations because high contents of Au and PGE were observed both in the vicinity of and at the distance from these dislocations. However, the absence of Cu deposit in the neighborhood of some faults may suggest tectonic control of oxidized solutions transfer. Small displacements of Cu deposit and Au+PGE horizons may suggest that some faults might have formed after Cu mineralisation whereas others might have been coeval with the precious metals mineralisation (Pieczonka & Piestrzyński, 2001). Shifting of precious metals horizons results from geological data interpretation. Explanation of this feature requires further, detailed studies on tectonics and metals distribution.

MODELING OF GOLD CONTENT VARIABILITY AND ACCURACY OF GOLD RESERVES ESTIMATIONS

Review of recent applications of statistical and geostatistical methods to the estimations of gold deposit parameters

According to Sharapov (1971), statistical methods were applied for the first time in economic and mining geology over 100 years ago for estimations of error in average Au content calculations made by Psaryev in 1899 for some Siberian gold deposits.

Most of available papers on statistical/geostatistical methods applied to gold deposits refer to those hosted in the Witwatersrand reef complex in South Africa. An interesting distribution model of Au grades in a deposit leading to log-normal probability distribution of this parameter was proposed by de Wijs (1953). His results were applied by Krige and Ueckermann (1963), and Krige (1968, 1976, 1978) to the development of a new geostatistical estimation method of Au contents and reserves (then called "kriging" in order to honor D.G. Krige) as well as to quantification of sampling errors. The authors mentioned above applied also other statistical methods: correlation, multidimensional regression and trend analysis. The optimization of sampling grid in South African deposits was studied by Rendu (1976). Clifton *et al.* (1969) investigated the proper size of samples taken from a deposit, which would ensure the required accuracy of Au grade estimation. The error of sample preparation for chemical analyses was estimated with the modified method developed by Gy (1983), who considered the specific character of Au concentration and occurrence (Ottley, 1965).

Estimation of Au reserves and quality of particular deposits required more advanced, parametric and nonparame-tric geostatistical methods (disjunctive, indicator and probability kriging), as shown by Kim *et al.* (1987) for Au-Ag deposit in Nevada, USA, by Sullivan (1984) and Verly and Sullivan (1985) for Jerritt Canyon deposit, Nevada, USA, and by Chiles and Liao (1992).

Parker (1991) proposed a new approach to the problem of outliers in the assessment of average Au grade at the Sunnyside Mine (Colorado), Jerritt Canyon and Sleeper mines (Nevada) in the USA. Examples of geostatistical descriptions with semivariograms applied to studies on variability structure of Au contents can be found in Armstrong (1998), whereas the development of integrated system for Au deposits validation in the Witwatersrand reef complex was presented by Camisani-Calzolari *et al.* (1992).

The world literature dealing with mathematical evaluation of Au deposits is very abundant. The presented above,

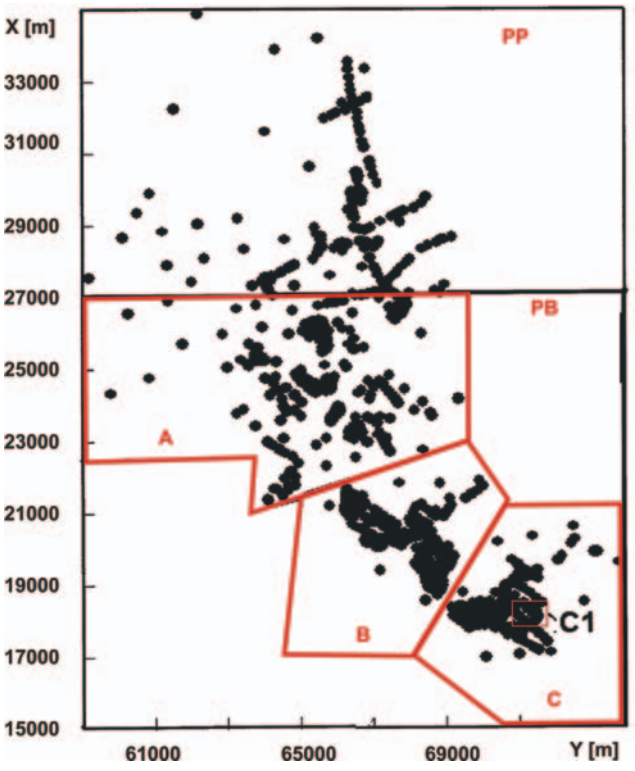

Fig. 89. Samples location in mine workings of the Cu-Ag ore deposit Polkowice-Sieroszowice and distinguished parts and areas of gold content estimation. PP – sub-economic part of the deposit, PB – economic part of the deposit; A, B, C – areas of exploration, C_1 – sub-area of exploration

brief review of most important papers illustrates the wide range of problems related to estimations of ore grades and reserves applied in exploration for and sampling of Au deposits.

The scope of studies and the source materials

The following report contains the results of statistical and geostatistical studies on variability and estimation accuracy of Au grade, and related parameters in a part of the Polkowice-Sieroszowice Cu-Ag deposit. The source materials were the results of chemical analyses for Au in point samples collected from mine workings along vertical lines (corresponding to lithostratigraphic sequences) with 20 cm spacing. Totally, 1,171 sampling sites were included. For each sampling site average Au contents were calculated for lithological varieties of host rocks and for the whole economic-grade deposit. The study area together with localization of sampling sites are shown in Fig. 89.

Taking into account the clustering of sampling sites (as an only criterion), two parts were distinguished in the study area: sub-economic (PP) and economic (PB). In the latter four exploration areas were contoured: A, B and C (A+B+C = PB), and C1 (a sub-area sampled in previous research project). Such procedure aimed to compare variabilities and Au contents in various parts of study area, and to recognize the areal variability of Au grade.

Apart from Au content, deposit thickness M [m] and product of both parameters: Au∗M [ppm m] (named "linear accumulation index") were considered. The latter parameter is an equivalent of "meter*Cu per cent" index applied by the Lubin Copper Company for contouring the economic-grade Cu-Ag deposit (see Regulation…, 2001). Thickness of Au deposit was determined as a distance between two extreme point samples in vertical sequence, in which Au grades exceeded cut-off value = 0.5 ppm. The deposit was categorized as economic-grade if arithmetic mean of Au contents in point samples enclosed between the extreme samples was higher than 0.5 ppm.

Methodology

For initial description of variability parameters the classic statistical methods were applied, i.e. histograms characterizing the probabilistic variability structure of parameters and calculations of principal variability measures of deposit parameters: arithmetic mean (as a measure of central tendency), variance, variability coefficients (as dispersion measures) and asymmetry coefficient (as a measure of distribution skewness). Additionally, the percentage was calculated of samples (N_b) which met the accepted cut-off grade (Au>0.5 ppm).

The following formulae were applied:

arithmetic mean: variance: $z \quad \frac{1}{n} \sum_{i\ 1}^{N} z_i$

variance: $s^2 \quad \frac{1}{N} \sum_{i\ 1}^{N} (z \quad \bar{z})^2$

variability coefficient: $v \quad \frac{s}{\bar{z}} \ 100\%$

asymmetry coefficient: $g_1 \quad \frac{1}{Ns^3} \quad (z_i \quad \bar{z})^3$

where: N – number of data (= number of collected samples), z_i – value of analyzed parameter in an "i"-th sample.

Variability structure of deposit parameters was analyzed with geostatistical method developed by Matheron (1962, 1963). Application of this method to geological and mining-engineering practices was described in details e.g., by David (1977), Journel and Huijbregts (1978), Isaaks and Srivastawy (1989), and Armstrong (1998). Thus, semivariograms were used for examination of parameters variability (directional and averaged for all directions), random and non-random variability components were selected, autocorrelation range was determined as well as geostatistical variability models were verified with the cross-validation test.

The semivariograms are usually visualized with scatter plots and characterize the power of diversification of parameters expressed as average squared increments (ordinates axis) *versus* average distance between measurement points of parameters (abscissae axis).

The formula for calculation of empirical semivariogram for data derived from deposit sampling is:

$$(h) \quad \frac{1}{N_h} \sum^{N_h} (z_i \quad z_{i\ h})^2$$

where: – number of samples pairs distant by "h",
z_i, z_{i+h} – values of analyzed parameter in points distant by "h"

Geostatistical models are continuous mathematical functions permitted by the theory of geostatistics, which approximate the empirical semivariograms.

Table 49

Statistics of Au contents [ppm] in studied parts of the Polkowice-Sieroszowice deposit

Study area	N	N_b [%] Au>0.5 ppm	$\bar{z}$ [ppm]	s^2 [ppm]^2	v [%]	g_1
Whole study area PB+PP	1,171	62.7	2.24 [0.0-37.4]	15.2	173.6	4.02
Economic-grade deposit PB=A+B+C	1,000	69.2	2.54 [0.0-37.4]	16.9	161.7	3.81
Exploration area A	310	69.8	2.81 [0.0-29.3]	16.4	144.2	3.14
Exploration area B	362	62.6	2.76 [0.0-37.4]	24.9	180.9	3.78
Exploration area C	328	76.4	2.05 [0.0-21.4]	8.2	140.2	3.19
Exploration sub-area C1	167	81.4	2.40 [0.0-21.4]	11.1	138.6	2.87
Sub-economic deposit PP	171	24.9	0.51 [0.0-9.7]	1.7	256.0	3.92

N – number of data (= number of collected samples)
N_b – percentage of samples above the cut-off grade (>0.5ppm)
$\bar{z}$ – arithmetic mean and [ ] – outliers
s^2 – variance, v – variability coefficient, g_1 – asymmetry coefficient

Table 50

Statistics of deposit thickness M [m] in studied parts of the Polkowice-Sieroszowice deposit

Study area	N	N_b [%]	$\bar{z}$ [m]	s^2 $[m]^2$	v [%]	g_1
Whole study area PB+PP	1,171	62.7	0.22 [0.0-1.6]	0.07	123.6	3.49
Economic-grade deposit PB=A+B+C	1,000	69.2	0.25 [0.0-1.6]	0.08	113.0	1.54
Exploration area A	310	69.8	0.25 [0.0-1.6]	0.08	111.3	1.76
Exploration area B	362	62.6	0.17 [0.0-1.3]	0.05	121.9	1.71
Exploration area C	328	76.4	0.33 [0.0-1.4]	0.10	98.8	1.05
Exploration sub-area C1	167	81.4	0.33 [0.0-1.3]	0.10	92.8	1.06
Sub-economic deposit PP	171	24.9	0.06 [0.0 - 0.8]	0.02	224.5	3.12

For explanation of symbols see Table 49

Table 51

Statistics of Au linear accumulation index Au∗M [ppm∗m] in studied parts of the Polkowice-Sieroszowice deposit

Study area	N	N_b [%]	$\bar{z}$ [ppm·m]	s^2 $[ppm·m]^2$	v [%]	g_1
Whole study area PB+PP	1,171	62.7	0.62 [0.0-10.0]	0.98	160.4	3.49
Economic-grade deposit PB=A+B+C	1,000	69.2	0.71 [0.0-10.0]	1.09	147.6	3.29
Exploration area A	310	69.8	0.93 [0.0-10.0]	1.99	152.1	2.79
Exploration area B	362	62.6	0.58 [0.0-6.9]	0.76	149.4	2.71
Exploration area C	328	76.4	0.63 [0.0-6.8]	0.53	115.1	3.03
Exploration sub-area C1	167	81,.4	0.66 [0.0-3.4]	0.40	96.5	1.46
Sub-economic deposit PP	171	24.9	0.10 [0.0-1.5]	0.07	252.3	3.27

For explanation of symbols see Table 49

Estimation accuracy of average values of deposit parameters in calculation blocks and in specific points of the deposit were determined with the kriging method. This procedure considers both the already determined geostatistical variability models fitted to point semivariograms as well as mutual configuration of sampling sites, their position in analyzed calculation block or in the whole deposit, dimensions and shape of particular block. When compared with other methods, the kriging provides most accurate estimations of parameters.

The range of procedures characterized above was applied to both the full data population and the particular subsets representing selected parts of study area.

Results

Statistical data processing

The results of all statistical calculations for selected areas are listed in Tables 49, 50 and 51 (for the vertical sequence of whole deposit) and in Table 52 for particular host-rocks. Histograms of deposit parameters values for selected data sets are presented in Figs 90 and 91.

Analysis of statistical data and histograms allowed the author to formulate several remarks on the variability character of studied deposit parameters.

Distribution of Au contents can be regarded as typical of the most of trace and accompanying elements in the Cu-Ag deposit of the Fore-Sudetic Monocline. It is reflected, first of all, by strong asymmetry of distribution with skewness coefficients about 3–4 and very high (v =100–150%) or extremely high (v>150%) variability expressed by variability coefficient.

Among the studied parts and areas (Fig. 89) the northern part showed exceptionally low Au grades, close to the accepted cut-off value. Only 25% of samples from this part revealed Au contents in the sequence over 0.5 ppm. Moreover, these samples were randomly distributed over the whole northern part and did not form larger clusters, which would enable the author to reasonably contour the zones of Au content over 0.5 ppm. Hence, the whole northern part of study area was categorized as sub economic deposit (PP).

The exploration areas (A, B and C), which constitute the economic-grade deposit (PB) show similar mean Au contents within the class 2.1–2.5 ppm and similar percentages of samples over cut-off grade (63–70%).

The two other deposit parameters: thickness and linear accumulation index reveal similar regularities. Mean thicknesses of economic-grade deposit in selected parts and areas

Table 52

Statistics of Au contents, deposit thickness and linear accumulation index for particular host-rocks (only for economic-grade deposit PB=A+B+C)

Parameter	Lithology	N	N_b [%]	$\bar{z}$	s^2	v	g_1
Au [ppm]	carbonates	1,000	2.3	0.08	0.5	869.5	13.2
	Kupfer-schiefer	1,000	30.3	0.96	7.0	275.2	5.18
	sandstones	1,000	54.0	2.23	22.4	212.2	5.56
M [m]	carbonates	1,000	2.3	0.01	0.00	827.8	12.4
	Kupfer-schiefer	1,000	30.3	0.06	0.01	178.5	1.86
	sandstones	1,000	54.0	0.18	0.07	145.3	1.87
Au·M [ppm·m]	carbonates	1,000	2.3	0.02	0.04	854.2	11.6
	Kupfer-schiefer	1,000	30.3	0.16	0.16	255.6	4.35
	sandstones	1,000	54.0	0.53	0.93	181.9	3.86

For explanation of symbols see Table 49

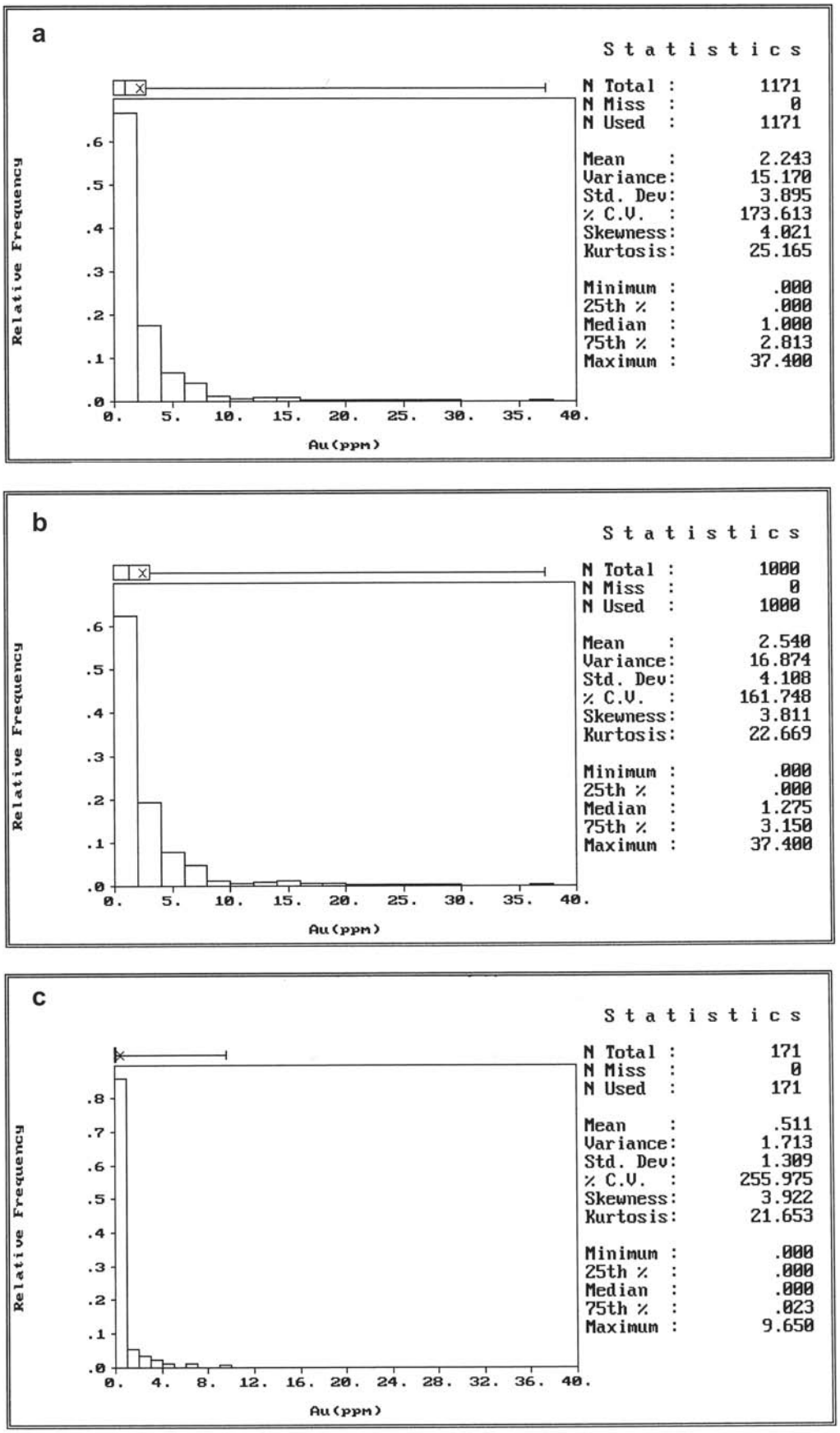

Fig. 90. Histograms of the gold content for the distinguished parts of the deposit. **a** – all samples, **b** – economic part of the deposit, **c** – sub-economic part of the deposit

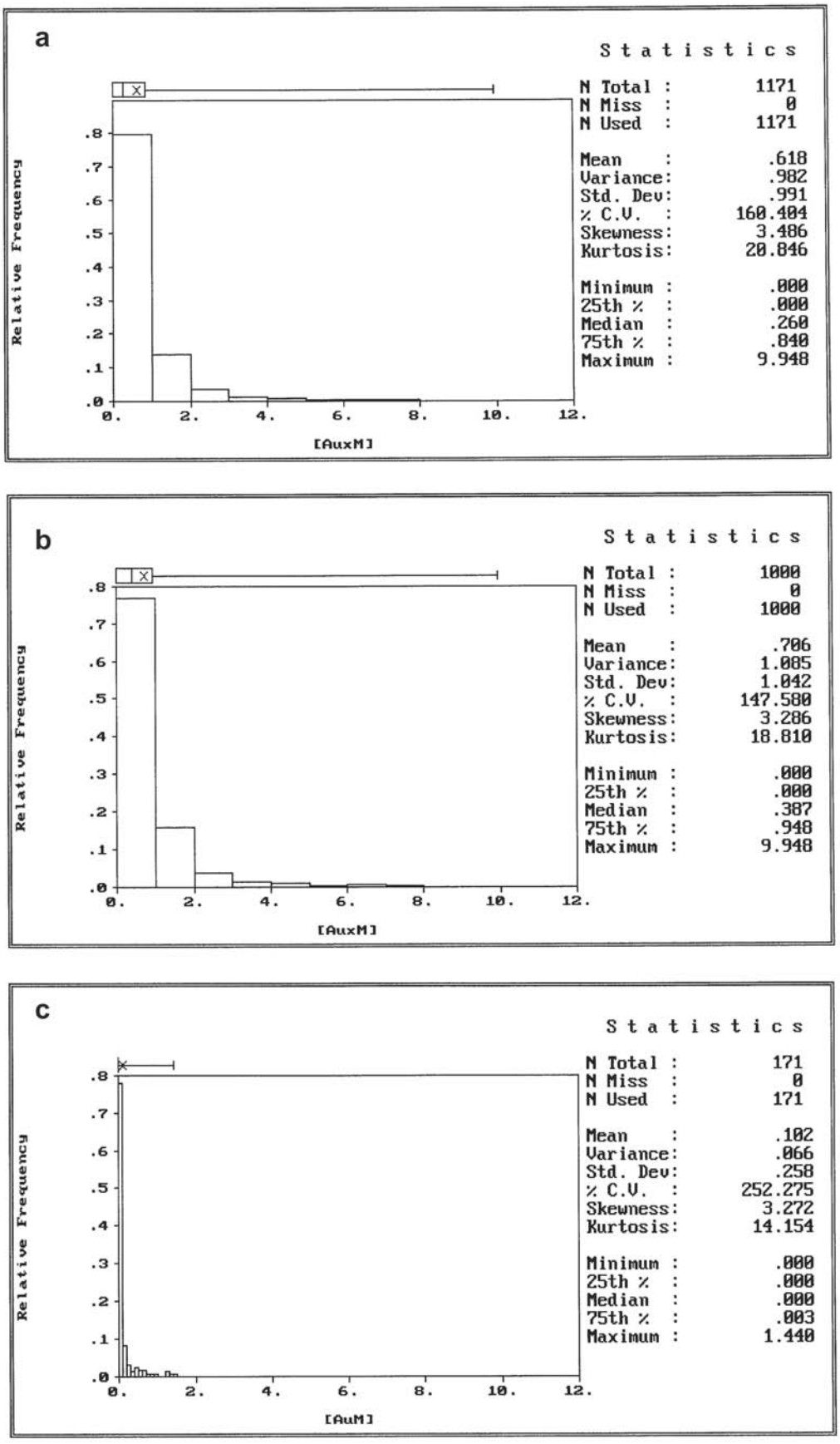

Fig. 91. Histograms of the gold accumulation [Au∗M] for the distinguished parts of the deposit. **a** – all samples, **b** – economic part of the deposit, **c** – sub-economic part of the deposit

fall into the range 0.17–0.33 m, whereas mean thickness of sub-economic deposit is only 0.06 m. Variability coefficients for thickness are somewhat lower than those for Au contents – v: 100–120% for economic-grade deposits and 225% for sub-economic deposit whereas asymmetry coefficients are significantly lower for the economic-grade deposit (1.1–1.8) but exceed 3 for sub-economic deposit.

The linear accumulation coefficient shows variability structure similar to that of Au grade, particularly if one compares variability coefficients (115–152% for economic-grade deposit) and asymmetry coefficients, which fall into the range 2.8–3.0 at mean linear accumulation index values 0.6–0.9 [ppm m]. In the subeconomic part of Au deposit mean value of this parameter is only 0.1 [ppm m] at high variability coefficient (252 %) and asymmetry coefficient 3.3.

For particular host-rocks significant differences were observed in percentages of samples with Au contents over cut-off grade (Au>0.5 ppm). Only 2.3% of samples from the Zechstein Limestone carbonates met this criterion whereas for the Kupferschiefer and the Weissliegend sandstone much higher values were calculated: 30.3 and 54.0%, respectively. Simultaneously, the sandstone showed the highest mean values of deposit parameters: Au content (2.2 ppm Au), thickness (0.18 m) and linear accumulation index (0.53 ppm*m) whereas the variability coefficients of deposit parameters was the lowest among the host-rocks (145–212%).

Geostatistical analysis of variability structure

The variability structure of deposit parameters was characterized with the geostatistical method after Matheron (1962, 1963) applying various semivariograms. First, the directional variability of was analyzed with the Variowin software. The results are displayed in maps (Fig. 92).

Analysis of maps indicates similar diversification values of three deposit parameters in all directions. This justifies the assumption on isotropic variability structure of these parameters. Therefore, the isotropic semivariograms ensure the sufficiently accurate description of variability structure. These semivariograms show diversification of parameters dependent only on the distances between various points in the deposit (excluding the spatial orientation of lines connecting these points).

Semivariograms of studied parameters together with fitting theoretical models for the whole study area and for the distinguished parts are illustrated in Figs 93 and 94. The following geostatistical variability models were applied: spherical, exponential, Gauss and random, generalized mathematical equations of which are shown in Fig. 93 and in Tab. 53.

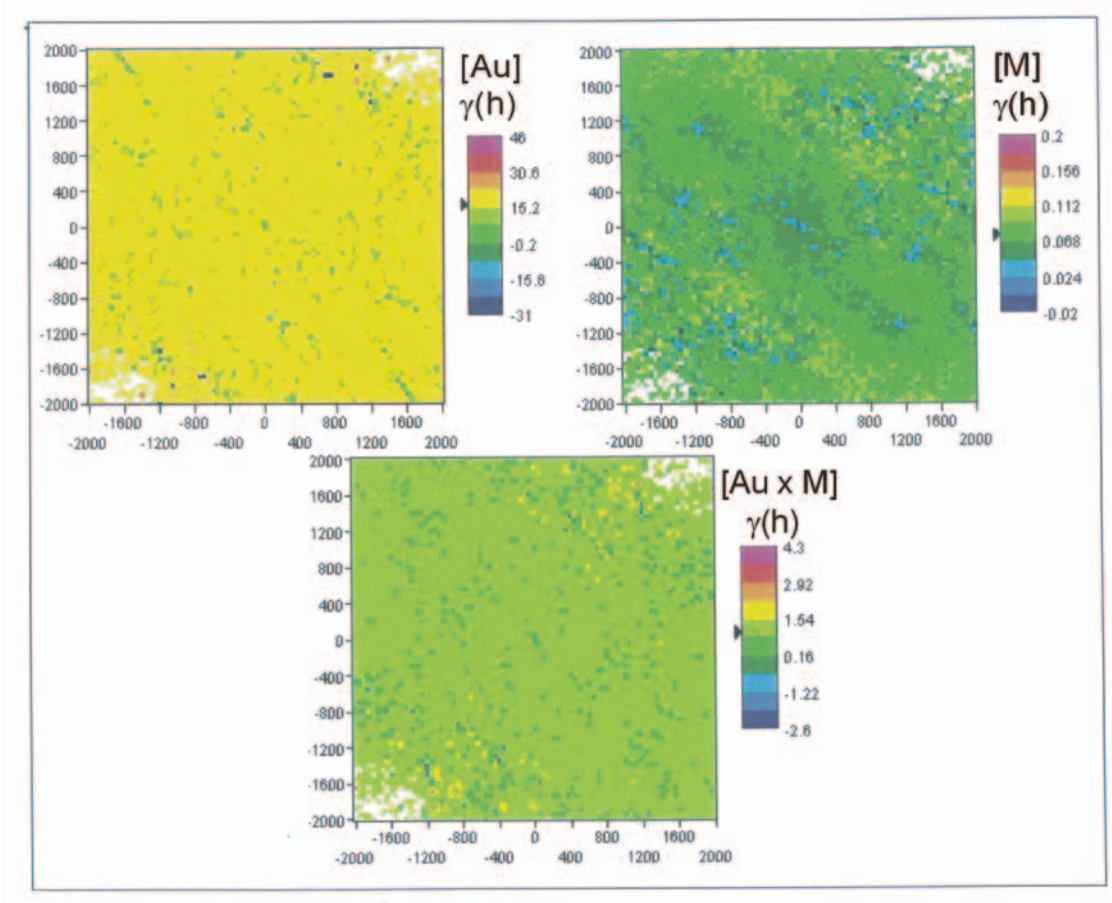

Fig. 92. Map of semivariogram surfaces of the gold content [Au], deposit thickness [M] and gold accumulation [Au∗M] for the economic part of the deposit

The equations of geostatistical models (in simplified and full notations) used for approximations of semivariograms are:

spherical model: $(h) \quad C_0 \quad Csph(h/a)$

$(h) \quad C_0 \quad C \frac{3}{2} \frac{1}{2}\frac{h^3}{a^3}$ for $h \quad a$ and

$(h) \quad C_0 \quad C$ for $h \quad a$

expotential model: $(h) \quad C_0 \quad C\exp(h/a)$

$(h) \quad C_0 \quad C\ 1 \quad e^{\frac{h}{a}}$ for $h \quad a$ and

$(h) \quad C_0 \quad C$ for $h \quad a$

Gauss model: $(h) \quad C_0 \quad CGaus(h/a)$

$(h) \quad C_0 \quad C\ 1 \quad e^{\frac{h^2}{a^2}}$ for $h \quad a$ and

$(h) \quad C_0 \quad C$ for $h \quad a$

random model: $(h) \quad C_0$;

where: C_0 – variance of local variability (random component of variability), C – variance of spatial variability (non-random component of variability), a – range of semivariogram (autocorrelation)

Analysis of calculated semivariograms and geostatistical variability models reveals several common features for Au content and linear accumulation index. Diversification of these parameters is very high even in adjacent sampling sites and only insignificantly increases with the distance between the sites. Such result is well-known from the papers by Krige published in the early 1950-ties and referred to South-African Au deposits. Strong local variability of Au contents resulting from the appearance of nuggets was rather unfortunately named by Krige as the "nugget effect". Such variability character dominated by local variability generally enables us to apply classic geostatistical methods for solution of practical, geological and mining-engineering problems.

Thickness of deposit reveals much less pronounced local variability and distinct increase of semivariograms values with the increasing distance between the sampling sites. That means more pronounced influence of non-random variability component, which reflects the regularities in its changes in the deposit than that of Au content and linear accumulation index.

Additionally, in order to verify the estimations correctness of mean values of deposit parameters in the selected parts of the deposit, so-called relative semivariograms were calculated and theoretical models were fitted, according to equations presented in Tab. 53. The relative semivariograms are obtained by division of values of basic semivariograms (calculated from the formula given in chapter "*Distribution...*") by the square of mean value of given parameter.

Such attempt enables one to compare variabilities of various parameters or the same parameters in various parts of a deposit. Examples of relative semivariograms are shown in Fig. 94 (exclusively for economic-grade deposit).

The relative semivariograms do not contribute to the knowledge of variability structure of the parameters, except for confirmation of earlier conclusions. However, these become important if accuracy of parameters estimation in calculation blocks and points is evaluated as these allow us to determine directly the relative errors and provide controls for calculations based upon the semivariograms.

Estimation of the error of sample preparation for chemical analyses with the formula after Pierre Gy

The variance of local variability quantified in a geostatistical model as an absolute term (C_0) is a sum of variances characterizing the variability of particular parameter in a small scale of observation (lower than basic sampling grid) and the variance of the error of sample preparation for chemical analyses (so-called "variance of secondary sampling error", Deverly, 1983) and the chemical analytical error itself. The variance of secondary sampling error can be determined with the highest credibility from the formula proposed by the creator of the comprehensive theory of sampling, Pierre Gy (Gy, 1983).

The total (relative) variance of the error of sample preparation for chemical analyses σ^2_T is not higher than doubled variance of sample reduction σ^2_{FE}, i.e.: $\sigma^2_{TE} \quad \sigma_{FE}$ (Scott & Whateley, 1995). This boundary, maximum, total variance $\sigma^2_{TE} = 2\sigma^2_{FE}$ can be accepted as a "safe" measure of the precision of sample preparation for chemical analyses.

The variance of sample reduction called the "fundamental error" is given by the formula:

$$^2 FE \quad \sum_{i\ 1}^{N} \frac{1}{M_i} \quad \frac{1}{M_{i\ 1}} \quad m\ f\ g_i\ l_i\ d_i^3$$

where: N – number of grain size reduction stages, M_i – mass of reduced sample at the "i" stage of grain size reduction [g], m – parameter representing mineral composition [g/cm^3], f – parameter representing the grain shape, g_i – parameter representing the distribution of grain size, l_i – coefficient of grain liberation from intergrowths (quantified as $l_i \quad \sqrt{\frac{d_L}{d_i}}$ – where: d_L – diameter of smallest intergrowths (taken here as $d_L = 5$ μm = 0.005 mm), d_i – equivalent diameter of largest grains after each stage of grain size reduction [mm]

In the case of gold minerals the estimation of the variance of sample preparation for chemical analyses is difficult due to rather limited estimation credibility of individual components in the Gy formula. It particularly concerns the grain size distribution in sample and the quantitative estimation of liberated gold grains at given stages of grain size reduction in given sample. For calculations the two extreme variants were considered:

– all the gold grains are free,

– all the gold grains occur in intergrowths with other minerals.

For the first case the following values of sampling parameters were taken (Ottley, 1965):

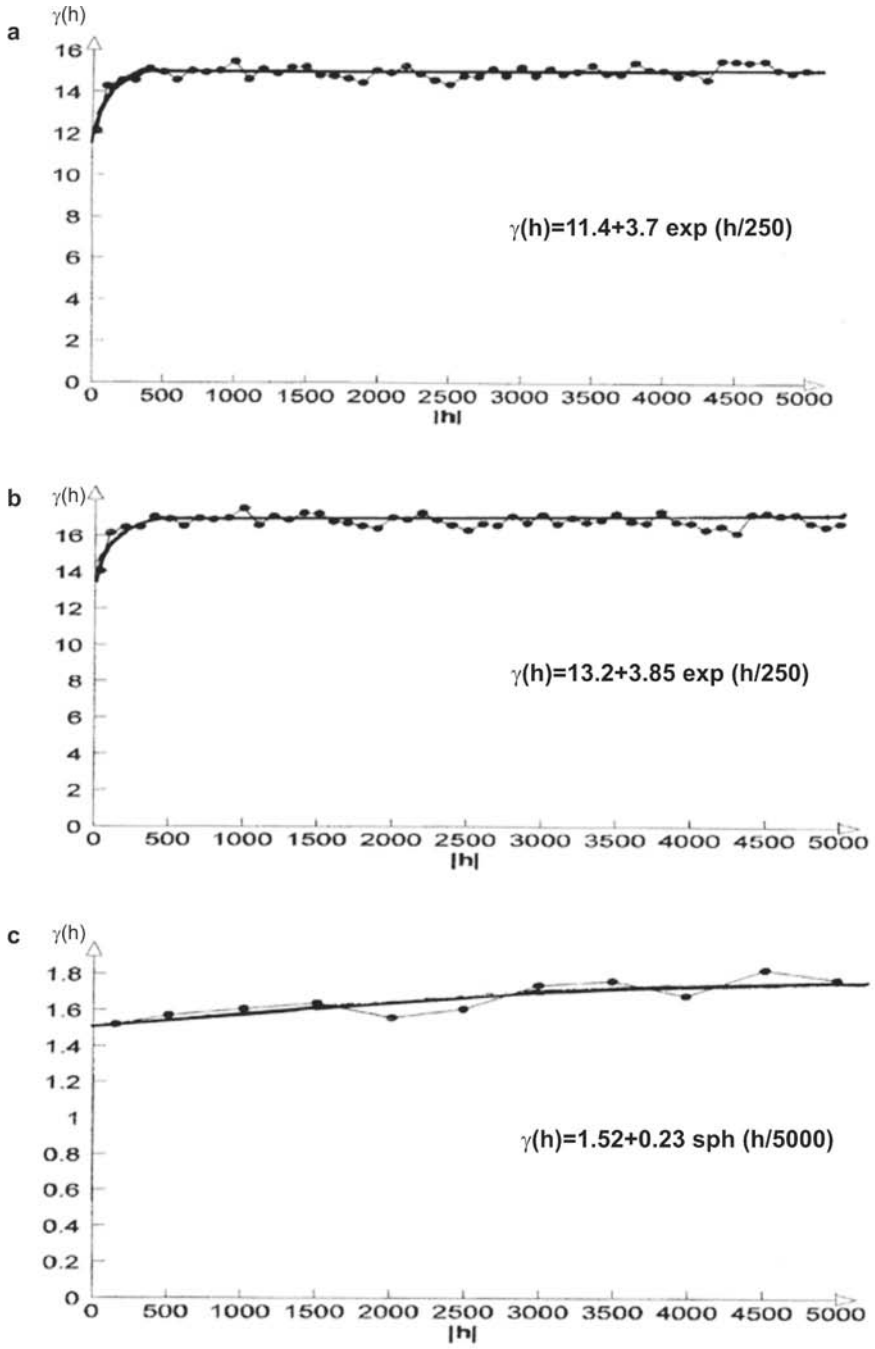

Fig. 93. Semivariograms and geostatistical models of the gold content variability in the distinguished parts of the deposit. **a** – all samples, **b** – economic part of the deposit, **c** – sub-economic part of the deposit

m = / $\bar{z}$ (specific gravity of Au/mean content of Au) = 19.5/2.5g/cm^3 ppm = 7.8 10^{6}g/cm^3

f = g = 0.2 and l = 1

d – diameter of largest native gold grains, taken as d = 0.04 cm after Pieczonka (1998).

For the second case the calculations should follow the basic formula and particular parameters should be red from relevant tables and expressions.

In both cases the masses of samples at the two stages of grain size reduction are the same: M_0 = 1000g, M_1 = 50g, M_2 = 35g (M_0 – mass of a sample collected from the deposit, M_1 – mass of reduced sample after first grain size reduction stage down to maximum diameter d_1 = 1mm, M_2 – mass of sample collected for analysis after sample milling to maximum grain diameter d_2 = 0.07mm).

At the above presented assumptions the estimation of relative variances of grain size reduction σ^2_{FE} and the total error of sample preparation for chemical analyses σ^2_{TE} are as follows:

– all native Au grains free of intergrowths:

σ^2_{FE} = (1/35 – 1/1000) 7.8 10^{6}0.20.2 10.04^3=0.55

andi σ^2_{TE} = 1.10

– all native Au grains in intergrowths:

(at the liberation coefficients of native Au grains from

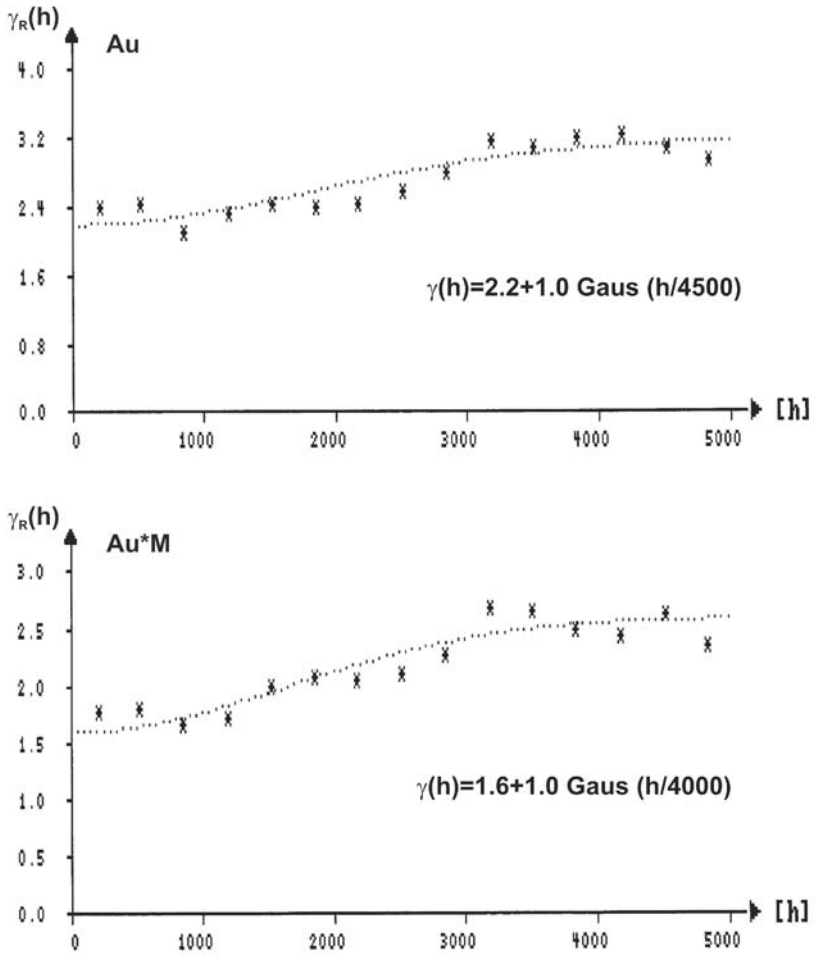

Fig. 94. Relative semivariograms and geostatistical models of the gold content [Au], deposit thickness [M] and gold accumulation [Au M] variability for the economic part of the deposit. (Range of calculation: 5 000 m)

intergrowths at the two stages of comminution:
l_1 = 0.005/l = 0.071, l_2= 0.005/0.07=0.27)
σ^2_{FE} = (1/50 – 1/1000) 7.8 10^6 0.2 0.25 0.0710.1^3 +
+ (1/35 – 1/50) 7.8 10^6 0.2 0.25 0.27 0.007^3) = 0.526 +
0.0003 = 0.53
and σ^2_{TE} = 1.06

The results obtained for both variants of native Au occurrence are surprisingly similar and, despite several simplifications, these results justify the supposition that errors of sample preparation for chemical analyses can significantly influence the accuracy of estimations of Au contents and reserves. The value of the variance of total sample preparation

Table 53

Models of selected relative semivariograms of gold deposit parameters
(models equations were explained in chapter "*Distribution...*")

Area	Au [ppm]	M [m]	Au*M [ppm·m]
Economic-grade deposit**(PB)PB = A+B+C*	γR(h) = 2.2+1.0Gaus(h/4500)	γR(h) = 0.8+0.77Gaus(h/4300)	γR(h) =1.6+1.0 Gaus(h/4000)
	γR(h) = 2.35	γR(h) = 0.76+0.3sph(h/650)	γR(h) = 1.82
Exploration area A*	γR(h) = 1.7+0.37sph(h/1700)	γR(h) = 0.88+0.4sph(h/1500)	γR(h) = 2.3
Exploration area B*	γR(h) = 2.8+0.8Gaus(h/1300)	γR(h) = 0.87+0.72sph(h/1400)	γR(h) = 1.20 + 1.25 sph(h/700)
Exploration area C*	γR(h) = 1.48+0.38sph(h/1200)	γR(h) = 0.36+0.48sph(h/450)	γR(h) = 0.93
Exploration sub-area C1*	γR(h) = 1.65+0.5sph(h/2000)	γR(h) = 0.34+0.53sph(h/300)	γR(h) = 0.75 + 0.3 sph(h/2000)
Sub-economic deposit (PP)*	γR(h) = 5.1+3.4sph(h/480)	γR(h) = 7.5	γR(h) = 10.0

** – applicability distance – up to 5 km; * – applicability distance – up to 2 km

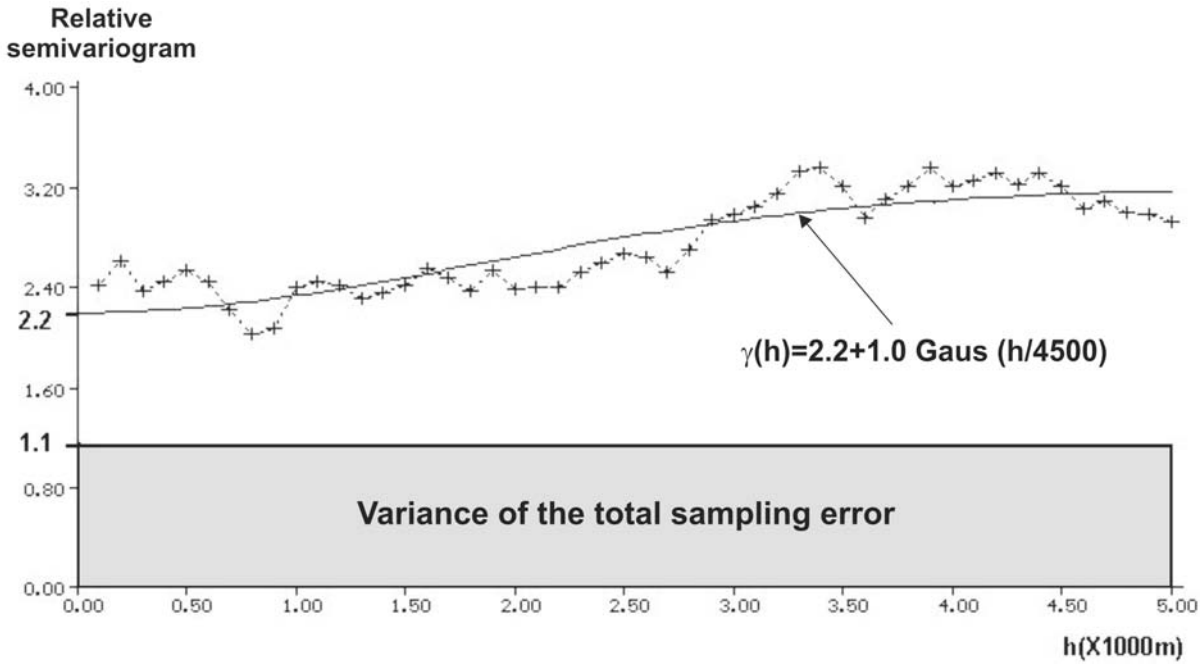

Fig. 95. Contribution of the total sampling error variance to the global variability of the gold content represented by relative semivariogram (the economic part of the deposit – PB=A+B+C). σ^2_{TE} – variance of the total sampling error

error (σ^2_{TE} =1.10) related to the variance of local variability (C_0=2.2) in the relative model of Au content for the economic-grade part of the deposit (Tab. 53) constitutes 50%, as illustrated in Fig. 95. It means that the observed variability of metal content is highly overestimated due to apparent variability caused by the sample preparation errors. Simultaneously, some opportunities arise of the improvement of estimation accuracy of Au reserves by the change in sample preparation procedure for chemical analyses, which may result in the reduction of secondary sampling error. However, it requires the verification of estimated variances, which, in turn, depends on precise determination of grain size distribution in samples and the degree of grain liberation from intergrowths at various stages of grain comminution.

As compared to the secondary sampling errors, the analytical errors are of minor importance (Scott, Whateley, 1995) and were neglected in further considerations.

Table 54

Estimation errors of mean values of Au deposit parameters for exploration area A determined with the block kriging

Coordinates of the center of calculation block	Block dimensions [m]	N	$\sigma_{k[Au]}$ [%]	$\sigma_{k[M]}$ [%]	$\sigma_{k[AuxM]}$ [%]
X_0=65300, Y_0=26000	200×200	12	39.1	29.4	43.8
	500×500	34	25.8	20.7	26.0
	800×800	40	23.5	18.8	24.0

N – number of samples,
σ_k – standard relative estimation error of mean value of a deposit parameter [Au] – Au content, [M] – deposit thickness, [Au*M] – linear accumulation index

Table 55

Estimation errors of mean values of Au deposit parameters for exploration area B determined with the block kriging

Coordinates of the center of calculation block	Block dimensions [m]	N	$\sigma_{k[Au]}$ [%]	$\sigma_{k[M]}$ [%]	$\sigma_{k[AuxM]}$ [%]
X_0=68700 Y_0=19000	200×200	55	22.7	15.4	16.9
	500×500	62	21.7	14.7	15.9
	800×800	63	24.9	21.7	22.0

For explanation of symbols see Table 54

Table 56

Estimation errors of mean values of Au deposit parameters for exploration area C determined with the block kriging

Coordinates of the center of calculation block	Block dimensions [m]	N	$\sigma_{k[Au]}$ [%]	$\sigma_{k[M]}$ [%]	$\sigma_{k[AuxM]}$ [%
X_0=69700 Y_0=18300	200×200	21	29.5	19.2	21.0
	500×500	56	19.1	14.9	12.9
	800×800	58	19.1	17.1	12.7

For explanation of symbols see Table 54

Table 57

Minimum number of samples required for estimation of mean deposit parameters at the accuracy of deposit assessment categories A, B and C_1

Deposit assessment category	Au				M				Au M			
	R.A	R.B	R.C	PB	R.A	R.B	R.C	PB	R.A	R.B	R.C	PB
A	832	1,309	787	1,046	496	595	391	511	926	893	530	871
B	208	328	197	262	124	149	98	128	232	224	133	218
C_1	93	146	88	117	56	67	44	57	103	100	59	97

R.A, R.B, R.C – exploration areas: A, B, C; PB – economic-grade deposit

Estimation accuracy of mean values of deposit parameters in calculation blocks

The estimation accuracy of mean values of deposit parameters were studied in three variants of calculation blocks of dimensions: 200×200 m, 500×500 m and 800×800 m. The area of the largest block corresponds to the total area of Cu-Ag deposit worked out during 1 year of exploitation. Each studied block was localized within the selected zones of highest sampling density (coordinates of the centers of blocks are quoted in Tables 54, 55 and 56). The values of relative estimation errors of mean deposit parameters were determined with the block kriging procedure based upon the relative geostatistical models (Tab. 53).

At the applied sampling system the estimation accuracy of mean Au contents in calculation blocks is generally low. For the largest block the relative (standard) errors of mean Au content fall into the range of 18–25% and those of Au linear accumulation (practically equivalent to Au reserves) are between 13 and 24%. From the formal point of view such values correspond to the highest accuracy required for deposit assessment categories C_2 and C_1, respectively.

Estimation accuracy for deposit thickness is only slightly higher that those for above mentioned parameters as the errors are between 13 and 22%.

For calculation blocks 200×200m estimation errors are very high and may exceed even 40%, which indicates highly unsatisfactory accuracy of deposit parameters estimations in too small blocks.

Determination of the minimum number of samples required for presumed accuracy of deposit parameters estimations

Due to the dominance of random component in overall variability of deposit parameters, the sufficiently credible determination of the minimum number of samples required for estimation of mean values of deposit parameters at presumed accuracy can be done with the following formula:

$$N_{min} = t^2 v^2 / \varepsilon^2_{wmax}$$

where: t = 2 – parameter for probability 95%, v – variability coefficient [%], ε_{wmax} – permissible (maximum) relative estimation error of mean values of deposit parameters [%].

In calculations the requirements for deposit assessment categories A, B and C_1 were taken into account for which the permissible estimation errors at probability P = 0.95 are 10%, 20% and 30%, respectively. The determined minimum numbers of samples should guarantee the required estimation accuracy of mean values of deposit parameters at the risk below 5%.

The results of calculations presented in Tab. 57 point out that for estimation of mean Au content and Au reserves under the requirements of the assessment category A the number of samples must be very high – from 530 to 1,309, depending on the part of deposit. It seems however, that for Au, which is only an accompanying element in the Cu-Ag deposit the requirements for assessment category C_1 are fully satisfactory. For this category the minimum number of samples necessary for proper estimation of Au content in the economic-grade deposit is 117 (for exploration areas considered separately: from 88 to 146) and that of linear accumulation index (which practically corresponds to Au reserves) is 97 (from 59 to 103 for particular exploration areas). Thus, it can be proposed that the rough number of about 100 samples should allows us to estimate the Au deposit parameters and reserves in the economic-grade deposit with the accuracy of the assessment category C_1 (Tab. 57).

The determination of spacing grid for sampling in the mine workings requires further information on the considered sampling area, total length of workings and their localization.

Summary and conclusions

1.Variabilities of Au content and linear accumulation index and, to lesser degree, also the deposit thickness can be described as very high or extremely high, and probability distributions of these parameters show strong positive asymmetry. Both variability features are typical of most trace elements hosted in the Cu-Ag deposit of the Lubin-Sieroszowice Copper District and cause serious troubles in accurate estimations of their mean contents and reserves.

2. Variability of [Au] content and its daughter parameters is isotropic, which means that there are no privileged directions in the deposit along which this deposit parameter is clearly more or less diversified than along other directions.

3. The variability structures of [Au] content and [Au] linear accumulation index reveal very high contribution

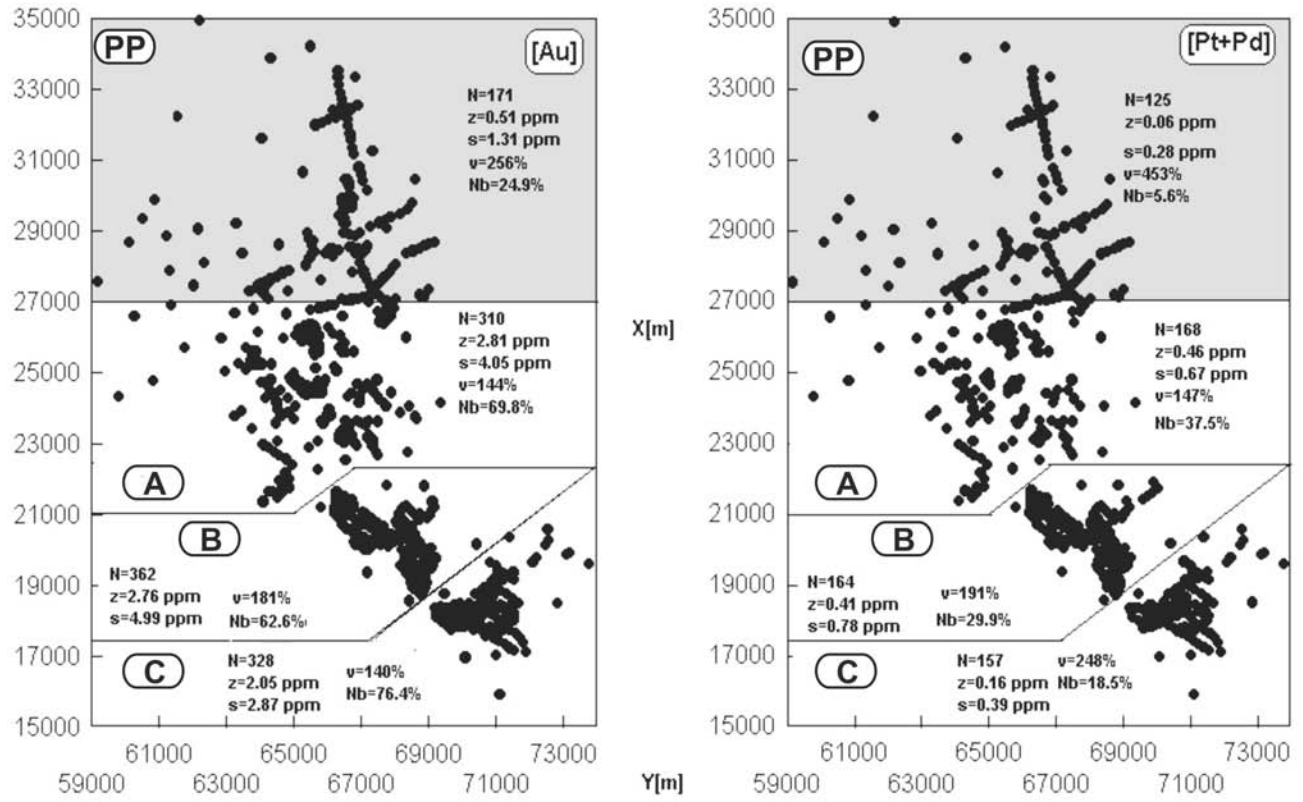

Fig. 96. Samples location for assaying of the gold content [Au] and the platinum and palladium content [Pt+Pd] in the Cu – Ag ore deposit Polkowice-Sieroszowice. PP – sub-economic part of deposit, PB – economic part of the deposit, A, B, C – areas of exploration. N – Number of samples, $\bar{z}$ – arithmetic mean, s – standard deviation, v – coefficient of variation, Nb – proportion of samples with grade above 0.5 ppm

from random component, which justifies in practice the acceptance of random variability model of these parameters and its application for the simple statistical formulae.

4. Significant contribution to the observed variability of [Au] content may originate from the apparent variability resulting from errors of sample preparation for chemical analyses. This assumption has important practical implications for estimation accuracy of Au content and reserves but it must be verified by studies on grain size distribution of samples and on the mode of Au occurrence in products of particular grain-size reduction stages.

5. Estimation accuracy of mean Au contents and Au reserves in small calculation blocks (200×200 m) is very low and meets the requirements only for assessment category D_1 (hypothetical resources). For calculation blocks of areas close to those worked out during 1 year of Cu-Ag ore exploitation (i.e. of dimensions 800×800 m) and at the sampling system applied in this project the estimation accuracy for mean Au content fits only to the criteria of deposit assessment category C_2 and the estimation accuracy of Au reserves corresponds only to that required for assessment category C_1.

6. It seems reasonable (and sufficient for practical purposes) to accept the estimation accuracy of assessment category C_1 (with permissible error 30% at probability level P=95%) for estimations of mean Au contents and Au reserves (regarding Au as an accompanying element in the Cu-Ag deposit). However, such attempt is possible only for calculation blocks in which at least 100 samples were collected.

VARIABILITY MODELING AND ESTIMATION ACCURACY OF (Pt+Pd) CONTENT

Source material

Both the variability description and the accuracy estimation of total PGE (Pt+Pd) contents were based upon somewhat less abundant database than that for Au. The database included the results of chemical analyses of 604 samples collected from the same parts of the Polkowice-Sieroszowice deposit. The distribution of sampling sites for PGE analyses is shown in Fig. 96 with the basic statistical parameters quoted for distinguished areas. For comparison the sketch map of Au sampling sites was included. As for Au, the whole study area was divided into 4 parts corresponding to most dense sampling grids. Moreover, the same names and symbols of the areas were applied, as for Au deposit. Both the statistical and geostatistical analyses were made separately for the selected parts.

The scope and methodology of variability analysis of Pt+Pd contents were identical as for Au (see chapter "*Distribution...*").

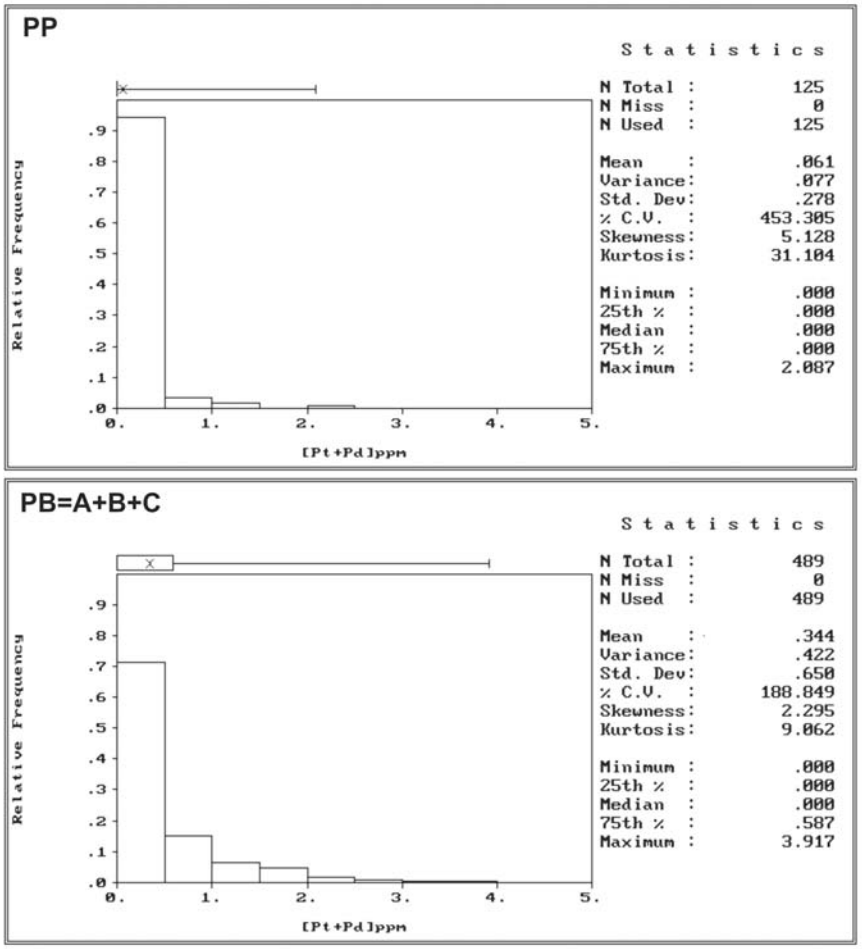

Fig. 97. Histograms of the [Pt+Pd] content in the sub-economic (PP) and economic (PB) parts of the deposit

Statistical characterization of Pt+Pd contents

Results of calculations of principal statistical parameters for Pt+Pd contents in the whole study area and in distinguished parts are listed in Table 58. Probability distributions of Pt+Pd contents are displayed as histograms in Fig. 97.

As concluded from Table 58, the study area is inhomogeneous from the point of view of both the mean Pt+Pd contents and the intensity of their diversification. Only the exploration areas A and B show similarities in statistical parameters. The remaining areas PP and C (particularly the PP) are much lower in PGE, as revealed by lower mean values and by very low percentages of samples in which Pt+Pd contents exceed presumed cut-off value 0.5 ppm. If only the mean values are considered, the distinguished exploration areas show identical regularities in Au and Pt+Pd contents. However, no statistically significant correlations were found for Au and Pt+Pd contents. Variability coefficients for Pt+Pd are higher than those for Au, which suggests that accurate estimations of Pt+Pd mean contents and reserves at the applied sampling density will be even more difficult than in the case of Au. Similarly to Au, distributions of Pt+Pd contents show strong positive asymmetry (Fig. 97) but the variability range of asymmetry coefficient is higher.

Variability structure of Pt+Pd contents

The variability structure of Pt+Pd contents was studied with the directional and isotropic semivariograms to which the theoretical models were fitted. Similarly to Au, directional semivariograms displayed in color map (Fig. 98) did not reveal privileged directions along which the diversity of Pt+Pd contents would be distinctly higher or lower than along other directions. It is a sufficient argument supporting the working hypothesis on isotropic distribution of Pt+Pd contents. Practical consequence of this hypothesis is the investigation of Pt+Pd distribution only with the averaged semivariograms for all directions and their theoretical models, examples of which are shown in Fig. 99. Equations of theoretical models of relative semivariograms are listed in Table 59.

Estimation accuracy for mean Pt+Pd contents

Estimation accuracy of mean Pt+Pd contents was studied with the block kriging method, separately for each of four exploration areas (PP, A, B, C) and in 3 square calculation blocks of various size (500×500 m, 1,000×1,000 m and 2,000×2,000 m) The larger sizes of blocks in comparison with those applied in the estimations of Au contents (see

Table 58

Statistics of Pt+Pd contents in the whole study area and in the exploration areas

Study area	N	N_b [%]	$\bar{z}$ [ppm]	Range [from - to] [ppm]	s [ppm]	v [%]	g_1
Whole study area PB+PP	614	24.1	0.29	0 - 3.92	0.60	210.8	2.58
Economic-grade deposit PB=A+B+C	489	28.8	0.34	0 - 3.92	0.65	188.8	2.30
Exploration area A	331	33.8	0.43	0 - 3.92	0.73	167.4	1.92
Exploration area B	125	5.6	0.06	0 - 2.09	0.28	453.3	5.13
Exploration area C	168	37.5	0.46	0 - 2.83	0.67	147.0	1.30
Exploration sub-area C1	164	29.9	0.41	0 - 3.92	0.78	190.9	2.33
Sub-economic deposit PP	157	18.5	0.16	0 - 2.87	0.39	247.5	3.46

PB – Au economic-grade deposit, PP – Au sub-economic deposit, N – number of data, N_b – percentage of samples with [Pt+Pd]>0.5ppm, $\bar{z}$ – mean content (arithmetic), s – standard deviation, v – variability coefficient, g_1 – asymmetry coefficient

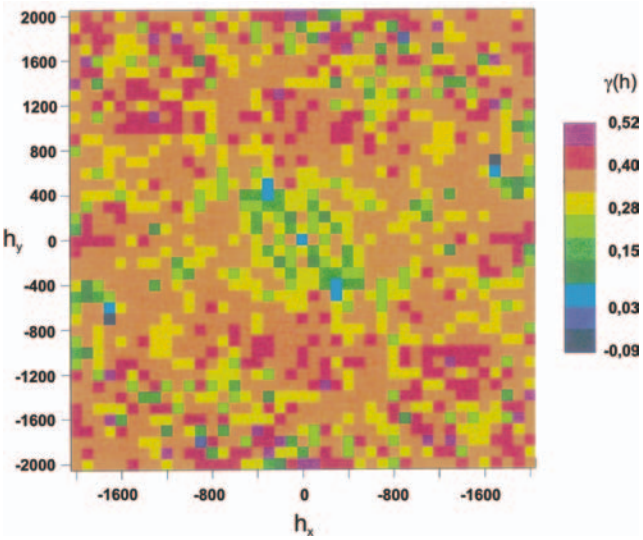

Fig. 98. Map of semivariogram surface of the [Pt+Pd] content

chapter "*Distribution...*") resulted from lower sampling density for PGE, due to which the number of data obtained for 200×200 m blocks appeared to be insufficient. All three blocks of various sizes were concentric. Coordinates of their centers are shown in Tab. 60. Calculations of standard estimation errors of mean Pt+Pd contents were based upon the relative models of variability. Calculations for models of basic semivariograms made for a few cases were treated as controls. Three types of geostatistical models were applied: local (i.e. exclusively for data from a particular area), general (for all data) and models for higher-grade areas conventionally called the economic-grade deposit (PB=A+B+C). The results of calculations are presented in Tab. 60. The largest discrepancies in estimation accuracy were found in the sub-economic area (PP) of lowest Pt+Pd contents. The local model gave estimation errors several times higher than the general model. For the remaining areas estimation errors calculated with geostatistical method are similar. The most credible are the results based upon local geostatistical models. For exploration areas enriched in Pt+Pd (A, B, C) good results are provided also by the general model.

Table 59

Models of relative semivariograms of Pt+Pd contents in the whole study area and in the distinguished exploration areas. For explanation of formulae notations see chapter "*Distribution....*")

Study area	Model equation
Whole study area PB+PP	γ(h)=0.92+3.25sph(h/940)
Economic-grade deposit PB=A+B+C	γ(h)=0.88+2.85sph(h/750)
Exploration area A	γ(h)=0+50sph(h/500)
Exploration area B	γ(h)=0.4+1.75sph(h/600)
Exploration area C	γ(h)=0.15+5.35sph(h/1150)
Exploration sub-area C1	γ(h)=3.2+0.001325h

However, these results have rather low practical importance due to significant standard errors of estimation which, for calculation blocks localized in the A, B and C exploration areas, fall into the range of 24–54% for local models. Low estimation accuracy of mean Pt+Pd contents enables us to categorize the recognition of these metals into the assessment category D_1, thus, their reserves can be regarded only as hypothetical. For the sub-economic area (PP) the calculated errors are unrealistically high: from 174 to 259%, depending on the size of calculation blocks. Generally, the low estimation accuracy of Pt+Pd contents and reserves is caused by their high variability and low contents of metals (particularly in PP area), which influences the relative estimation errors, and by low density of sampling grid.

Determination of the minimum number of samples required for estimation of mean Pt+Pd contents with presumed accuracy

Due to high variability of Pt+Pd contents the minimum number of samples was determined only for the requirements of deposit assessment categories C1 and C2. For higher assessment categories such determination seems to be useless because of huge costs of sampling, sample preparation and chemical analyses. Similarly to Au, the classic

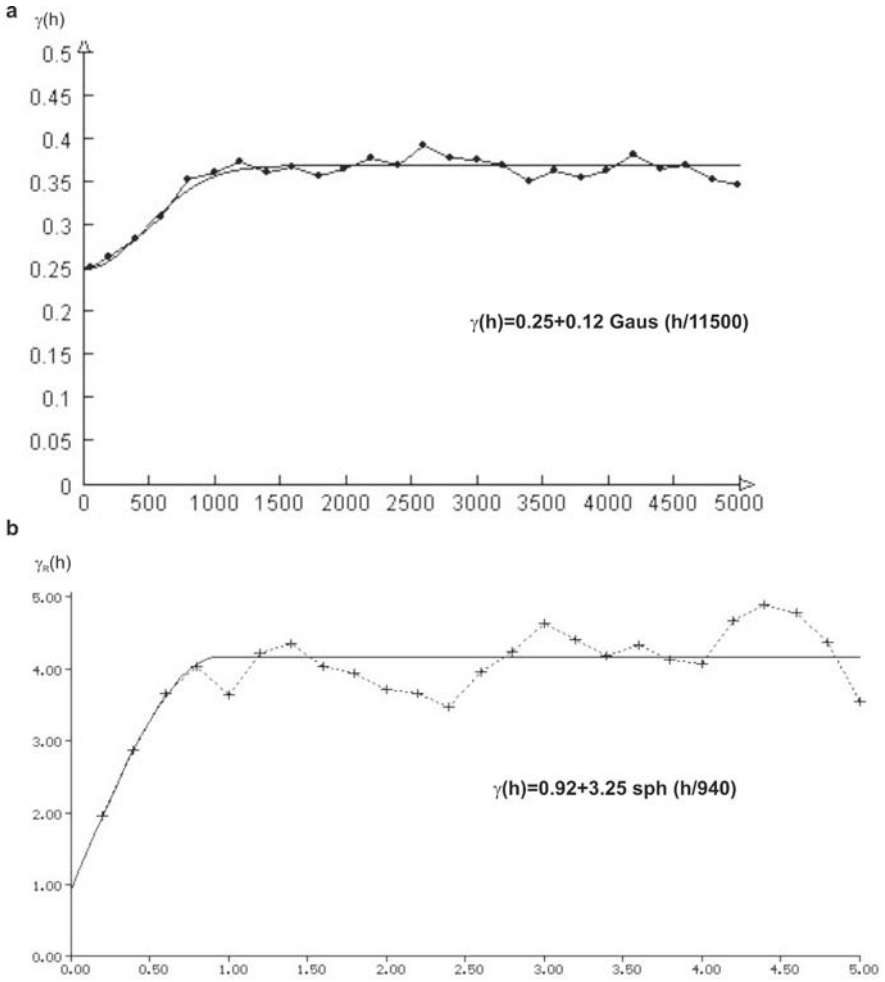

Fig. 99. Semivariogram (a) and relative semivariogram (b) of the [Pt+Pd] content in the economic part of the depositdata (PB+A+B+C)

Table 60

Estimation of relative standard errors of mean [Pt+Pd] contents with the kriging method in calculation blocks of various sizes

Study area(coordinates of the block center)	Block dimensions [m] and number of samples (N)	Local model	General model	Model for PB=A+B+C
Sub economic deposit PP Y_0 = 67000 X_0 = 29000	500×500N=5	259%	69.3%	nc
	1,000×1,000N=16	220%	53.9%	nc
	2,000×2,000N=49	174%	44.1%	nc
Exploration area A Y_0 = 65000 X_0 = 24500	500×500N=18	53.5%	63.3%	65.3%
	1,000×1,000N=39	37.2%	42.7%	44.6%
	2,000×2,000N=64	28.6%	35.7%	35.3%
Exploration area B Y_0 = 67000 X_0 = 20600	500×500N=24	35.0%	43.0%	43.9%
	1,000×1,000N=50	24.3%	27.2%	27.9%
	2,000×2,000N=59	45.7%	41.9%	40.1%
Exploration area C Y_0 = 70800 X_0 = 18200	500×500N=23	42.9%	35.7%	36.4%
	1,000×1,000N=62	28.4%	25.2%	25.9%
	2,000×2,000N=64	30.6%	36.5%	35.5%

Table 61

Minimum number of samples necessary for estimation of Pt+Pd mean contents at the accuracy required for deposit assessment categories C_1 and C_2

Assessment category	Exploration areas						
	Whole study area	PB=A+B+C	A+B	PP	A	B	C
C_1	198	159	125	913	97	162	273
C_2	112	90	71	514	54	92	153

PB – economic-grade deposit, PP – sub-economic deposit

statistical formula was applied for estimation of the number of samples. However, it must be taken into account that the non-random component of variability is more pronounced for Pt+Pd than for Au, which may influence the results. Better results can be expected if geostatistical method is applied but this method requires some additional assumptions concerning the size of area for which Pt+Pd contents are estimated, the development mode of the area with mine workings and the anticipated localization of sampling sites. If these data are lacking the geostatistical kriging method cannot be applied at the recent stage of studies. Hence, the estimations of required number of samples made with the statistical method, presented in Table 61, should be regarded as an approximation.

The results shown in Tab. 61 reveal enormous dispersion of prognozed amounts of samples – from 97 to 913 (from 97 to 273 for economic deposit PB) for assessment category C_1 and from 54 to 514 (from 54 to 153 for economic deposit PB) for assessment category C_2. Extremely high numbers of samples were estimated for the area of lowest Pt+Pd contents (sub-economic deposit PP). This low-grade deposit should not be taken as a reference level for estimation of sample numbers as it requires several times higher density of sampling grid. If the sub-economic deposit PP is excluded, the accuracy required for the assessment category C_1 implies the collection of about 160 samples from the higher-grade parts of the deposit (where mean Pt+Pd contents are over 0.1ppm). For the assessment category C_2 about 90 samples should be taken. Therefore, the proposed number of samples for Au reserves assessment (100 for assessment category C_1) should ensure the proper estimation of Pt+Pd reserves in the assessment category C_2.

Summary and conclusions

1. The Pt+Pd contents reveal higher variability that those of Au and can be described qualitatively as extremely high.

2. Similarly to Au, the variability of Pt+Pd contents in the study area is isotropic, i.e. the intensity of content changes in all directions is similar.

3. The relative models of Pt+Pd semivariograms show higher diversity and much stronger non-random component than Au semivariograms.

4. Similarly to Au, detailed studies (also quantitative) should be undertaken on grain size of collected samples and on the forms of Au occurrence. These results would enable us to estimate the sample preparation error and its importance for the estimation accuracy of Pt+Pd mean contents and reserves.

5. With the sampling system applied in this project the estimation accuracy of Pt+Pd contents and reserves in calculation blocks of dimensions 500×500 m, 1,000×1,000 m and 2,000×2,000 m is exceptionally low and is sufficient only for deposit assessment category D_1 (hypothetical resources).

6. The number of about 100 samples approximated with the statistical method should be sufficient for general estimation of Pt+Pd contents and reserves with the accuracy required for assessment categories C_2 with permissible error 40% at probability level P=95% (and for category C_1 for Au contents and reserves with permissible error 30% at probability level P=95%). However, these results should be verified with the geostatistical kriging method when additional information is available, i.e. the size of area of estimation, the distribution of sampling sites and the number of samples to be collected.

GENETIC CONCEPTS ON DEPOSITION OF PRECIOUS METALS

Jadwiga Pieczonka & Adam Piestrzyński

TRANSPORT OF Au AND Pt

The transport of Au in hydrothermal solutions has been discussed in many papers, e.g., Krupp and Weiser (1992), Foster (1993), Piestrzyński and Wodzicki (2000). Their concepts were reviewed by Pieczonka and Piestrzyński (2000) and supplemented by author's opinion.

The behavior of PGE and Au in geological environments is diversified. In the ultrabasics the contents of Au and Pt are similar but only the PGE form economic-grade accumulations (Stenina, 1997). The reason for such fractionation is the structure of outer electron shells of these metals: Pt has one electron less than Au in 5d shell (i.e. $5d^9 6s^1$ in Pt *versus* $5d^{10} 6s^1$ in Au) (Stenina, 1997). Iron is third most widespread cation after Si and Al. In water complexes the replacement of Al and M^+ (multivalence cation) allows to "save" 23 kcal/mol of energy. Moreover, among all transitional metals Fe (electron shell structure $3d^6 4s$) is closest and best partner for Au in the formation of water complexes (Stenina *et al.*, 2001). Such complexes were discovered in hydrothermal solutions of metamorphic provenance. The presence of electron vacancy in 5d shell of Pt atoms releases positive charge, which secures the internal electrovalent bond and hampers the complexing of Pt with

other elements (Stenina, 1997). Therefore, the joint migration of Au and Fe is very probable and may lead to the accumulation of both elements at the same site. On the contrary to Au, Pt is more inert in chemical reactions. Volumes of metals transported in water systems require their uniform energetic structure in relation to other complexing compounds (Stenina, 1997). Among the PGE only Ru, Rh and Pd show behaviors similar to Fe. Hence, these metals may migrate for much longer distances than the remaining PGE.

According to Piestrzyński *et al.* (1996a) and Piestrzyński and Wodzicki (2000), the most probable is the transport of Au in thiosulphate complexes $\{Au(S_2O_3)_2^{-3}\}$. These compounds are stable at temperatures below 200°C, i.e., corresponding to crystallization temperature of Cu-sulphides in the Fore-Sudetic Monocline deposit. Au can be dissolved as thiosulphate complex according the reaction (Krupp & Weiser, 1992):

$$Au + 2S_2O_3^{-2} + H^+ + 1/4O_2 = Au(S_2O_3)_2^{-3} + 1/2H_2O$$

According to Piestrzyński *et al.* (1996a), thiosulphate complexes formed close to the sulphide/sulphate equilibrium boundary and dissolved Au. The sources of Au were clastic basement rocks. Metal was then transported with ascending oxidizing solutions. Bierlein *et al.* (1997) reported that 50% extraction of Au (20 ppb) from clastic rock slab of size 20x50 km and 10 m thick may lead to deposition of 600 t Au. Due to energetic similarity of Au and Fe, transport of these metals in thiosulphate complexes is very probable. Thus, such a complex may have formula $(FeAu)(S_2O_3)_2^{-1}$, which explains the joint precipitation of Au and hematite variety called "hydrothermal hematite" by Piestrzyński *et al.*, (2002). The chemically inert character of PGE results in much limited accumulation of these metals in the environment of Au precipitation. This precipitation occurred when solution entered the stability field of sulphates. The abrupt change of P and T is necessary to break the gold complexes, which took place at the contact with the Cu deposit representing the reducing environment. Such reactions may release sulphur, which contributes to further breakdown of the complexes (Stenina, 1997). The result of such reactions is the coexistence of sulphides, native Au and hematite. Oxidizing solution which migrated through the sandstone and the Kupferschiefer successively dissolved Au hosted in these rocks. Therefore, the highest concentrations of Au should correlate with the maximum thickness of clastic pile. Paragenesis of native Au with covellite and hematite found at the boundary between the oxidizing and the reducing environments confirms the theory of Au transport in thiosulphate complexes (Piestrzyński *et al.*, 1996a; Piestrzyński & Wodzicki, 2000).

Piestrzyński and Pieczonka (1998) proposed two other models of Au deposition in these zones. The first model includes selective precipitation of Au from suspension which was in equilibrium with the enclosing rocks. Such a process supplied collomorph-type Au. The second model comprises the transport of Au as polysulphide complexes in reducing solutions derived from the overlying evaporites. The polysulphides were subsequently oxidized during downward migration. Such model is supported by the native Au-hematite paragenesis described above from the carbonate rocks. The model is correct from the point of view of thermodynamics, however, no structural evidence has been found up to date for such reactions. Reducing solutions carrying the polysulphides might have been easily oxidized in the zone of red spots occurrence. However, the accumulation of most part of Au (about 75%) in the sandstone indicates that the decisive role in Au transport was played by oxidizing solutions ascending from the basement rocks. Moreover, the amount of Au in the deposit is too high to be sourced in the Lower Zechstein sediments (Piestrzyński & Wodzicki, 2000).

RELATIONSHIPS WITH THE TECTONICS

It appears difficult to evaluate the role of tectonics in the formation of Au deposit. Up to now, the southern boundary of Au concentrations has not been recognized as this part of Cu deposit has not been developed, as yet. Determination of this boundary may contribute to the modeling of Au source and transport. It is very probable that the zones with high Au concentrations extend as far as to the Fore-Sudetic Block.

The mining sectors with high contents of Au form a NW–SE-trending belt (Fig. 78–80 i 100). The coexistence of these sectors with the number of faults have not been proven. Moreover, the arrangement of Au-bearing zones in relation to the strikes of fault systems is highly variable and presumably depends on the transfer rate of oxidizing solution through the rocks surrounding the fault as well as on the rate of its gradual change of solution milieu from oxidizing to reducing. Hence, the main role is played by the chemistry and the physical properties of rocks. Undoubtedly, faults were important patches for the transfer of oxidizing solutions from deep basement but the formation of Au concentrations in such sites is rather improbable due to oxidizing conditions dominating in their vicinity.

Small faults visible in cross-sections (Figs 81–85) did not influence the formation of precious metals concentrations as high contents of these metals occur in their vicinity and at large distances from the dislocations. Faults cause only insignificant displacements of rocks in the Cu deposit and in the Au-bearing horizons, which may suggest the post-ore character of these type tectonics.

RELATIONSHIP TO THE Cu DEPOSIT

The results obtained up to date led to the genetic model of Au concentration in the oxidized zones of the Polkowice-Sieroszowice deposit (Figs 101, 102). This model is valid for the current research stage and will evolve in the future with the progressing development of the deposit. Considering the fact that Au accumulates at the bottom of Cu deposit (Fig. 101), the origin of its concentrations is closely related to the specific stage of Cu deposit formation. The succession of geological processes leading to the formation of Cu deposit and to the accumulation of Au in the studied part of the mine area is shown in Fig. 102. It is difficult to determine unequivocally at which stage of Cu deposit formation

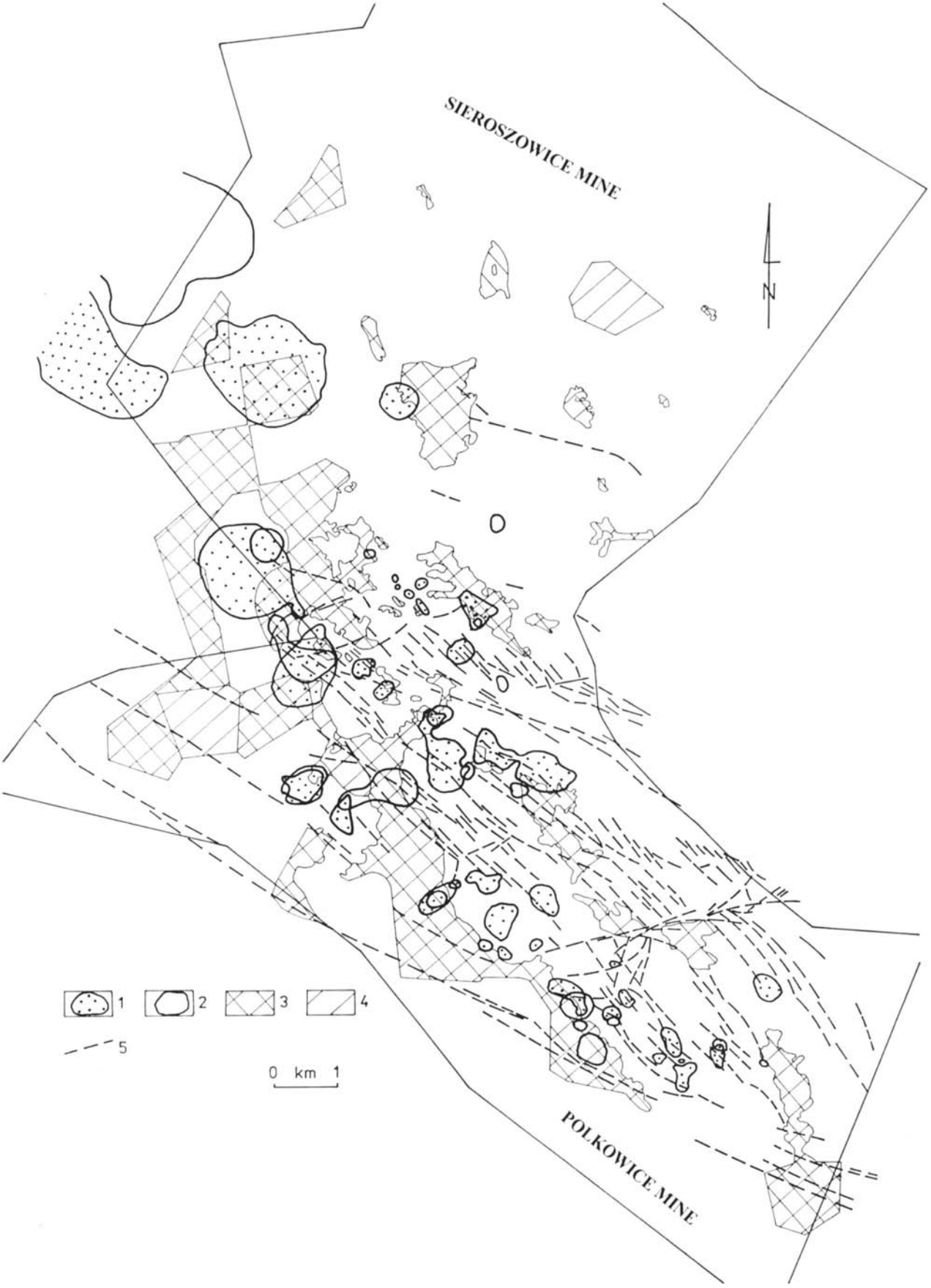

Fig. 100. Superposition map of rich gold and PGM fields on the back ground of basic tectonics. *1* – area with minimum content of Au = 2 ppm, *2* – area with minimum content of Pt + Pd = 1 ppm, *3* – area without economic copper deposit, *4* – area with sub-economic copper deposit, *5* – documented faults

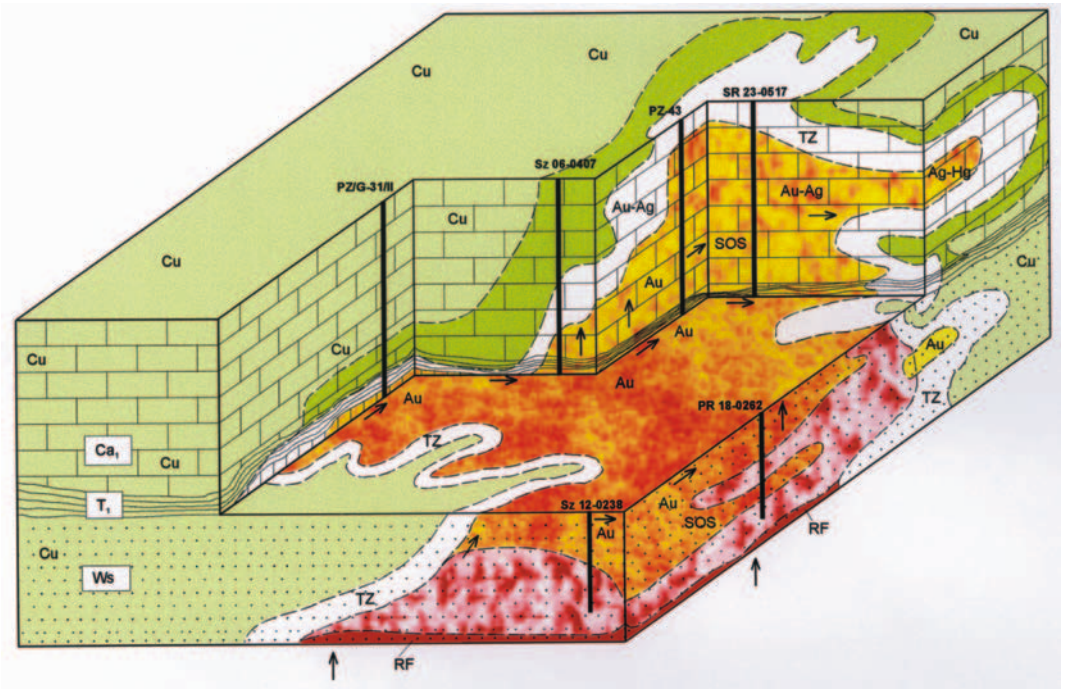

Fig. 101. 3-D model of gold deposit. Lithology is as shown in Fig. 2. Sz 06-0407 – position of channel sampling, pale green – copper deposit (Cu), dark green – secondary enrichment in copper, white – transition zone (TZ), yellow – gold deposit (Au), red – oxidation environment, SOS – secondary oxidizing system, RF (rote Fäule) – primary oxidizing system (after Pieczonka & Piestrzyński, 2000)

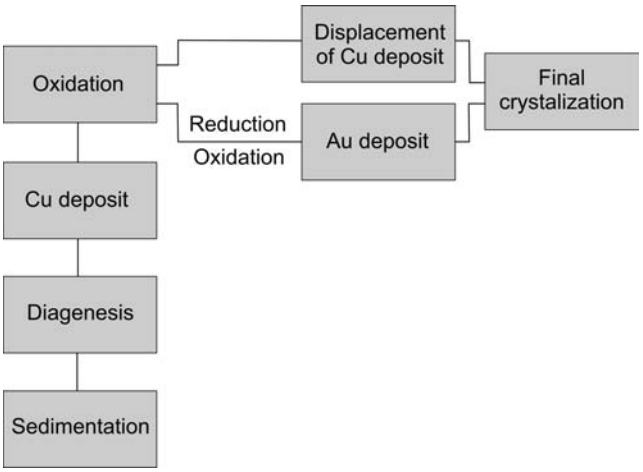

Fig. 102. Transformation of host rocks in the Lubin – Sieroszowice mining area

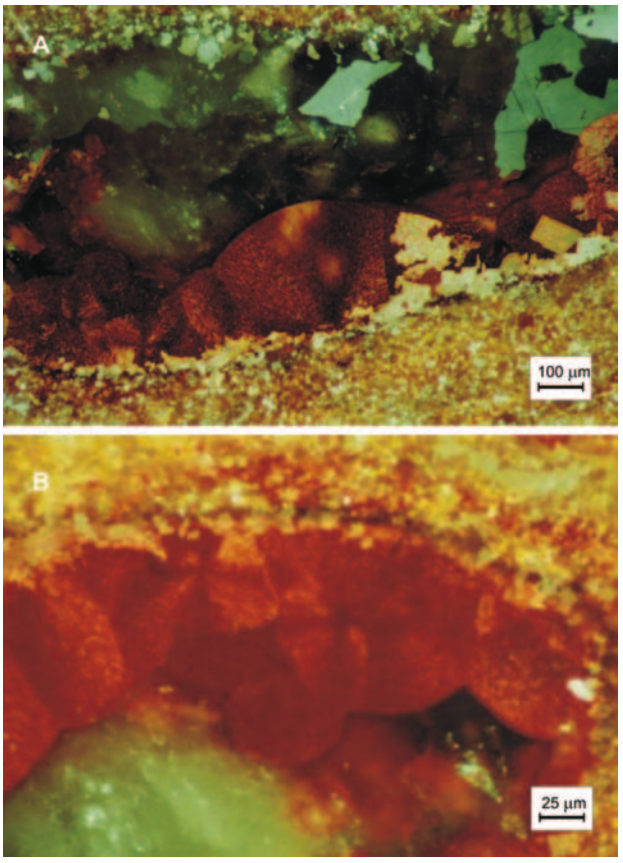

Fig. 103. Microphotographs in reflected light and crossed nicols showing final effect of the SOS activity. **A** – young, colloform aragonite colored in red by fine dispersed hydrothermal hematite, sample PZ-J-7; **B** – enlarged fragment of phot. A

the concentration of Au has commenced. In the Au-bearing zones the processes of sedimentation, diagenesis and formation of economic-grade Cu accumulation were identical as in the other parts of the Fore-Sudetic Monocline deposit. After formation of Cu deposit the oxidation processes have commenced, which were main factors leading to the formation of Au accumulations. Comparison of macroscopic physical properties, mineralogical and chemical composition of rocks from the oxidized and the Cu-bearing zones enabled the authors to reconstruct the processes leading to concentration of Au. After crystallization of Au minerals the final crystallization of sulphides from residual solution

in the transitional zone and in the youngest systems of cracks took place. The final stage of oxidation zone evolution was crystallization of collomorph calcites with small admixtures of Mg and with fine inclusions of hematite (Fig. 103).

ECONOMIC VALUE OF GOLD DEPOSIT IN THE FORE-SUDETIC MONOCLINE

Adam Piestrzyński

The preliminary economic evaluation of Au deposit was presented in the report from the research project run at the AGH-University of Science and Technology in 1997. This evaluation included the results of studies carried on in the years 1995–1996 and 1997. Results of the following project confirmed the extension of the zone enriched in precious metals into the newly developed mining fields (see chapter "*Distribution...*"). All collected data indicate the presence of the zone secondary enriched in precious metals beneath the Cu deposit and in its vicinity. The average thickness of this deposit is 0.23 m (Report AGH, 1997; Piestrzyński & Pieczonka, 1997a; Piestrzyński *et al.*, 2002) and average grade is 2.37 g Au/Mg (Report AGH, 1997; Piestrzyński & Pieczonka, 1997a). The measured Au reserves are **34.328 Mg** (worthy **442.9 mln USD** at Au price 400 USD/oz, February 2004). The inferred Au reserves are **51.56 Mg** (worthy **665.124 mln USD**) and the inferred Pt+Pd reserves amount **12.18 Mg** (worthy **196.45 mln USD**) (Report AGH, 1997; Piestrzyński & Pieczonka, 1997a). Taking into account 50% recovery of PGE minerals, the industrial value of accumulated Pt+Pd is about 98 mln USD. Hence, the cumulative value of precious metals hosted in calculation blocks (i.e. in the part of potential area of Au deposit, Tab. 62) amounts 442.9+98.0 = **540.9 mln USD**. According to bank experts, Au prices will rise due to instability of the market and general increase in demand for mineral raw-materials. At the end of 2005 the prices of precious metals raised for next 20%. In 2008 it is already clear, that prognoses for 2005 was correct, and we observer further increase of precious metals prices. The worthy of gold reserves for the price 959.8 USD/oz (29.02.2008) is 1062.284 mln USD and 1596.360 mln USD respectively. The worthy of Pt+Pd resources increases in 2008 up to 264.030 mln USD.

All the results obtained up to date confirm the extension of the precious metals zone outside the recently developed Cu deposit. The northern contour of the zone has already been defined (Report AGH, 1996, 1997; Piestrzyński & Pieczonka, 1997a) whereas the southern contour still remains unknown. Examination of samples collected from the southern part of Cu deposit (close to the Fore-Sudetic Block) revealed Au contents above 0.5 g/Mg. However, available data do not allow the authors to define precisely the southern boundary of precious metal deposit, close to the southern range of Lower Zechstein strata.

In order to determine the dressing properties of precious metals, the pilot concentration test has been carried on for 1 Mg samples using gravity separation and froth flotation methods (Report AGH, 1997; Piestrzyński & Pieczonka, 1997a). It was followed by the industrial-scale froth flotation test made on 12,882 Mg sample (known as "The Easter Test", run on April 12–13, 1998) (Wieniewski *et al.*, 1998). Similar dressing tests were made at the Wrocław Technical University (Łuszczkiewicz, 1998). The results demonstra- ted that good and very good Au concentrates can be obtained with traditional methods (gravity separation, froth flotation) (Łuszczkiewicz, 1998). However, the same methods applied for Pt and Pd concentration gave poor results (Łuszczkiewicz, 1998). On the contrary, very promissing effects for all precious metals were obtained with the pressure cyanide leaching process (up to 98–99% recovery, Chmielewski, 1998).

Both the microscopic studies and the chemical analyses revealed the presence of Au in the economic-grade copper ore. Here, gold should be regarded as a trace element accompanying the main commodity, i.e. copper. However, gold forms also a dispersion aureole around the zone of precious metals accumulation, which is located beneath the copper deposit. Hence, the precious metals (mainly Au) must be accepted as accompanying commodities in relation to copper. The results demonstrated that outside the currently mined copper orebody the zones exist, which enrichment in precious metals permits their classification as Au deposit. The Cu grade in these zones is low (<0.2 wt.%).

The studies on the effectiveness of Au ore dressing (based on industrial-scale pilot test) demonstrated that economically effective recovery of Au requires the "ore" grade over **1.627 g Au/Mg$_{ore}$** (Wieniewski *et al.*, 1998). However, this value is valid only for the ore which grades **1.007 g Au/Mg** and 0.67 wt.% Cu. The ore processed during the industrial-scale pilot test was not that containing the increased amounts of Au but was a mixture of Cu ore (about 30% by mass) and rocks grading 1.6 g Au/Mg and <0.1 wt.% Cu. Taking into account the assumptions made by Wieniewski *et al.*, (1998), and the gold price at the level of **9 mln USD/Mg Au**, the grade of such ore should be **2.47 g Au/Mg** in order to ensure the economic effectiveness of its extraction. Under the same assumptions (Wieniewski *et al.*, 1998) and the gold price **1,136,1290 USD/Mg** (at the exchange rate **1 USD = 3.74 PLN**) the economically effective ore grade should be **2.1 g/Mg**. According to the AGH Report (1997), 50% of ore reserves in calculation blocks, i.e., 17,537 Mg Au worthy 199,237 mln USD, shows average grade over 2.47 g Au/Mg. Thuds, even at this appraisal of average Au content, the studied zone should be regarded as an economic-grade gold deposit. Taking into account, that exchange rate of USD dropt down to the level of 2.48 PLN, and high prices of precious metals increase roughly 3 times, the grade of gold ore could be lower, as estimated above, to receive good results.

At the current Au price (about 12.9 mln USD/Mg) and at USD/PLN exchange rate similar to that quoted above, exploitation of ore grading over **1.72 g Au/Mg** will be profitable. Piestrzyński and Pieczonka (1997a) revealed that 80% of reserves calculation blocks show higher grades. Economic reserves accumulated in these blocks are about 27.4 Mg Au, which is an equivalent of 354 mln USD. This value can be even higher if PGE are recovered. The estimation of PGE value brings some problems as an unequivocal concept

Table 62

Gold reserves in selected calculation blocks (after Piestrzyński & Pieczonka, 1997a)

Calculation block	Grade [g Au/Mg]	Reserves: geostatistical method [kg]	Error [%]	Reserves: average values method [kg]	Difference	Estimation error [%]
A	0.901	2,388.54	64.0	2,256.085	132.455	5.54
B	1.887	1,197.92	32.8	1,257.817	59.897	5.00
C	2.449	566.50	18.0	531.151	35.349	6.23
D	1.829	1,248.75	88.9	2,301.863	1,053.113	84.33
E	3.581	1,743.04	55.9	1,905.276	162.236	9.30
H	5.246	6,612.27	48.5	4,362.048	1,250.222	22.27
I	2.196	2,158.65	165.0	4,167.634	2,008.984	93.06
L	2.078			1,178.445		
M	2.962	4,390.25	57.6	4,801.177	410.927	9.35

of their concentration has not been proposed, as yet. The principal assumption made for all these calculations is the elimination of capital costs of copper mines construction but, from the other side, total amount of Au already recovered in copper metallurgy is about 20 Mg. Moreover, there are significant Au reserves left in the sandstone, which has not been mined due to low Cu grade and which, unfortunately, will never be mined in the future as its reexploatation is impossible. The remaining reserves can be classified as technogenic deposit.

According to the BRGM classification (http://www.gl.rhulac.uk/geode/dbase1.html), gold accumulations are regarded as deposits if minimum total reserves of Au amount 1.0 Mg (class D). The Au deposit hosted in the secondary oxidation zones of the Fore-Sudetic Monocline Cu deposit fall into the class C (50–10 Mg Au). The modern world mining industry extracts Au deposits of minimum grade **1 g Au/Mg** of ore. This criterion is controlled by many factors and is usually dependent on the reserves – the larger reserves, the lower grade at which mining is profitable. The Au and PGE deposit described in this paper meet the world criteria for economic-grade accumulations.

DISCUSSION AND CONCLUSIONS

Jadwiga Pieczonka & Adam Piestrzyński

In the copper deposit of the Fore-Sudetic Monocline the secondary oxidation zones locally host economic-grade gold mineralization with accompanying platinum and palladium. Due to their economic importance, these zones were subjected to comprehensive studies. The results are summarized below.

- Both the spatial distribution and the variable shapes of oxidized zones in the Polkowice-Sieroszowice area advocate their epigenetic origin.
- The red spots – the indicators of oxidizing environment – are of epigenetic origin and were formed by reaction of oxidizing solutions ascending from the basement with the surrounding rocks,
- Both the character and spatial arrangement of red spots suggest at least two stages of red spots formation,
- Oxidizing solutions penetrated the rock complex after the formation of economic-grade copper mineralisation, as revealed by distribution of sulphide mineralisation in relation to the red spots,
- Gold was transported in oxidizing solutions mostly as thiosulphate complexes. Thiosulphates were identified in several samples. The precious metals mineralisation occurs exclusively in the oxidized zones, which are characterized by the lack of copper and other trace metals, typical of the copper deposit,
- The oxidizing solutions dissolved the already formed sulphides. Other metals were then transported together with gold. A part of sulphides and hematite crystallized contemporaneously with the gold, as indicated by the presence of Au in minerals from which native Au forms intergrowths,
- Highest-purity native Au crystallized in the sandstone and in the bottom part of the Kupferschiefer. Up the sequence electrum usually appears, a mineral characteristic for transitional zones,
- When the oxidized zone is more extended vertically, the higher is thickness of gold mineralized horizon, that also hits carbonates. Contents of sulphides in the oxidized zone usually does not exceed 0.5 wt.%.
- Between the oxidized zone and the copper deposit a narrow transitional zone exists, characterized by low content of sulphides and the presence of precious metals,
- Recrystallization of sulphides displaced by oxidizing solutions took place above the transitional zone. Particularly high concentrations of sulphides are observed along the boundary of transitional zone with the copper deposit,
- In the all studied zones veinlets and nests of coarse- crystallize carbonates with sulphide minerals appear, representing the latest mineralisation stage,
- Organic geochemical studies clearly indicated its secondary oxidation. The amount of organic matter in the oxidized zones decreased over 20 times, which supports the concept of secondary oxidation of copper deposit. Carbon dioxide was fixed by the formation of new generation of carbonates, including collomorph varieties with hematite,
- Mineralogical studies revealed the presence of diversified assemblage of precious metals minerals, which includes many phases described for the first time from this deposits

and many other, poorly known minerals which require further studies.

• Microporobe analyses demonstrated the presence of:

– several selenides from which the most common are: naumannite and clausthalite, and less frequent minerals of compositions: Pb_3Se_2 and $AgSe_2$,

– nine Te minerals. Traces of Te in the ore are confirmed by the bulk chemical analyses (ICP),

– fourteen Pd-arsenides from which only five were already described in the literature,

– one Pt mineral only of approximate composition $Pd_{11}Pt(AuAg)_3As_2$, which contains 11 wt.% Pt,

– two unknown natural alloys of approximate compositions BiCu and Bi_2Cu,

– seven new Pd-As-O phases of variable proportions between elements,

– two selenides containing up to 1.3 wt.% Rh. This is the only one reasonable accumulation of PGE members other than Pd and Pt,

– important admixtures of precious metals in accompanying Cu-sulphides, selenides, natural alloys and hematite.

All the results support the concept of the presence of secondary, hydrothermal precious metals deposit, which can be regarded as a new type: the red-bed-related precious metals deposit. Characteristic features of this new type are: discordant position of ore body in relation to lithology, diversified mineralogical and chemical compositions, localization close to the redox boundary and close to the deep fracture of the Odra River tectonic zone.

REFERENCES

Armstrong, M., 1998. *Basic linear geostatistics.* Springer, Berlin, 153 pp.

Banaś, M. & Kijewski, P., 1987. Metale szlachetne w cechsztyńskim złożu rud miedzi w obszarze LGOM. (In Polish). In: *Metale towarzyszące w złożu rud miedzi, stan badań i perspektywy dalszego wykorzystania.* Konferencja naukowo-techniczna w Rydzynie. Komisja do Spraw Polityki Surowcowej NOT, Wrocław, pp. 49–63.

Barrie, C. T., 1995. Magmatic platinum group elements. In: Eckstrand, O.R. *et al.* (eds), *Geology of Canadian Mineral Deposits Types*, Geological Survey of Canada, 8: 605–614.

Barns, S. J. & Francis, D., 1995. The distribution of platinum-group elements, nickel, copper, and gold in the Muskox layered intrusion, Northwest Territories, Canada. *Economic Geology*, 90/1: 135–154.

Bierlein, F. P., Ramsay, W. R. H. & Arne, D. C., 1997. Tholeites and interflow sediments from the Cambrian Heathcote Greenstone Belt, Australia: Sources for gold mineralization in Victoria. In: Papunen, H. (ed.), *Mineral Deposits: Research and Exploration, Where do They Meet? Proceedings of the Fourth Biennial SGA Meeting,* Turku, Finland, Balkema, pp. 145–148.

Błaszczyk, J. K., 1981. Paleomorfologia stropu białego spągowca a miąższość złoża miedzi w piaskowcach. (In Polish). *Rudy i Metale Nieżelazne*, 26: 14–17.

Borg, G., Trdoux, M., Maiden, K. J., Sellschop, J. P. F. & Wayward, O.F.D., 1987. PGE and Au distribution in rift-related volcanics, sediments and stratabound Cu/Ag ores of Middle Proterozoic age in central SWA/Namibia. In: Prichard, H.M. *et al.* (eds), *Geo-Platinum,* Elsevier, Amsterdam, pp. 303–317.

Cabral, A. L., Lehmann, B., Kwitko, R. & Cravo Costa, C. H., 2002. The Serra Pelada Au-Pd-Pt deposit, Carajas mineral province, Northern Brazil: Reconnaissance mineralogy and chemistry of very high grade palladian gold mineralization. *Economic Geol*ogy, 97/5: 1127–1138.

Camisani-Calzolari, F. A., Knox, G., Woodend, A. & Lorenzini, M., 1992. The development of an integrated evaluation system for a Witwatersrand gold mine. In: *Proceedings of the Fourth International Geostatistics Congress, 13-18 September*. Troia, Portugal, pp. 937–951.

Carville, D. P., Leckie, J. F., Moorhead, C. F., Rayner, J. G. & Durbin, A. A., 1990. *Coronation Hill* gold platinum palladium deposit. In: Hughes, F.E. (ed.), *Geology of the mineral deposits of Australia and Papua New Guinea,* Australasian Institute of Mining and Metallurgy Monography, 14: 759–762.

Chakrabarti, D. J. & Laughlin, D. E., 1990. Bi-Cu. In: Massalski, T.B. *et al.* (eds), *Binary alloy phase diagrams. ASM International*, pp. 732–733.

Chernyshov, N. M. & Korobkina, T. P., 1995. New type of platinoid mineralization in the Voronez province: platinoid-bearing highly carbonaceous black shales, Platinum of Russia. (In Russian). Moscow, *Nauka* 2/2: 55–83.

Chiles, J. P. & Liao, H. T., 1992. Estimating the recoverable reserves of gold deposits: Comparison between disjunctive kriging and indicator kriging. In: *Proceedings of the Fourth International Geostatistics Congress, 13-18 September*. Troia, Portugal, pp. 1053–1064.

Clifton, H. E., Hunter, R. E., Swanson, F. J. & Phillips, R. L., 1969. Sample size and meaning full gold analysis. *Geological Survey Professional Paper 625-C*, US Government Office, Washigton, p.17.

Chmielewski, T., 1998. Hydrometalurgiczne odzyskiwanie złota i metali szlachetnych z rud i koncentratów LGOM. (In Polish). *Prace Specjalne Polskiego Towarzystwa Mineralogicznego*, 12: 63–81.

Collier, R. W., 1985. Molybdenum in the northeast Pacific Ocean. *Limnology and Oceanography*, 30: 1351–1354.

Coveney, R. M. & Nansheng, C., 1991. Ni-Mo-PGE-Au-rich ores in Chinese black shale and speculations on possible analogues in the United States. *Mineralium Deposita*, 26/2: 83–88.

Crocket, J. H., 1993. Distribution of gold in the Earth's crust. In: Forster, R.P. (ed.), *Gold metallogeny and exploration,* Chapman & Hall., pp. 1–36.

Czajowski, W., 1987. Występowanie i koncentracja metali towarzyszących w poszczególnych fazach technologicznych produkcji miedzi. (In Polish). In: *Metale towarzyszące w złożu rud miedzi, stan badań i perspektywy dalszego wykorzystania. Konferencja naukowo-techniczna w Rydzynie. Komisja do Spraw Polityki Surowcowej NOT,* Wrocław, pp. 81–100.

Daltry, V. D. C. & Wilson, A. H., 1997. Review of platinum-group mineralogy: composition and elemental associations of the PG-minerals and unidentified PGE-phases. *Mineralogy and Petrology,* 60: 185–229.

David, M., 1977. *Geostatistical ore reserve estimation*. Elsevier SPC, Amsterdam-Oxford-New York, 364 pp.

Deczkowski, Z., 1977. Budowa geologiczna pokrywy permsko-mezozoicznej i jej podłoża we wschodniej części monokliny przedsudeckiej. (In Polish). *Prace Instytutu Geologicznego*, 82: 1–63.

Deverly, F., 1983. Application de la geostatistique aux problèmes d'echantillonage. *Science de la Terre*, *S. Informatique Geolo-*

gique, 18: 27–45.

Distler, V. V., Dyuzhikov, O.A. & Genkin, A. D., 1993. The Talnakh Ore Field: A copper-nickel-platinum giant. *Geology of Ore Deposits*, 35: 1–14.

Dyjor, S., 1978. Wykształcenie i stratygrafia utworów trzeciorzędowych na obszarze legnicko-głogowskim okręgu miedziowego. (In Polish). *Przewodnik L Zjazdu Polskiego Towarzystwa Geologicznego*, Zielona Góra, pp. 210–214.

Eckstrand, O. R., 1995. Magmatic nickel-copper-platinum group elements. In: Eckstrand, O.R. *et al.* (eds), *Geology of Canadian Mineral Deposits Types*, *Geological Survey of Canada,* 8: 583–605.

Espitalié, J., Laporte, J., Madec, M., Marquis, F., Leplat, P., Paulet, J. & Boutefeu, A., 1977. Méthode rapide de characterisation des roches mères, leur potential petrolier et de leur degré d'evolution. *Rev. IFP*, 32: 23 – 42.

Espitalié, J., Deroo, G. & Marquis, F., 1985. La pyrolyse Rock Eval et ses applications. *Revue IFP*, 40, 41: 563 – 579, 755 – 784.

Fan, D., 1983. Polyelements in the Lower Cambrian black shales series in Southern China. In: Augustithis, S.S. (ed.), *The significance of trace metals in solving petrogenetic problems and controversies*: Athens, Theophrastus Publications, pp. 447–474.

Foster, R. P., 1993. *Gold metallogeny and exploration*. Chapman & Hall., 432 pp.

Fulda, E., 1928. The problem of copper shale. *Jahrbuch Preussische Geologie, L-A*, 49.

Gillitzer, C., 1936. The geology of ore enrichments in the copper shale of the Central Germany. *Jahrbuch Halle Verb.,* 15: 1–19.

Goble, R. J., 1980. Copper sulphides from Alberta: yarrowite Cu_9S_8 and spionkopite $Cu_{39}S_{28}$. *The Canadian Mineralogist,* 18: 511–518.

Goble, R. J., 1981. Then leaching of copper from anilite and the production of a metastable copper sulphide structure. *The Canadian Mineralogist,* 19: 583–591.

Gy, P., 1983. Les erreurs d'echantillonage. *Analysis*, 11/ 9: 413–440.

Harańczyk, Cz., 1972. Mineralizacja kruszcowa dolnocechsztyńskich osadów euksynicznych monokliny przedsudeckiej. (In Polish). *Archiwum Mineralogiczne,* XXX: 1–172.

Harańczyk, C. & Jarosz, J., 1966. Wtórne minerały w osadowym złożu miedzi. (In Polish). *Rudy i Metale Nieżel*azne*,* 6: 290–296.

Harańczyk, C. & Bryniarska, J., 1967. Badania stromeyerytu miedziowego z Lubina. (In Polish). *Rudy i Metale Nieżel*azne, 12: 408–412.

Hudson, D. R., 1986. Platinum-group minerals from the Kambalda nickel deposits, Western Australia. *Economic Geol*ogy, 81/5: 1218–1225.

Hunt, J. M., 1979. *Petroleum geochemistry and geology.* W.H. Freeman, San Francisco, 617 pp.

Hunt, J. M., 1996. *Petroleum geochemistry and geology.* W.H. Freeman and Company, New York, 743 pp.

Hulbert, L., Carne, R. C., Gregoire, D. C. & Paktunc, D., 1992. Sedimentary nickel, zinc and platinum group element mineralization in Devonian black shales at the Nick property, Yukon, Canada: A new deposit type. *Exploration and Mining Geology,* 1: 39–62.

Inan, E. E. & Einaudi, M. T., 2002. Nukundamit ($Cu_{3.38}Fe_{0.62}S_4$) bearing copper ore in the Bingham porphyry deposit, Utah: Result of upflow through quartzite. *Economic Geol*ogy, 97/3: 499–515.

Isaaks, E. H. & Srivastava, R. M., 1989. *An Introduction to Applied Geostatistics.* Oxford University Press, New York, 561 pp.

Jacobs, L., Emerson, S. & Huested, S. S., 1987. Trace metal chemistry of the Cariaco trench. *Deep-Sea Research*, 34: 965–981.

Janczyszyn, J., Loska, L., Mayer, W., Piestrzyński, A. & Domańska, G., 1986. Badania łupków miedzionośnych metodą neutronowej analizy aktywacyjnej ze szczególnym uwzględnieniem metali szlachetnych, pierwiastków ziem rzadkich oraz uranu i toru. (In Polish). *Gospodarka Surowcami Mineralnymi*, 2/3-4: 483–496.

Jarosz, J., 1966. Minerały z grupy stromeyerytu w piaskowcach miedzionośnych. (In Polish). *Rudy i Metale Nieżel*azne, 11: 464–465.

Jerzykiewicz, T., Kijewski, P., Mroczkowski, J. & Teisseyre, A. K., 1976. Geneza osadów białego spągowca monokliny przedsudeckiej. (In Polish, English summary). *Geologia Sudetica*, 11(1): 57–89.

Journel, A. C. & Huijbregts, Ch.J., 1978. *Mining Geostatistics*. Academic Press., London, 600 pp.

Jowett, E. C., 1986. Genesis of Kupferschiefer Cu-Ag deposits by convective flow of Rotliegendes brines during Triassic rifting. *Economic Geology*, 81: 1823–1837.

Jowett, E. C., Roth, T., Rydzewski, A. & Oszczepalski, S., 1991. "Background" 34S values of Kupferschiefer sulphides in Poland: Pyrite-markasite nodules. *Mineralium Deposita,* 26: 89–98.

Jung, W., 1960. The conditions of sedimentation during the Upper Rotliegendes and the Zechstein times in SE Fore-Harz region. *Zeitschrift für angewandte Geologie, 6*/12: 598–604.

Jung, W. & Knitzschke G., 1976. Kupferschiefer in the German Democratic Republic (GDR) with special references to the Kupferschiefer deposits in the southeastern Harz foreland. In: Wolf, K.H. (ed.), *Handbook of strata-bound and stratiform ore deposits,* Elsevier, Amsterdam, 6: 353–406.

Juroszek, C., Kłapciński, J. & Sachanbiński, M., 1981. Wulkanity dolnego permu południowej części monokliny przedsudeckiej i perykliny Żar. (In Polish, English summary). *Rocznik Polskiego Towarzystwa Geologicznego*, 51: 517–544.

Karakaya, I. & Thompson, W.T., 1990. Ag-Se. In: Massalski, T. B. *et al.* (eds), Binary alloy phase diagrams, *ASM International*, pp. 88–92.

Kautzch, E., 1942. Untersuchungsergebnisse über die Metallverteilung im Kupferschiefer. *Archivum Lagerstättenforsch.,* Berlin, 74 pp.

Kerswill, J. A., 1995. Iron-formation-hosted stratabound gold. In: Eckstrand, O.R. *et al.* (eds), *Geology of Canadian Mineral Deposits Types*, *Geological Survey of Canada,* 8: 367–382.

Kijewski, P. & Jarosz J., 1987. Mineralizacja kruszcowa i formy występowania pierwiastków towarzyszących w złożu rud miedzi. (In Polish). In: *Metale towarzyszące w złożu rud miedzi, stan badań i perspektywy dalszego wykorzystania*. Konferencja naukowo-techniczna w Rydzynie. Komisja do Spraw Polityki Surowcowej NOT, Wrocław, pp. 21–47.

Kim, Y. C., Medhi, P. K. & Roditis, I. S., 1987. Performance evaluation of indicator kriging in a gold deposit. *Mining Engineering*, 39/10: 947–952.

Kłapciński, J., 1958. Trias na północny-wschód od wału przedsudeckiego. (In Polish, English summary). *Rocznik Polskiego Towarzystwa Geologicznego,* 28: 361–408.

Kłapciński, J., 1964. Stratygrafia cechsztynu okolic Lubina, Sieroszowic i Wschowy (monoklina przedsudecka). (In Polish, English summary). *Rocznik Polskiego Towarzystwa Geologicznego*, 34: 65–93.

Kłapciński, J., 1966. Stratygrafia anhydrytów Werra w rejonie Lubina i Sieroszowic (monoklina przedsudecka). (In Polish,

English summary). *Rocznik Polskiego Towarzystwa Geologicznego*, 36: 65–78.

Kłapciński, J., 1967. Stratygrafia anhydrytów Stassfurt w rejonie Lubina i Sieroszowic. (In Polish, English summary). *Kwartalnik Geologiczny*, 11: 303–311.

Kłapciński, J., 1971. Litologia, fauna, stratygrafia i paleogeografia permu monokliny przedsudeckiej. (In Polish, English summary). *Geologia Sudetica*, 5: 1–135.

Kłapciński, J., 1986. The Leine Anhydrite of the Polish Zechstein: a significant lithostratigraphical marker-unit. *Geological Society London, Special Publication*, 22: 217–222.

Kłapciński, J., 1991. Zechstein anhydrites in western Poland**.** *Zentralblatt für Mineralogie, Geologie und Paläontologie*, I/4: 1171–1188.

Kłapciński, J. & Peryt, T. M., 1996. Budowa geologiczna monokliny przedsudeckiej. (In Polish). In: Piestrzyński, A. *et al.* (eds), *Monografia KGHM Polska Miedź S.A.*, pp. 75–88.

Kłapciński, J., Juroszek, C. & Sachanbiński, M., 1975. Nowe dane o geologii fundamentu krystalicznego obszaru przedsudeckiego. (In Polish, English summary). *Geologia Sudetica*, 10 (2): 7–46.

Kłapciński, J., Juroszek, Cz. & Sachanbiński, M., 1988. Wulkanity dolnego permu północnej części monokliny przedsudeckiej. (In Polish, English summary). *Acta Universitatis Wratislaviensis, 875*, *Prace Geologiczno-Mineralogiczne*, 11(1)*:* 3–31.

Kłapciński, J., Konstantynowicz, E., Salski, W., Kienig, E., Preidl, M., Dubiński, K. & Drozdowski S., 1984. *Atlas obszaru miedzionośnego (monoklina przedsudecka).* (In Polish). Wydawnictwo "Śląsk", Katowice.

Koblański, A., 1996. Budowa geologiczna podłoża monokliny w ujęciu geofizycznym. (In Polish). In: A. Piestrzyński *et al.* (eds), *Monografia KGHM Polska Miedź S.A*., pp. 109–114.

Konstantynowicz, E., 1965. Mineralizacja utworów cechsztynu niecki północno-sudeckiej (Dolny Śląsk). (In Polish, English summary). *Prace Geologiczne Komisji Nauk Geologicznych PAN, Oddział w Krakowie*, 18: 1–99.

Konstantynowicz, E., 1971. Geologia złóż rud miedzi i przejawów miedzionośnych w Polsce. (In Polish). In: Konstantynowicz, E. (ed.), *Monografia przemysłu miedziowego w Polsce*, Wyd. Geol., Warszawa, 432 pp.

Kotarba, M. & Szafran, S., 1985. Zastosowanie analizatorów Rock-Eval i Oil Show w poszukiwaniach naftowych. (In Polish). *Nafta*, 41: 81–88.

Kotarba, M. J., Peryt, T. M., Kosakowski, P. & Więcław, D., 2006. Organic geochemistry, depositional history and hydrocarbon generation modelling of the Upper Permian Kupferschiefer and Zechstein Limestone strata in south-west Poland. *Marine Petrol. Geol.*, 23: 371–386.

Krasoń, J., 1964. Podział stratygraficzny cechsztynu północnosudeckiego w świetle badań facjalnych. (In Polish). *Geologia Sudetica,* 1: 221–255.

Krasoń, J. & Grodzicki, A., 1964. Uwagi o genezie, wieku i mineralizacji białego spągowca. (In Polish). *Przegląd Geologiczny*, 12: 323–325.

Krasoń, J. & Grodzicki, A., 1965. Die Sedimentations-und Mineralisationsbedingungen des "Weissliegenden" in Dolny Śląsk (VR Polen). In: *Freiberger Forschungshefte, Kupferschiefer und "Rote Fäule*", C 193: 183–195.

Krige, D. G., 1968. Rol matematicheskoy statistiki w metodakh utochnennoy otsenki promyshhlennogo orudenenia na rudnikach Yuzhnoy Afriki. (In Russian). *Voprosy matematicheskoj gieologii*, Nauka, AN SSSR, Leningrad, pp. 252–272.

Krige, D. G., 1976. Some basic cosiderations in the application of geostatistics to the evaluation of ore in South African gold mines. *Journal of the South African Institute of Mining and Metallurgy*, 76/9: 383 – 391.

Krige, D. H., 1978. Obzor nekotorykh geostatisticheskich modeley dla otsenki zolotonosnykh rud w Yuzhnoy Afrikie. (In Russian). *Issledowania po matematicheskoj geołogii*. Nauka, AN SSSR, Leningrad, pp. 124–133.

Krige, D. G. & Ueckermann, H. J., 1963. Value contours in improved regressions techniques for ore reserve valuations. *Journal of the South African Institute of Mining and Metallurgy*, Johannesburg, pp. 429–452.

Krup, R. E. & Weiser, T., 1992. On the stability of gold-silver alloys in the weathering environment. *Mineralium Deposita*, 27: 268–275.

Kucha, H., 1973. Organiczne związki złota w łupku miedzionośnym z monokliny przedsudeckiej. (In Polish). *Rudy i Metale Nieżelazne*, 6: 302–303.

Kucha, H., 1974: Złoto rodzime w złożach miedzi na monoklinie przedsudeckiej. (In Polish). *Rudy i Metale Nieżelazne,* 4: 174–175.

Kucha, H., 1975. Preliminary report on the occurrence of palladium minerals in Zechstein rocks of the Fore-Sudetic Monocline. *Mineralogia Polonica,* 6/2: 87–92.

Kucha, H., 1976a. Platyna, pallad, rtęć i złoto w utworach cechsztyńskich monokliny przedsudeckiej. (In Polish). *Rudy i Metale Nieżelazne*, 1: 24–26.

Kucha, H., 1976b. Materia organiczna Au, Ni i Co w utworach cechsztynu monokliny przedsudeckiej. (In Polish, English summary). *Rocznik Polskiego Towarzystwa Geologicznego*, 46: 369–417.

Kucha, H., 1981. Precious metal, alloys and organic matter in the Zechstein copper deposits, Poland. *TMPM Tschermaks Mineralogische und Petrographische Mitteilungen*, 28: 1–16.

Kucha, H., 1982a. Platinum-group metals in the Zechstein copper deposits, Poland. *Economic Geology,* 77: 1578–1591.

Kucha, H., 1982b. Rozmieszczenie złota i metali grupy platyny w złożach miedzi na monoklinie przedsudeckiej. (In Polish). *Rudy i Metale Nieżelazne,* 5: 211–213.

Kucha, H., 1984. Palladium minerals in the Zechstein copper deposits in Poland. *Chemie der Erde,* 43: 27–43.

Kucha, H., 1986. Eugenite, $Ag_{11}Hg_2$ – a new mineral from Zechstein copper deposits in Poland. *Mineralogia Polon*ica, 17(2): 3–12.

Kucha, H., 1995. Redefinition of Rote Fäule, Kupferschiefer, Poland. In: Pasava, J., Kribek, B. & Zak, K. (eds), *Mineral deposits from their origin to their environmental impacts. Proceedings of the III Biennial SGA Meeting,* Balkema, Prague, pp. 953–965.

Kucha, H. & Pocheć. J., 1983. Organogeniczny wapień ankerytowy z glaukonitem i metalami rodzimymi Au, Pt, Pd i Pb z rejonu Lubina Zachodniego. (In Polish, English summary). *Rocznik Polskiego Towarzystwa Geologicznego*, 53: 169–176.

Kucha, H. & Pawlikowski, M., 1986. Two brine model of the genesis of strata-bound Zechstein deposits (Kupferschiefer Type), Poland. *Mineralium Deposita,* 21: 70–80.

Kucha, H. & Piestrzyński A., 1991. The role of thiosulphates in the accumulation of sulphur and metals in Kupferschiefer, Poland. In: Pagel, M. & Leroy, J. L. (eds), *Source, Transport and Deposition of Metals,* pp. 197–200.

Kucha, H. & Mayer, W., 1996. Geochemia. (In Polish). W: Piestrzyński, A. *et al.* (eds), *Monografia KGHM Polska Miedź S.A.*, pp. 237–251.

Kucha, H. & Przybyłowicz, W., 1999. Noble metals in organic matter and clay-organic matrices, Kupferschiefer, Poland. *Economic Geology*, 94: 1137–1162.

Kucha, H. & Plimer, J., 2001. Au-silicates from mesothermal gold deposits. In: Piestrzyński A. *et al.* (eds), Mineral deposits at the beginning of the 21st century. *Proceedings of the Sixth Biennial SGA-SEG Meeting*, Kraków, Poland, pp. 775–778.

Kucha, H., Mayer, W. & Piestrzyński A., 1982. Mineralogia i geochemia srebra złoża kopalni Konrad. (In Polish). *Rudy i Metale Nieżelazne*, 6: 254–258.

Kucha, H., Stumpf, E.F. & Prochaska, W., 1997. Au-oxysulphide inclusions in gold and their meaning for gold transport and deposition, Mitterberg, Austria. In: Papunen, H. (ed.), *Mineral Deposits: Research and Exploration, Where do They Meet? Proceedings of the Fourth Biennial SGA Meeting,* Turku, Finland, pp. 225–228.

Kucha, H., Mayer, W., Piestrzyńsk,i A. & Wieczorek, A., 1981. The replacement of rutile by chalcocite in the Zechstein copper ores of the Fore-Sudetic Monocline. *Mineralogia Polonica,* 12/1: 69–74.

Langford, F. F. & Blanc-Valleron, M. M., 1990. Interpreting Rock-Eval pyrolysis data using graphs of pyrolizable hydrocarbons vs. Total organic carbon*. AAPG Bulletin*, 74: 799 – 804.

Leenheer, M. J., 1984. Missisippian Bakken and equivalent formations as source rocks in the Western Canadian Basin. *Organogenic Geochemistry*, 6: 521–532.

Loukola-Ruskeeniemi, K., 1991. Geochemical evidence for the hydrothermal origin of sulphur, base metals and gold in proterozoic metamorphosed blac shales, Kainuu and Outokumpu areas, Finland. *Mineralium Deposita,* 26/2: 152–164.

Loukola-Ruskeeniemi, K. & Heino T., 1996. Geochemistry and genesis of the black shale-hosted Ni-Cu-Zn deposit at Talvivaara, Finland, *Economic Geology*, 91: 80–110.

Łuszczkiewicz, A., 1998. Wydzielenie koncentratów złota i platynowców z pozabilansowej rudy miedzi. (In Polish). *Prace Specjalne Polskiego Towarzystwa Minineralogicznego*, 12: 41–62.

Maier, W. D. & Barnes, S.-J., 2003. Platinum-group elements in the Boulder Bed western Bushveld Complex, South Africa. *Mineralium Dep*osita, 98: 370–380.

Maier, W. D., Marsh, J. S., Barnes, S.-J. & Dodd, D. C., 2002. The distribution of platinum group elements in the Insizawa Lobe, Mount Ayliff Complex, South Africa: Implication for Ni-Cu-PGE sulphide exploration in the Karoo Igneous Province. *Economic Geology,* 97: 1293–1306.

Makariev, L. B., Bylinskaya, L. V. & Pavlov, M. V., 1999. Platinum group elements in the Kodar-Udokan copper district. In: Orlov, V.P. (ed.), Platinum of Russia, Moskva, *Geoinformmark,* 3: 300–306.

Mao, J., Lehmann, B., Du, A., Zhang, G., Ma, D., Wan, Y., Zeng, M. & Kerrich, R., 2002. Re-Os dating of polymetallic Ni-Mo-PGE-Au mineralization in Lower Cambrian black shales of South China and its geologic significance. *Economic Geology,* 97/5: 1051–1061.

Matheron, G., 1962. *Traîté de géostatistique appliquée*. T.1, Editions Technip, Paris, 334 pp.

Matheron, G., 1963. *Traîté de géostatistique appliquée*. T.2, Editions Technip, Paris, 172 pp.

Mayer, W. & Piestrzyński, A., 1982. Geologia i okruszcowanie złoża miedzi Rudna. (In Polish). *Unpublished PhD Thesis*, AGH-University of Science and Technology, Kraków, 232 ms. pp.

Mayer, W. & Piestrzyński, A., 1985. Ore minerals from Lower Zechstein sediments at Rudna mine, Fore-Sudetic monocline, SW Poland. *Prace Mineralogiczne PAN*, *Oddział w Krakowie*, 75: 1–80.

Mączka, W., Piestrzyński, A. & Pieczonka, J., 2003. Wzbogacanie grawitacyjne złota występującego w łupku czerwonym. (In Polish). *Inżynieria Mineralna,* 3 (10): 141–149.

Michalik, M., 1979. Utwory plamiste (rote Fäule) występujące w cechsztynie Z-1 na południe od Głogowa. (In Polish). In: Z badań mineralogicznych skał Polski. *Prace Mineralogiczne PAN, Oddział w Krakowie*, 54: 23–41.

Nemec, W. & Porębski, S., 1977. Weissliegendes sandstones: a transition from fluvial-aeolian to shallow-marine sedimentation (Lower Permian of the Fore-Sudetic Monocline) 1. Sedimentary structures and textural differentiation. *Rocznik Polskiego Towarzystwa Geologicznego*, 47: 387–418.

Nieć, M. & Piestrzyński, A., 1996. Forma i budowa złoża. (In Polish). In: Piestrzyński, A. *et al.* (eds), *Monografia KGHM Polska Miedź S.A.*, pp. 185–194.

Nowak G. J., Speczik S., Oszczepalski S., 2001. Petrographic composition of organic matter in the Kupferschiefer horizon of Poland. In: A. Piestrzyński *et al.* (eds), *Mineral Deposits.* Balkema, Rotterdam, 67–70.

Oberc, J., 1967. Budowa tektoniczna terenów XL Zjazdu PTG w Zgorzelcu. (In Polish). *Przegląd Geologiczny*, 6: 253–261.

Oberc, J., 1995. Schemat budowy geologicznej Dolnego Śląska. (In Polish). *Materiały Sesji LXVI Zjazdu Polskiego Towarzystwa Geologicznego*, pp. 2–9.

Oberc, J. & Tomaszewski, J., 1963. Niektóre zagadnienia stratygrafii i podziału cechsztynu monokliny przedsudeckiej. (In Polish). *Przegląd Geologiczny*, 11: 505–509.

Obermajer, M., Fowler, M. G. & Snowdon, L. R., 1999. Depositional environment and oil generation in Ordovican source rocks from southwestern Ontario, Canada: organic geochemical and petrological approach**.** *AAPG Bulletin*, 83: 1426 – 1453.

Oberthür, T., Weise, T. W., Gast, L. & Kojonen, K., 2003. Geochemistry and mineralogy of platinum-group elements at Hartley Platinum Mine, Zimbabwe. *Mineralium Deposita*, 38: 327–343.

Okamoto, H., 1990: As-Pd. In: Massalski, T. B. *et al.* (eds), *Binary alloy phase diagrams. ASM International*, pp. 308–310.

Oszczepalski, S., 1980. Paleogeography, sedimentation and mineralization of the Z_1 carbonate series (Zechstein) in the western part of the Fore-Sudetic Monocline (western Poland). *Contribution to Sedimentology*, 9: 307–323.

Oszczepalski, S., 1989. Kupferschiefer in southwestern Poland: sedimentary environments, metal zoning and ore controls. *Geological Associacion of Canada Special Paper,* 36: 571–600.

Oszczepalski, S., 1999. Origin of the Kupferschiefer polymetallic mineralization in Poland. *Mineralium Deposita*, 34: 599–613.

Oszczepalski, S. & Rydzewski, A., 1983. Miedzionośność utworów permu na obszarze przylegającym do złoża Lubin-Sieroszowice. (In Polish). *Przegląd Geologiczny*, 31: 437–444.

Oszczepalski, S. & Rydzewski, A., 1996. Rozmieszczenie metali w basenie cechsztyńskim. (In Polish). In: Piestrzyński, A. *et al.* (eds), *Monografia KGHM Polska Miedź S.A.*, pp. 115–122.

Oszczepalski, S. & Rydzewski, A., 1997. *Atlas metalogeniczny cechsztyńskiej serii miedzionośnej w Polsce.* (In Polish). Państwowy Instytut Geologiczmy, Warszawa.

Ottley, D. J., 1965. Gy's sampling slide rule. *Revue de l' industrie minerale*, 8 pp.

Parker, H. M., 1991. Statistical treatment of outlier data in epithermal gold deposit reserve estimation. *Mathematical Geology*, 23: 175–199.

Pasava, J., Hladikova, J. & Dobes, P., 1990. Comparison between the distribution of PGM in black shales from the Bohemian Massif (CSFR) and other black shale occurrences. *Minera-*

lium Deposita, 26: 99–103.

Pasava, J., Vavrin, I., Fryda, J., Janousek, V. & Jelinek, E., 2003. Geochemistry and mineralogy of Platinum-group elements in the Ransko gabro-peridotite massif, Bohemian Massif (Czech Republic). *Mineralium Deposita,* 38/3: 298–311.

Peryt, T. M., 1977. Cechsztyn w rejonie Wrocławia. (In Polish, English summary). *Kwartalnik Geologiczny*, 21: 741–756.

Peryt, T. M., 1984. Sedymentacja i wczesna diageneza utworów wapienia cechsztyńskiego w Polsce zachodniej. (In Polish, English summary). *Prace Państwowego Instytutu Geologicznego*, 109: 1–80.

Peryt, T. M., 1988. Cechsztyński dolomit płytowy (Ca3) w rejonie Wrocławia. (In Polish, English summary). *Biuletyn Instytutu Geologicznego*, 358: 5–24.

Peters, K. E., 1986. Guidelines for evaluating petroleum source rock using programmed pyrolisis**.** *AAPG Bulletin*, 70: 318–329.

Pieczonka, J., 1998. Okruszcowanie utworów typu rote Fäule w złożu rud miedzi na monoklinie przedsudeckiej w obszarze Polkowice-Sieroszowice. (In Polish). *Unpublished PhD Thesis,* AGH-University of Science and Technology, Kraków, 158 ms. pp.

Pieczonka, J., 2000. Strefy utlenienia w złożu rud miedzi na monoklinie przedsudeckiej. (In Polish). *Prace Specjalne Polskiego Towarzystwa Mineralogicznego*, 16: 9–54.

Pieczonka, J. & Piestrzyński, A., 2000. Model genetyczny koncentracji złota w obszarze występowania złóż rud miedzi na monoklinie przedsudeckiej. (In Polish). *Prace Specjalne Polskiego Towarzystwa Mineralogicznego*, 16: 55–82.

Pieczonka, J. & Piestrzyński, A., 2001. Złoże złota na monoklinie przedsudeckiej – fakty i hipotezy. (In Polish). *Geologia, Kwartalnik AGH*, 27: 411–434.

Piestrzyński, A., 1989. Uranium and thorium in copper ore deposits in the Fore-Sudetic Monocline (SW Poland). *Mineralogia Polonica,* 20/1: 41–57.

Piestrzyński, A., 1990. Uranium and thorium in the Kupferschiefer formation, Lower Zechstein. *Mineralium Deposita,* 25/2: 146–152.

Piestrzyński, A., 1995. Materiały archiwalne dotyczące obrony pracy habilitacyjnej. (In Polish). AGH Kraków. Archival data.

Piestrzyński, A., 1996a. Okruszcowanie. (In Polish). In: Piestrzyński, A. *et al.* (eds), *Monografia KGHM Polska Miedź S.A.*, pp. 200–237.

Piestrzyński, A., 1996b. Geneza złoża. (In Polish). In: Piestrzyński, A. *et al.* (eds), *Monografia KGHM Polska Miedź S.A.*, pp. 282–302.

Piestrzyński, A. & Pieczonka, J., 1997a. Analiza mineralogiczno-złożowa w strefach wzbogaconych w metale szlachetne. Praca wykonana na zlecenie KGHM Polska Miedź S.A., ZG Polkowice-Sieroszowice. (In Polish, English summary). *Archiwum Zakładu Złóż Rud i Soli AGH Kraków*, 250 pp.

Piestrzyński, A. & Pieczonka, J., 1997b. Gold and PGE on an oxide-reducing interface in Lower Zechstein sediments of the Fore-Sudetic Monocline, SW Poland. In: Papunen, H. (ed.), *Mineral Deposits: Research and Exploration, Where do They Meet? Proceedings of the Fourth Biennial SGA Meeting,* Turku, Finland, pp. 99–102.

Piestrzyński, A. & Pieczonka, J., 1998. Tetraauricupride from the Kupferschiefer type deposit, SW Poland – first occurrence. *Mineralogia Polonica*, 29/1: 11–18.

Piestrzyński, A. & Wodzicki, A., 2000. Origin of the gold deposit in the Polkowice-West Mine, Lubin-Sieroszowice Mining District, Poland. *Mineralium Deposita,* 35: 37–47.

Piestrzyński, A., Wodzicki, A. & Banaszak, A., 1996a. Złoto w złożu rud miedzi na monoklinie przedsudeckiej. (In Polish). *Przegląd Geologiczny*, 44(11): 1098–1102.

Piestrzyński, A., Schmidt, S. & Franco, H., 1991. Gold-bearing chalcopyrite from the Philex-Sto. Tomas II porphyry copper deposit, Tuba, Beguet, Philippines. *Neues Jahrbuch Miner. Abh*., 163: 238–241.

Piestrzyński, A., Schmidt, S. Th. & Franco, H., 1994. Pd-minerals in the Sto. Tomas II, porphyry copper deposit, Tuba Benguet, Philippines. *Mieralogia Polonica*, 25/2: 21–31.

Piestrzyński, A., Głuszek, A. & Michalik, A., 1996c. Istrukcja opróbowania horyzontu z metalami szlachetnymi. (In Polish). Archival data. *Archiwum ZG Polkowice*.

Piestrzyński, A., Kucha, H. & Reut, R., 2000. Występowanie żył kruszcowych typu Rücken w złożu rud miedzi na monoklinie przedsudeckiej (In Polish). *Prace Specjalne Polskiego Towarzystwa Mineralogicznego*, 16: 83–94.

Piestrzyński, A., Pieczonka, J. & Głuszek, A., 2002. Redbed-type gold mineralisation, Kupferschiefer, south-west Poland. *Mineralium Deposita,* 37: 512–528.

Piestrzyński, A., Banaszak, A., Oszczepalski, S., Rydzewski, A.& Speczik, S., 1996b. Jakość złoża KGHM Polska Miedź S.A. w świetle najnowszych wyników badań. (In Polish). In: *Uroczysta Sesja Naukowa, 40-lecie odkrycia złóż rud miedzi i 35-lecie KGHM Polska Miedź S.A.,* pp. 24–29.

Podemski, M., 1973. Sedymentacja cechsztyńska w zachodniej części monokliny przedsudeckiej na przykładzie okolic Nowej Soli. (In Polish, English summary). *Prace Państwowego Instytutu Geologicznego,* 71: 1–101.

Pokorski, J., 1978. Zarys rozwoju basenu czerwonego spągowca na obszarze Niżu Polskiego. (In Polish, English summary). *Przegląd Geologiczny*, 12: 686–694.

Pokorski, J., 1981. Propozycja formalnego podziału litostratygraficznego czerwonego spągowca na Niżu Polskim. (In Polish, English summary). *Kwartalnik Geologiczny,* 25: 41–57.

Pokorski, J. & Ryka, W., 1978. Rotliegend. In: Piątkowski, T.S., Pokorski, J. & Wagner, R. (eds), *Symposium on Central European Permian. Guide to Excursions, Pt. 1*: *Permian of the Polish Lowlands*, Warszawa, pp. 34–43.

Preidl, M., 1967. Budowa tektoniczna obszaru Lubina i Sieroszowic. (In Polish). *Przegląd Geologiczny,* 6: 265–267.

Rendu, J. M.,1976. The optimization of sample spacing in South African gold mines. *Journal of the South African Institute of Mining and Metallurgy*, 76/ 9: 392–399.

Rentzsch, J., 1991. Die Rote-Fäule-Fazies als wichtigster erzkontrollierender Faktor der Vererzung des Typs Kupferschiefer. *Zbl. Geologie und Paläontologie*, I/4: 945–956.

Rentzsch, J., 1995. Revision of the metal distribution controls in the Kupferschiefer of Germany. In: Pasava, J., Kribek, B. & Zak, K. (eds), *Mineral deposits from their origin to their environmental impacts*. *Proceedings of the III Biennial SGA Meeting,* Balkema, Prague, pp. 975–976.

Report AGH, 1996. Występowanie Au, Pt i Pd w złożach rud miedzi i zachowanie się tych pierwiastków w procesach technologicznych. Praca zbiorowa pod kierunkiem A. Piestrzyńskiego (In Polish). Archival data. *Archiwum Zakładu Złóż Rud i Soli, WGGiOŚ*, AGH Kraków, manuscript, 450 pp.

Report AGH, 1997. Analiza mineralogiczno-złożowa w strefach wzbogacenia w metale szlachetne. Praca zbiorowa pod kierunkiem A. Piestrzyńskiego. (In Polish). Archival data. *Archiwum Zakładu Złóż Rud i Soli, WGGiOŚ,* AGH Kraków, manuscript, 350 pp.

Richter, G., 1941. *Geologische Gesetzmässigkeite in der Metallführung des Kupferschiefers – Zwei Beitrage zu Fazies, Tektonik und Kupferführung des Zechsteins I, Waldeck II Nordsudeten.* Berlin, 61 pp.

Rospondek, M. J., Fijałkowska, A. & Lewandowska, A., 1993 – The origin of organic matter in Lower Silesian copper-bearing shales. *Annales Societatis Geologorum Poloniae*, 63: 85–89.

Rydzewski, A., 1969. Petrografia łupków miedzionośnych cechsztynu na monoklinie przedsudeckiej. (In Polish, English summary). *Biuletyn Instytutu Geologicznego*, 217: 113–167.

Rydzewski, A., 1976. Geneza polimetalicznej mineralizacji dolnocechsztyńskiej. (In Polish). *Przegląd Geologiczny,* 4: 176–181.

Rydzewski, A., 1978. Facja utleniona cechsztyńskiego łupku miedzionośnego na obszarze monokliny przedsudeckiej. (In Polish). *Przegląd Geologiczny,* 2: 102–107.

Ryka, W., 1978. Skały wylewne czerwonego spągowca w Polsce. (In Polish). *Przegląd Geol*ogiczny, 12: 694–698.

Ryka, W., 1981. Some problems of the Autunian volcanism in Poland. In: *Proceedings, International Symposium Central European Permian*, Warszawa: 165–179.

Ryka, W. & Maliszewska, A., 1982. *Słownik petrograficzny*. (in Polish). Wydawnictwa Geologiczne, Warszawa, 403 pp.

Salamon, W., 1976. Metale szlachetne w czarnych łupkach cechsztyńskich na monoklinie przedsudeckiej. (In Polish). *Rudy i Metale Nieżelazne*, 12: 472–477.

Salamon, W., 1979. Ag i Mo w cechsztyńskich osadach monokliny przedsudeckiej. (In Polish, English summary). *Prace Mineralogiczne PAN, Oddział w Krakowie*, 62: 1–56.

Salski, W., 1965. Problemy małej tektoniki w rejonie Lubina. (In Polish). *Rudy i Metale Nieżelazne,* 4: 485– 489.

Salski, W., 1968. Charakterystyka litologiczna i drobne struktury łupków miedzionośnych monokliny przedsudeckiej. (In Polish, English summary). *Kwartalnik Geologiczny,* 12: 855–873.

Salski, W., 1975a. Tektonika okolic Lubina. (In Polish, English summary). *Biuletyn Instytutu Geologicznego,* 287: 61–178.

Salski, W., 1975b. Zmiany układu spękań w cechsztyńskich skałach węglanowych monokliny przedsudeckiej. (In Polish, English summary). *Kwartalnik Geologiczny*, 19: 583–595.

Salski, W., 1977. Rozwój tektoniczny obszaru miedzionośnego monokliny przedsudeckiej. (In Polish, English summary). *Rocznik Polskiego Towarzystwa Geologicznego*, 47: 27–48.

Salski, W., 1996. Tektonika złoża. (In Polish). In: Piestrzyński, A. *et al.* (eds), *Monografia KGHM Polska Miedź S.A*., pp. 141–155.

Sawłowicz, Z., 1993. Iridium and other platinum-group elements as geochemical markers in sedimentary environments. *Palaeogeography, Palaeoclimatology, Palaeoecology*, 104: 253–270.

Sawłowicz, Z., 1994. PGE and Re in the Zechstein Cu-Deposit (Kupferschiefer) from the Lubin-Glogow Mining Area (Poland). *IX Symposium of International Association on the Genesis of Ore Deposits.* Beijing, China, pp. 884–885.

Sawłowicz, Z., Gize, A. P. & Rospondek, M., 2000. Organic matter from Zechstein copper deposits (Kupferschiefer) in Poland. In: Gikson, M., Mastalerz, M. (eds), *Organic matter and mineralization: thermal alternation, hydrocarbon generation and role in metallogenesis*. Kluwer Academic Publishers, Dordrecht/Boston/London: 220–242.

Schissel, D., Tsvetkov, A. A., Mitrofanov, F. P. & Korchagin, A. U., 2002. Basal Platinum-group element mineralization in the Federov Pansky Layerd mafic intrusion, Kola Peninsula, Russia. *Economic Geology*, 97: 1657–1677.

Schneiderhöhn, H., 1926. Erzführung und Gefüge des Mansfelder Kupferschiefers. *Metall und Erz,* 23: 143–146.

Schröcke, H. & Weiner, K. L., 1981. *Mineralogie.* W De G Berlin, New York, 952 pp.

Scott, B. C. & Whateley, M.K.G.,1995. Evaluation techniques. In: Evans, A.M. (ed.), *Introduction to mineral exploration*. Blackwell Science Ltd, London: 61–202.

Sharapov J. P., 1971. *Primienienie matiematicheskoy statistiki w geologii.* (In Russian). Nedra, Moskwa, 245 pp.

Siemaszko, E., 1978. Permskie skały wylewne w południowozachodniej części monokliny przedsudeckiej. (In Polish, English summary). *Kwartalnik Geologiczny*, 22: 571–581.

Sillito, R. H., 2003. Iron oxide-copper-gold deposits: an Andean view. *Mineralium Deposita*, 38: 787–812.

Skirrow, R. G. & Walshe, J. L., 2002. Reduced and oxidized Au-Cu-Bi iron oxide deposit of the Tennant Creek Inlier, Australia: An intergraded geologic and chemical model. *Economic Geology*, 97: 1167–1202.

Skowronek, C., 1968. Czerwone plamy w utworach dolnego cechsztynu. (In Polish). *Rudy i Metale Nieżelazne,* 3: 134–137.

Smith J. T., 1994. Petroleum system logic as an exploration tool in a frontier setting. In: Magoon L.B. & Dow W.G. (eds), *The petroleum system – from source to trap.* AAPG Memoir 60: 25– 49.

Sofer, Z., 1984. Stable carbon isotope compositions of crude oils: applicaton to source depositional environments and petroleum alteration. *AAPG Bulletin*, 68: 31–49.

Sokołowski, J., 1967. Charakterystyka geologiczna i strukturalna obszaru przedsudeckiego. (In Polish, English summary). *Geologia Sudetica*, 3: 297–367.

Speczik, S., 1979. Mineralizacja kruszcowa w utworach karbońskich podłoża monokliny przedsudeckiej. (In Polish, English summary). *Geologia Sudetica,* 14(1): 77–124.

Speczik, S., 1985. Metalogeneza podłoża podcechsztyńskiego monokliny przedsudeckiej. (In Polish, English summary). *Geologia Sudetica*, 20(1): 37–97.

Speczik S., Püttmann W. 1987. Origin of Kupferschiefer mineralization as suggested by coal petrology and organic geochemical studies. *Acta Geologica Polonica*, 37: 167–187.

Stenina, N.G., 1997. Behaviour of gold and platinum in natural processes. In: Papunen, H. (ed.), *Mineral Deposits: Research and Exploration, Where do They Meet? Proceedings of the Fourth Biennial SGA Meeting,* Turku, Finland, pp. 319–321.

Stenina, N. G., Alabin, L. V. & Dolzhenko, V. N., 2001. Metamorphic reaction as a basis of gold mineralization. In: Piestrzyński, A. *et al.* (eds), *Mineral deposits at the beginning of the 21st centuary, Proceedings of the VI Biennial SGA-SEG Meeting*, Kraków: 917–920.

Sullivan, J., 1984. Conditional recovery estimation through probability kriging – theory and practice. In: Verly, G. (ed.), *Geostatistics for natural Resources Characterization*. Part 1, Reidel Publishing Company, pp. 365–384.

Talkington, R. W. & Lipin, B. R., 1986. Platinum-group minerals in chromite seams of the Stillwater Complex, Montana. *Economic Geology,* 81/5: 1179–1186.

Tarkian, M., Economu-Eliopulos, M. & Eliopulos, D. G., 1992. Platinum-group minerals and tetraauricupride in ophiolite rocks of Skyros island, Greece. *Mineralogy and Petrology*, 47: 55–66.

The 2001.18.12. Regulation of the Minister of Environment on the economic criteria for deposits of mineral raw-materials, Dz. U. (Official Journal) No. 153, item 1774.

Tomaszewski, J. B., 1962a. Problemy stratygrafii monokliny przedsudeckiej. (In Polish). *Rudy i Metale Nieżelazne,* 7: 547–551.

Tomaszewski, J.B., 1962b. Utwory solne cechsztynu monokliny przedsudeckiej w rejonie Lubin-Sieroszowice. (In Polish). *Przegląd Geologiczny,* 12: 668–671.

Tomaszewski, J. B., 1963. Tektonika brzeżnej części monokliny przedsudeckiej. (In Polish). *Rudy i Metale Nieżelazne,* 2: 207–210.

Tomaszewski, J. B., 1966. Charakterystyka litofacjalna utworów cechsztyńskich brzeżnej części monokliny przedsudeckiej. (In Polish). In: *Z geologii Ziem Zachodnich*. PWN, Wrocław: 265–276.

Tomaszewski, J. B., 1978. Budowa geologiczna okolic Lubina i Sieroszowic (Dolny Śląsk). (In Polish, English summary). *Geologia Sudetica*, 13(2): 85–132.

Tomaszewski, J. B., 1981. Development of Zechstein deposits in the vicinity of Lubin and Sieroszowice. *Proceedings of the International Symposium on Central European Permian*. Wydawnictwa Geologiczne, Warszawa, pp. 341–355.

Tomaszewski, J. B. & Kienig, E., 1972. Zagadnienie dolomitu lubińskiego w osadach cechsztynu monokliny przedsudeckiej. (In Polish). *CBiPM "Cuprum"*, 2: 26–33.

Verly, G. & Sullivan, J., 1985. Multigaussian and probability krigings – application to the Jerritt Canyon deposit. *Mining Engineering*, 37: 586–574.

Wagner, R., Piątkowski, T. S. & Peryt, T. M., 1978. Polski basen cechsztyński. (In Polish). *Przegląd Geologiczny,* 26: 673–685.

de Wijs, H. J., 1951. Statistics of ore distribution. *Geologie en Mijnbouw*, I/11:365–375.

de Wijs, H. J., 1953. Statistics of ore distribution. *Geologie en Mijnbouw*, II/1: 12–24.

Wilczek, T. & Merta, H., 1992. Wstępne wyniki badań pirolitycznych metody Rock Eval. (In Polish). *Nafta*, 48: 109 – 116.

Wild, A., Edwards, A. & Yakubchuk, A., 2003. Unconventional deposits of Pt and Pd: A review with implications for exploration. *SEG Newsletter,* 52: 1, 10–18.

Wieniewski, A., Kubacz, N. & Kowalska, M., 1998. Wyniki wstępnych badań wzbogacania pozabilansowej rudy miedzi o podwyższonej zawartości złota. (In Polish). *Prace Specjalne Polskiego Towarzystwa Mineralogicznego*, 12: 11–28.

Więcław, D., Kotarba M. J., Pieczonka J., Piestrzyński A., Oszczepalski S. & Marynowski, L., 2007. The new view on reduced, transitional and oxidised zones distribution in the Kupferschiefer in Foresudetic Monocline (SW Poland) based on indices of organic matter. *Biuletyn Państwowego Instytutu Geologicznego*, 423: 125–138.

Wodzicki, A. & Piestrzyński, A., 1994. An ore genetic model for the Lubin-Sieroszowice mining district, Poland. *Mineralium Deposita,* 29: 30–43.

Wojciechowska, J. & Serkies, J., 1967. Traces of gold in the Fore-Sudetic copper deposits of the Lubin region. *Bulletin de L`Academie Polonaise des Sciences, serie des sciences géologiques et geographiques,* 3: 107–112.

Wyżykowski, J., 1961. Północno-zachodni zasięg krystaliniku bloku przedsudeckiego i możliwości poszukiwań cechsztyńskich rud miedzi w tym rejonie. (In Polish). *Przegląd Geologiczny,* 4: 182–186.

Wyżykowski, J., 1964. Utwory czerwonego spągowca na przedgórzu Sudetów. (In Polish). *Przegląd Geologiczny,* 12: 319–323.

Wyżykowski, J., 1971. Cechsztyńska formacja miedzionośna w Polsce. (In Polish). *Przegląd Geologiczny,* 3: 117–122.